Failure mechanisms in glass-ceramic matrix composite laminates

Davies, C. M. A.

Award date:
1994

Awarding institution:
University of Bath

FAILURE MECHANISMS IN GLASS-CERAMIC MATRIX COMPOSITE LAMINATES

Submitted by C.M.A.Davies

for the degree of PhD

of the University of Bath

1994

ProQuest LLC
789 East Eisenhower Parkway
P.O. Box 1346
Ann Arbor, MI 48106-1346

SUMMARY

The room-temperature tensile mechanical properties of a range of silicon carbide fibre-reinforced glass-ceramic matrix composite laminates have been studied in detail and the results compared with predictions based on available models of composite behaviour.

The longitudinal and transverse stress-strain responses of unidirectional, off-axis and simple angle-ply laminates of a Nicalon/CAS composite have been monitored during continuous and incremental loading. Attempts to correlate the stress-strain behaviour with the initiation and development of matrix cracks have been made by means of acoustic emission, edge replication and optical microscopy.

The stress-strain behaviour of unidirectional composite was in reasonable agreement with that predicted by the Aveston, Cooper, Kelly (ACK) model. Matrix cracking was found to commence at stresses much lower than the limit of proportionality on the stress-strain curve and was indicated by the onset of acoustic emission activity. Continued matrix cracking occurred over a range of stress and was found to be accompanied by an increasing cumulative residual strain and a reduction in composite modulus. The transverse strain behaviour was found to be most closely associated with matrix cracking damage. Subsequent damage was thought to be by progressive fibre fragmentation and/or fibre-matrix sliding.

The tensile stress-strain behaviour of a range of simple angle-ply laminates was discussed in terms of observed damage and in the light of results from unidirectional and off-axis Nicalon/CAS composite. Again, the transverse strain behaviour was found to be most closely associated with matrix cracking and continued cracking appeared to be limited in some laminates by the ability of fibres to withstand extra load. A behavioural model was proposed in which failure mechanisms are

superimposed and which enables the form and extent of damage to be predicted. Acoustic emission activity and damage observations were in accord with predictions based on this type of approach.

ACKNOWLEDGEMENTS

The author would like to acknowledge contributions made by the following individuals and institutions throughout the course of this work:

I would like to thank Professor Bryan Harris and Dr. Robin Cooke for their supervision, advice and many helpful discussions. I would also like to thank Rolls-Royce plc for their significant financial contribution to the project, for the provision of materials and for their technical support. Contributions made by members of the Composites and Ceramics Group are greatly appreciated. Acknowledgement is also made to the SERC for provision of a CASE award. Thanks are due to members of the School of Materials Science at Bath University, in particular to Mark Deven and Dr. Tim Mays. A debt of gratitude to Dr. Richard Russell-Floyd is acknowledged.

To my family - and to the finding of many more banana trees!

To the memory of Richard Russell-Floyd

and

To Iain Banks for 'The Crow Road' and for "The man who put the Bore in Borosilicate"!

CONTENTS

CHAPTER 1 : BACKGROUND AND AIMS OF PROJECT

1.1 Background

Gas turbine engines are complex engineering structures which contain some of the most demanding and aggressive operating conditions seen by any material. The gas turbine operates on essentially simple principles. Air is compressed and passed into a combustion chamber where energy is produced in the system by burning fuel. The hot gas then passes through a series of turbines, where some of the energy is expended in causing them to rotate in order to drive the compressor, and is expelled into the atmosphere at high velocity thus creating the thrust which propels the aircraft forward.

The major factors influencing the continued development of gas turbine engines are the need to increase thrust and fuel efficiency whilst decreasing weight and cost. Over the last 50 years improvements in design and materials technologies have enabled thrust-to-weight ratios and compression ratios to be increased from 3:1 to 10:1 and from 4:1 to 30:1 respectively, and turbine entry temperatures (TETs) to be increased from 800 °C to 1400 °C[1]. The TET is a measure of the thermal efficiency of an aero-engine for which the ultimate aim is that of stoichiometric combustion at approximately 2000 °C. However, even at current gas temperatures some components (e.g. high-pressure turbine blades situated directly behind the combustion chamber and which experience the full TET) are required to operate at temperatures higher than the melting point of the superalloy from which they are manufactured. This is achieved by extensive use of cooling air and ceramic thermal barrier coatings which, together, can reduce the metal temperature by up to 150 °C. Obviously the use of cooling air is a source of great loss in engine power which can only be eliminated by the use of materials with higher temperature capabilities.

The design goals for military gas turbine engines entering service in the 21st century are a thrust-to-weight ratio of 20:1, a compression ratio of 40:1 and a TET of 2000 °C[1]. The extent of these improvements is beyond that achievable by the development

of current metallic materials alone. However ceramic materials, which offer high specific stiffness and strength at high temperatures, have the potential to achieve the desired performance increase and a range of these materials is currently being considered by aero-engine manufacturers such as Rolls-Royce for a number of low weight, high-temperature components.

Although ceramics do have high-temperature stability, together with good wear and corrosion resistance, their low fracture toughness has hitherto severely limited their use in engineering applications since any replacement of a metal component needs to demonstrate predictable behaviour and a guaranteed life. The fracture toughness is a measure of the sensitivity of the strength of a material to the presence of defects. Monolithic ceramics such as SiC, Si_3N_4, and Sialon typically have fracture toughnesses in the range 3 - 8 $MPa.m^{1/2}$ which means that flaw sizes of the order of 100 μm or less are critical. This, together with typical strength distributions having Weibull moduli of 10 - 15, gives unacceptably high failure probabilities for most aero-engine applications since, once the fracture strength is reached, the stored elastic energy is far in excess of that required to fracture the material and failure is thus catastrophic.

Since the late 1950s efforts have been made to improve the toughness and reliability of structural ceramics by the incorporation of a second discontinuous phase which modifies crack growth behaviour[2,3]. One such method of toughness enhancement is through energy absorption by the stress-induced transformation of a second-phase particle ahead of the crack tip (i.e. zirconia transformation toughening). Particle, whisker and platelet dispersions have also been used to toughen the above monolithic matrices.

The most dramatic improvements in the fracture properties of ceramics have been obtained by reinforcing ceramic matrices with continuous high-strength fibres to

produce a ceramic-matrix composite (CMC) exhibiting controlled failure with a high fracture energy resulting from crack deflection, crack bridging and fibre pull-out. However, the enhanced tensile properties and damage tolerance are achieved at the expense of degraded transverse and shear properties requiring composites to be designed specific to each application under consideration.

1.2 Aims of Project

In order for the potential of ceramic-matrix composites to be fully exploited, a detailed understanding of the micro-mechanics of failure under a wide range of loading conditions is required.

Of particular concern in CMCs is matrix cracking which represents the onset of permanent damage and a loss of protection for the fibre-matrix interface against oxidation. The stress at which matrix cracking commences is the current design limit for this class of materials and as such must be quantifiable and predictable. To an extent, the relationship between mechanical and microstructural properties for the tensile fracture of unidirectionally reinforced composite is understood (e.g. the Aveston Cooper and Kelly model [4]). However, in view of the limited application of unidirectionally reinforced composite in an aero-engine environment, similar advances need to be made to describe other composite structures and failure mechanisms.

In the present work, the failure mechanisms of unidirectional, off-axis and simple angle-ply laminates of a glass-ceramic matrix composite are investigated with the aim of understanding their stress-strain behaviour.

CHAPTER 2 : BEHAVIOURAL MODELS

2.1 Introduction

This chapter examines some of the available models that attempt to describe the mechanical behaviour of ceramic and composite materials and acts as a precursor to interpreting the behaviour of ceramic-matrix composites.

Initially, the strength and fracture toughness of monolithic ceramics are considered together with the statistical nature of their failure processes. As the present study is predominantly concerned with the behaviour of continuous-reinforced ceramic-matrix composites this section aims to present the fundamentals of fracture mechanics which form the basis of a number of later models for predicting the matrix cracking behaviour of ceramic-matrix composites.

Traditional theories for predicting the elastic properties of composites are then presented and this is followed by a detailed review of models for predicting the matrix cracking behaviour of unidirectionally-reinforced brittle matrix composites. Transverse ply cracking in cross-ply polymer composites is briefly considered.

The final section of this chapter critically examines existing composite strength models and failure criteria which were predominantly developed for polymer-matrix composites but which may be applicable to the current system.

Experimental studies which assess the applicability of the above models for predicting the behaviour of glass and glass-ceramic matrix composites will be discussed in Chapter 3.

2.2 Properties of Ceramics

2.2.1 Introduction - Definition of a Ceramic

Ceramics are defined as inorganic, crystalline materials with ionic and covalent atomic bondings[5]. The bonds are highly stable and ceramics thus have very high melting points and high chemical stability. Traditional ceramics, such as earthenware, china and porcelain, have long been used in the pottery industry as a result of their refractoriness and are principally based on clay (hydrated aluminosilicates). The term now encompasses new ceramics such as highly dense single oxides, carbides and nitrides; cement and concrete; glass and glass-ceramics. All are characterised by their low thermal and electrical conductivity, high hardness and stiffness, good compressive strength and lack of plasticity.

This lack of plasticity is due to the limited number of independent slip systems (maximum of five) within the crystal structure and in covalently bonded ceramics, additionally, to the high resistance to dislocation movement. However, in both cases this results in brittleness and strengths well below theoretical values.

2.2.2 Brittle Fracture - The Griffith Concept

The ideal, or theoretical strength of a crystalline body is the stress which must be applied to cause it to fracture across a particular crystallographic plane[6]. By assuming that the force required to fracture a material is equal to that required to separate an isolated pair of atoms (i.e. ignoring any interaction with other adjacent atoms) and that the total amount of energy which must be supplied to separate the two atoms is equal to that required to create two new surfaces, then an expression for the theoretical fracture strength can be derived:

$$\sigma_{max} = \sqrt{\left(\frac{E\,\gamma}{b_0}\right)} \qquad (2.1)$$

where E is Young's modulus, γ the surface energy and b_0 the equilibrium lattice spacing. The theoretical fracture strength of a solid is thus of the order of $E/10$. In practice, however, most brittle materials fracture at around $E/1000$ although very fine carefully made fibres of glass and ceramic can achieve strengths approaching the theoretical. The reason for this discrepancy between actual and predicted values was first suggested by Griffith[7] as a result of a classic investigation into the strength of glass which he carried out in the 1920s. Griffith suggested that the low strength of glass was due to the presence of small defects which enabled the stress to be concentrated so that the theoretical fracture stress is reached in localised regions of the sample. In order to quantify this effect, he considered the total energy change of a cracked body as the crack length was increased and by doing this realised that it was possible to derive a thermodynamic criterion for fracture. The advantage of this energetic approach, compared with earlier solutions based on Inglis's work[8], is by considering the energy change as a whole rather than stress concentrations at the vicinity of crack tips. Only if the total energy decreased would the crack extend spontaneously under the applied load.

Griffith considered the energy changes that would occur if an elliptical crack, with a major axis length of $2a$, situated within an infinite body normal to an applied tensile stress σ was extended by an infinitesimal amount. This is depicted in Figure 2.1. In extending the crack, new surfaces are produced and if the crack extension is infinitesimally small then the stresses and displacements immediately ahead of the new crack tip are essentially identical to those ahead of the initial crack tip. Griffith recognised that the driving force for crack extension was the difference between the energy which could be released if the crack were extended and that needed to create new surfaces (2γ). He calculated the energy release per unit plate thickness as a function of crack length by considering energy changes in the body as a whole. This

can also be expressed as the potential energy release for crack extension under constant load. For a given crack length, a, the Griffith fracture stress (σ_f) is given by:

$$\sigma_f = \sqrt{\left(\frac{2E\gamma}{\pi a}\right)} \qquad (2.2)$$

for plane stress, and

$$\sigma_f = \sqrt{\left(\frac{2E\gamma}{\pi(1-\upsilon^2)a}\right)} \qquad (2.3)$$

for plane strain.

The thermodynamic nature of this approach must be emphasised as it considers only the initial and final states and ignores the details of the fracture process at the crack tip. It therefore represents only a necessary condition for fracture which may not be a sufficient one since, even if the Griffith criterion is satisfied, the crack would not extend unless the stress was sufficiently concentrated at the crack tip to attain the local fracture stress. In the case of ductile metals, which exhibit plastic deformation at the crack tip, the energy required to fracture the material is much greater than that necessary to create new surfaces (2γ) and the Griffith energy-balance approach is not able to deal with this situation. However, Griffith's revolutionary work introduced the concept of the flaw as a source of weakness in a solid and forms the basis of present day fracture mechanics.

2.2.3 Brittle Fracture - The Stress Intensity Approach

In this approach, the energy released as a result of crack extension is calculated by consideration of the crack tip region and incremental extension of the crack, rather than by following Griffith's method, and as such is a continuum analysis.

If a crack of length $2a$, situated within an infinite solid, is subjected to a tensile stress, σ_a, normal to the crack length, then the stress distribution ahead of the crack, σ_{ij}, may be expressed by Irwin's crack tip solution[9] as:

$$\sigma_{ij} = \frac{K}{\sqrt{2\pi r}} \cdot f(\theta) \qquad (2.4)$$

where r is the distance ahead of the crack tip and $f(\theta)$ is a geometric function. It should be noted that this expression is only valid when linear elasticity theory applies and is not valid for $r \approx 0$ or $r \approx a$. K is defined as the stress intensity factor and can be related to the applied stress and crack length by

$$K = \sigma_a Y \sqrt{a} \qquad (2.5)$$

where Y is a dimensionless constant which depends on the geometry of the crack and the loading configuration.

The energy per unit thickness released during incremental crack extension may be defined as the strain energy (or equivalent potential energy) release rate and given the symbol G, such that

$$G = \frac{K^2}{E} \qquad (2.6)$$

for plane stress conditions.

The Griffith criterion for perfectly elastic fractures requires that the strain energy release must atleast equal the work needed to separate the two surfaces i.e. that failure will occur when G reaches a critical value of $G_c = 2\gamma$.

This then enables a critical stress intensity factor, K_c, for the onset of failure to be defined.

There are three basic modes of crack-surface diplacement in relation to the applied load. These are: Mode I (opening) which corresponds to crack separation normal to the applied stress; Mode II (sliding) which corresponds to longitudinal shearing of the crack normal to the crack front; and Mode III (tearing) which corresponds to lateral shearing parallel to the crack front. Of the three modes, the first is most applicable to crack propagation through highly brittle solids. The critical stress intensity factor for failure in Mode I is termed K_{Ic} - the fracture toughness of the material - and may be regarded as a material parameter.

2.2.4 The Statistical Nature of Strength in Brittle Materials

An important consequence of the initiation of failure by the presence of Griffith cracks is that the strength of a brittle solid shows a large degree of scatter about the mean as a consequence of the distribution of flaw sizes within the material, the strength also being dependent on the volume of material tested. Since it is generally not possible to detect defects of critical dimensions in ceramics by current non-destructive testing techniques it is therefore necessary to apply statistical theory to the strength of this class of materials. This enables the probability of survival of a specimen at a given stress level and loading configuration to be predicted.

In the early 1950s Weibull[10] developed statistical methods which have been found to be applicable to strength distributions in brittle materials. In its simplest form the Weibull analysis is based on a 'weakest link' model which is analogous to failure from a single defect within a body, assuming that no interaction between defects occurs.

The Weibull distribution may be expressed in the form

$$P_s(V) = \exp\left[-V\left(\frac{\sigma - \sigma_u}{\sigma_0}\right)^m\right] \qquad (2.7)$$

where: $P_S(V)$ is the probability of survival of a volume V of material at a stress σ; m is a shape parameter usually called the Weibull modulus and reflects the degree of variability in strength - a higher value of m corresponding to a narrower range of strength values; σ_u is the stress below which fracture is assumed to have zero probability and in many cases can be taken as zero; σ_0 is a normalising parameter and has no physical significance.

For the purposes of plotting data it is convenient to take logarithms twice to give the expression

$$\ln \ln\left(\frac{1}{P_s}\right) = \ln V + m \ln(\sigma - \sigma_u) - m \ln \sigma_0 \qquad (2.8)$$

Thus the gradient of a plot of $\ln\ln(1/P_s)$ against $\ln(\sigma - \sigma_u)$ is the Weibull modulus, m, and can be used to predict survival probabilities at particular stress levels.

As stated previously, the measured strength is also dependent on the volume of material tested since a larger volume of material has a higher probability of containing a critical flaw. If two different specimens of the same material, i.e. having the same Weibull modulus, are tested under a uniform stress then the failure stresses can be equated thus[11]

$$\frac{\sigma_{V1}}{\sigma_{V2}} = \left(\frac{V_2}{V_1}\right)^{\frac{1}{m}} \qquad (2.9)$$

where V_1 and V_2 are the volumes of the two specimens and σ_{V1} and σ_{V2} are their corresponding strengths. This is derived from equation 2.7 since, if the probability of survival is the same for both, then $V_1 (\sigma_{V1})^m = V_2 (\sigma_{V2})^m$. Equation 2.7 can also be used to account for stress variations through a beam - for example, to compare the strength of a given volume of material when tested in tension (σ_t) or three-point bending (σ_{3b}). By integrating equation 2.7 with respect to volume and accounting for the distribution of tensile stress in the bending beam (ignoring compressive stresses) then assuming an equal probability of survival, the expressions obtained for tensile and three-point bending can be equated and the following ratio derived:

$$\frac{\sigma_{3b}}{\sigma_t} = \left[2(m+1)^2\right]^{1/m} \qquad (2.10)$$

However, although the expression predicts the bend strength of a ceramic to be much greater then the tensile strength (which is indeed found to be the case), the effect of surface flaws on the initiation of fracture is ignored.

2.3 Elastic Properties of Composite Laminates

2.3.1 Introduction

In the designing of composite structures it is of great importance to have the ability to calculate the elastic properties of a laminate so that its response to extenal loads can be predicted. A number of empirically derived expressions exist for prediction of composite elastic constants in terms of the elastic moduli and geometric parameters of the constituents. A number of these are discussed below. The orthotropic nature of composite materials means that the elastic response will be different in different directions. A system of co-ordinates is therefore used to distinguish these moduli. The notation used throughout this work is detailed in Figure 2.2. However, care must be taken when cross-referencing with other works to ensure that the terminology is consistent.

2.3.2 Elastic Properties of Unidirectional Laminates

If a tensile or compressive load is applied parallel to the fibres in a unidirectional composite, then the strain in the matrix will be the same as the strain in the fibres, assuming that both the fibre and matrix behave elastically and that the bond between them is perfect. This leads to an expression[12] for the longitudinal composite elastic modulus, E_1

$$E_1 = E_f V_f + E_m V_m \qquad (2.11)$$

where E_f and E_m are the fibre and matrix elastic moduli respectively, and V_f and V_m their corresponding volume fractions. This is often referred to as the 'Rule of Mixtures' equation. It should be noted that this approach assumes that the Poisson ratios of fibre and matrix are identical. Hull[12] suggests that the error involved in this

assumption is likely to be 1-2% at most and that good agreement has been found between experimental and predicted values for glass/polyester systems. The accuracy of predictions based on rule of mixtures for the longitudinal modulus of glass and glass-ceramic matrix composites is discussed in Chapter 3.

A similar approach can be used to predict the transverse modulus of a unidirectional laminate, E_2, by considering a load applied transverse to the fibres. It is assumed that the stresses in the fibres and matrix are equal and this gives an expression

$$E_2 = \frac{E_f E_m}{E_f(1 - V_f) + E_m V_f} \qquad (2.12)$$

In order to determine the effect of fibre orientation on the principal composite modulus, Krenchel (given in Hull[12]) introduced an efficiency factor η such that

$$\eta = \sum a_n \cos^4 \theta \qquad (2.13)$$

where a_n is the proportion of fibres orientated at angle θ to the direction of applied load. This approach can be used to calculate the composite modulus, E_c, of both unidirectional off-axis and angle-ply laminates where

$$E_c = \eta E_f V_f + E_m V_m \qquad (2.14)$$

Again, equality between Poisson's ratio of fibre and matrix is assumed and plies at 90° to the loading direction are considered to make no contribution to the overall stiffness.

A rule-of-mixtures type approach may also be used to predict linear thermal expansion coefficients, and the following expression has been derived by Shapery (again given in Hull[11]) for the thermal expansion coefficient (α) parallel to the fibres of a unidirectional composite:

$$\alpha = \frac{E_f \alpha_f V_f + E_m \alpha_m (1 - V_f)}{E_f V_f + E_m (1 - V_f)} \qquad (2.15)$$

where α_f and α_m are the expansion coefficients of the fibre and matrix respectively. Modulus terms enter into the expression since the overall composite thermal expansion is dependent on the relative elastic properties of the fibre and matrix.

2.3.3 Laminate Plate Theory

An orthotropic body, such as a unidirectionally reinforced composite lamina, is characterised by having three mutually perpendicular planes of material symmetry and the properties at any point within the solid are different in three mutually perpendicular directions. Laminated plate theory (LPT) is a method by which the elastic properties of laminates can be calculated from the properties, orientation and distribution of individual laminae. This approach is detailed in Jones[13], Tsai[14] and Kelly[15] and is summarised below.

Nine stress components must be used to define the state of stress at a point - namely three normal stresses σ_{11}, σ_{22}, σ_{33} and six shear stresses τ_{23}, τ_{31}, τ_{12}, τ_{32}, τ_{13} and τ_{21}. The first suffix refers to the direction normal to the plane in which the stress is acting and the second suffix to the direction in which the stress is acting. These stresses are depicted in Figure 2.3. It can be seen that for equilibrium at any point, $\tau_{23} = \tau_{32}$, $\tau_{31} = \tau_{13}$ and $\tau_{12} = \tau_{21}$ in order to prevent any unbalanced couple from acting on the cube. The corresponding strains are given the notation ε_{11}, ε_{22}, ε_{33}, γ_{23}, γ_{31} and γ_{12}. It should be noted that the γ terms are engineering shear strains and as such are related to the individual shear stresses simply by the shear modulus, *G*.

The above stresses and strains are related by a generalised form of Hooke's law

$$\sigma_i = \sum_{j=1}^{6} C_{ij} \varepsilon_j \qquad (2.16)$$

where σ_i and ε_j are the stresses and strains in contracted notation form i.e. σ_{11}, σ_{22}, σ_{33}, τ_{23}, τ_{31} and τ_{12} become σ_1, σ_2, σ_3, σ_4, σ_5 and σ_6. C_{ij} is referred to as the 'stiffness matrix'. A similar expression relates strain to stress by a 'compliance matrix', S_{ij}. The compliances can be expressed in terms of engineering constants E, ν and G.

For laminae and laminates, it is assumed that conditions of plane stress exist i.e. that the composite plate is thin enough so that the through thickness stresses are zero - $\sigma_{33} = \tau_{23} = \tau_{31} = 0$. Composite laminae can also be considered to be transversely isotropic since in the plane normal to the 1-axis the properties are independent of direction.

With these assumptions, the strain-stress relationship becomes

$$\begin{bmatrix} \varepsilon_1 \\ \varepsilon_2 \\ \gamma_{12} \end{bmatrix} = \begin{bmatrix} S_{11} & S_{12} & 0 \\ S_{12} & S_{22} & 0 \\ 0 & 0 & S_{66} \end{bmatrix} \cdot \begin{bmatrix} \sigma_1 \\ \sigma_2 \\ \tau_{12} \end{bmatrix} \qquad (2.17)$$

where $S_{11} = 1/E_1$, $S_{22} = 1/E_2$, $S_{12} = -\nu_{12}/E_1 = -\nu_{21}/E_2$ and $S_{66} = 1/G_{12}$.

The stress-strain relationship for a unidirectional lamina is

$$\begin{bmatrix} \sigma_1 \\ \sigma_2 \\ \tau_{12} \end{bmatrix} = \begin{bmatrix} Q_{11} & Q_{12} & 0 \\ Q_{12} & Q_{22} & 0 \\ 0 & 0 & Q_{66} \end{bmatrix} \cdot \begin{bmatrix} \varepsilon_1 \\ \varepsilon_2 \\ \gamma_{12} \end{bmatrix} \qquad (2.18)$$

where Q_{11}, Q_{12}, Q_{22} and Q_{66} are called reduced stiffnesses and are defined in terms of only four independent constants, namely the engineering constants E_1, E_2, ν_{12} and ν_{21}:

$$Q_{11} = C_{11} = \frac{E_1}{1 - \nu_{12}\nu_{21}} \quad , \quad Q_{22} = C_{22} = \frac{E_2}{1 - \nu_{12}\nu_{21}}$$

$$Q_{12} = C_{12} = \frac{\nu_{12}E_2}{1 - \nu_{12}\nu_{21}} = \frac{\nu_{21}E_1}{1 - \nu_{12}\nu_{21}} \quad , \quad Q_{66} = \tfrac{1}{2}(C_{11} - C_{12}) = G_{12} \qquad (2.19)$$

It may be noted from the above expressions that for a unidirectional composite tested in tension (or compression) along the principal material directions, no shear strains are produced and the deformation is independent of G_{12}. Similarly, a shear stress produces only shear strains which are independent of E_2, ν_{12} and ν_{21}. There is thus no coupling between shear and extensional strains under the assumed conditions. This does not apply when a lamina is tested at arbitrary angles to the principal material directions. Under these circumstances, the stresses and strains can be rotated and the above expressions transformed to an x-y co-ordinate system in which the x-axis is at an angle θ to the 1-direction, as depicted in Figure 2.4. The stress-strain relationship can then be expressed in terms of a transformed reduced stiffness matrix. Using this approach, expressions for the elastic properties E_x, E_y, G_{xy} and ν_{xy} can be derived:

$$\frac{1}{E_x} = \frac{1}{E_1}c^4 + \left(\frac{1}{G_{12}} - \frac{2\nu_{12}}{E_1}\right)s^2c^2 + \frac{1}{E_2}s^4$$

$$\frac{1}{E_y} = \frac{1}{E_1}s^4 + \left(\frac{1}{G_{12}} - \frac{2\nu_{12}}{E_1}\right)s^2c^2 + \frac{1}{E_2}c^4$$

$$\frac{1}{G_{xy}} = 2\left(\frac{2}{E_1} + \frac{2}{E_2} + \frac{4\nu_{12}}{E_1} - \frac{1}{G_{12}}\right)s^2c^2 + \frac{1}{G_{12}}(s^4 + c^4)$$

$$\nu_{xy} = E_x\left[\frac{\nu_{12}}{E_1}(s^4 + c^4) - \left(\frac{1}{E_1} + \frac{1}{E_2} - \frac{1}{G_{12}}\right)s^2c^2\right] \qquad (2.20)$$

Thus if E_1, E_2, G_{12} and ν_{12} are known, the elastic properties at any angle may be calculated (s and c are $\sin\theta$ and $\cos\theta$, respectively).

The basis of laminated plate theory is that a composite laminate is built up of individual laminae having properties described by the above expressions. Assuming that the laminates are perfectly bonded, that the bond is infinitely thin and is non-shear-deformable and that the laminate as a whole behaves as a thin sheet, then for a given strain distribution the stresses within the individual laminae can be calculated

and failure criteria applied. A number of commercially available computer programs are able to perform this analysis e.g. LAMANAL[16].

An important limitation of this approach is that, in view of the assumptions detailed in the previous paragraph, interlaminar shear stresses are ignored and thus low stress failures due to (for example) delamination at free edges are not predicted.

2.4 Matrix Cracking in Unidirectional Laminates

2.4.1 Introduction

Of particular concern in CMCs is the onset of matrix cracking as this represents the onset of permanent damage and a loss of protection for the fibre-matrix interface against oxidation. The stress at which matrix cracking occurs is the current design limit for this class of material and as such must be predictable. A number of models exist which attempt to describe the matrix cracking of unidirectional composite when tested parallel to the fibres. Early studies took an energy balance approach using data from model composites such as glass-fibre-reinforced plaster whereas later studies examined the mechanics of matrix cracking. These two approaches are discussed below, together with a third based on finite element analysis, followed by more recently developed predictions of matrix crack spacings.

2.4.2 Energy Balance Models

The foremost energy balance model for the prediction of matrix cracking in unidirectional laminates is the Aveston, Cooper & Kelly[4] (ACK) model. The model attempts to describe the stress-strain behaviour of a unidirectionally reinforced composite tested in tension parallel to its fibres. The model assumes that both the fibre and matrix have well-defined and single-valued failure strains (and stresses) and that the fibre and matrix are unbonded with a constant interfacial shear strength.

It is shown for a composite in which the failure strain of the matrix is significantly less than that of the fibres that on loading to the matrix failure strain, the matrix will crack and the load will be locally redistributed to the fibres. Assuming that there are sufficient fibres to withstand the additional load thrown upon them, the crack will be sustained. However, as a result of the (assumed constant) fibre-matrix interfacial

shear strength, the stress is shed back into the matrix and increases linearly from zero with distance away from the crack plane (see Figure 2.5). At a distance x' either side of the crack the matrix failure strain will again be reached and multiple cracking will occur with no further increase in applied load. The length x' is determined by the rate of stress transfer between the matrix and fibres which is in turn determined by the interfacial shear strength, τ. Cracking will continue until the limiting crack separation is reached where the matrix is broken into blocks by cracks spanning the entire width and thickness of the specimen and which are between $2x'$ and x' apart. By consideration of a simple force balance, an expression for x' was derived such that

$$x' = \frac{V_m}{V_f}\left(\frac{\sigma_{mu} r}{2\tau}\right) \qquad (2.21)$$

where σ_{mu} is the matrix strength and r the fibre radius.

By considering the energy associated with the formation of a single crack, Aveston and co-workers derived an expresson for the matrix failure strain, ε_{mu}. To do this, it is assumed that the stress in the matrix is equal to the matrix cracking stress and that the crack traverses the entire width of the specimen normal to the fibres. An energy balance can then be constructed in which the work done by the applied stress in extending the composite and the decrease in the matrix strain energy over the distance x' on either side of the crack must equal the work of fracture.

The work of fracture comprises : the matrix fracture surface energy in creating a crack within the matrix (γ_m); the energy to debond the interface over a length x'; frictional work as the fibres slide over the matrix; and the increase in elastic strain energy of the fibres.

Equating these energy terms gives an expression for the matrix failure strain

$$\varepsilon_{mu} = \left(\frac{12\tau\gamma_m E_f V_f^2}{E_f E_m^2 r V_m}\right)^{\frac{1}{3}} \qquad (2.22)$$

From equation 2.22, it is evident that the matrix cracking strain can be increased by incorporating fibres of smaller diameter. Cooper & Sillwood[17] investigated this subsequently and showed that matrix cracking could be suppressed in composites containing very small diameter fibres.

Most usefully, the ACK analysis can be used to describe the stress-strain behaviour of a unidirectional laminate, as in Figure (2.6 a)). From zero applied load the composite deforms elastically with modulus E_c until the stress in the matrix reaches the matrix cracking stress. At this point, multiple cracking of the matrix takes place with no further increase in load until the saturation crack spacing is reached. The load is transferred to the fibres and any additional load then results in further elongation of the fibres and slipping of the fibres through the matrix, giving an overall slope of $E_f V_f$ (ignoring fibre damage). The specimen will eventually fail at a stress corresponding to the strength and proportion of fibres within the composite.

It should be noted that the ACK analysis has a number of limitations, one of which is that it is only valid for a system of fibres and matrix with single-valued strengths - unlike glass and glass-ceramic matrix composites in which both matrix and fibres have a distribution of failure strengths (as discussed in section 2.2). For a matrix having such a strength distribution, Aveston et al offer the qualitative argument that matrix cracking will occur over a range of applied loads, as shown in Figure (2.6 b)). A second limitation is that the ACK energy balance only considers the energy of the system before and after cracking with no consideration given to the source of a crack nor its mechanism of growth.

In more recent work the shortfalls of the ACK approach have been addressed. For example, Aveston and Kelly[18] further developed their ideas by considering flexible fibres and a well-bonded system (obviously inapplicable here). Budiansky and co-workers[19] also develop ACK theory by considering three types of matrix fracture,

viz. (a) no interface debonding with no fibre slippage, (b) an unbonded interface with frictional slippage of fibres, and (c) the case of initially bonded, de-bonding fibres to which a fracture mechanics criterion for steady-state crack propagation is applied. In the light of experiments carried out by Marshall & Evans[20] on a SiC/LAS composite they conclude that the frictional slip model is most applicable. However, the assumed steady-state conditions for crack propagation predict a fall in stress on formation of a first matrix crack and the many other simplifying assumptions used make an incorrect prediction of zero for the matrix cracking stress when the fibre volume fraction tends to zero. These factors aside, Budiansky et al introduce a number of points concerning fibre-matrix strain mismatches resulting from processing which lead to initial matrix stresses and to interface pressures, and they suggest that the frictional slip obeys a Coulombic friction law. Their results imply that an optimum strain mismatch exists which would increase the externally applied cracking stress, although they caution that this may not necessarily be desirable in terms of the post-cracking composite strength and toughness.

More successful predictions of behaviour have been made by using continuum models.

2.4.3 Continuum Models

Marshall, Cox & Evans[21] first proposed continuum models to describe the cracking behaviour of brittle-matrix composites by considering stress intensity factors for long and short cracks where long cracks are considered to be more than a few fibre diameters in length. This approach has been further developed more recently by McCartney[22]. Both studies first consider a discrete fibre model (fibres as separate entities) as shown in Figure 2.7. A crack in the matrix is bridged by unbroken fibres that exert tractions on the crack surfaces. By examining the relative displacements of fibre and matrix, the crack opening displacement for a given traction may be

determined. A continuum model is then introduced by assuming that the effective traction distribution is a smooth, continuous function. This enables an expression for the composite stress intensity factor to be defined. The condition for equilibrium crack growth is that the stress intensity, K, equals the critical stress intensity factor, K_{1c}. Marshall et al assume that the matrix and composite stress intensity factors scale with the ratio E_m:E_c since they state that in the region immediately ahead of the crack tip the matrix and fibre strains must be compatible. McCartney, however, shows that this assumption is unnecessary and energetically inconsistent and that K_{1c} is related to the plane-strain fracture toughness of the matrix alone by a factor $(V_m E_c/E_m)^{1/2}$.

Both studies examine the growth of long cracks. Marshall et al consider 'steady-state' crack propagation in the derivation of their matrix cracking stress. They show that in the steady-state region of a crack (where equilibrium crack opening displacement is obtained), the net tractions on the crack faces exactly equal the applied force and that the stress required to extend the crack is independent of the crack length. An energy balance based on ACK theory is then applied to their continuum model to derive an expression for the matrix cracking stress. Although the Marshall et al and ACK approaches yield very similar expressions, the energy balance analysis used by Marshall is too approximate to demonstrate equivalence between ACK theory and a fracture mechanics approach.

McCartney[22] modifies the ACK expression so that it is valid for plane strain conditions by considering the changes in stored and frictional energy associated with crack growth in the discrete model, although the change in the expression merely amounts to replacing the E_c term with $E_c/(1-\nu^2)$ and similarly for E_f and E_m:

$$\sigma_{mu} = \left\{ \frac{12\gamma_m \tau(1-\nu^2)E_f}{rV_m E_m^2 E_c} \right\}^{1/3} \cdot \frac{E_c}{(1-\nu^2)} \qquad (2.23)$$

A similar energy calculation is then carried out for the continuum model. Equating these two expressions so that the energy available for matrix cracking is the same for both the discrete and continuum models yields a different boundary condition to that used by Marshall et al. The matrix cracking stress is then calculated by using the corrected boundary condition. From this it is possible to generate a curve which describes the dependence of the critical stress for matrix cracking, σ^c_∞, on the length '*a*' of a pre-existing defect, as shown in Figure 2.8. This result shows a limiting threshold for the matrix cracking stress which is exactly equivalent to that of the ACK theory corrected for plane strain conditions. McCartney also shows that crack growth is not possible unless the Griffith fracture criterion is satisfied, i.e. that any stress below this threshold level will not result in crack growth. Two other important features of the curve should also be noted. The first is that it is unique, being independent of the specific values of any material parameters, and it is therefore applicable to any composite system in which $\varepsilon_f > \varepsilon_m$. Secondly, the curve is a smooth, single-valued function which means that once cracking is initiated at a pre-existing defect the matrix cracks completely if the applied stress is maintained. Thus stable crack growth is not encountered. However, with regard to this second point, it was assumed in McCartney's original derivation that cracks formed instantaneously and this may therefore be of direct consequence.

In the case of the treatment of Marshall et al[21], they were unable to give a full analytical solution for the crack opening displacement when considering short cracks. However, they were able to show that in this case, the entire crack contributes to the stress concentration and that the stress required to propagate the crack is sensitive to the length of a pre-existing crack. These points (taken from Marshall) are also shown in Figure 2.8. They showed that in terms of the flaw size, the transition from short crack to long crack behaviour corresponds to a pre-existing crack length of a few fibre diameters for a Nicalon/LAS composite.

Later work by McCartney[23] has further addressed the limitations of the above models in terms of stress transfer between matrix and fibre in the vicinity of cracks, namely that the interface is assumed frictional with a constant shear stress, τ, and that the fibre and matrix have the same Poisson's ratio. The stress-transfer problem is addressed by the use of a concentric cylinder model as illustrated in Figure 2.9, which is representative of a uniaxial composite having a volume fraction, V_f, of fibres of radius R. A series of cylindrical polar co-ordinates (r, θ, z) are defined such that z lies along the fibre axis. A crack lies at position $z = 0$ and frictional slip at the fibre-matrix interface occurs over a distance ℓ away from the crack (with $\ell = 0$ corresponding to a perfectly bonded system) and that no slip occurs for $\ell \leq z < \infty$. The frictional slip is thought to obey a Coulomb friction law and an estimate of the coefficient of interfacial friction, η, is required for subsequent calculations. McCartney takes values of $\eta = 0.3, 0.5$ and 0.7.

The major conclusion drawn from the model is that the interfacial shear strength is not uniform in the region of interfacial slip and cannot therefore be assumed as a material constant. The shear stress distribution is found to be dependent on the applied strain and the difference, T, between the test temperature and the composite manufacturing temperature. A critical strain parameter ε^+ is defined at which the shear stress and normal pressure at the interface and the stress in the matrix are all zero and at which the slip length tends to infinity :

$$\varepsilon^+ = (V_f E_f / \nu_f E_c)(\alpha_f - \alpha_m)\Delta T \qquad (2.24)$$

It should be noted that at strains approaching ε^+, long lengths of fibre will be subjected to an axial stress σ/V_f (σ being the applied stress) since at this point the load is borne entirely by the fibres. Models that assume constant interfacial shear strength predict that the maximum axial stress in the fibres occurs at the location of the crack and McCartney suggests that, when used in conjunction with weakest link statistics, this will lead to an underestimate of the pull-out length.

It follows from the above expression that the critical strain is almost independent of the Poisson ratio for the matrix and consequently of the Poisson ratio mismatch between the fibre and matrix. It is also apparent that when E_f and E_m are of the same order, the volume fraction of fibres will have a strong influence on ε^+. It is predicted that the slip length ℓ decreases as the volume fraction increases so long as it is not so great that the fibres nearly touch.

2.4.4 Local Flaw Model

Recent work by Wang, Huang & Barsoum[24] has taken what they term a 'quasi-microscopic' approach in which they make the basic assumption that microcracks in the matrix are due to the propagation and coalescence of randomly distributed manufacturing flaws and that these flaws are situated initially within the matrix and at the fibre/matrix interface. They take an 'initiator cell' containing a matrix flaw and an interface flaw and assume that the joining up of these defects will initiate the matrix cracking process. Fracture analysis of the initiator cell is done by calculation of the strain energy release rate at the tip of the matrix flaw by finite element analysis. The model requires details of the initiator cell in terms of constituent properties and geometrical layout. Wang et al assume a hexagonal array of fibres and an initial matrix defect of the order of the fibre spacing in length. Their model predicts that for interface flaws or debonds of the order of the fibre diameter, the presence of the fibre has no constraining effect on the propagation of matrix cracks.

2.4.5 Predictions of Matrix Crack Spacing

In the original ACK theory the limiting crack separation in a brittle matrix composite was shown to be between x' and $2x'$, where x' is calculated from equation 2.21. Work by Cooper and Sillwood[17] on a steel fibre-reinforced epoxy composite concluded that measured crack spacings were in good agreement with theory and that exceptionally high or low values were generally associated with crack branching. Subsequent work by Aveston Mercer and Sillwood[25] showed that the theoretical mean crack spacing, s, was 1.364 x' . This was calculated, in a purely mathematical approach, by considering the minimum average spacing between cars of length x parked at random in a given space. The model was further developed by Kimber and Keer[26] for a composite of infinite length, i.e. large compared to x. The theoretical mean crack spacing in this case was shown to be 1.337 x'.

Yang and Knowles[27] also use a car-parking model but with a computer generated database of 300,000 car lengths, each of the car lengths being associated with a failure stress and with the overall distribution being that of Weibull. This model recognises the fact that matrix cracking occurs over a range of stresses rather than at a single well-defined stress level.

Zok and Spearing[28] address the interaction of cracks and the overlapping of slip lengths of adjacent cracks, calculating the steady-state strain energy release rate of interacting cracks by the ACK approach. They examine both periodic and random arrays of cracks. In both cases it is assumed that the interfacial shear stress is constant and the strain distribution on either side of each crack is linear. They conclude that the crack spacing at the onset of matrix cracking (i.e. at σ_{mu}) is twice that predicted by ACK and that the crack spacing decreases with applied stress, not reaching saturation until the applied stress, σ, is approximately 1.3 σ_{mu}. A computer simulation of random matrix cracks using the above results for a given initial flaw density and specimen gauge length gave the average saturation crack spacing as 1.75 x', although

this solution provided no information on the crack spacing distibution. A lower flaw density was found to give a higher average crack spacing with a wider distribution.

2.5 Transverse Ply Cracking in Cross-Ply Laminates

2.5.1 Introduction

Transverse ply cracking has been studied extensively in cross-ply polymer matrix composites for over twenty years. Cracking of the matrix in the transverse ply is the first type of damage to form when a load is applied to the composite. The cracks run perpendicular to the applied stress (parallel to the transverse fibres) and span the entire width and thickness of the ply. Figure 2.10 shows the configuration of a tranverse ply crack. 'Sub-critical' damage of this type occurs at lower strains than the 'critical' failure of fibres within the longitudinal plies. Thus, many design criteria for polymer-matrix composites are based on 'first-ply failure' - i.e. the stress or strain at which 90° ply cracking initiates. It is anticipated that such design principles may also be applied to ceramic-matrix composites.

2.5.2 First-Ply Failure

In an early experimental study by Garrett & Bailey[29] the strain levels at which the initial cracking occurred in the 90° plies of a series of $(0/90_n)_s$ glass-fibre/polyester laminates were measured by means of optical observation, acoustic emission and the first deviation from linearity of the stress-strain curve. The results from all three methods were coincident and it was found that the initial cracking strain increased with decreasing transverse ply thickness (i.e. with decreasing n).

Further work was carried out by Parvizi, Garrett & Bailey[30] on a series of glass/epoxy cross-ply laminates having a much wider range of transverse ply thicknesses. They noted two types of failure initiation, the instantaneous propagation of cracks spanning the entire transverse ply, for ply thicknesses greater than about 0.4 mm, and the formation of cracks at ply edges which multiplied and grew slowly across the ply with increasing load for thicknesses less than 0.4 mm. This latter

phenomenon they termed 'constrained' cracking. It was also observed that in the case of a transverse ply thickness of 0.1 mm, transverse ply cracking was completely suppressed prior to ultimate failure of the composite.

A further detailed study by Bailey & Parvizi[31] showed, by in situ scanning electron microscopy of polished test specimen edges loaded to different levels of strain, that transverse ply cracks in glass fibre-reinforced polyester cross-ply laminates originated from fibre-matrix debonding. Debonds observed at low strains were seen to coalesce at higher strains to form 90° ply cracks and a corresponding drop in laminate modulus was detected.

In the work of Garrett & Bailey[29] and Parvizi et al[30] it was found that the interface between the longitudinal and transverse plies remained bonded during transverse ply cracking. It was thus assumed that the laminate behaved in a fully elastic manner, enabling the transverse ply cracking behaviour to be modelled by using the energy-based Aveston & Kelly[18] theory of multiple fracture. It was found that predicted values of the tranverse ply failure strain were in good agreement with experimental data for ply thicknesses ($2d$) of less than 0.5 mm. The theory also predicted complete constraint for $2d < 0.1$ mm. However, experimental values at large values of $2d$ were much greater than those predicted. It should also be noted that this type of approach gives no consideration to the origin of the crack nor the way it propagates throught the matrix.

Subsequent studies of transverse cracking by several workers, e.g. Wang et al[32], Ogin & Smith[33] and Laws & Dvorak[34], have taken a fracture mechanics approach and assume that the mechanism of transverse ply cracking is by the propagation of flaws. It was shown that in the case of constrained cracking, the first-ply failure stress increased with decreasing ply thickness as greater energy was required to propagate a crack. However, this approach was generally found to underestimate the first-ply failure strain of thick (unconstrained) plies.

Alternatively, Fukanaga et al[35] take a statistical strength approach, in which it is assumed that the strength of the transverse ply obeys a two-parameter Weibull distribution, due to the presence of a distribution of flaws, and that the Weibull modulus decreases with increasing ply thickness. The statistical approach was found to predict the first ply failure of carbon/epoxy cross-ply laminates with greater accuracy at large ply thicknesses than energy-based theories but was insufficient to describe the behaviour of thin (constrained) plies.

2.5.2 Multiple Cracking

In the work of Garrett & Bailey[29] and Parvizi et al[30], it was found that after, initial cracks had formed, the crack spacing decreased sharply with increasing stress and appeared to reach a limiting value that was dependent on the transverse ply thickness.

The redistribution of stress in the transverse and longitudinal plies in the presence of 90° ply cracks can be described by shear lag analysis. This type of approach was originally used by Aveston and Kelly[18] to decribe the stress-strain behaviour of unidirectional brittle matrix composites containing fully-formed cracks and by considering fibres bonded to the matrix. Aveston and Kelly determined that multiple matrix cracking occurred in unidirectional composites in which the failure strain of the matrix was less than that of the fibres. The analysis was modified by Garrett & Bailey[29] to describe the stress redistribution in cross-ply composites containing fully-formed 90° ply cracks by assuming that the transverse ply of a composite acted as a material of low failure strain sandwiched between plies of a higher failure strain. The approach is described below.

A crack which is formed in the 90° ply of a cross-ply composite at the first-ply-failure stress and which traverses the entire width and thickness of the ply is arrested by the adjacent 0° plies. The load is then carried by the longitudinal plies in the vicinity of

the crack and, if it is assumed that the plies are elastically bonded and remain so, then load is transferred back into the 90° plies, over a certain distance away from and on either side of the crack, via shear at the ply interfaces. The 90° ply failure strain may again be reached at other parts of the transverse ply and the process repeated to cause multiple cracking. Garrett and Bailey assume the profile of stress decay in the longitudinal plies to be symmetric about the crack and in the form of an exponential function. It is also assumed that the transverse ply has a unique failure strain and that a constant shear stress acts at the interface between the longitudinal and transverse plies. The approach of Garrett and Bailey predicts a stepped curve of crack spacing with applied stress, as shown in Figure 2.11. They suggest that the expected crack spacing will depend on the position of the first crack and the length of the test specimen. Figure 2.11 shows an envelope drawn around the stepped curve which indicates the region in which the crack spacing is expected to fall for a specimen of any length and with a random position of the first crack. In practice, the decrease of cracking spacing with increasing applied stress takes the form of a smooth curve due to variations in transverse ply strength and the progressive, rather than instantaneous, growth of cracks.

It may be noted that the approach predicts the location of new cracks is always midway between existing cracks, where the transverse ply stress is greatest, as the statistical distribution of transverse ply strength is ignored. Fukanaga et al[35] attempted to address this shortfall by combining shear lag analysis with a statistical distribution of ply strength, as discussed in the previous section.

2.5.4 Stiffness Reduction

When damage is sustained by the transverse ply, its contribution to the overall laminate mechanical properties is reduced. One such property is the laminate longitudinal modulus. Shear-lag anaysis enables an expression for the longitudinal modulus of the laminate to be written in terms of the transverse ply crack spacing.

This type of approach was used by Ogin & Smith[33] to describe the stiffness reduction in glass-fibre-reinforced plastic composites and good agreement with experimental results was found.

Highsmith & Reifsnider[36] studied stiffness reduction in glass-epoxy laminates and determined that, since transverse cracking, delamination and fibre failure could all contribute to the degradation in mechanical response of the laminate, no single stiffness measurement was sufficient to classify the damage. Highsmith & Reifsnider[36] examined the effect of cracking on the longitudinal modulus by using a degraded value of the transverse modulus, E_2 (calculated with the aid of shear lag anlaysis for different states of damage) and using laminate plate analysis to predict laminate stiffnesses. Although the predicted trend in behaviour was in accord with experimental observations, the stiffnesses were generally overestimated and this was thought to be a result of additional damage modes.

2.6 Ultimate Strength of Unidirectional Composites

2.6.1 Introduction

This section examines models for predicting ultimate strength which may be applicable to continuous-fibre reinforced unidirectional ceramic matrix composites under monotonic loading conditions. The majority of models were originally developed for polymer-matrix composites. This area is reviewed extensively by Rowlands[37], Tripp et al[38] and both Kelly[39] and Kim[40]. Initially models for predicting longitudinal tensile strength are considered, followed by models for predicting failure of composites under multiaxial loading conditions i.e. the effect of fibre orientation on strength.

2.6.2 Longitudinal Tensile Strength

In the work of Aveston Cooper and Kelly[4] it is predicted that once saturation of matrix cracking has occurred the load will be borne solely by the fibres and that they will continue to deform elastically (giving a second linear region of the stress-strain curve with gradient $E_f V_f$) until ultimate failure of the composite occurs at a stress equal to $\sigma_{fu} V_f$ (see Figure 2.6 a)) where σ_{fu} is the fibre failure stress. These predictions are based on a rule of mixtures approach and neglect the significant effect of the statistical nature of fibre failure stress (resulting from flaw distributions along the fibre length) on the overall composite strength. It should also be noted that the strength of fibre bundles or tows is significantly less than that of the mean fibre failure stress for this same reason. This was originally investigated by Daniels[41] and was later related to a Weibull distribution of fibre failure strengths by Coleman[42]. It was shown that the lower the Weibull modulus (i.e. the wider the fibre strength distribution and hence also the flaw size distribution) the further the bundle strength differed from the mean fibre failure stress.

A number of statistics-based models have been developed to predict composite strength. Historically, the most notable of these are the 'cumulative weakening' model of Rosen[43] and the 'fibre break propagation' model of Zweben[44]. Both models calculate the composite strength from the statistical distribution of single fibre strengths. As each fibre breaks, the load carried by that fibre is redistributed. Rosen assumes that a length of broken fibre nearest the break can no longer carry load and the load is redistributed equally among all the unbroken fibres in the same cross-section of the fibre break. Complete failure occurs when the weakest cross-section can no longer sustain the applied load. Predictions based on Rosen's theory are generally higher than experimental values and in reality failure does not occur at a single cross-section in any but the most brittle composites (i.e. those with very strong fibre-matrix interactions). In the Zweben model, load redistribution is to neighbouring fibres and thus fibre breaks have a stress concentration effect which gives a greater probability of fibre failure in adjacent fibres. A combined effort by Zweben & Rosen[45] that attempted a cumulative weakening-load concentration analysis was unsuccessful in establishing a usable failure criterion.

More recently, attempts have been made by a number of workers[46-50] to develop statistical models for predicting the ultimate tensile strength in the particular case of ceramic matrix composites.

On the basis of earlier work by Thouless & Evans[46], Cao & Thouless[47] develop an approximate failure model by assuming that the saturation density of matrix cracks exists in the composite prior to the application of load. They also assume that the fibres have a statistical variation of strength according to a two-parameter Weibull distribution and that a failed fibre, anywhere within the overall gauge length, is incapable of carrying load. On the basis of these assumptions, they calculate the probability of a fibre failing within a length equal to half the saturation crack spacing at or below a stress equal to the fibre stress in the plane of a matrix crack. They then relate this to the average stress applied to the composite and the probability that a fibre will fail anywhere within the gauge length. This yields an expression for the

average stress in the composite and, with a corresponding expression for the average composite strain, allows the stress-strain behaviour of the composite to be modelled. By assuming that the applied strain is very much greater than the residual strain in the fibre, the latter can be neglected and a more approximate solution obtained. The maximum in the stress-strain relation is then assumed to be associated with ultimate failure of the composite at a stress, σ_u, and a strain, ε_u, for which they derive estimates. Cao & Thouless[47] quote the scale and shape parameters of the Weibull distribution of fibre strengths as being 2.988 MPa and 2.1 respectively. Cao & Thouless also enabled the compliance of the test equipment to be taken into consideration so that a prediction of the full exponentially decaying tail of the stress-strain curve could be obtained.

Some of the shortfalls of the above approach were later addressed by Curtin[48,49,50]. Curtin developed a theory of fibre-fragmentation in a single-fibre composite[48] and by direct application of this theory he obtained expressions for the strength and fibre pull-out of a multi-fibre composite[49,50].

Curtin assumes that the composite behaves according to the ACK model and that multiple matrix cracking, up to crack saturation, occurs at a constant stress equal to the matrix cracking stress, σ_{mc}. It is assumed that in the plane of the crack the fibres carry the entire applied stress (σ_{mc}) and the stress per fibre is then σ_{mc} / V_f. After matrix crack saturation, any subsequently applied load is carried by the fibres. Any load carried by the matrix is neglected and the ultimate strength of the composite is then assumed to be solely dependent on how the load is redistributed among the fibres as the fibres begin to fail. When a fibre fails, the stress in the fibre at the break drops to zero and, as in the case of matrix cracking, the stress is shed back into the fibre through stress transfer across the fibre-matrix interface over a sliding length, l_f (where l_f is generally greater than the matrix sliding length x'). The mechanism of stress transfer is not considered. Curtin's theory assumes *global load sharing* i.e. that the load shed by the broken fibre is redistributed equally among the unbroken fibres in a

chosen plane and that no stress concentration of fibres occurs close to a broken fibre. Curtin defines an 'unbroken' fibre as one that has no fibre breaks within $\pm l_f$ (the sliding length) of the chosen plane. However, this theory, unlike that of Cao & Thouless, recognises that broken fibres also have a substantial load-carrying capability as a result of the interfacial sliding resistance, τ. The average load carried by broken fibres within $\pm l_f$ of the chosen plane depends on the average distance, $<L>$, of the breaks from that plane. Curtin performs a force balance which assumes that, in the chosen plane, all the applied load is carried by the fibres and that the average stress per fibre comprises the stress carried by unbroken fibres plus the average stress carried by broken fibres within $\pm l_f$. Since the location of fibre breaks within $\pm l_f$ is random, Curtin approximates $<L> / l_f$ to be 1/2 (which also gives an estimate of the pull-out length as $l_f/2$). It is also assumed that the probability of finding a break within $\pm l_f$ is independent of any fibre breaks outside this distance and is described by Weibull statistics. The number of breaks within the gauge length $2l_f$ is thus a function of the gauge length and the stress on unbroken fibres. Incorporation of these assumptions within the force balance and maximisation of the stress, yields an expression for the ultimate strength, σ_u, of the composite:

$$\sigma_u = V_f \sigma_c \left(\frac{2}{m+2}\right)^{1/(m+1)} \cdot \left(\frac{m+1}{m+2}\right) \qquad (2.25)$$

The first two terms in equation 2.28, V_f and σ_c, essentially give a rule of mixtures prediction of strength whilst the two expressions in brackets account for the reduced strength of fibre bundles compared to that of individual fibres.

σ_c is defined as the characteristic strength of a fibre at a characteristic sliding length, δ_c. For $m \leq \infty$, $\delta_c = r \sigma_c / \tau$ and in the limit when $m = \infty$, i.e. the fibres have a single failure strength, then δ_c is identical to the critical length, l_c, as defined by Kelly[15]. The characteristic fibre strength, σ_c, may be calculated from the mean strength, σ_0, of *as-processed* fibres having an arbitrary testing gauge length of L_0 and strength distribution m, by using the following equation

$$\sigma_c = \left[\frac{\sigma_0^m \tau L_0}{r}\right]^{1/(m+1)} \qquad (2.26)$$

where the mean fibre strength, σ_0, and distribution m are obtained by testing fibres extracted from the composite. However, the characteristic fibre strength, σ_c, and distribution can be obtained more directly by measuring the fracture mirror radii of pulled-out fibres on the fracture surface of the composite and converting the values to fibre strengths. It should be noted that $\sigma_c > \sigma_0$ since $\delta_c < L_0$.

Curtin quotes a characteristic fibre strength of 2 GPa with a Weibull modulus of 3.6 for a Nicalon/CAS composite, values which were obtained from the measurement of fracture mirror radii, and reasonable agreement was found between the measured and predicted strengths for this composite system (430 MPa and 480 MPa respectively). Curtin suggests that the theory predicts an upper-bound composite strength as additional fibre failures can occur in the wake of matrix cracks or during processing. Additional features of the theory are that the fraction of failed fibres at the ultimate tensile strength of the composite is approximately $2/(m+2)$ per length δ_c and that the fibre pull-out length is of the order of $\delta_c/4$. This type of fibre fragmentation and pull-out is depicted in Figure 2.12. With reference to this figure, Curtin suggests that the fibre pull-out will be the shorter of the two pieces formed when a matrix crack intersects a fibre fragment and this is indicated by the arrows.

2.6.3 Orientation Dependence of Strength

A number of empirically-derived failure criteria have been developed which attempt to predict the strength of a laminate under biaxial loading conditions from data obtained from simple uniaxial tension, compression and shear tests[37-40,51-55]. These are termed 'phenomenological failure criteria' since only the occurrence of failure is predicted, not the mechanism. In all cases it is assumed that behaviour is linear elastic

to failure i.e. sub-critical failure events (those that do not lead to ultimate failure) are neglected. The theories were originally developed to predict the failure of homogeneous, isotropic materials but have since been adopted as failure criteria in the design of composite components by taking a ply-by-ply approach. The stresses and strains in each lamina are calculated by using the laminated plate theory described in section 2.3.3 and are transformed to the principal material axes. Failure criteria can then be applied to each lamina. An outline of these procedures follows.

a) Maximum Stress Theory

It is envisaged that a unidirectional lamina tested in uniaxial tension at an angle θ to the fibre direction can fail by one of three mechanisms, i.e. transverse tensile failure, longitudinal tensile failure and intralaminar shear failure. The maximum stress theory assumes that ultimate failure occurs when the longitudinal, transverse or shear stress (σ_{11}, σ_{22} or τ_{12}) reaches a critical value defined by the strength in that direction (σ^*_{11}, σ^*_{22} or τ^*_{12}) and that failure occurs by the mechanism associated with that strength. The theory is thus in the form of three inequalities, as follows

$$\begin{aligned} \sigma_{11} &\leq \sigma^*_{11} \\ \sigma_{22} &\leq \sigma^*_{22} \\ \tau_{12} &\leq \tau^*_{12} \end{aligned} \qquad (2.27)$$

and as such is an example of a 'limit criterion'.
Equations to transform the applied stress, σ_{xx}, to those of the principal material axes can be derived from force-equilibrium considerations, with the notation defined in Figure 2.4, such that

$$\begin{aligned} \sigma_{11} &= \sigma_{xx} \cos^2 \theta \\ \sigma_{22} &= \sigma_{xx} \sin^2 \theta \\ \tau_{12} &= \sigma_{xx} \sin \theta \cos \theta \end{aligned} \qquad (2.28)$$

The variation of material axes stresses with load direction for a unidirectional composite is given in Figure 2.13.

By rearrangement of equations 2.28, and combining with the inequalities of 2.27, the uniaxial strength of the composite is determined by

$$\sigma_{xx} \leq \frac{\sigma^*_{11}}{\cos^2\theta} \quad , \quad \sigma_{xx} \leq \frac{\sigma^*_{22}}{\sin^2\theta} \quad , \quad \sigma_{xx} \leq \frac{\tau^*_{12}}{\sin\theta\cos\theta} \qquad (2.29)$$

The predicted failure envelope, i.e. strength versus orientation, together with experimental values for an E-glasss/epoxy composite, is depicted in Figure 2.14. The poor agreement between the results at intermediate angles is due to the occurrence of mixed mode failure of the composite, something which is not taken into consideration by the theory.

b) Maximum Strain Theory

The maximum stress theory and the maximum strain theory are analogous although in the latter case the strength of the composite is limited by the corresponding allowable strains such that the relative displacement of the component parts cannot exceed a certain amount. Again the theory can be expressed in the form of three inequalities

$$\begin{aligned} \varepsilon_{11} &\leq \varepsilon^*_{11} \\ \varepsilon_{22} &\leq \varepsilon^*_{22} \\ \gamma_{12} &\leq \gamma^*_{12} \end{aligned} \qquad (2.30)$$

The general stress-strain relations for an isotropic material may be adapted for the case of an orthotropic material, and assuming that no through-thickness stresses exist, can be written as

$$\varepsilon_{11} = \frac{1}{E_{11}}(\sigma_{11} - \nu_{12}\sigma_{22})$$
$$\varepsilon_{22} = \frac{1}{E_{22}}(\sigma_{22} - \nu_{21}\sigma_{11})$$
$$\gamma_{12} = \frac{1}{G_{12}}\tau_{12} \qquad (2.31)$$

Assuming that the material exhibits linear elastic behaviour to failure, then the ultimate strains can be related directly to the strengths by $\varepsilon^*_{11} = \sigma^*_{11}/E_{11}$, $\varepsilon^*_{22} = \sigma^*_{22}/E_{22}$, $\gamma^*_{12} = \tau^*_{12}/G_{12}$. Thus, by substituting these expressions for the failure strains into the inequalities of 2.30 together with the stress-strain relations of 2.31 and expressing the material axis stresses in terms of the applied stress by the transformation equations of 2.28, then the uniaxial strength based on the maximum strain theory is

$$\sigma_{xx} \leq \frac{\sigma^*_{11}}{\cos^2\theta - \nu_{12}\sin^2\theta} \quad , \quad \sigma_{xx} \leq \frac{\sigma^*_{22}}{\sin^2\theta - \nu_{21}\cos^2\theta}$$
$$\sigma_{xx} \leq \frac{\tau^*_{12}}{\sin\theta\cos\theta} \qquad (2.32)$$

The only difference between the above equations and those of the maximum stress theory is the inclusion of Poisson ratio terms. The predicted strength as a function of fibre orientation and measured values (for the same example referred to previously) are given in Figure 2.15. The variation of material-axes strains in unidirectional composite versus load direction for a Mod-I/epoxy composite are given in Figure 2.15. The material-axis shear strain is shown to be a maximum (for this material) at a load orientation angle of about 10°, and this led Chamis and Sinclair[56] to propose a 10° off-axis test for the measurement of intralaminar-shear modulus and fracture shear stress. This technique is discussed in Appendix 1.

Like the maximum stress theory, the maximum strain theory overestimates the composite strength at intermediate angles where in-plane shear loads dominate. Hart-Smith[54] considers the maximum strain theory and suggests that it is more applicable

for predicting the failure of a fibre-dominated unidirectional lamina than the maximum stress theory. However, he notes that the corners of the failure envelope are pinned by the two values of Poisson ratio chosen which may not necessarily be considered equal nor the same as the Poisson ratios of a laminate. Hart-Smith then presents a truncated maximum strain theory as a simplification which he suggests eliminates the overestimated strengths at intermediate angles although it only remains applicable to fibre-dominated failures. He suggests that this may be overcome by investigating the fibre and matrix shear failure characteristics separately and superimposing to give the failure envelope of the lamina. This would also allow residual thermal stresses to be accounted for by off-setting the origins of the constituent failure envelopes. Attempts to truncate the fibre-dominated maximum strain theory to allow for matrix-dominated failures at intermediate angles have been made by Puck and Schneider[57] although residual curing stresses in the matrix were ignored.

c) Interactive Criteria

One of the best known composite failure criteria is the 'maximum work theory' which is commonly referred to as the Tsai-Hill criterion[51]. This theory was developed from the von Mises isotropic yield criterion which was adapted for plastic yielding in anisotropic ductile metals by Hill[58] and later applied to the failure of composite materials by Tsai. The criterion is interactive and, assuming that the composite is transversely isotropic and is subject to plane stress conditions, it may be expressed as:

$$\frac{1}{\sigma_{xx}^2} = \frac{\cos^4\theta}{(\sigma_{11}^*)^2} + \left(\frac{1}{(\tau_{12}^*)^2} - \frac{1}{(\sigma_{11}^*)^2}\right)\sin^2\theta\cos^2\theta + \frac{\sin^4\theta}{(\sigma_{22}^*)^2} \qquad (2.33)$$

The advantages of this approach are that there is considerable interaction between failure strengths and that there is only one criterion. This gives the variation of strength with orientation as a smooth function which continually decreases with

increasing θ from 0° (without the initial increase as predicted by the maximum stress and strain theories) and in the example used by Tsai (Figure 2.17) gives a better fit to the data. However, it should be noted that the central interaction term is biased in that it contains only the longitudinal strength.

Further development of these ideas by Tsai & Wu[52], taking a similar approach to that for elastic moduli and compliance (as described in section 2.3.3), enabled a strength criterion to be described using a scalar function of strength tensors which may be expressed in general form as

$$f(\sigma) = F_i \sigma_i + F_{ij} \sigma_i \sigma_j = 1 \qquad i, j = 1, 6 \qquad (2.34)$$

This defines (as they term it) a failure surface in stress-space and, to ensure that the surface is closed, the stability condition $F_{ij}F_{jj} - F^2_{ij} > 0$ must be satisfied.
The number of independent and non-zero strength components can be reduced by assuming degrees of material symmetry in the same way as for laminate plate theory. For a transversely isotropic material under plane stress conditions the expression reduces to

$$F_1 \sigma_1 + F_2 \sigma_2 + F_6 \tau_{12} + F_{11} \sigma_1^2 + F_{22} \sigma_2^2 + 2F_{12} \sigma_1 \sigma_2 + F_{66} \tau_{12}^2 = 1 \qquad (2.35)$$

The strength components F_i and F_{ij} are related to the engineering strengths of the material. F_{12}, however, is related to the interaction of two stress components and has to be determined experimentally from a combined stress test (i.e. under biaxial loading conditions). In practice this is difficult to perform and the Tsai-Wu criterion has, as a consequence, not been widely adopted. However, Wu[53] suggests that most phenomenological failure criteria are in fact special cases of the Tsai-Wu theory.

It should be borne in mind that this type of approach is purely an empirical curve fittting procedure and given enough constants it may always be possible to describe experimentally determined off-axis properties adequately - also, that a change in any one of the engineering strengths alters almost every point on the failure envelope. Hart-Smith[55] suggests that this invalidates tensor polynomial anisotropic strength models since, for example, a decrease in transverse tensile strength falsely predicts an increase in biaxial compression strength. Hart-Smith[55] states that this is as a result of a fundamental misapplication of Hill's work to composite materials and presents an alternative based on a maximum shear stress (Tresca) condition, as mentioned previously. He suggests that individual failure modes should be superimposed, not interacted, and that the superimposed envelopes would truncate each other locally so that one or another would govern as the state of stress varied. This gives a flat-faceted failure envelope, with each facet defined by the failure of one particular fibre direction under a uniform failure mode throughout. Intersection of the facets denotes simultaneous failure in two or three fibre directions.

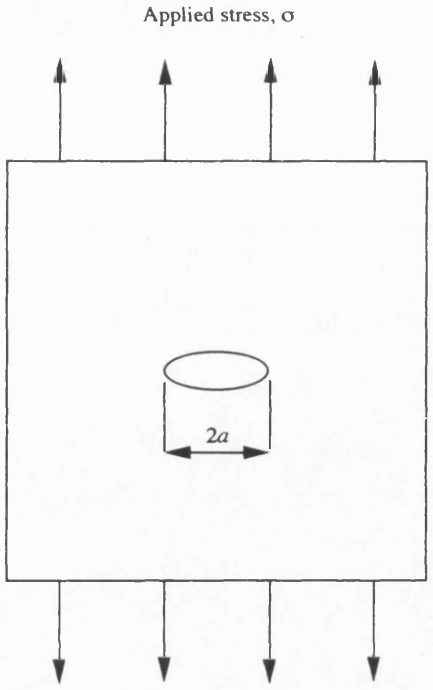

Figure 2.1: Diagram showing an elliptical hole in an infinite plate subjected to a uniform applied stress, σ

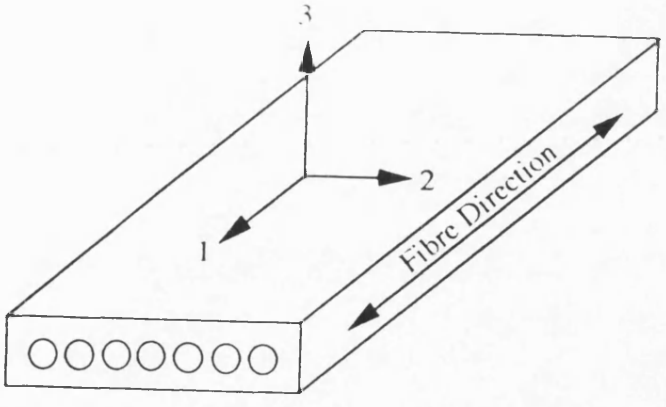

Figure 2.2: Diagram defining material (1, 2, 3) co-ordinate system in relation to the fibre direction within a unidirectional composite lamina

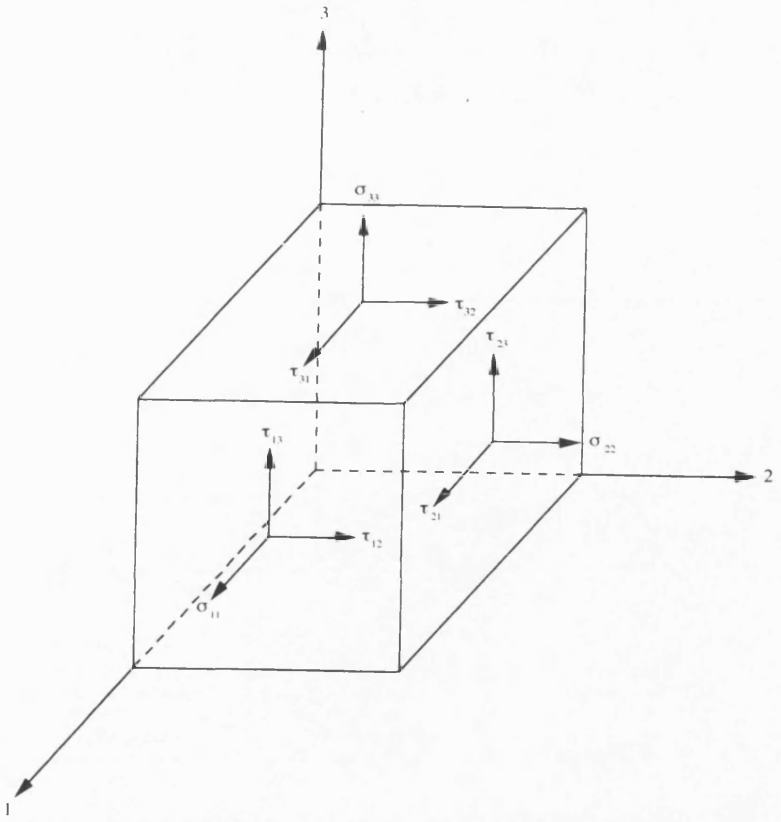

Figure 2.3: Diagram showing nine components of stress acting on an elemental unit cube of material

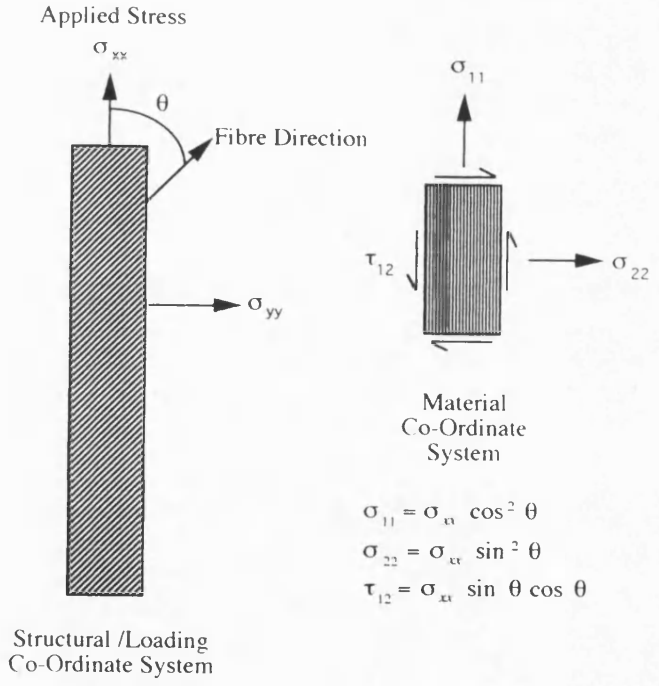

Figure 2.4: Schematic depicting the transformation of stresses from the material to strucural (x-y) co-ordinate system for a unidirectional composite

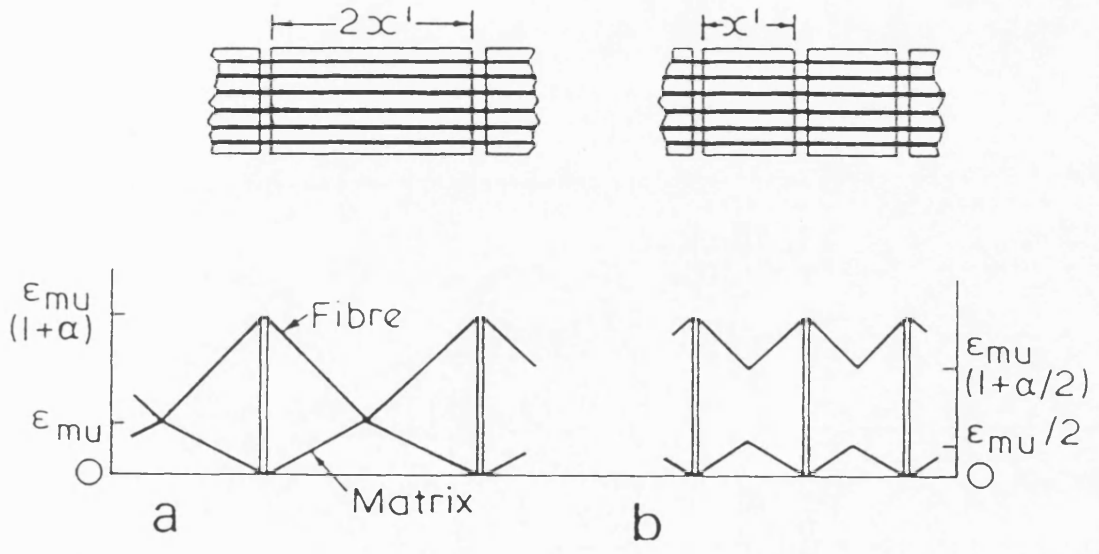

Figure 2.5: Strain profile in the fibres and matrix of a cracked unidirectional laminate for a crack spacing of a) $2x'$ and b) x' (after Aveston, Cooper & Kelly[4])

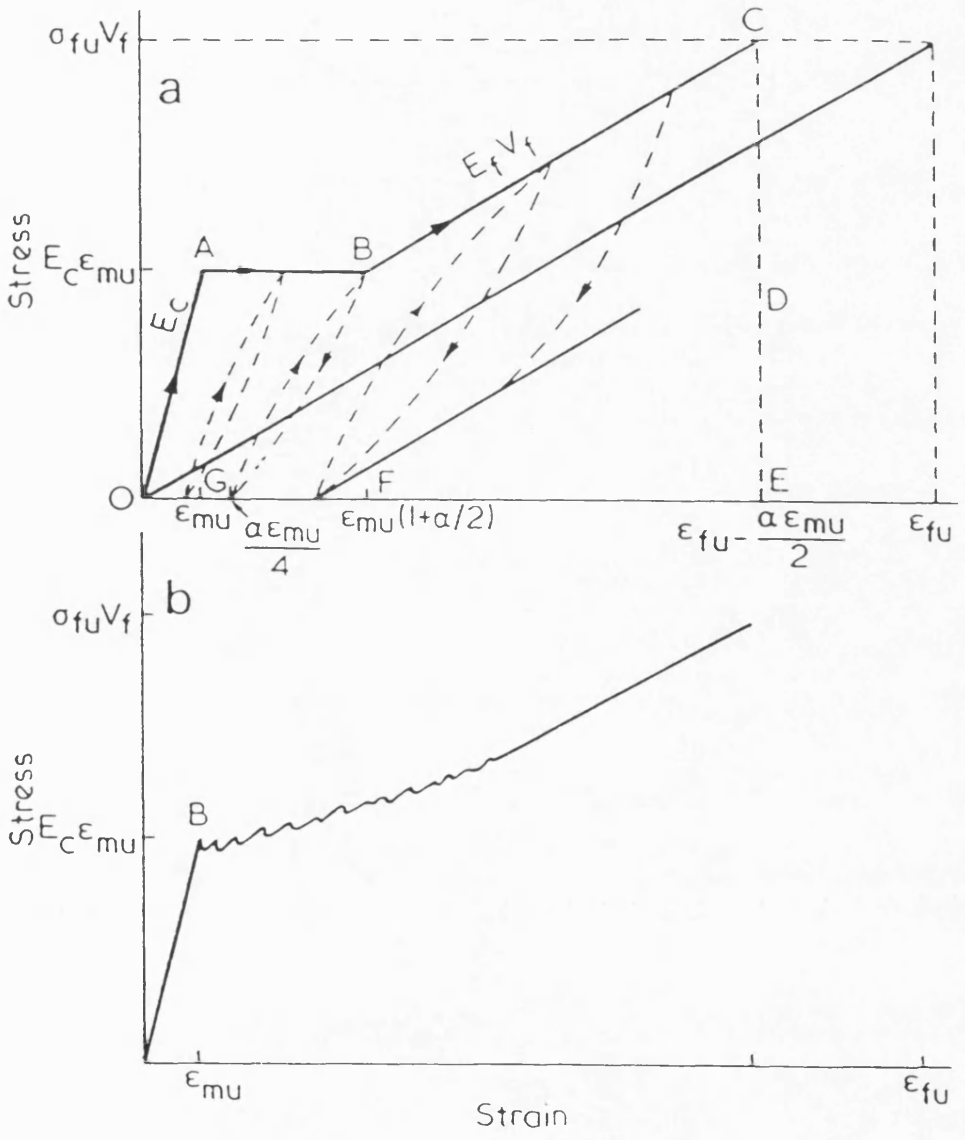

Figure 2.6: Stress-strain curve of a unidirectional laminate for a matrix with a) a single-valued failure strength and b) a strength variation (after Aveston, Cooper & Kelly[4])

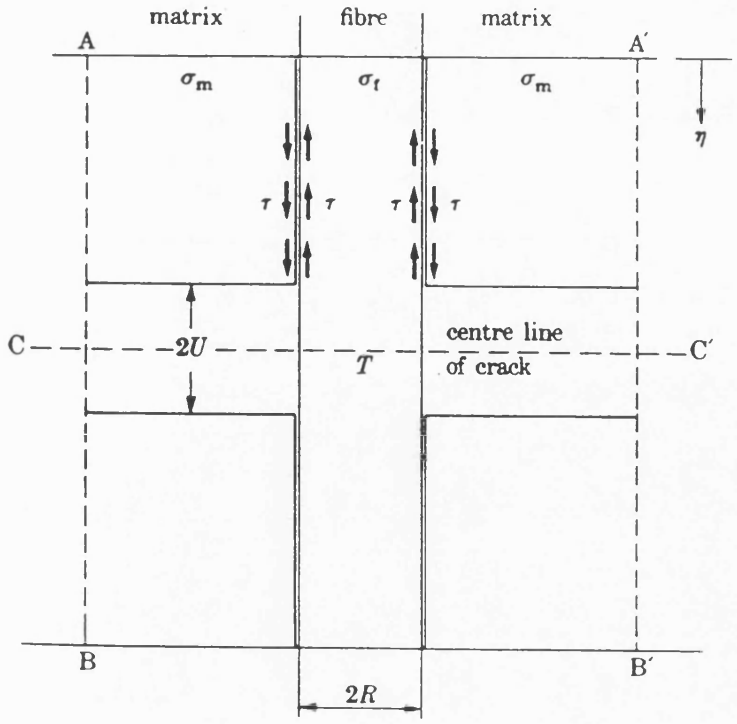

Figure 2.7: Schematic diagram of a discrete fibre model used in continuum analyses of matrix cracking in unidirectional composite (after McCartney[22])

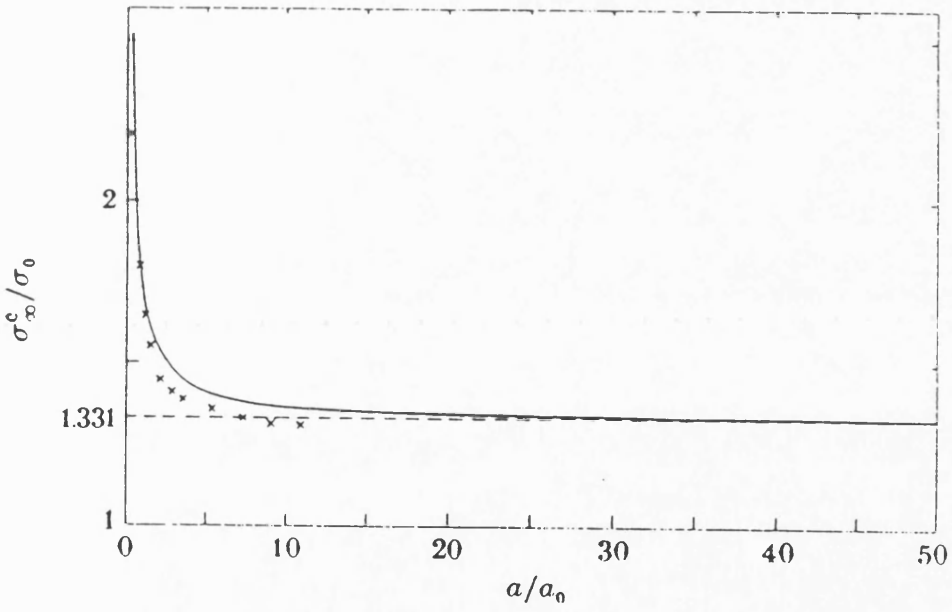

Figure 2.8: Dependence of the matrix cracking stress on the length of pre-existing flaw in unidirectional laminates (after McCartney[22])

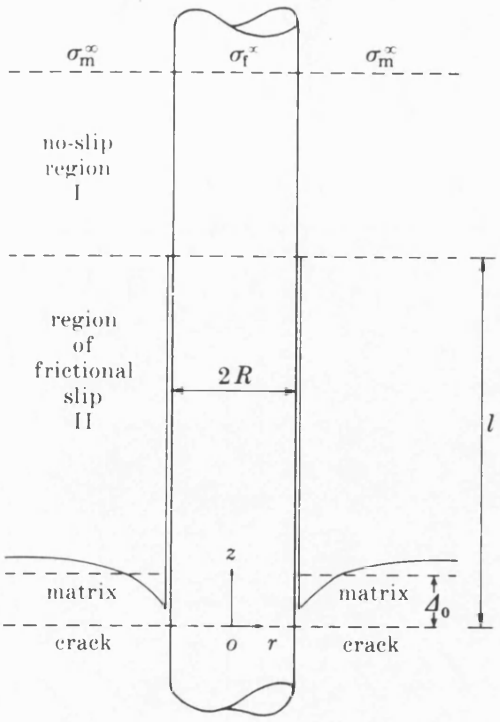

Figure 2.9: A concentric cylinder model of a composite showing a matrix crack and a region where there is frictional slip at the fibre-matrix interface (after McCartney[23])

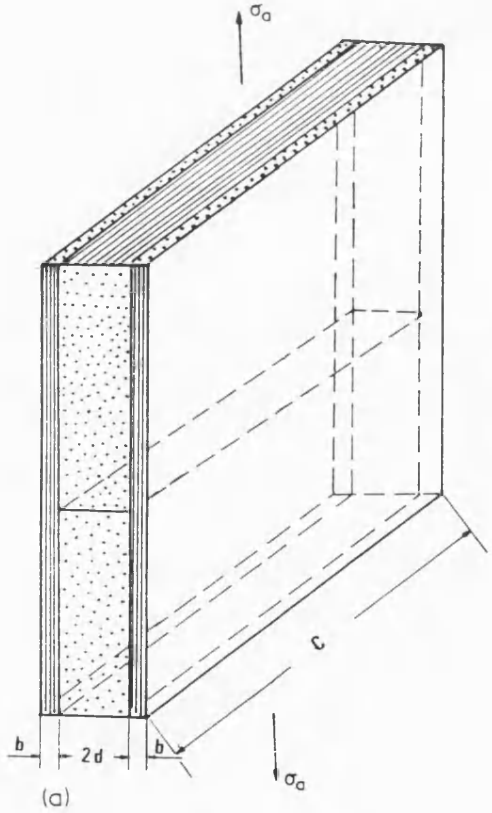

Figure 2.10: Schematic diagram of a cross-ply laminate containing a transverse ply crack (after Parvizi, Garrett & Bailey[30])

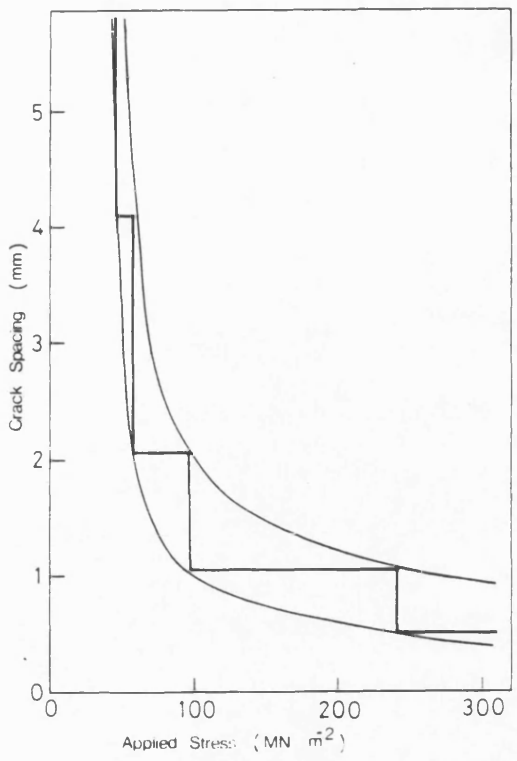

Figure 2.11: Theoretical crack spacing as a function of spplied stress for a cross-ply composite having elastically bonded plies (after Garrett & Bailey[29])

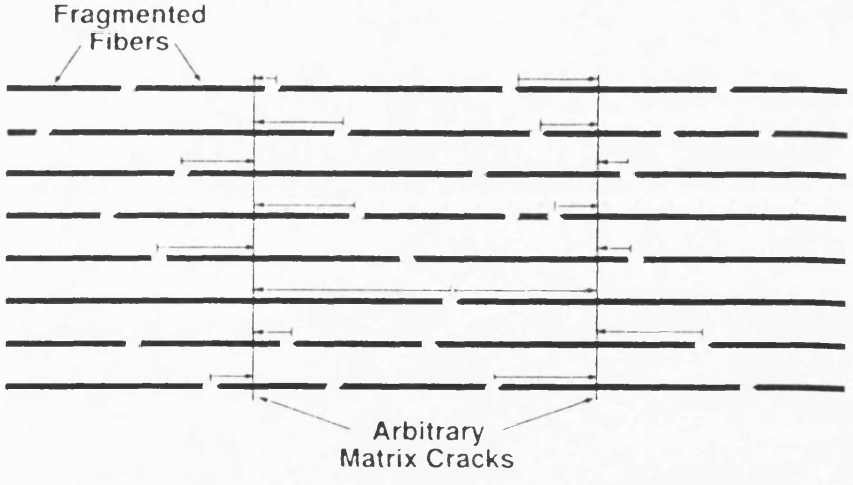

Figure 2.12: Schematic diagram showing fibre fragmentation and the determination of pull-out lengths (after Curtin[49])

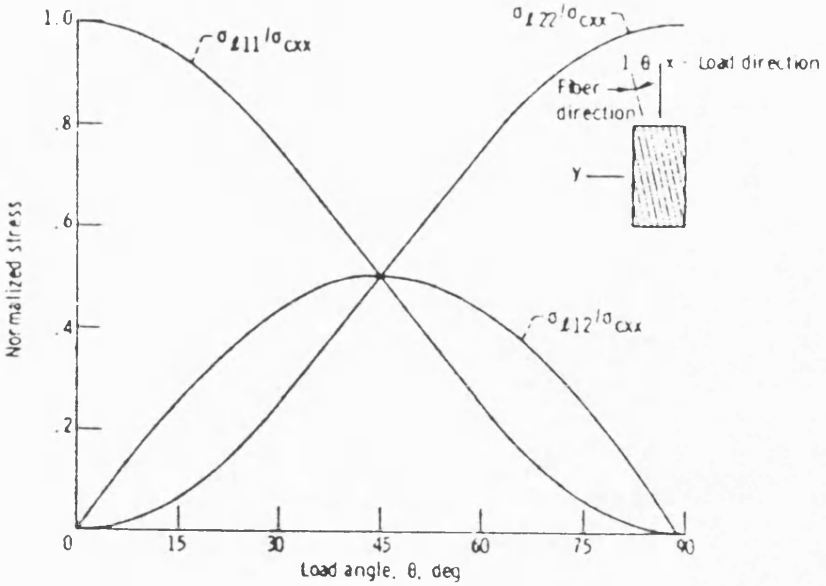

Figure 2.13: Variation of material-axes stresses with fibre orientation fo a unidirectional composite (after Chamis & Sinclair[56])

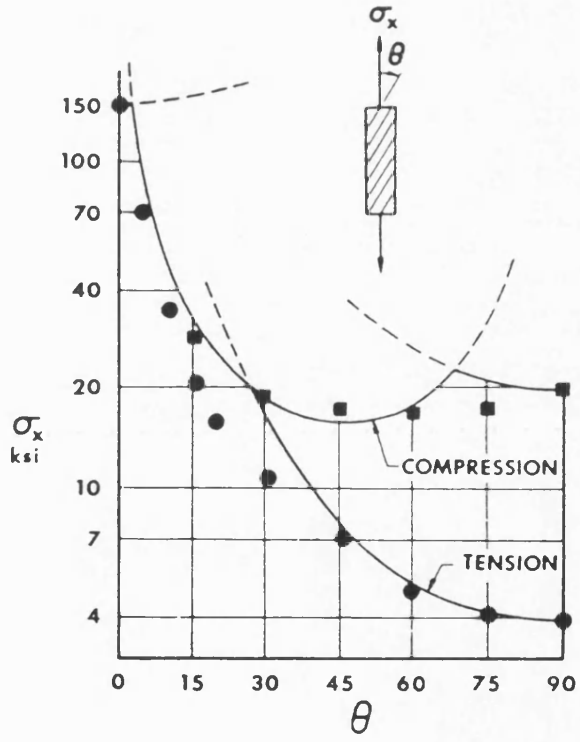

Figure 2.14: Strength of glass/epoxy unidirectional composite as a function of fibre orientation together with predictions based on maximum stress theory (after Tsai[51])

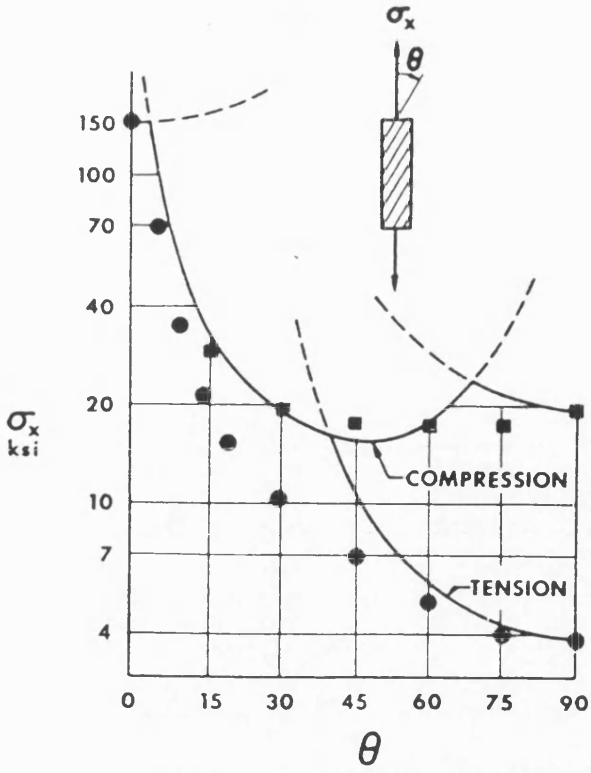

Figure 2.15: Strength of glass/epoxy unidirectional composite as a function of fibre orientation together with predictions based on maximum strain theory (after Tsai[51])

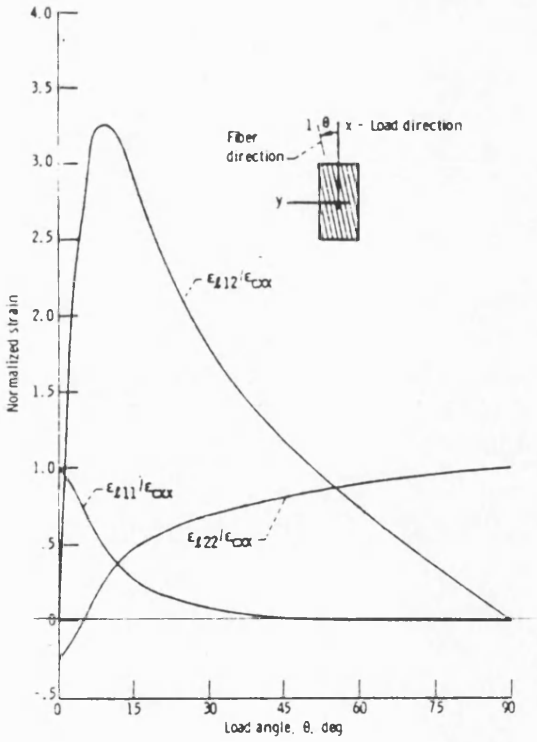

Figure 2.16: Variation of material axis strains with fibre orientation for a Mod-I/epoxy unidirectional composite (after Chamis & Sinclair[56])

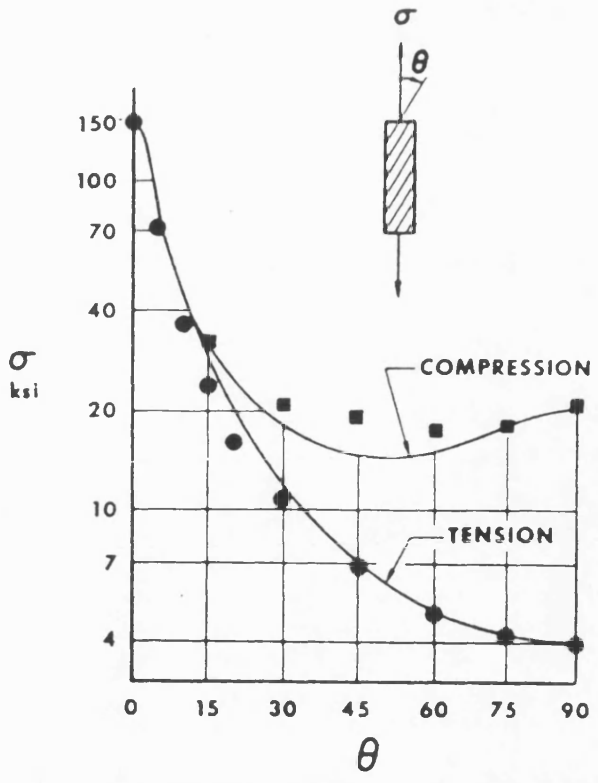

Figure 2.17: Strength of glass/epoxy unidirectional composite as a function of fibre orientation together with predictions based on Tsai-Hill theory (after Tsai[51])

CHAPTER 3 : GLASS AND GLASS-CERAMIC COMPOSITES

3.1 Development and Mechanical Properties of Glass and Glass-Ceramic Matrix Composites

Technology for the fabrication of fibre-reinforced glass and glass-ceramics was developed in the late 1960s at AERE Harwell by Sambell et al[59,60]. Initial studies were carried out on a series of glass and glass-ceramic matrices hot-pressed with discontinuous carbon fibre reinforcement and later with continuous carbon fibres. Continuous, aligned carbon-fibre-reinforced composites based upon matrices of Pyrex, lithium aluminosilicate (LAS), soda glass and alumina were produced. In particular, carbon-fibre-reinforced Pyrex glass showed significant improvements in mechanical properties (strength and toughness) compared to the unreinforced matrix. Changes in fabrication parameters, i.e. temperature and pressure, produced further improvements in strength by reducing porosity and fibre damage. Composite strengths were found to be in reasonable agreement with rule of mixtures predictions. The temperature capability of the composite was limited, by softening of the matrix, to 500°C in an inert atmosphere. However, when heated in air, the composite strength was degraded as a result of the poor oxidation resistance of the carbon fibre. Further studies of the mechanical properties of the carbon/Pyrex composite were carried out by Phillips et al[61]. Composite bend strengths were measured as a function of fibre volume fraction and fibre orientation. Strengths were found to deviate from rule of mixtures predictions for a fibre content of greater than 30 vol% and this was attributed to a shift in the neutral axis of bending towards the compressive face as a result of matrix cracking prior to ultimate composite failure. Phillips et al noted that multiple cracking of the matrix occurred on the tensile face and sides of bend specimens at stresses well below the ultimate strength of the composite and that this caused a 'bendover' in the load-deflection curve. The matrix cracks were regularly spaced with a separation of the order of a few hundred microns. The strength of the matrix was calculated to have been increased by the presence of

fibres and this increase was found to be in good agreement with the predictions of Aveston, Cooper and Kelly[4].

Modulus values increased with fibre content, up to about 60 vol%, but were consistently less than rule of mixtures predictions - a discrepancy which they attributed to fibre misalignment. At a fibre content of about 60 vol% both strength and modulus were significantly reduced by a high level of porosity present in the matrix.

The orientation dependence of strength appeared to be in reasonable agreement with predictions based on the maximum stress theory although interpretation of the results was hindered by a large degree of scatter. It was also not possible to distinguish between shear and transverse tensile failures at intermediate angles from the bend specimen fracture faces.

Further work was carried out by Phillips[62,63] on the carbon/Pyrex and carbon/LAS composites to determine their fracture energies as a function of fibre volume fraction and strain-rate.

However, the main limitation on the use of carbon-fibre-reinforced composites was fibre oxidation and little work relevant to the present study was published on ceramic matrix composites from the mid-1970s until the development of alternative, more refractory fibres. With the commercial availability of a cost-effective silicon carbide yarn such as Nicalon[64,65], the interest in CMCs was renewed. Prewo and his co-workers[66] at United Technologies Research Center first investigated the properties of Pyrex glass reinforced with CVD SiC monofilaments and the new Nicalon fibres. From a series of flexural tests conducted at temperatures of up to 700°C they found that both forms of the material exhibited high levels of flexural strength and toughness up to high temperatures. The strengths were equivalent to those of the carbon/Pyrex composite but the temperature stability was found to be enhanced. Softening of the matrix gave an upper composite use limit of about 600°C, above which plastic deformation of the matrix made the measurement of strength inaccurate

by this method. Further improvements in the Nicalon/Pyrex composite properties were later made by the development of a continuous fibre, tape-making process for the infiltration of fibre tows with matrix slurry prior to hot-pressing[67]. Unidirectional and cross-ply Nicalon/Pyrex composites were produced by Prewo and Brennan using this method. Flexural properties of the cross-ply material were between 65 and 75% of the unidirectional properties, indicating that the 90° plies contributed to the composite strength. Thermal ageing of unidirectional composite at 540°C for up to 500 hours was found to have no effect on flexural strength. Preliminary findings of a Nicalon-fibre-reinforced high silica glass matrix composite were also presented and properties were found to be retained up to 1100°C, limited again by softening of the matrix. However, although a higher use temperature was achieved, the higher viscosity of the matrix during consolidation introduced significant manufacturing difficulties in terms of composite densification without fibre damage. Further work by Brennan and Prewo[68] concentrated on glass-ceramics for high temperature matrices as this allowed composite densification whilst the matrix was in a low viscosity glassy state after which the matrix could be crystallised by a 'ceraming' heat treatment to give the required high temperature stability. A lithium aluminosilicate glass-ceramic matrix was chosen with a ZrO_2 nucleating agent. Hot pressing was carried out at temperatures of over 1300°C, followed by a heat treatment of between 880 and 1100°C for 1 to 2 hours. Both unidirectional and cross-ply composites with fibre volume fractions of approximately 50% were manufactured by this method and their flexural properties measured at temperatures of up to 1200°C. Bend strengths were retained up to about 1000°C, above which viscous flow of residual glass within the matrix caused a drop off in composite strength. Specimens did not fail completely and retained some load-carrying capability. This contrasted with the behaviour of the monolithic LAS which had very little useful strength at 1000°C and fractured catastrophically into two pieces. Composite elastic moduli were very close to those predicted from rule of mixtures and were retained to higher temperatures than the monolithic LAS. Predictions of axial and transverse thermal expansion coefficients

from matrix and fibre properties were in reasonable agreement with measured values. A thermal expansion coefficient of 1 x 10^{-6} /°C was taken for the LAS matrix which corresponded to it being fully crystallised to β-spodumene. It was suggested that this value would be reduced for a β-spodumene-silica solution but higher if a substantial amount of glassy phase were retained.

Microstructural examination of Nicalon/LAS composite during ceraming trials identified the formation of a thick glaze-like layer on the exposed surfaces at temperatures above 900 °C, and this was associated with pore formation within the matrix. The exact mechanism for the formation of this layer was not known although it was suggested that an oxidative reaction had occurred between the fibre and matrix close to the surface, with the evolution of SiO or CO gas.

In later work by Prewo[69] the properties of both LAS-I and LAS-II (a slight modification of the original composition which was designed to be more compatible with the Nicalon fibre) were reported. Tensile tests were carried out at room temperature on unidirectional composites of both type. Stress-strain curves for the ceramed LAS-I composite were linear to failure, whereas those for both as-pressed and ceramed LAS-II composite showed a marked discontinuity at a strain of about 0.3 % after which the composite modulus decreased, a phenomenon that was attributed to matrix cracking. Initial composite elastic moduli were found to be in good agreement with rule of mixtures predictions.

Tensile tests were also carried out on individual as-received Nicalon fibres and those extracted from the composite by use of hydrofluoric acid. It was found that fibres extracted from LAS-I and LAS-II matrix composites had strengths degraded by 40% and 30% respectively. Composite strengths were compared to predictions based on a rule of mixtures approach, by taking either extracted fibre strengths or fibre bundle strengths and multiplying by the fibre volume fraction, and also predictions by the Zweben and Rosen model (outlined in section 2.6.2). The best agreement with measured strengths was found surprisingly to be a rule of mixtures approach using

extracted fibre strengths, even though this method neglects the fibre strength distribution.

Prewo also compared the measured tensile strengths of the glass-ceramic matrix composites with those measured by flexure and found that the latter significantly overestimated the tensile strength. It was thought that non-linear behaviour on the tensile face of bend specimens caused the neutral axis of stress to be displaced towards the compression side and made the use of simple beam theory equations invalid.

Fracture surfaces of all specimens from both types of composite exhibited extensive fibre pull-out when tested at room temperature or at elevated temperature in argon. However, it was observed that the fracture of Nicalon/LAS-II composite tested by flexure in air showed increasingly brittle characteristics above 600°C and this was thought to be due to either a local decrease in fibre strength or an increase in fibre-matrix interfacial strength.

Further work was carried out by Prewo[70] on the fatigue and stress-rupture of both LAS-I and LAS-II unidirectional composites. Room temperature tensile-tensile fatigue of the LAS-I composite at a range of stresses below the static fracture stress caused no decrease in composite elastic modulus, and residual strengths were equivalent to those of the unfatigued composite strength. This was also the case for Nicalon/LAS-II composite fatigued at stresses below the previously mentioned proportional limit. However, when fatigued at higher stress levels, a significant reduction in the proportional limit stress was observed as was the appearance of a second linear stress-strain region having an elastic modulus less than that measured originally. The effect of fatigue and stress-rupture at stresses above the proportional limit of the LAS-II composite was made more evident by flexural testing in air at high temperatures. Testing at both 600 and 900°C caused composite embrittlement, as the oxidising environment was able to penetrate through the microcracked matrix. At lower stresses, samples survived for 50 hours at both 600 and 900°C. However, the

residual strength of 600 °C tested material was reduced to the level of the proportional limit. This was not the case for 900°C tested material and the mechanism for this 'recovery' was not known.

Marshall and Evans[20] examined the failure mechanisms of a silicon carbide fibre reinforced glass-ceramic matrix composite under both flexural and tensile loading. In both cases the stress-strain curves consisted of an initially linear elastic region, followed by non-linear load increase up to a maximum, after which a continuous load decrease occurred. From direct observation of the specimen surface during tensile tests, it was possible to determine that the onset of non-linearity of the stress-strain curve coincided with the formation of a single matrix crack which traversed the width and thickness of the specimen. Further loading caused the formation of multiple, regularly-spaced cracks in the matrix. Marshall and Evans derived an estimate for the interfacial friction stress from measured matrix crack spacings using the Aveston Cooper Kelly model (outlined in section 2.4.2) and found it to be comparable with values obtained by direct methods of measurement using an indentation technique earlier developed by Marshall[71] (to be discussed in Chapter 4). Values of interfacial friction stress of approximately 2 MPa were obtained by both methods.
Marshall and Evans also determined that the flexure test could only be used to determine stress up to the level at which matrix cracking occurs as, on loading beyond this point, simple beam theory is no longer valid and the relation between peak load and failure stress is thus obscure.

Mah et al[72] conducted a series of room-temperature flexural and tensile tests on Nicalon/LAS and Nicalon/MAS (magnesium aluminosilicate) composites. From macroscopic observations of failed flexural specimens they found that the Nicalon/LAS had failed in a compression/shear mode with no evidence of cracking on the tensile side of the specimen, whereas the Nicalon/MAS specimens had failed in tension with some secondary microcracking. The load-displacement curves of both

materials exhibited a discontinuity which they termed a 'blip' and which took the form of a slight load drop after an initially linear region. This was then followed by a non-linear region up to failure of the composite at which a significant load drop-off occurred.

Microscopic observations of the edges of failed Nicalon/LAS tensile specimens revealed a series of parallel, equally-spaced microcracks which became progressively narrower with distance away from the main failure site. It is presumed that 'narrower' refers to the crack opening rather than the spacing. They found that the cracks were bridged by fibres. Mah et al measured the average crack spacing to be 300 μm and from this calculated the fibre-matrix interfacial shear strength to be about 7 MPa by using the Aveston Cooper Kelly model (equation 2.21 in section 2.4.2). The load-displacement curves obtained in tension were of similar form to those from flexural tests. Composite modulus was in good agreement with rule of mixtures predictions and the 'blip' was found to occur at a strain equivalent to the failure strain of the monolithic matrix. Specimens from tests stopped after the 'blip' had occurred showed no evidence of cracking. However, Mah et al comment that cracks may have been formed but that they may not have grown sufficiently to reach the specimen surface or may have closed on release of the load.

Mah et al[73] further developed their test capability to include elevated temperature tensile testing. They conducted tensile tests on waisted specimens of a Nicalon/LAS composite at temperatures of up to 1000°C both in air and argon. It was found that the load-displacement behaviour in air at 900°C and 1000°C was identical to that at room-temperature but that the specimen failed catastrophically at a strain equivalent to that of the 'blip' at room-temperature. No secondary cracking was observed and a region of approximately 150 μm around the edges of the specimen was found to have failed in a completely brittle manner with the inner region showing fibre pull-out. They postulate that the blip coincides with the formation of a single crack that spans the entire width and thickness of the specimen and that at room temperature the load is redistributed via the fibre-matrix interface and causes other large cracks to form in

the matrix. However, at high temperatures, environmental effects at the fibre-matrix interface lead to fibre failure thus preventing load transfer and the generation of multiple matrix cracks.

The high temperature properties of glass and glass-ceramic matrix composites were further investigated by Mandell, Grande and Jacobs[74] and Luh and Evans[75]. Mandell et al conducted tensile tests in air on a Nicalon fibre-reinforced '1723' glass and Nicalon/BMAS (barium magnesium aluminosilicate) glass-ceramic composite. The properties of the latter composite were found to decrease above about 650°C. They found that a sharp drop in strength and strain to failure occurred at test temperatures of 800°C and 1000°C compared to those measured at lower temperatures. It was also noted that at 1000°C a region of flat, brittle fracture had occurred around the exposed edges of the specimen whilst at temperatures below this, fibre pull-out had occurred over the whole fracture surface.
Luh and Evans[75] conducted flexural tests on notched and un-notched samples of Nicalon/LAS composite and found that the behaviour changed from being notch insensitive at room temperature, where failure occurred in the form of delamination at the crack tip, to notch sensitive at 1000°C, where crack growth occurred normal to the stress axis and was a function of notch depth. The fibre-matrix interfacial shear resistance was estimated to be $\approx$ 2 MPa at room temperature and $\approx$ 40 MPa at 1000°C in air after an exposure of about 1 hour. The behaviour transition was attributed to this increase in interface strength together with a decrease in fibre strength.

At about this time, the processing conditions for a Nicalon/Pyrex composite were developed in the UK by Dawson, Preston and Purser[76] using the slurry infiltration and hot-pressing route illustrated in Figure 3.1. Flexural strengths of over 1GPa were obtained for a standard fibre volume fraction of about 0.5 and the properties were retained up to 500°C. A Weibull modulus of 30 was calculated from failure strengths,

showing a high degree of reproducibility. The composite strength was found to be strain-rate independent and unaffected by holding under load for 1000 hours.

The Nicalon/Pyrex composite was studied by many workers in the UK, whilst American workers appeared to resurrect the carbon/Pyrex composite system for fundamental property determination. Although tensile testing at elevated temperatures was now possible, many workers continued to compare room-temperature flexural and tensile properties.
The room temperature mechanical properties of a range of unidirectionally reinforced glass and glass-ceramic matrix composites are given in Table 3.1.

The properties of optimised Nicalon/Pyrex material were examined by Ford, Cooke and Newsam[77] alongside two other composites manufactured by non-optimised routes and which were termed 'brittle' and 'delaminating'. Flexural tests were carried out at room temperature and acoustic emissions were monitored throughout. The 'optimised' material failed in a tough, fibrous manner with extensive fibre pull-out. Matrix on the tensile surface of test specimens was broken into a series of parallel cracks with an average crack spacing of about 63 μm. Using the Aveston Cooper Kelly model, the interfacial friction stress was calculated to be about 18 MPa. Acoustic emission activity below the onset of matrix cracking was attributed to fibre slipping which was dependent on the nature of the fibre-matrix interface. In the case of 'brittle' composite, no acoustic emissions were detected prior to failure whilst for the 'delaminating' material acoustic emission activity was detected throughout the test.
Kim & Katz[78] compared the 4-point bend and tensile properties of a unidirectional Nicalon-fibre-reinforced barium magnesium aluminosilicate (BMAS) glass-ceramic matrix composite and first noted a phenomenon which they termed 'transverse strain reversal', where the strain transverse to the fibres begins to become less negative and in some cases may even be positive at final fracture. The onset of this transverse

strain reversal was found to be coincident with the first deviation from linearity of the axial strain and was thought to be due to axial cracking and fibre-matrix debonding. This phenomenon was further investigated by Habib et al[79] for a range of Nicalon/Pyrex composite laminates. They concluded that determination of the Poisson ratio after matrix cracking had occurred was probably invalid because of this.

Davidge and Briggs[80] compared the flexural and tensile properties of a Nicalon fibre-reinforced Borosilicate glass. They conducted tensile tests on $\approx$ 10 samples and obtained a Weibull modulus of 12 for the range of strength values (compared with a Weibull modulus of 30 from $\approx$ 100 bend tests). Some of the specimens had failed by a mixture of tension and shear, with failure extending into the gripped region, and this was thought to account for the wide scatter in results. The measured tensile strength was found to be in good agreement with predictions based on rule of mixtures, assuming that the load was born solely by the fibres and taking a fibre bundle strength to average fibre strength ratio of 0.65. Comparison was then made between bend and flexural strengths by taking into account the differences in stressed volume and stress distribution in the two types of specimen.

Up to this point, very little work had been carried out on the mechanical properties of glass and glass-ceramic cross-ply composites. Sbaizero and Evans[81] measured the tensile and 4-point flexural properties of a (0/90) Nicalon/LAS laminate tested with one set of fibres along the tensile axis. They also measured the shear properties of the same laminate by tensile testing specimens with fibres orientated at $\pm 45^{\circ}$ to the loading axis. The tensile stress-strain curve of (0/90) orientated material was found to have two discontinuities, the first at about 70 MPa which coincided with the formation of delamination cracks within the transverse plies and adjacent to the lamina interfaces, and the second at a stress of about 130 MPa due to the formation of cracks normal to the stress axis and predominantly in the axial laminae. At this latter stress level, cracks normal to the stress axis also formed in the transverse plies and

some cracks propagated across two or three layers. They observed that further propagation was impeded by interaction with delamination cracks. They also comment that the crack opening of cracks normal to the stress axis is significantly reduced upon load removal, making the cracks difficult to detect at zero load, whereas delamination cracks remained visible throughout. Shear failure of specimens tested at $\pm 45^{\circ}$ was in the form of an array of matrix cracks that formed at the ulimate stress.

Seerat un Nabi and Derby[82] conducted both tensile and flexural tests on Nicalon/Pyrex cross-ply composites. Tensile testing revealed the existence of two discontinuities in the stress-strain curve. The first occured at 25 MPa and was found to coincide with the onset of cracking in the transverse plies, whilst the second more pronounced knee occurred at a stress of about 60 MPa after which a second linear region was observed until final failure of the composite. The onset of acoustic emission activity was found to coincide roughly with the first knee on the stress-strain curve. Between the first and second knees, progressive cracking of the transverse plies was observed and the decreasing crack spacing with increasing stress was found to be in accord with a model first proposed for resin matrix composites by Garrett and Bailey (discussed in section 2.5). Bend specimens were found to fail by shear in the central plies of the specimen.

Prewo[83] conducted room temperature tensile and flexural tests on both unidirectional and cross-ply carbon/Pyrex laminates. Flexural strengths of unidirectional composite were found to be significantly greater than tensile strengths and it was also noted that failure in flexure was by combined tensile and shear. A permanent decrease in elastic modulus was observed in tensile specimens loaded to high stresses, unloaded then reloaded to failure and this was thought to be due to matrix cracking. The tensile strength of cross-ply composite was less than half that of unidirectional material of the same fibre volume fraction, indicating that the 0° plies were weakened by the presence of the 90° plies. Elastic modulus of the cross-ply

composite was also half that measured from uniaxial tests, indicating that the 90° plies contributed almost nothing to the composite stiffness. Prewo also examined the effect of fibre volume fraction on the proportional limit of unidirectional composite and found it to increase with increasing fibre content in accord with the Aveston Cooper Kelly model.
The effect of matrix chemistry on the fibre-matrix interface and composite mechanical properties was investigated by altering the composition of the borosilicate glass by various reactive element additions. They concluded that although by increasing the strength of the fibre-matrix interface the shear strength of the composite was increased, this was achieved at the expense of tensile strength and toughness.

Prewo, Johnson and Starrett[84] conducted a series of tensile tests at elevated temperature on cross-ply laminates of a Nicalon/LAS-III composite. (The LAS-III matrix composition was described as having been tailored to be more compatible with SiC-type fibres.) Room temperature stress-strain curves of the cross-ply composite exhibited two discontinuities. The first occurred at about 39 MPa and was due to matrix cracking or fibre-matrix interfacial debonding in the 90° plies. The second discontinuity occurred at approximately 175 MPa and coincided with similar damage occurring in the 0° plies. Again, testing at elevated temperature in air limited the tensile strength to that associated with the 0° ply proportional limit.

An even smaller amount of published work exists on the off-axis properties of glass and glass-ceramic matrix composites. A study by Nardone & Prewo[85] examined the tensile properties of off-axis unidirectional and $(\pm \theta)_s$ carbon fibre reinforced borosilicate glass laminates. Transverse strain reversal of the type mentioned above was observed in 0° samples, which they associate with 'brooming out' of fibres during matrix microcracking, but this was not seen in off-axis measurements. Stress-strain curves of off-axis samples were linear to failure and little matrix microcracking

occurred. They also concluded that matrix cracking in $(\pm \theta)_s$ laminates occurs over a much greater proportion of the stress-strain curve than for 0° composite. Good agreement was found between measured strengths and those predicted by the Tsai-Hill failure criterion for both types of laminate using an in-plane shear strength, τ, of 32 MPa. However, agreement with maximum stress theory predicted values was poor.

Dawson et al[86] also measured the off-axis tensile properties of unidirectional Nicalon/Pyrex composite and found that the best fit for the strength versus orientation data was the Tsai-Hill failure criterion. They found that the maximum stress theory overestimated the strengths, by up to 60% for 10° to 60° aligned composite. A transition between tensile and shear failure was predicted to occur at an off-axis angle of 6.5°. Dawson et al observed this transition to take place at between 5° and 10°, with transverse shear occuring from 45° and 90°. They found that strength predictions based on the maximum stress theory could be made closer to measured values by assuming that the transverse and in-plane shear moduli were of similar magnitudes, of the order of the matrix strength, although large discrepancies were still present in the intermediate 15° - 50° range. They plotted the variation of Poisson ratio with strain for each orientation. For the 0° aligned case the Poisson ratio decreased continuously during loading, followed by a sharp increase shortly before failure. They suggest that the final increase is an artefact caused by the positioning of the strain gauge in relation to matrix cracks. The variation of Poisson ratio with strain at other fibre orientations was found to be far more complex and no attempt was made to describe the behaviour.

It was in the late 1980s that the presence of cristobalite, a form of silica, was identified in the Pyrex matrix of Nicalon/Pyrex composites[87,88]. This was formed by devitrification of the glass during processing and, since its thermal expansion coefficient is of the order of ten times that of the parent matrix, its presence led to microcracking of the composite on cooling from the processing temperature. The

formation of cristobalite occurred because of the mobility of the ions in the matrix and because the processing temperature lies within the optimum region for its nucleation and growth[89,90].

Large variations in the mechanical properties of the Nicalon/Pyrex composite were observed as a result of cristobalite associated damage and this obviously had serious implications for the practical application of such a composite. Pryce, Hill and Smith[91] found that laminate plate theory overestimated the initial elastic modulus of a range of cristobalite-containg Nicalon/Pyrex laminates, by as much as 60% in some cases, and that this was due to the presence of critobalite-associated cracking in the matrix prior to loading such that the matrix did not contribute fully to the overall laminate stiffness. In order to calculate laminate stiffness from laminate plate theory, the elastic properties of a unidirectional lamina were required - i.e. the longitudinal and transverse elastic moduli, the in-plane shear modulus and the principal Poisson ratio. Pryce et al developed a novel compression technique for the measurement of the transverse elastic modulus and obtained a value that was in reasonable agreement with predictions based on a rule of mixtures approach whereby the property was assumed to be controlled solely by the matrix.

Shin & Knowles[92], however, concluded that matrix crystallisation did not affect the room-temperature flexural strength of Nicalon/Pyrex, but that increased diffusion of aluminium into the fibres caused lower strength, brittle failures.

Bleay and Scott[88] studied the fibre-matrix interface of composites containing cristobalite and concluded that the formation of cristobalite led to local variations in matrix composition and consequent variation in reaction with the fibre.

3.2 Glass and Glass-Ceramic Matrix Composite Fibre-Matrix Interfaces

From all of the above work it becomes clear that a critical factor in the performance of glass and glass-ceramic matrix composites is control of the nature and strength of the fibre-matrix interaction. The rôle of the interface on the mechanical properties of ceramic-matrix composites has been reviewed extensively by Kerans et al[93], Thouless et al[94], Cao et al[95], and Evans et al[96].

The structure of the interface between Nicalon fibres and a range of glass-ceramic matrices has been examined by several workers (e.g. Chaim & Heuer[97], Cooper & Chyung[98], Bischoff et al[99], Chen et al[100], and Bonney & Cooper[101]), who have found that in the most successful systems the interface takes the form of an in-situ developed carbon layer which has a low cohesion and interfacial shear strength. The kinetics of carbon layer formation are controlled by the chemistries of the fibre and matrix together with the pressing time and temperature and are characterised by the chemical equilibrium[98]

$$SiC + O_2 \rightarrow SiO_2 + C$$

with the primary driving force being the silica composition gradient across the interface.

In view of the fundamental effect of fibre-matrix interface strength on the overall composite properties it is necessary to be able to quantify this parameter. An experimental technique developed by Marshall[71] was developed which involves the in-situ indentation of fibres parallel to their axis with a Vickers indentation instrument. Further developments of this technique by Marshall and Oliver[102] involved the use of an ultra-low load or nano- indenter which enabled the displacement to be measured as a function of indentor load. By this method they attempted to determine the relative magnitude of the fibre-matrix bond strength and interfacial friction stress for a Nicalon/LAS composite, concluding that the bond

strength was negligible. Another improvement in the technique was made by Mandell et al[103] who used a rounded indentor. They determined the bond strength to be an order of magnitude greater than the friction stress. These techniques are discussed in further detail in Chapter 4. More recently, a novel indent system which operates within an SEM has been developed by Lewis et al[104] for the determination of interface de-bond and shear stresses in silicate matrix composites. This enables simultaneous monitoring of both image and load-displacement curve and allows much higher loads to be used than conventional nano-indentors. Values of interfacial fiction stress of between 5 MPa and 10 MPa have been measured by this technique on a range of glass-ceramic matrix composites,

3.3 Current Understanding of Nicalon/CAS Glass-Ceramic Matrix Composite

As may be noted from the above, the majority of work up to 1990 was carried out in the UK on Nicalon/Pyrex and in the USA on Nicalon/LAS. At this point a Nicalon-fibre reinforced calcium aluminosilicate (CAS) glass-ceramic matrix composite[105] manufactured by Corning Glass became commercially available.

The mechanical and structural properties of the Nicalon/CAS composite have been studied by several groups of workers both in the USA and UK[106-117]. Comparison of the room temperature mechanical properties of unidirectional Nicalon/CAS from a number of sources is given in Table 3.2.

Tensile stress-strain curves for unidirectionally reinforced Nicalon/CAS composite were of the form described in the previous section and in the majority of cases[106,108,111] good agreement was found between measured values of initial elastic modulus and rule of mixtures predictions based on constituent properties. The transverse strain reversal mentioned in the previous section was also noted by several workers[106,109, 111]. Daniel et al[108] and Harris et al[111] measured the gradient of the second linear region of the stress-strain curve, assumed to be deformation of the fibres

alone, and both found that this was less than $E_f V_f$ predictions. Harris and his co-workers assume that this is due to degraded fibre properties as a result of manufacturing conditions, whereas Daniel observes failure of some fibres prior to matrix crack saturation.

Many workers[107,110,111] also found reasonable agreement between the onset of matrix cracking and predictions based on the Aveston Cooper Kelly model for multiple fracture. Kim and Pagano[106], however, carried out tensile tests on a range of unidirectionally reinforced glass and glass-ceramic matrix composites and attempted to identify the onset of matrix cracking by use of acoustic emission and strain gauge monitoring together with replication techniques. They confirmed that for a Nicalon/CAS composite the onset of the first few matrix cracks coincided with detection of the first few acoustic emission events but that this occurred at a stress level of $\approx$ 132 MPa which is greatly below the matrix cracking stress predicted from ACK theory ($\approx$ 360 MPa) and is within the initial linear portion of the stress-strain curve. They deduce that the short gauge-length strain gauges used for increased sensitivity are in fact only sensitive to cracks in the immediate vicinity of the gauge and are therefore unreliable for detecting the first matrix cracks. It should be noted that the matrix fracture surface energy (γ_m) used in their ACK calculations was 40Jm^{-2} which is considerably larger than that adopted by most other workers (cf γ_m = 12.5 Jm^{-2} measured by Beyerle et al[107] in tests on chevron-notched bend specimens of monolithic matrix material; γ_m = 3 Jm^{-2} used by Pryce and Smith[110] in their calculations) although in accord with that used by Harris et al[111]. Kim and Pagano also determined by unloading and reloading that the Nicalon/CAS obeyed the Kaiser effect (i.e. that no further acoustic emissions were detected until the previous stress level was reached). Harris et al[111], however, detected acoustic emissions in all laminates tested at strains as low as 0.01% and found that the Kaiser effect was not obeyed on reloading even when no change in elastic modulus was observed.

Kim and Pagano conclude that the onset of matrix cracking occurs at strains within the range of failure strains of the monolithic matrix (0.07 - 0.15%) and that the fibres offer no true reinforcement in the manner predicted by ACK theory.

Beyerle et al[107], who conducted four-point bend and tensile tests on unidirectional Nicalon/CAS, determined by direct optical observation that the first matrix cracks appeared at stresses in the range 130 - 150 MPa and were coincident with the onset of acoustic emission activity, which is in accord with the findings of Kim and Pagano. Bend and tensile tests were conducted on specimens with faces and edges polished so that a matrix-rich outer surface layer was removed. A number of tensile tests conducted on specimens without this layer removed showed similar stress-strain behaviour although surface matrix cracks were observed to form at stresses as low as 50 MPa. They comment that this demonstrates the importance of local fibre content on matrix cracking.

Beyerle et al measured the actual saturation crack spacings of bend test specimens (as opposed to the majority of workers who count cracks over a small gauge length) and obtained an average value of 103 μm which gave an estimate for the interfacial shear stress (from ACK) of τ = 25 -28 MPa. This is considerably higher than their estimate from fibre pull-out lengths (τ in the range 10 -15 MPa) and generally higher than that adopted by other workers and which in most cases are estimated (τ = 7 MPa by Kim and Pagano[106]; τ = 8 - 10 MPa by Pryce and Smith[110,112]; τ = 5 MPa by Harris et al[111]; τ = 9 MPa by Evans et al[96]). Beyerle and his co-workers conclude that the lower-bound matrix cracking stress predicted from the ACK model is in good agreement with their measured values for τ in the range 10 - 15 MPa and by taking account of the residual thermal stresses in the matrix. They measured a value of 89 MPa (tensile) for the matrix residual stress by using a dissolution technique and this is in excellent agreement with that calculated from a concentric-cylinder model by Powell et al[113]. This residual tensile stress in the matrix arises from thermal expansion coefficient mismatch between matrix and fibre (α_m = 5 x10^{-6} /°C and α_f = 3.1 x 10^{-6} /°C - as given in Tables 3.3 and 3.4 respectively) and results from cooling

from the processing temperature (assumed to be of the order of 1000 -1200 °C). Kim and Pagano[106] and Harris et al[111] estimate the matrix residual stress to be of the order of 130 -140 MPa, whereas Pryce and Smith[112] incorporate a value of 50 MPa for the compressive stress in the fibres in their calculations of predicted stress-strain behaviour. In the work of Daniel et al[108] the matrix residual thermal stress, which is calculated to be 55 MPa, is ignored. However, their approach is to use a modified shear lag rather than the ACK model to predict crack density and stress-strain behaviour. They observe cracking to commence at stresses of about 100 MPa and to reach saturation at a stress of about 275 MPa with a minimum crack spacing of 36 μm.

Evans, Zok and Davis[96], in their review of the rôle of interfaces in brittle matrix composites, present measured and calculated values for the matrix cracking stress of a unidirectional Nicalon/CAS composite which show excellent agreement (160 MPa and 140 -160 MPa respectively). Their calculations are based on ACK theory with residual stresses taken into account. However, only the interfacial shear strength used in their calculations (obtained from saturation crack spacings) is quoted.

It becomes clear from the above results the accuracy of the ACK model predictions of matrix cracking stress, when compared to measured values, is extremely sensitive to the chosen values of matrix fracture surface energy, interfacial shear stress and matrix residual stress - all of which are difficult to determine experimentally.

Karandikar & Chou[109] and Pryce & Smith[110,112] have modelled modulus reductions in both unidirectional and cross-ply Nicalon/CAS laminates as a function of stress during quasi-static tensile tests, using a shear lag approach.

Pryce and Smith[110] conducted discontinuous tensile tests on unidirectional composite and on a range of crossply laminates having different transverse ply thicknesses. They measured elastic modulus and crack density as a function of both stress and strain for each lay-up. Prediction of crack density versus stress behaviour

for unidirectional composite, based on an ACK approach, was found to be an oversimplification compared with measured trends as the statistical distribution of matrix strengths was not taken into consideration by the model. Predictions of the crack density versus stress behaviour of the transverse plies within crossply laminates, based on a shear-lag approach, were found to be in reasonable agreement with measured values. However, the statistical nature of the 90° failure processes was not taken into consideration by the model, nor was the stiffness degradation of the constraining 0° plies at high strains. By extrapolating crack density versus strain curves back to the point where they crossed the strain axis, Pryce and Smith estimated the 90° ply cracking threshold for each laminate and determined that the lowest threshold occurred in the laminate with the thickest transverse ply. This is in accord with the findings of Karandikar and Chou[109]. From these threshold values, and by taking a fracture mechanics approach, Pryce and Smith estimated the initial diameter of flaws within the transverse plies of the crossply laminates and determined that in each case this was less than the transverse ply thickness and that the flaw size increased with increasing ply thickness. They inferred from this that, for practical ply thicknesses, transverse ply cracking in the Nicalon/CAS composite would be 'unconstrained' by the 0° plies. The saturation crack spacing was found to be influenced by the transverse ply thickness, although they did not quantify the effect. They also found that the limiting value of the elastic modulus was lower than rule of mixtures predictions based only on the fibres within the 0° plies. They attributed this to fibre breakage prior to ultimate failure of the composite.

Karandikar and Chou[109] concluded from their work on Nicalon/CAS unidirectional and cross-ply laminates that the presence of transverse plies had little effect on the matrix cracking in unidirectional plies in terms of initiation strain and saturation densities. The variation of unloading and secant Young's moduli was measured as a function of strain during discontinuous tests and reductions of 30 - 55% for unidirectional material and 45 - 69% for cross-ply material occurred as a consequence of damage. Similarly, values of the instantaneous Poisson ratio decreased as a

function of applied strain and became negative at saturation damage as the transverse strain became positive. The decrease in Young's modulus was successfully predicted by a modified shear lag model.

Further work by Pryce and Smith[112] concentrated on modelling the stress-strain behaviour of unidirectional Nicalon/CAS composite. They conducted discontinuous tensile tests and found that loading and un-loading curves were of the form of hysteresis loops with an increasing strain offset at zero applied stress. Once cracking had occurred in the laminates the stress-strain curves became non-linear over the whole loading range and secant modulus values had to be measured. Measurements of crack density versus stress behaviour from these tests were then used to model the continuous stress-strain behaviour by modifying the ACK analysis.

Work by Allen et al[114] on the properties of chevron-notched, unidirectional samples of Nicalon/CAS during cyclic flexural loading up to 1000°C has shown that the failure mode changes from that of multiple matrix cracking and fibre debonding at ambient temperature to dominant angled cracks at 600 °C and to a single mode I crack at 1000 °C. This behaviour transition was found to be due to environmental attack at the fibre-matrix interface.

In-situ observations of delamination cracking in double cantilever beam specimens situated within the loading stage of an SEM have been carried out by Kaute et al[115]. Delamination cracks were found to be bridged by fibres which span the crack wake at a low angle. This bridging is caused by the waviness of fibres within the composite. They estimated the tensile stresses on the bridging fibres to be between 0.5 and 1.2 GPa, by using a bridge column theory, which when resolved perpendicular to the crack face gives a crack closing force of between 15 and 40 mN. They determined that the peak stress in bridging fibres was limited by the fibres debonding from the matrix over a distance of up to 800 μm and that this was then followed by fibre failure due to bending.

Microstructural analysis of the as-received Nicalon/CAS composite carried out by Bleay et al[116], using a wide range of techniques, determined that the matrix consisted almost entirely of the crystalline phase Anorthite ($CaAl_2Si_2O_8$) together with approximately 1 vol. % α - Al_2O_3, less than 0.5 vol.% of a silicon-rich glassy phase and zirconium-rich particles thought to originate from a nucleating agent. TEM analysis of the fibre-matrix interface region revealed a carbon-rich band of approximately 50nm thickness. This region was also found to contain elements from both the fibre and matrix. Measurement of the interfacial friction stress by the Marshall technique described previously gave a value of the order of 3 MPa for the as-received composite. Heat treatment at temperatures of up to 1000 °C caused little change in this value although voids formed at the interface in samples heated to 800°C and this was thought to be due to the evolution of CO or CO_2. In specimens heated to 1100°C, degradation of the interface was more pronounced. A silica band of about 100nm thickness and containing voids had formed at the interface and the friction stress had increased to between 5 and 25MPa around the outer edges of the specimens. This did not affect the overall strength of the composite but led to brittle fracture around the outer edges.

Pharaoh et al[117] also studied the stability of fibre-matrix interfaces in Nicalon/CAS by heat treating samples of unidirectional and cross-ply composite for 100 hours in air at temperatures of between 600°C and 1200°C. Samples were subsequently tested in three-point bend and interfacial shear stresses were determined by the Marshall technique. Pharaoh et al found that the microhardness of Nicalon fibres (to be used in interfacial shear stress calculations) varied from 18.5 to 23.5 MPa and that this variation had a large effect on the calculated shear stress. Values of interfacial shear stress were found to increase from 5-10MPa in the as-received composite to 20-25MPa after exposure to temperatures $\geq$700°C. Three-point bend strengths were found to have decreased after exposure to intermediate temperatures (600 and 700°C) but recovered after exposure to 800°C and above. They determined by electron

microscopy that the fibre-matrix interface in as-received composite consisted of a carbon-rich layer and that this was unaffected by temperatures below 500°C. At temperatures of between 500°C and 800°C, pipe diffusion of oxygen along fibre-matrix interfaces caused oxidation of the carbon producing voids. However, oxidation of the carbon interface at higher temperatures was accompanied by oxidation of the silicon carbide fibre and a silica bridge was formed between fibre and matrix in the outer 30μm of samples. This effectively created a 'plug' at the fibre ends thus preventing further oxidation of the interface by this method. They state that oxygen diffusion through the matrix then becomes an important factor.

3.4 Properties of Constituent Materials

3.4.1 Glass-Ceramics for Composite Matrices

Glass-ceramics are defined as 'polycrystalline solids prepared by the controlled crystallisation of glasses'[118]. This crystallisation is accomplished by subjecting suitable glasses to a heat-treatment schedule which results in the nucleation and growth of crystal phases within the glass. Glass-ceramic materials that have so far been studied as CMC matrices are generally based on compositions which form a low thermal expansion, near-monophasic microstructure - for example, compositions of lithium aluminosilicate (LAS), magnesium aluminosiliocate (MAS), calcium aluminosilicate (CAS) and barium aluminosilicate (BAS). The selection of a specific composition is normally a compromise between high-temperature capability and ease of fabrication or microstructure control[104,119]. Ideal process conditions to produce optimum composite mechanical performance are those in which densification and fibre-matrix interface development occur prior to the controlled crystallisation of the matrix by nucleation and growth. An idealised composite processing cycle is illustrated schematically in Figure 3.2. The interface development and matrix crystallisation kinetics are shown in the form of time/temperature/transformation

(TTT) curves. For the ideal conditions to be met, processing has to be carried out at temperatures above the liquidus temperature of the matrix, T_e, as the low viscosity of the matrix in this regime allows full (generally greater than 98%) densification to be achieved. The matrix can then be crystallised by heat treatment at a lower temperature. However, stoichiometric glass-ceramic compositions which form near monophase microstructures, and which are thus of interest as high-temperature composite matrices, generally have liquidus temperatures greater than 1200°C which is above the stability limit of currently available silicon carbide fibres.

Although compositions which form di- or tri-phasic structures are more readily melted, control of the relative size and proportions of the crystalline phases to give the required mean thermal expansion may not be achieved and there is a greater probability of having glassy residues. In many cases the addition of nucleating agents such as Cr_2O_3, Nb_2O_5 and ZrO_2 is required to ensure the formation of an even distribution of fine grains[120,121].

Table 3.3 lists some properties of a range of glass-ceramic matrix materials found suitable for incorporation in high-temperature composites. However, little published information on the mechanical properties of the monolithic glass-ceramics exists and it is suspected that some of the data have been calculated from composite properties. The properties of CAS were provided by Corning[122].

The most notable feature of the data is the wide range of thermal expansion coefficients that can be obtained with changes in composition thus giving the potential to tailor this property with respect to the fibres and to the applications considered.

3.4.2 Ceramic Fibres for Glass-Ceramic Matrix Composites

A major impetus in the development of continuous-fibre-reinforced ceramic-matrix composites, following earlier experiments with oxidation-susceptible carbon fibre, was the commercial availability of silicon carbide yarns.

Nicalon silicon carbide fibres were developed in the 1970s by Yajima and his co-workers[64,65] at the Nippon Carbon Co. The fibres are manufactured by the controlled pyrolysis of an organometallic (polycarbosilane) precursor. Fibres are supplied in the form of tows consisting of approximately 500 filaments. Manufacturer's data for the properties of the Nicalon fibre are given in Table 3.4.

The structure, properties and thermal stability of Nicalon fibres have been investigated by several workers[123-128] and are reviewed by Andersson & Warren[129]. An average fibre diameter of 15μm has been measured although diameters in excess of 20μm have been observed. The fibres are generally considered to be predominantly microcrystalline β-SiC, having a grain size of the order of 2nm, with excess carbon and oxygen. The oxygen was originally thought to be present in the form of SiO_2, situated mostly at the fibre surface in the form of an outer layer, and the carbon as graphitic microcrystals. Estimates of the relative proportions of the constituent phases have been given as 65% β-SiC and 20% free carbon, the remainder being SiO_2. However, more recent studies by Bleay et al[128] have concluded that the oxygen is present in the form of silicon oxycarbide situated throughout the fibre, with oxycarbide in the outer 200nm being significantly richer in oxygen, and that the total oxycarbide content represented 34% of the fibre volume with 34% SiC and 20% free carbon.

The isotropic microstructure of Nicalon means that the axial and radial thermal expansion coefficients (α) are identical and equal to 3.1×10^{-6} /°C. The lower value in α, by comparison with bulk β-SiC, is consistent with the presence of free carbon and oxygen. The density of Nicalon is similarly reduced to 2.6 g/cc in comparison with that of β-SiC.

The as-received Nicalon fibre is coated with an acrylic size which is generally removed either by dissolution in acetone or by heat treatment prior to mechanical testing. The room temperature tensile strength of de-sized Nicalon fibres has been

found to lie within the broad range 1-4 GPa with a distribution described by Weibull statistics and consistent with the presence of a single defect population. As a consequence of this defect population, the measured strength is dependent on gauge length with higher strength values being obtained from shorter gauge lengths. The Weibull moduli for gauge lengths between 80 and 220 mm were found by Simon and Bunsell[123] to be of the order of 3. Values of Young's modulus varying from 118-185 GPa have been reported (cf manufacturer's data in Table 3.4) with the higher value corresponding to a gauge length of 15mm.

Heat treatment of Nicalon fibres in both air and argon at temperatures of up to 1300/1400°C, followed by room temperature evaluation, has been carried out by several of the above workers. All have observed the formation or thickening of an SiO_2 layer on the outer surface of the fibre during exposure in air to temperatures between 600-1000°C. Above 1000°C reductions in both strength and Young's modulus were observed, these changes being attributed to coarsening of the β-SiC grain size and evolution of CO (formed from a reaction between the free carbon and either atmospheric oxygen or oxygen within the fibre).
Studies of the long-term behaviour of Nicalon fibres under steady loading conditions[127] have revealed that creep deformation occurs at temperatures above 1000°C and this deformation initially follows a logarithmic creep law. This primary creep is thought to be due to recrystallisation of the β-SiC. Failure strains up to 6% were measured at 1300°C.

A second type of silicon carbide reinforcement is the Tyranno fibre which was originally developed in the early 1980s[130,131] to be more compatible with an aluminium matrix than Nicalon fibre was found to be. Tyranno fibres are manufactured in a similar manner to Nicalon except that they are produced from a polytitanocarbosilane polymer precursor. Pyrolysis of the fibre is carried out at

1400°C and thus the fibre has high-temperature properties which are superior to those of Nicalon.

The physical and mechanical properties of the Si-Ti-C-O fibre are given in Table 3.4, together with comparative data for the Nicalon Si-C-O fibre. The average diameter of the fibre is 8-12μm and this can be controlled to within ±1.5μm. The smaller diameter and higher strain to failure are beneficial in the production of weaves, braids and knits and in the manufacture of complex composite components. The higher temperature capability of the Tyranno fibre is thought to be attributable to the retention of an amorphous state and to the bonding of non-stoichiometric carbon to the titanium, giving greater microstructural stability.

The current limitation on the temperature capability of ceramic-matrix composites is that of the fibre (1000-1200°C) and this must be increased in order for the composite performance requirements to be achieved. The aim of fibre developments for ceramic-matrix composites is to produce small-diameter, weavable fibres which are structurally and mechanically stable to at least 1600°C and which may be manufactured at low cost from polymer precursors. Recently, fibres which have improved thermal stability have been developed, for example the Si-N-based Dow-Corning HPZ fibre and stoichiometric SiC fibres[104]. Another method of potentially improving the temperature capability of glass-ceramic matrix composites is by the pre-coating of existing Nicalon fibres, with for example carbon or boron nitride, so that a synthetic partially sacrificial interface is formed when consolidated within the composite. Some of the problems associated with this method are discussed by Evans et al[96].

	Nicalon/Pyrex Davidge & Briggs[80]	**Nicalon/LAS-II** Prewo[69]	**Nicalon/LAS-III** Kim & Pagano[106]	**Nicalon/BMAS** Kim & Katz[78] and Kim & Pagano[106]
Fibre Volume Fraction	0.45	0.44	0.39	0.43
Elastic Modulus (GPa)	110	136	131	149
Poisson Ratio	-	-	-	0.26
Longitudinal Tensile Strength (MPa)	600	680	-	416
Strain to Failure (%)	0.55	1.03	-	-
Proportional Limit Stress (MPa)	500	391	306	254
Proportional Limit Strain (MPa)	0.4	0.29	0.23	0.17
Matrix Crack Initiation Stress (MPa)	-	-	195	< 214
Matrix Crack Initiation Strain (%)	-	-	0.15	< 0.14

Table 3.1 : Published data on the room-temperature tensile properties of unidirectional glass and glass-ceramic matrix composites

	Kim & Pagano[106]	Beyerle et al[107]	Harris et al[111]	Pryce & Smith[110,112]
Fibre Volume Fraction	0.40	0.37	0.37	0.34
Elastic Modulus (GPa)	127	-	124	128
Poisson Ratio	-	-	0.24	0.24
Longitudinal Tensile Strength (MPa)	505	430	334	400
Strain to Failure (%)	-	~ 0.8	~ 0.7	0.78
Proportional Limit Stress (MPa)	212	150 - 200	~ 175	96
Proportional Limit Strain (MPa)	0.17	-	~ 0.15	0.08
Matrix Crack Initiation Stress (MPa)	132	130 - 150	-	-
Matrix Crack Initiation Strain (%)	0.10	-	-	-
Assumed $\Gamma_m = 2\gamma_m$ (Jm^{-2})	80	25	80	6
Assumed τ (MPa)	7	10 - 15	5	8 - 10
Matrix Residual Stress (MPa)	127	89	140	- 50 (in fibres)

Table 3.2 : Published data on the room-temperature tensile properties of unidirectional Nicalon/CAS composite

	LAS	BMAS[74]	MAS	CAS[122]
Predominant Phase	β-Spodumene	Barium Osumilite	Cordierite	Anorthite
Thermal Expansion Coefficient ($x10^{-6}$ /°C)	1.0[68]	1.7	2.6[118]	5
Density (g/cc)	-	2.77	-	2.45
Ultimate Strength (MPa)	-	-	-	80 - 170
Elastic Modulus (GPa)	86[69]	106	-	85 - 110
Composite Use Temperature (°C)	1200[120]	1200-1250	1200[120]	> 1200

Table 3.3 : Published data on the physical and mechanical properties of glass-ceramic matrices

	NICALON	TYRANNO
Composition	Si - C - O	Si - Ti - C - O
Diameter	15 μm	8 - 12 μm
Number of Filaments	500	200·n (n = 1-8)
Tensile Strength	2.5 - 3.0 GPa	3.0 ± 0.5 GPa
Young's Modulus	180 GPa	220 ± 20 GPa
Strain to Failure	1.4 %	1.4 - 1.5 %
Axial Coefficient of Thermal Expansion	3.1 x 10^{-6} /°C	3.1 x 10^{-6} /°C
Transverse CTE	3.1 x 10^{-6} /°C	-
Density	2.55 g/cc	2.3 - 2.4 g/cc

Table 3.4 : Silicon carbide fibre manufacturers' data

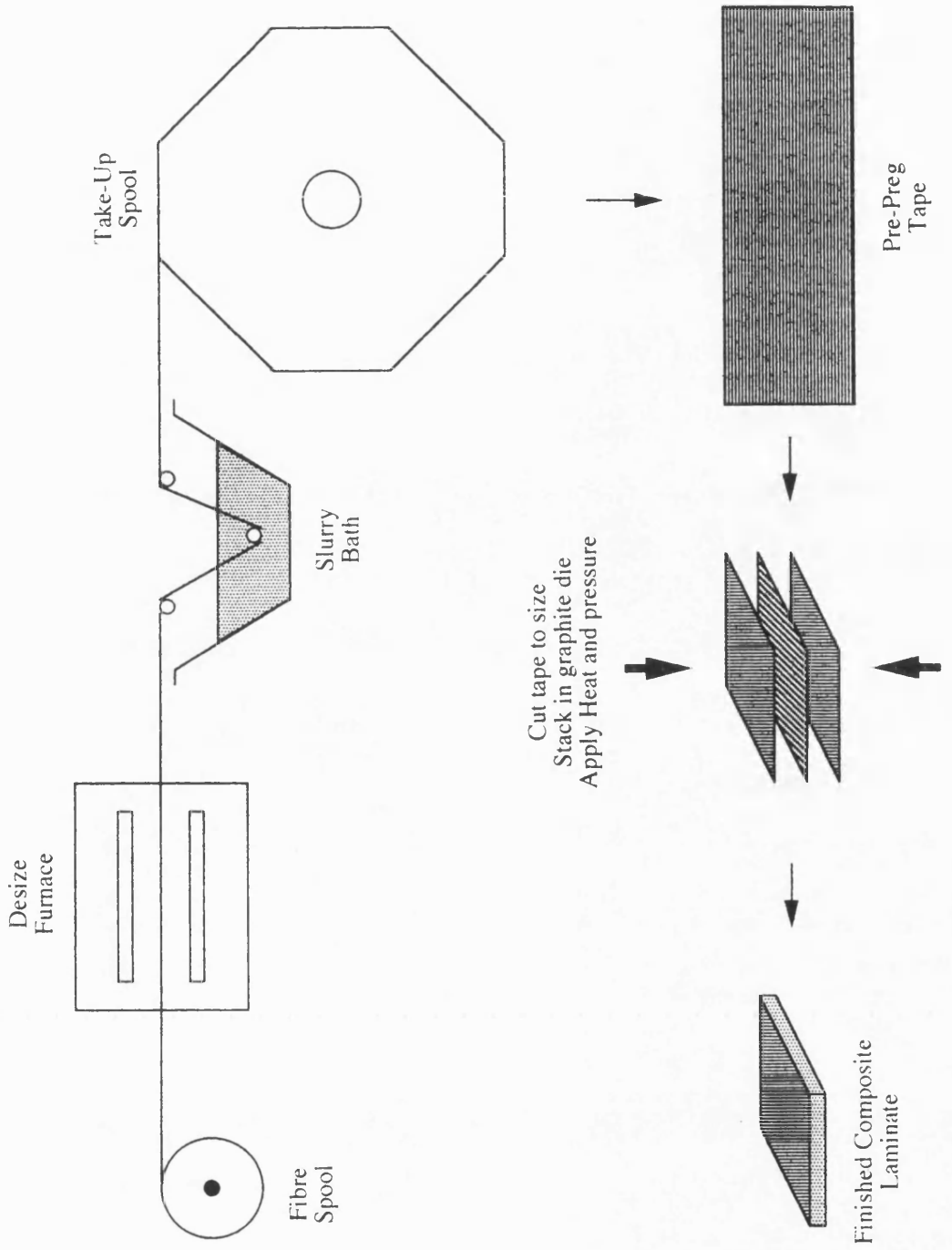

Figure 3.1 : Glass and glass-ceramic matrix composite manufacture by slurry impregnation and hot-pressing route

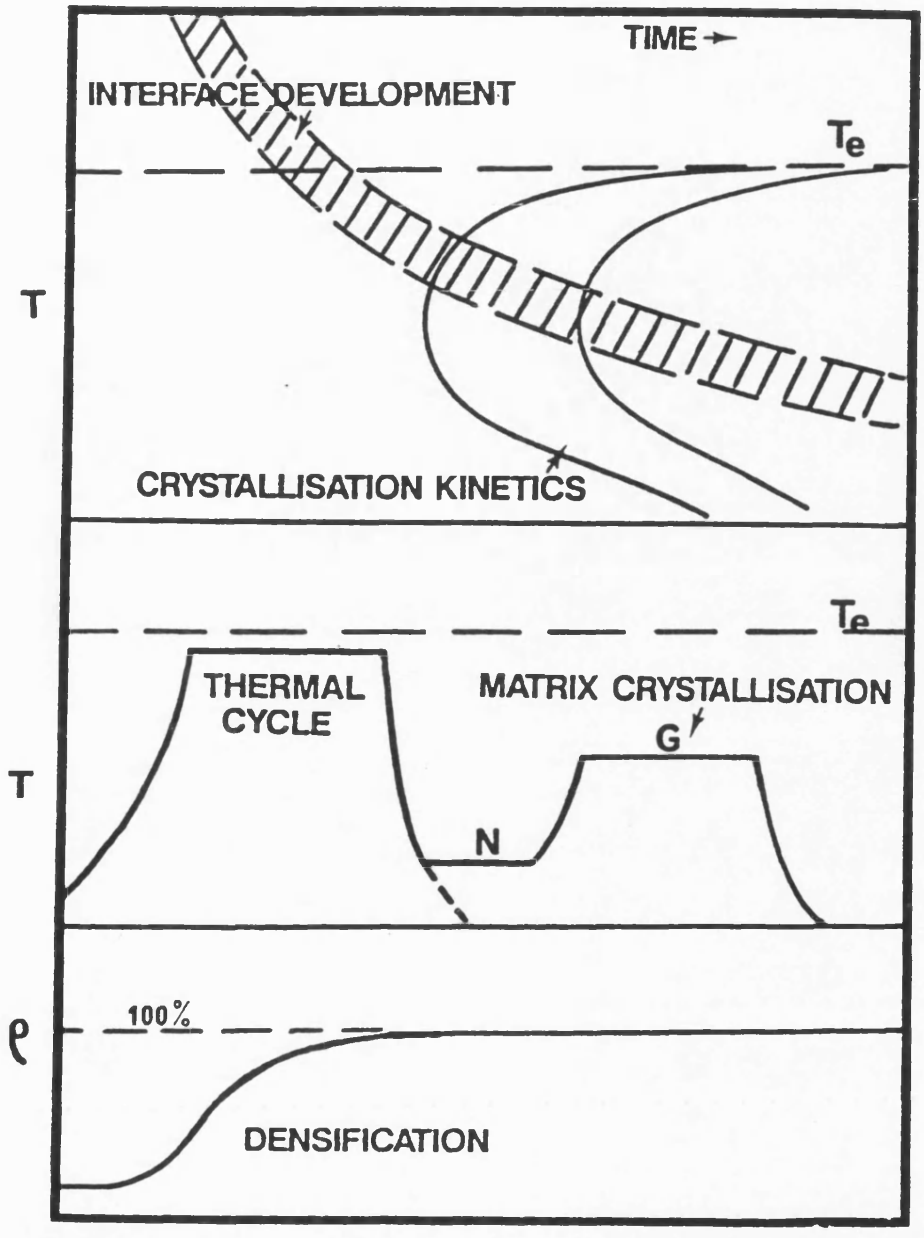

Figure 3.2 : Schematic time-temperature plots illustrating the competition between kinetics of matrix crystallisation, densification and interface development during hot-pressing (after Murthy, Pharaoh and Lewis[119])

CHAPTER 4 : MATERIALS AND EXPERIMENTAL DETAILS

4.1 Materials and Manufacture

4.1.1 Source and Form of Material Supply

Material was supplied by Corning Glass Works, Corning, New York via Rolls-Royce plc and was in the form of flat plates of dimensions 150 mm x 150 mm and of variable thickness. The lay-up, laminate thickness and nominal ply thickness of each plate is given in Table 4.1. A small number of machined test pieces of dimensions 100 mm x 10 mm originating from an unspecified plate having a $(0)_{12}$ construction were also provided. The plates were black in appearance and the orientation of the fibres in the outer plies was evident from surface inspection. All plates were examined non-destructively by the ultrasonic C-scan method in an attempt to identify regions of gross defect e.g. delamination, voidage, matrix-rich regions. The perimeter region of each plate (~ 2 mm wide) was found to be poorly impregnated and consolidated and this was removed prior to the cutting of specimens.

A 150 mm diameter disc of monolithic CAS having a thickness of 10 mm and made ostensibly under the same process conditions (time, temperature and pressure) as the composite was also supplied by the manufacturer. The as-received disc was black in appearance although it later became apparent that this was merely a surface condition thought to be due to contact with the graphite die and the possible use of a release agent. The bulk material had an off-white, mottled appearance. No non-destructive structural evaluation of the as-received disc was made.

4.1.2 Material Manufacture

Details of the composite process are proprietary to the manufacturer. However, it is possible to infer likely conditions from knowledge of the manufacture of other composite systems. It is assumed that the composite was produced by the slurry impregnation, hot-pressing route first developed by Sambell et al[59,60] for carbon-

fibre-reinforced Pyrex which was further adapted by Prewo & Brennan[67] and later by Dawson et al[76] for Nicalon/Pyrex production. This process route is depicted in Figure 3.1 of the previous chapter and involves the removal of organic size from the surface of fibres by passing through a furnace; the impregnation of fibre tows with a slurry of powdered matrix, solvent and organic binder; filament winding the impregnated tows to form 'pre-preg' sheets; cutting and stacking the sheets to the required configuration in a graphite die; and hot-pressing to form a densified composite. In the case of glass-ceramic-matrix composites, a post-forming heat treatment is required to crystallise the glass fully. The important variables which have a direct effect on the composite properties are discussed by Briggs and Davidge[132]. Fibre handling in terms of desizing time and temperature, efficiency of fibre separation, path length of fibre through slurry, winding speed, and fibre tension are all mentioned as affecting composite performance. However, the most critical of the process variables is the hot-pressing schedule in terms of time at temperature, temperature and pressure. The conditions are generally dictated by the matrix chemistry and the need to achieve full densification but are most deleterious to the fibres. A compromise therefore has to be reached so that fibre degradation and damage are minimised. Prewo, Brennan and Layden[120] state that pressure should only be applied once the process temperature is reached in order to reduce fibre damage.

Little information on the exact process times, temperatures and pressures is given in the literature. Brennan and Prewo[68] hot-pressed their LAS-I composite, which contained a ZrO_2 addition, at a temperature of over 1300°C followed by a ceraming heat treatment at 880-1100°C for 1 to 2 hours. However this composite had a linear stress-strain curve possibly as a result of the formation of a strong fibre-matrix bond. Later compositions of LAS contained additions of both Nb_2O_5 and ZrO_2. Chaim & Heuer[97] refer to Brennan as quoting a pressing schedule of 1250 - 1300°C for 15 minutes at 7 MPa pressure and ceraming at 1050°C for 24 hours. Chaim et al[121] hot-pressed Nicalon/Cordierite (MAS) composites containing either Cr_2O_3 or Nb_2O_5

additions at 1000 - 1200°C and a pressure no higher than 14 MPa, followed by a heat treatment at 1300°C for 1 hour without pressure. However, they failed to identify the presence of a carbon-rich interface. Cooper & Chyung[98] found that a thicker graphitic interface was formed in as-pressed CAS composite when annealed at 1200°C for 2 hours or by adding 1 wt% As_2O_3.

From the above information it appears reasonable to assume that the overall hot-pressing and ceraming schedule for a Nicalon/CAS composite would involve exposure to temperatures of about 1200°C for a couple of hours and that some form of nucleating agent would have been added to the stoichiometric matrix composition. It is also likely that several (possibly up to 4) plates would have been hot-pressed at a given time with graphite spacers between them.

4.2 Monolithic CAS Evaluation

4.2.1 Microstructural Analysis

In order to determine whether the structure and composition of the monolithic material was in fact equivalent to that of the composite matrix, samples were analysed by using a wide range of techniques. In all cases the black outer surface was removed prior to examination. A sample of the bulk material was analysed by X-ray diffraction (XRD) to determine the composition of phases present. Polished samples were examined by scanning electron microscope (SEM) in both secondary electron and back-scattered electron imaging modes - the former to identify flaws (e.g. porosity) and the latter to determine the size and distribution of phases. The sample also underwent electron probe microanalysis (EPMA) to measure quantitatively the composition of the apparent phases by both energy dispersive and wavelength dispersive spectroscopy (EDS and WDS).

4.2.2 Physical Property Determination

The bulk density of the monolithic CAS was evaluated by measuring the weight and dimensions of specimens subsequently to be used for elastic property determination. The linear coefficient of thermal expansion was measured up to 1000°C in a Dupont Thermomechanical Analyser (TMA) at a ramp rate of 5°C per minute.

4.2.3 Elastic Property Determination

A number of methods exist for the measurement of the elastic properties of materials. These include monotonic loading techniques, involving the recording of mechanical load-displacement profiles, and dynamic techniques, either pulse velocity or natural frequency methods. In view of the low strain to failure of ceramic materials, dynamic techniques are generally employed.

Measurement of the elastic constants of the monolithic CAS in this case was made by a resonant frequency method according to ASTM C 848 - 78[133] and which is outlined in a paper by Davis[134]. Tests were carried out on rectangular specimens of nominal dimensions 100mm x 10mm x 6 mm in flexural, longitudinal and torsional modes of vibration to generate values of elastic modulus (E), shear modulus (G) and Poisson's ratio (ν). The apparatus arrangement for each mode of vibration is depicted in Figure 4.1. The bar is excited by means of a driving transducer and the resulting oscillation of the beam detected by a second transducer. The relative positioning of the support(s) and transducers dictates the mode of vibration of the beam. Beams of either rectangular or circular cross-section can be used although difficulties arise in generating torsional modes of vibration with rod specimens - hence the use of a rectangular beam in this instance.

The elastic constants are calculated from the fundamental (1st) resonant frequency of vibration - i.e. elastic modulus from either longitudinal or flexural modes, and shear

modulus from torsional mode (Figure 4.1 shows the positioning of the nodes for the fundamental frequencies). Since there are only two independent elastic constants for isotropic materials, Poisson's ratio can then be calculated from the well-known expression $\nu = (E/2G) - 1$.

The expressions used to calculate the moduli from the fundamental frequency are derived from consideration of the velocity of stress waves in the material (i.e. $C = \sqrt{(E/\rho)}$, where C is the wave velocity) and are dependent on the size and shape of the specimen. For the simplest case of longitudinal vibration, in which the specimen is supported at its mid-point and the length of the specimen is equal to half the wavelength at the resonant frequency, the basic equation for Young's Modulus (E, in N/m^2) is[134]:

$$E = 4 \times 10^{-6} n^2 l^2 \rho \qquad (4.1)$$

where n is the resonant frequency of vibration in Hz, l is the specimen length in mm, and ρ is the bulk density in kg/m^3.

The expressions are generally made more complex, particularly in the case of flexural vibration, by the need to allow for lateral expansion and contraction of the beam (Poisson ratio effect) by use of a correction factor. For the case of longitudinal resonance in a rectangular bar, the correction factor is:

$$\frac{1}{\left[1 - \frac{(\pi\nu)^2}{2l^2}\frac{(b^2 + h^2)}{12}\right]^2} \qquad (4.2)$$

where b is the width of the bar (in mm), h is its thickness and ν the material Poisson ratio. Equation 4.1 has to be multiplied by the correction factor. This is only necessary if the length of the beam, and hence the wavelength at the resonant frequency, is less than about 10 times the thickness of the beam. This condition is satisfied in the present specimens.

Factors which can affect the accuracy of the modulus measurements are specimen machining and dimensional accuracy, accuracy of bulk density measurement, degree of material porosity, and the presence of cracks.

4.2.4 Matrix Strength Determination

Strength measurements of the monolithic CAS material were made by testing in three-point bending. A standard has been proposed by the CEN European Committee for Standardization which describes methods for determining the nominal flexural strength of advanced monolithic technical ceramic materials at ambient temperature by either three- or four-point bending. These methods are detailed in a draft document prEN 843-1:1992[135]. The test is described as being suitable for the purposes of material development, quality control, characterisation and design data acquisition. The strength determined by the test is calculated on the basis of linear elastic bending of a thin beam on the assumption that the material being tested is elastically homogeneous and isotropic and shows linear (Hookean) stress-strain behaviour. The value obtained can be affected by many factors - e.g. the microstructure of the material, surface finishing procedure during specimen preparation, size and shape of specimen, function of test apparatus, loading rate and humidity of atmosphere. In the present study a screening test developed by Rolls-Royce plc, which falls largely within the recommendations of the CEN standard, was employed.

The CEN standard does not specify the precise test jig design but states that the test jig shall function so as to minimise misalignments, twist and frictional forces applied to the test piece and recommend that one of the support rollers and the loading roller should be articulated so that they are able to rotate freely about an axis parallel to the specimen length. The rollers were not articulated in the present study. The CEN standard also states that the test apparatus should be capable of applying force at a constant loading or displacement rate, be equipped to record the peak load applied to

the test piece, and that the loading rate should be selected such that fracture occurs in a time period of between 5 and 15 seconds. In the present study, tests were carried out on an Instron 1380 loadframe under load control at a rate equivalent to 15 kN/min in a three-point bend fixture of 10 mm fixed span.

The CEN standard states that the strength of monolithic ceramics is strongly influenced by the machining procedure adopted during specimen preparation and are specific as regards specimen machining. Some flexibility on actual dimensions of the test-piece is allowed but maximum tolerances of ± 0.2 mm are quoted. They also state that the two long edges bounding the face of the test-piece should be chamfered at approximately 45° to a distance of 0.12 mm and that all grinding should be performed parallel to the length of the test-piece. A surface roughness of not greater than 2 μm is also specified. The CEN standard recommends that for statistical evaluation of strength data the minimum number of test specimens should be 30.
In the present study, twenty five specimens of nominal dimensions 50mm x 3mm x 3 mm were diamond ground from the as-received material. The tensile face was ground to a surface finish of $\leq 0.4\mu$m and the edges chamfered at 45°. Specimens were sufficiently long to allow three to four tests to be carried out on each, giving a total of 93 results in this particular case. Only the failure load was recorded and this enabled a strength value to be calculated from the standard beam-theory equation. The broken specimens were caught by means of a plastic bag secured around the base of the bend fixture and were examined in the SEM.

4.2.5 Determination of Fracture Mechanics Parameters

The fracture surface energy, γ, and its related stress intensity factor, K_{Ic}, may both be regarded as material parameters which describe the sensitivity of the strength of a material to the presence of flaws. As such, they are a key to the understanding of the mechanical properties of ceramics and to the designing of engineering structures. A

number of experimental techniques have thus been devised for their measurement. In this case a Single Edge Notched Beam (SENB) configuration was used.

A standard test method for measurement of the fracture toughness of metallic materials by SENB is defined in ASTM E 399[136]. The recommended test piece geometry is given in Figure 4.2. A crack of known length, a, is introduced by machining a notch into the specimen and is made to propagate by the application of an increasing bending moment in a three-point bend loading configuration. It is essential that the notch be narrow and effectively atomically sharp at the tip and that the size of the specimen should be large compared to the microstructural features of the material. A number of analytical approaches exist for the determination of fracture mechanics parameters from this type of test. That given in ASTM E 399 allows the calculation of the fracture toughness (K_Q) from the formula

$$K_Q = \left(\frac{P_Q S}{BW^{3/2}}\right) \cdot f\left(\frac{a}{W}\right) \qquad (4.3)$$

where P_Q is the failure load (if the load-displacement plot is linear to failure), S is the span, B the specimen width and W the specimen thickness (defined in Figure 4.2). The compliance function, $f(a/W)$, is dependent on the notch-to-depth ratio and loading configuration and for three-point bending where the span to depth ratio is 4:1 can be calculated from the equation

$$f\left(\frac{a}{W}\right) = \frac{3\left(\frac{a}{W}\right)^{\frac{1}{2}}}{2} \cdot \frac{\left[1.99 - \left(\frac{a}{W}\right)\left(1 - \frac{a}{W}\right) \times \left(2.15 - 3.93\frac{a}{W} + 2.7\left(\frac{a}{W}\right)^2\right)\right]}{\left(1 + 2\frac{a}{W}\right)\left(1 - \frac{a}{W}\right)^{\frac{3}{2}}} \qquad (4.4)$$

Both the crack length and specimen thickness should be greater than about $2.5(K_Q/\sigma_Y)^2$ for plane strain conditions to exist, where σ_Y is the yield stress of the

material. However, this is irrelevant for ceramics in view of their non-yielding behaviour.

Compliance analysis[6,11] is another method of obtaining fracture mechanics parameters from this type of test. This approach considers the force/deflection behaviour of samples over a wide range of crack sizes and requires no knowledge of the stress distribution within the specimen. Experimentally, one has to measure the specimen compliance, C, and plot it as a function of notch-to-depth ratio. For constant loading, the strain energy release rate, G, is then calculated from

$$G = \frac{P^2\left(\frac{dC}{da}\right)}{2B} \qquad (4.5)$$

where dC/da is the gradient of the above plot at a given crack length. If the load P is set to the maximum load P_Q, then a value of γ_i (the fracture initiation energy) can be calculated from G. This is only applicable if the specimen exhibits controlled or semi-controlled failure characteristics which is generally only achieved at large notch-to-depth ratios. For shallow notches the stored elastic energy in the test apparatus at the point of failure initiation is usually far in excess of that required to fracture the material completely.

The compliance method requires a large number of test specimens and is therefore not often employed. However, the use of the bend specimen is particularly economical on material and requires no method of gripping.

Specimens exibiting controlled or semi-controlled failure can also be used to calculate the energy for fracture propagation in ceramics - usually referred to as the work of fracture γ_f. Tattersall and Tappin[137] proposed the use of a bend-test bar with a chevron notch symmetrical about the centre line introduced by two saw-cuts which left a triangular cross-section at the point of maximum load. This means that the crack moves into an ever widening region of the material as it propagates through the specimen and gives a greater degree of control of crack propagation. The work of

fracture is then simply defined as the work done on the specimen during the complete fracture process, which is indicated by the area under the force/deflection curve to failure divided by twice the cross-sectional area at the notched part of the specimen. This test requires no knowledge of the stress distribution within the specimen nor the elastic properties of the material being tested. However, its major disadvantage is that it integrates the total energy requirement over the whole fracture process and gives only the work of fracture, which is most useful for comparison with other materials.

SENB tests were carried out on CAS specimens of dimensions 33 mm x 6 mm (W) x 4.7 mm (B) which were cut from the dynamic modulus specimens described in section 4.2.3 by slicing in half lengthways and then into three by means of a Buehler ISOMET fitted with water-cooled peripheral diamond wheel. A cutter speed of 3000 rpm and a cutting force of 150 g were used. This gave a total of 30 specimens which satisfied the criterion that the depth (W) must be at least equal to the width (B) (i.e. that $1 \leq W/B \leq 4$). Notches of lengths (a) 1.2 mm, 1.8 mm, 2.4 mm, 3.0 mm, 3.6 mm and 4.2 mm were cut along the centre of specimens using a 0.5 mm diamond slitting saw to give a/W ratios of 0.2, 0.3, 0.4, 0.5, 0.6 and 0.7 (5 off of each). Tests were conducted in an Instron 1195 fitted with a 500 kg load cell set to its most sensitive range (10 kg $\approx$ 1 N). A three-point bend fixture having a span (S) of 24 mm and the minimum available pin diameter of 6 mm were used. ASTM E 399 recommends that the span to depth ratio (S/W) be 4:1 and that the pin diameter (D) be $W/2 < D < W$. Both of these criteria were satisfied. Tests were carried out at the minimum cross-head speed of 0.5 mm/min and load-displacement curves were recorded by both chart recorder and computer (outlined in section 4.3.1). An unnotched specimen, having the same nominal dimensions as notched specimens, was tested under these conditions with a strain gauge fitted centrally to its narrow face and positioned opposite the central loading pin. This was to determine the relative specimen displacement to the cross-head deflection (as no suitable clip gauges were available). Values of elastic modulus and strain to failure were also obtained from this test.

4.3 Nicalon/CAS Composite Evaluation

4.3.1 Room-Temperature Tensile Test Procedure

Parallel-sided specimens of dimensions 100mm x 10 mm were machined from the as-received panels by means of a water-cooled peripheral diamond wheel. In the case of the two $(0)_{12}$ panels, specimens were cut at angles of 0°, 5°, 10°, 20°, 30°, 45° and 60° to the direction of fibre reinforcement. A total of three specimens of each orientation were obtained from the two panels with the only cross-check being between the 0° samples, as a result of material economy. In the case of (0/θ/0) panels, all specimens were cut parallel to the direction of fibres in the outer plies.

Abraded aluminium end tabs were bonded to the specimen ends with epoxy resin to give an overall gauge length of 50 mm. Small-diameter wires were positioned between the specimen and end tab to control the glue-line thickness and to prevent resin escaping during curing. Biaxial strain gauges manufactured by Micro-Measurement and of the type CEA-06-062WT (120 or 350 Ω resistance) were bonded centrally to the broad face of the specimen by using the standard technique of cleaning, etching, neutralising, marking, positioning, catalysing and bonding (with cyanoacrylate adhesive). Any excess glue was removed with solvent. In the case of one 10° off-axis test, specimens were fitted (additional to a uniaxial gauge and on the opposite face) with a three-way strain gauge rosette to give strain measurements at 0°, 45° and 90° to the loading axis and so that a measure of the intralaminar shear stress might be obtained according to the test devised by Chamis & Sinclair[56] for polymer-matrix composites described in Appendix 1.

Specimens were tested in an Instron 1195 universal testing machine fitted with a 500 kg load cell and wedge-action grips, at a cross-head speed of 0.5 mm/min. Both longitudinal and transverse strains, together with the load output from the Instron, were monitored throughout each test. Strain gauges were connected to separate

channels on a series of rack-mounted strain gauge amplifiers and the data recorded by a PC fitted with custom-built software. Data files were converted to ASCII files after each test and loaded into a spreadsheet for analysis. The apparatus is shown schematically in Figure 4.3.

The strain is measured by the change in resistance of the strain gauge during deformation by connecting it within a Wheatstone bridge. The output voltage of the Wheatstone bridge is then amplified, numerically converted and stored in a computer file. The ouput voltage, V, is converted to strain directly from the following formula (derived from the equation of the Wheatstone bridge and the electrical components values):

$$\varepsilon_{corr} = \frac{2V}{k\,(500 - V)} \qquad (4.6)$$

where ε_{corr} is the corrected strain and k the gauge factor (supplied by the manufacturer on each packet of strain gauges). The sensitivity of the gauge is directly dependent on the amplification gain. Only 200 and 1000 gains were available on the equipment used in the present study. The 200 gain was selected for longitudinal strain measurement and 1000 for transverse strain measurement. Equation 4.6 is calculated for a 200 gain and V should be divided by 5 if the 1000 gain is used.

In an attempt to develop a standard tensile test method for brittle-matrix composites, Morrell & McCartney[138] have highlighted a number of possible sources of error with respect to the misuse of strain gauges. These errors may be due to poor bonding of the gauge to the specimen (which they state depends on the skill of the operator) and the use of an inaccurate gauge factor. Great care was taken in bonding the strain gauges to ensure accuracy of alignment and good adhesion. However, the surface etchant seemed to have little effect and it was thought that the use of a more abrasive technique might have implications for the onset of matrix cracking. In the case of the gauge factor, errors can arise when the gauge is calibrated for a material of different

Poisson's ratio, e.g. aluminium or steel, than that on which it is to be used. Errors are due to the gauge output being affected by the lateral strain, which is normally taken into account by the calibration. If used on a material of significantly different Poisson's ratio, a systematic error is introduced. In this case, gauges of '06' category were chosen, indicating that the gauges were calibrated on steel[139]. This error can be compensated for by using the following equations:

$$\varepsilon_x^{true} = \varepsilon_x - k_t \varepsilon_y$$

$$\varepsilon_y^{true} = \varepsilon_y - k_t \varepsilon_x \qquad (4.7)$$

where ε_x and ε_y are the longitudinal and transverse strains (respectively) measured by a 0/90 strain gauge rosette, and k_t is the transverse sensitivity factor supplied by the manufacturer with the strain gauges.

Another source of error can be due to a change in the resistance of the strain gauge with temperature. This may be compensated for by the use of a similar but unstressed gauge in place of the dummy gauge, thus cancelling out any temperature effects. The facilities to do this were not available nor were they thought necessary for the present short-duration, room-temperature tensile tests.

In the present study, 350 Ω gauges were used where possible as this reduces lead-wire effects and improves the signal-to-noise ratio in the gauge circuit[139].

4.3.2 Acoustic Emission Monitoring

The phenomenon of sound generation in materials under stress is termed acoustic emission (AE) and is produced by the release of elastic energy within the material during deformation and cracking[140]. These elastic or stress waves can be detected, usually in the form of discrete pulses, by a piezoelectric transducer placed on the material surface. Acoustic emission pulses are generally assumed to be of the form of a decaying sinusoid that can be characterised in a number of ways, as depicted in

Figure 4.4, e.g. by peak amplitude, rise time, frequency and energy - together with the rate of emissions received and the total count number. Early studies of acoustic emissions included 'ringdown counting', a method in which the number of times a pulse exceeds the threshold voltage is counted. This parameter is a measure of the duration of a signal and is indirectly dependent on amplitude but is also a function of the signal frequency and attenuation. More commonly, the severity of an event is measured by energy analysis, a measure of which can be obtained by squaring the initial pulse amplitude (peak amplitude).

In the current study a small, flat, copper-cased broad-band acoustic emission transducer made by Rolls-Royce and having a resonant frequency in the range 200-400 kHz was secured to the specimen face by a rubber-lined clip and good acoustic coupling was ensured by the use of silicone grease. The transducer was then connected via an AECL 60 dB pre-amplifier, fitted with 0.125 - 2 MHz band-pass filters and placed on a rubber mat, to a Marandy MR1004, 25 channel amplitude sorter and ringdown counter. This set-up is depicted in Figure 4.3. The Marandy AE Analyser incorporates a highly accurate amplitude level and threshold digital setting (± 0.1 dB) and has four analogue inputs for monitoring load and strain data (as described in section 4.3.1). The Marandy sorts the AE events with maximum amplitude above 10 mV into 26 amplitude levels each of 2.4 dB width. Events with an amplitude greater than 10 V are registered in Channel 26 as 'over-range'. The decibel scale gives the voltage amplitude (V) relative to a reference voltage (V_i), which in this case is the minimum instrument threshold of 10 mV, by the following formula

$$\left(\frac{V}{V_i}\right) \text{ ratio in decibels } = 20 \log_{10}\left(\frac{V}{V_i}\right) \qquad (4.8)$$

Thus Channel 1 registers voltages from 10 mV to 13.2 mV, Channel 2 registers voltages from 13.2 mV to 17.4 mV, and so on.

The data were recorded by an IBM-compatible PC fitted with custom-built software and stored as a *.AEB binary datafile. By default, the Marandy updates the *.AEB file every second although this can be increased to up to every 5 minutes. In addition to the time, load, strain and AE event count, the *.AEB file also contains cumulative ringdown counts, event and ringdown rates, and cumulative event counts. After each test the data file was converted to an ASCII file in the form of comma separated variables (*.CSV) and subsequently loaded into a package for analysis.

Many workers have tried to relate the acoustic emissions generated by composite materials during testing with individual failure mechanisms, for example Rotem[141], Valentin et al[142] and Guild et al[143]. In these cases tensile tests on resin-matrix composites were monitored for acoustic emissions. Different failure mechanisms were induced by testing samples with fibres orientated at different angles to the loading axis. In all cases the amplitude distribution of acoustic emissions from each test was analysed and attempts to correlate the distribution with the observed failure mechanisms were made. A method of analysing amplitude distributions was developed by Pollock[144] and is described in Appendix 2.

A number of errors in AE detection can be introduced as a result of electromagnetic interference (radio signals and from electrical cables) and mechanical noise interference (from the testing machine). The measurement of mechanical background noises can be reduced by pre-setting an amplitude threshold, as this type of interference is generally of low amplitude and short duration. A major source of error in composite materials is due to signal attenuation within the material. It should be noted that the waveform detected by the AE equipment is an electrical response resulting from the excitation of the piezoelectric crystal within the AE transducer by a stress wave. Modifications to the AE wave occur during propagation through both the material and the transducer due to discontinuities or from reflections at free surfaces. Composite materials, in particular, offer many internal surfaces for wave scattering

and this can cause a major reduction of energy in the wave and thus the detected energy of the wave.

The technique is therefore highly sensitive to experimental conditions and the AE testing of different specimens must be done under comparable circumstances. The use of different AE systems to compare similar responses must be treated with extreme caution.

4.3.3 Damage Monitoring Techniques

A number of unidirectional and off-axis tests were subjected to discontinuous loading to progressively higher strain levels, up to ultimate failure of the composite. Stress-strain data were measured and acoustic emissions monitored during both loading and unloading to each level.

A method often employed for the detection and monitoring of crack growth in metallic materials is that of producing a replica of the specimen surface on acetate film and examining it microscopically. This method was used in the present study and is described below. Specimen edges were polished prior to testing by using the routine for metallographic preparation (described in Appendix 3). Edge replicas were taken prior to testing to determine the as-received, unloaded microstructure. Specimens were loaded to the desired strain and then held at that level, although some instantaneous relaxation did occur. The acoustic emission transducer had to be detached and the silicone grease removed with acetone in order that replicas could be taken. Microscope slides and strips of cellulose acetate sheet were cut to approximately 50 mm length so that the whole of the gauge length could be sampled with one replica. For each replica, a microscope slide was wetted with acetone, and an acetate sheet applied followed by a liberal amount of acetone. The assembly was then pressed against the polished edge of the loaded specimen and held there until dry. After the dried film was removed from the sample the top and bottom of the specimen were noted on each replica so that damage could be related to the specimen

configuration. The acoustic emission transducer was then replaced and the specimen unloaded. Unloading data were recorded as a separate file in each case. Replicas were subsequently examined by optical microscopy at a magnification of x 160 and the crack spacings measured. As mentioned in section 3.4, the majority of workers have counted cracks over a given gauge length generally of about 5 - 20 mm. In the present study, when possible, the distance between neighbouring cracks in a given line along the specimen was measured over the whole gauge length by means of a graticule eyepiece which was calibrated at the selected magnification with a stage micrometer. At low strain levels, when only a few widely-spaced cracks had formed, cracks had to be counted over the whole gauge length. Measurement of the actual spacing of these cracks would have had to be carried out at low magnification, making the cracks more difficult to determine, and it was thought that this would introduce greater error. However, the crack counting method gave no information about the crack spacing distribution.

In the case of (0/θ/0) laminates, the material was too thin and delicate either to edge-polish prior to testing or to apply the replica technique to. In this case, a number of separate specimens were loaded to different strain levels. The end tabs were then removed by machining carefully and the entire specimen set in Epofix cold-setting resin. The samples were subsequently polished by the technique given in Appendix 3 and the cracks examined as above. Even at x 160 magnification cracks in these specimens were difficult to see and had to be counted over the whole gauge length, again in order to minimise errors.

4.3.4 Fibre Volume Fraction and Orientation Determination

The fibre volume fraction was measured by image analysis of polished sections with the equipment depicted in Figure 4.5. In the case of unidirectional composites, sections were taken from material within the end tabs of tensile test specimens (with the end tabs removed), set in cold-setting Epofix resin with the fibres situated

perpendicular to the flat surface of the mount, and polished according to the routine in Appendix 3. The specimens were placed on the stage of an optical microscope and a x80 magnified image was transferred via a high-resolution black and white camera to an 8 bit frame grabber in a 486 IBM-type PC and displayed on a monitor. The image was frozen and then sharpened by filtering. A threshold grey-level was set so as to separate the fibres from the background and a 'percent area' option selected which counted the number of pixels with grey levels above and below the threshold - the ratio of which gave the area fraction of fibres to matrix which was assumed to be equal to the volume fraction. Figure 4.6 demonstrates that, provided the fibres present elliptical cross-sections to the reference surface, the measured fibre volume fraction of unidirectional composite will be independent of fibre orientation and will be equal to the true fibre volume fraction. However, as Figure 4.7 demonstrates, for the measured fibre volume fraction of angle-ply laminates to be equal to the true value, measurements must be taken from sections cut at $-(\theta/2)$ to the direction of 0° fibres. In view of the difficulty of cutting such sections accurately, and assuming that all (0/θ/0) plates were made in the same batch from the same pre-preg, fibre volume fraction measurements were made on $(0)_3$ and (0/90/0) material only, with the latter cut at 45° to the outer fibre direction.

Measurement of the fibre orientation in the θ° ply of (0/θ/0) laminates was made by taking sections as above, with the outer 0° fibres situated perpendicular to the reference surface, and by measuring the major and minor axis lengths of the fibre ellipses presented to the surface. The orientation of the fibres to the surface is then calculated from the projected fibre dimensions, by the procedure shown in Figure 4.8, and by assuming that the fibres orientated at angle θ to the reference surface are circular in cross-section and that the projected cross-section is elliptical so that the minor axis length equals the fibre diameter. Work by Toll & Anderson[145] on the image analysis of injection-moulded composites demonstrated that greater precision in fibre orientation measurement could be obtained by substituting $(4A)/(\pi b)$ for the

minor axis length (where A is the area of an ellipse with major axis length b). This arises from the fact that the lengths a and b can only assume whole numbers of pixels, with a (the smaller measurement) being more prone to error.

The 'region of interest' (ROI) was selected so that it contained only fibres in the θ ply. Prior to measuring the projected dimensions of fibres within the ROI, it was necessary to ensure that the images of all fibres were whole and discrete. This required the use of a 'separate blobs' sub-routine. The first step was to produce a binary image based on a previously set threshold. Each 'blob' (in this case a fibre) was then dilated by one pixel to remove any holes within it. By then eroding back to the original size (i.e. removing one pixel) the holes remained removed. Further erosions were carried out until isolated pixels and tendrils were removed and all blobs were separated. On enlarging to their original size the blobs remained separate and could be measured as whole and disrete entities. All blobs touching the ROI were rejected. Measurements were made of the lengths of the major and minor axes and of the area of each selected fibre within the ROI and the data automatically exported to a computer spreadsheet package for subsequent analyis. Similar measurements were made within the 0° plies of the same section in an attempt to determine the accuracy of the section alignment.

4.3.5 Interface Friction Stress Measurement

The nature and strength of the fibre-matrix interaction is of crucial importance in controlling the properties of ceramic-matrix composites, with a weak interface being required to give the desired toughness enhancement over the monolithic ceramic. In order to relate the bulk mechanical properties of the composite to the interface properties, it is necessary to be able to determine the strength of the fibre-matrix interaction. The interfacial friction stress (τ) is a measure of the resistance of the interface to fibre sliding, and hence a low value of τ relates to a weak interface.

Early estimates of the interfacial friction stress were obtained from measurements of the saturation crack spacing in composites exhibiting multiple matrix cracking and by using a rearrangement of the Aveston Cooper Kelly[4] equation for x' (see section 2.4.2)

However, a technique for measuring the interfacial friction stress at individual interfaces which uses a Vickers microhardness tester was later developed by Marshall[71]. This method involves loading a Vickers pyramid indentor onto the centre of a fibre in a polished section where the fibres are normal to the reference surface. The applied force, F, causes the fibre to slide along the fibre/matrix interface over a distance L and depresses the fibre below the level of the surface by a distance U - as depicted in Figure 4.9. For specimens in which the slip length, L, is small compared with the thickness of the specimen, i.e. in which the fibre does not protrude from the opposite surface, the interfacial friction stress may be calculated from the expression :

$$\tau = \frac{F^2}{4\pi^2 U R^3 E_f} \qquad (4.9)$$

where R is the fibre radius and E_f is the elastic modulus of the fibre (taken as being about 180 GPa for Nicalon).

The fibre displacement, U, is defined as occurring whilst the fibre is under load. This cannot be measured directly by the microindentation technique, but is done by choosing the indentation load so that the corners of the indentation contact the matrix at the edges of the hole left by the depressed fibre. The displacement may then be calculated by geometric considerations (as defined in Figure 4.9), such that

$$U = (b - a)\cot \psi \qquad (4.10)$$

It should be noted that 2ψ is defined as the angle between diagonally opposite corners of the indentor and is 148° for the Vickers pyramid (not the 136° angle between the

opposite faces of the indentor used in hardness calculations). It should also be noted that, by this method, part of the total load is supported by the matrix. The force, F, applied to the fibre can be calculated from

$$F = 2a^2H \qquad (4.11)$$

where H is the fibre hardness which may be obtained from independent measurements of fibre indentations carried out at loads sufficiently low that fibre sliding does not occur.

Equation 4.9 which is used to calculate the interfacial friction stress is derived from a force balance and assumes that the matrix does not slip relative to the surrounding fibres. Any elastic depression of the matrix is also neglected, although Marshall estimates this to be about two orders of magnitude smaller than the observed fibre depressions. It is also assumed in the derivation of equation 4.9, that the slip length is very much greater than the fibre radius and that stresses at $z > L$ may be neglected.

Marshall & Oliver[102] further developed these ideas by using an ultra-low load or nano- indentor. This technique allowed the indentor forces and fibre displacements to be measured continuously during loading, unloading and load cycling at loads sufficiently small to prevent the indentation from extending into the matrix. Mandell, Hong & Grande[103] adapted a microdebonding tester, originally developed for polymer composites, for the measurement of interfacial bond strength (rather than interfacial shear strength) in glass-matrix- and glass-ceramic-matrix composites. The apparatus used a rounded indentor to apply sequentially higher loads in steps until debonding occurred. Debonding was identified by optical microscopy between loading steps. Finite element analysis was used to give an approximation of the stress field at the interface at the debonding load. Further loading after debonding enabled the friction stress to be calculated in the same way as before. Interfacial friction stress measurements made by Marshall, Marshall & Oliver and by Mandell, Hong &

Grande, using the three separate indentation techniques outlined above, have obtained comparable values for a Nicalon/LAS composite.

In the present study a LECO M400 Vickers microindentor was used to measure the interfacial friction stress of samples of unidirectional composite by the Marshall technique described above. The specimens were mounted in Epofix cold setting resin with fibres normal to the reference surface and polished according to the routine in Appendix 3.

Plate I.D. No.	Lay-up	Laminate Thickness (mm)	Nominal Ply Thickness (mm)
# 9012101 L	$(0)_{12}$	2.3	0.19
# 9012102 L	$(0)_{12}$	2.3	0.19
# 8924207 L	$(0)_3$	0.52	0.17
# 8913927 L	(0/5/0)	0.52	0.17
# 8913928 L	(0/10/0)	0.52	0.17
# 8917081 L	(0/20/0)	0.52	0.17
# 8913930 L	(0/45/0)	0.52	0.17
# 8913931 L	(0/90/0)	0.52	0.17

Table 4.1: Nicalon/CAS composite material supply

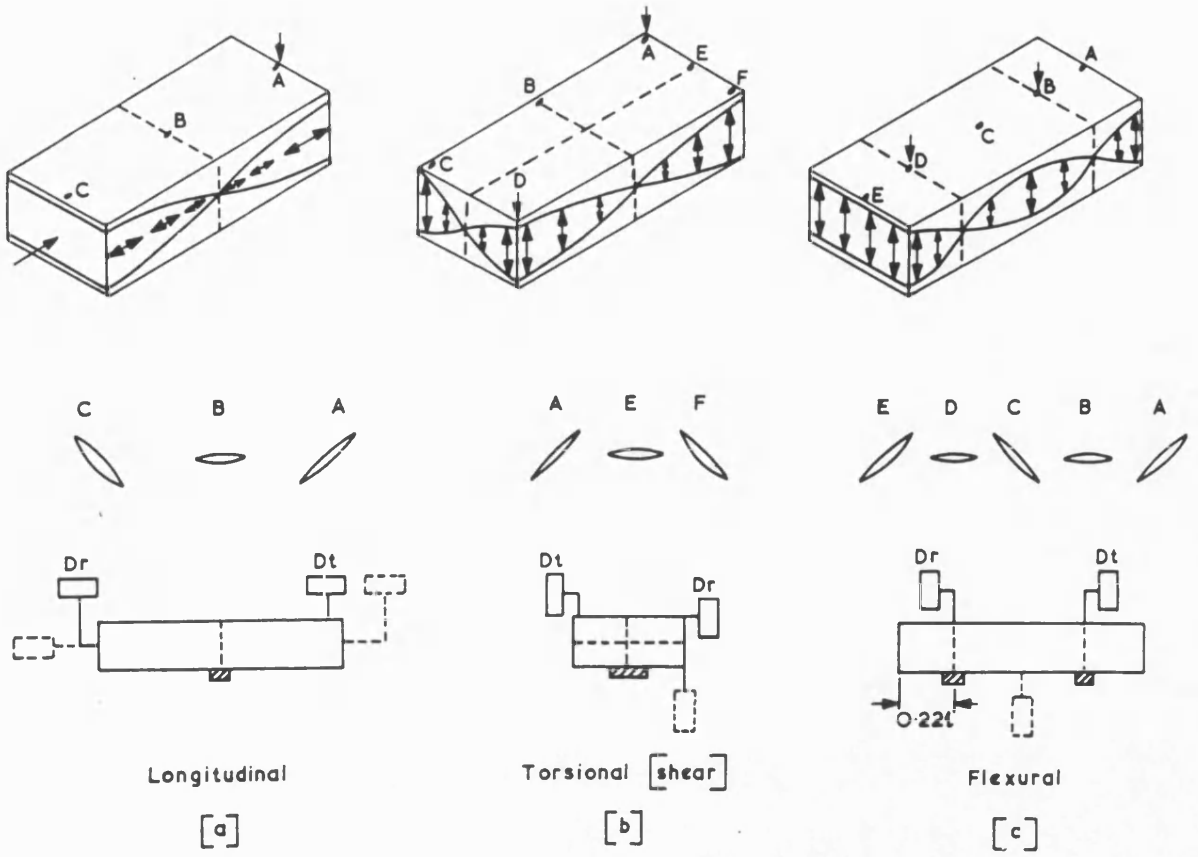

Figure 4.1: Schematic representation of the vibration modes of a rectangular prism (after Davis[134])

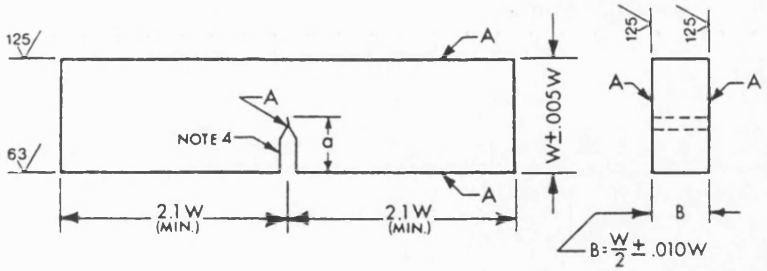

Figure 4.2: Standard specimen for single edge-notched bend tests (according to ASTM E 399[136])

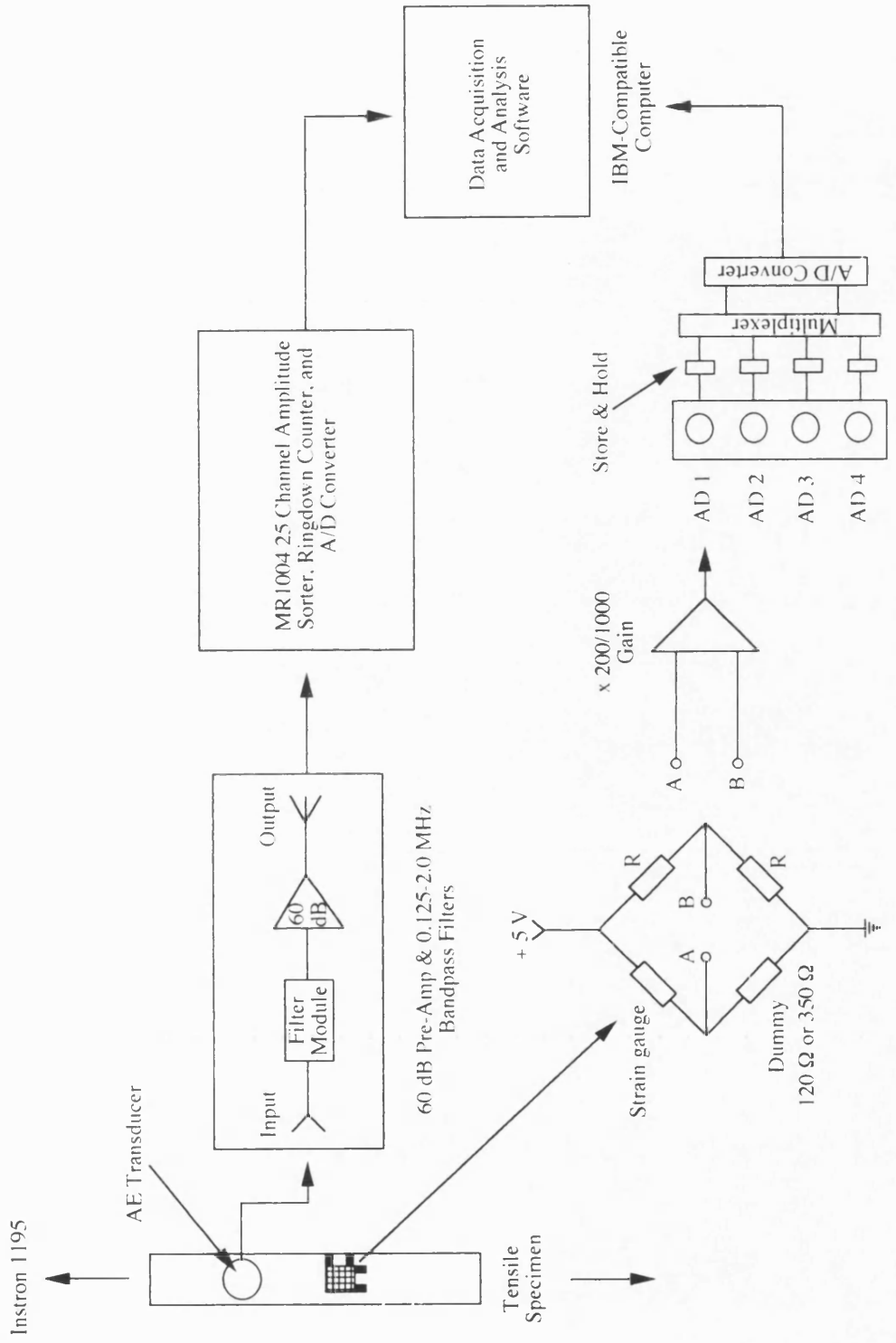

Figure 4.3: Diagrammatic representation of Marandy MR1004 strain-gauge and AE monitoring equipment

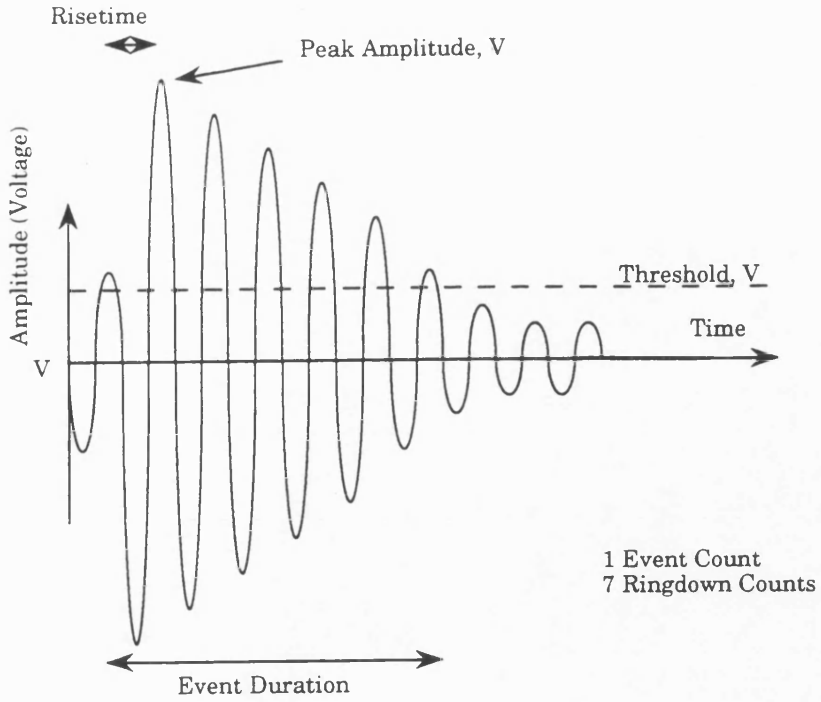

Figure 4.4: Idealised AE event showing definition of terms

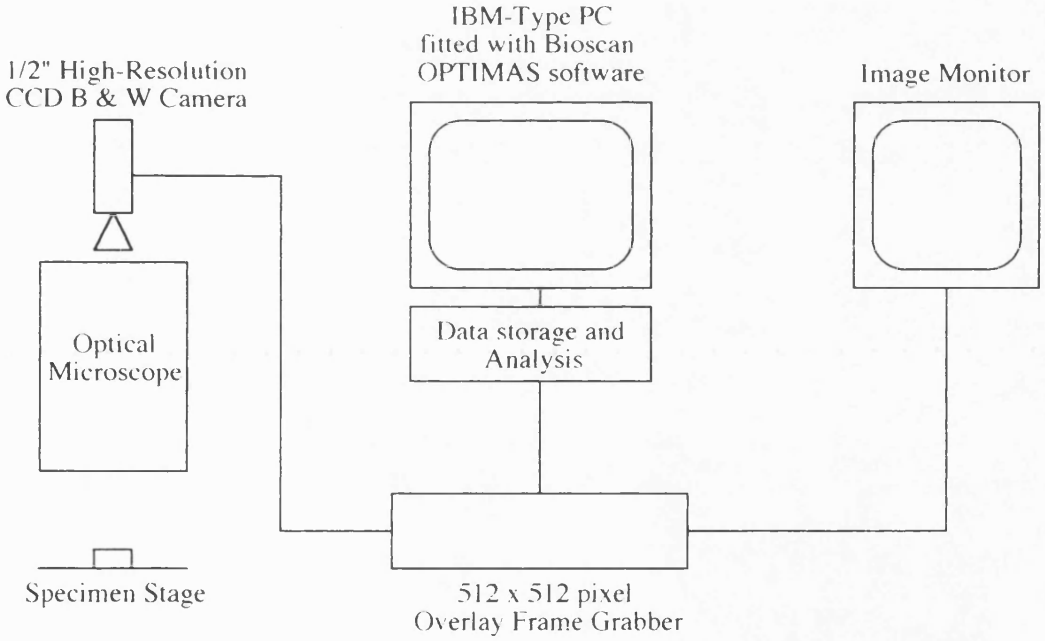

Figure 4.5: Schematic representation of image analysis equipment

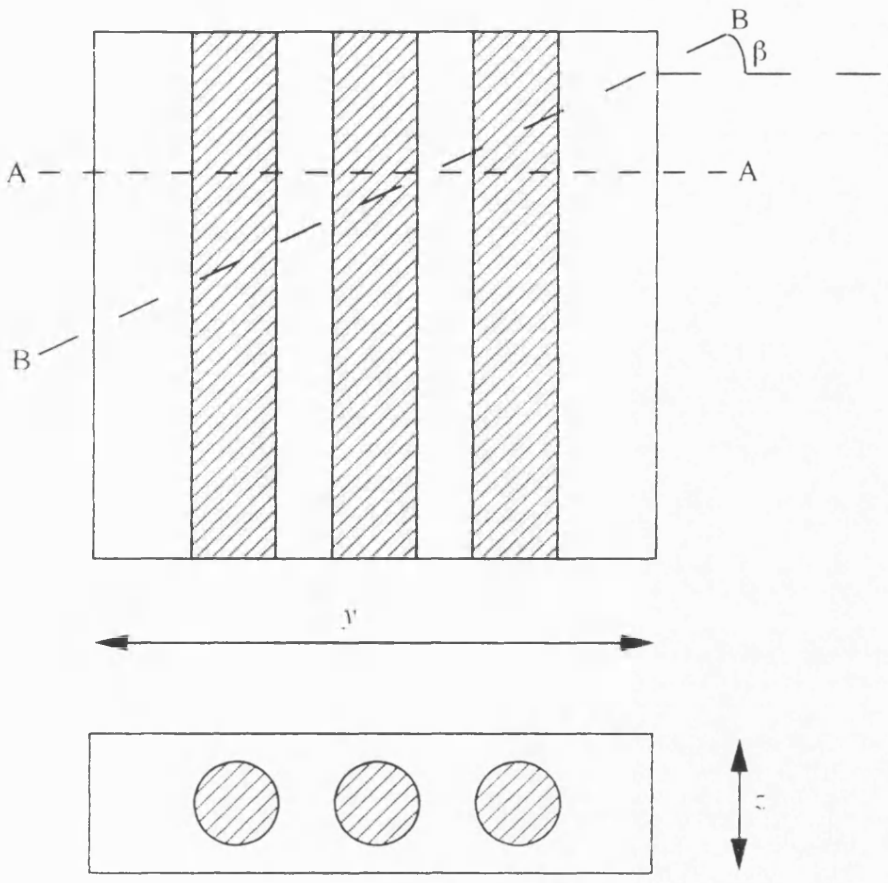

Section AA

$$A_f = \frac{3\pi r^2}{y \times z} \qquad A_f = V_f$$

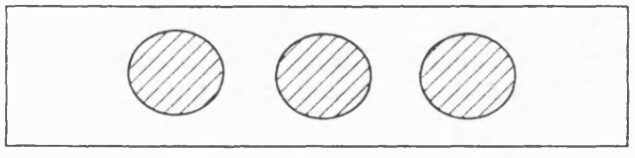

Section BB

$$A_f = \frac{\frac{3\pi r^2}{\cos\beta}}{\frac{y}{\cos\beta} \times z} \qquad A_f = A_f = V_f$$

Figure 4.6: Diagram showing the effect of section angle on the measured fibre volume fraction of unidirectional composite laminates

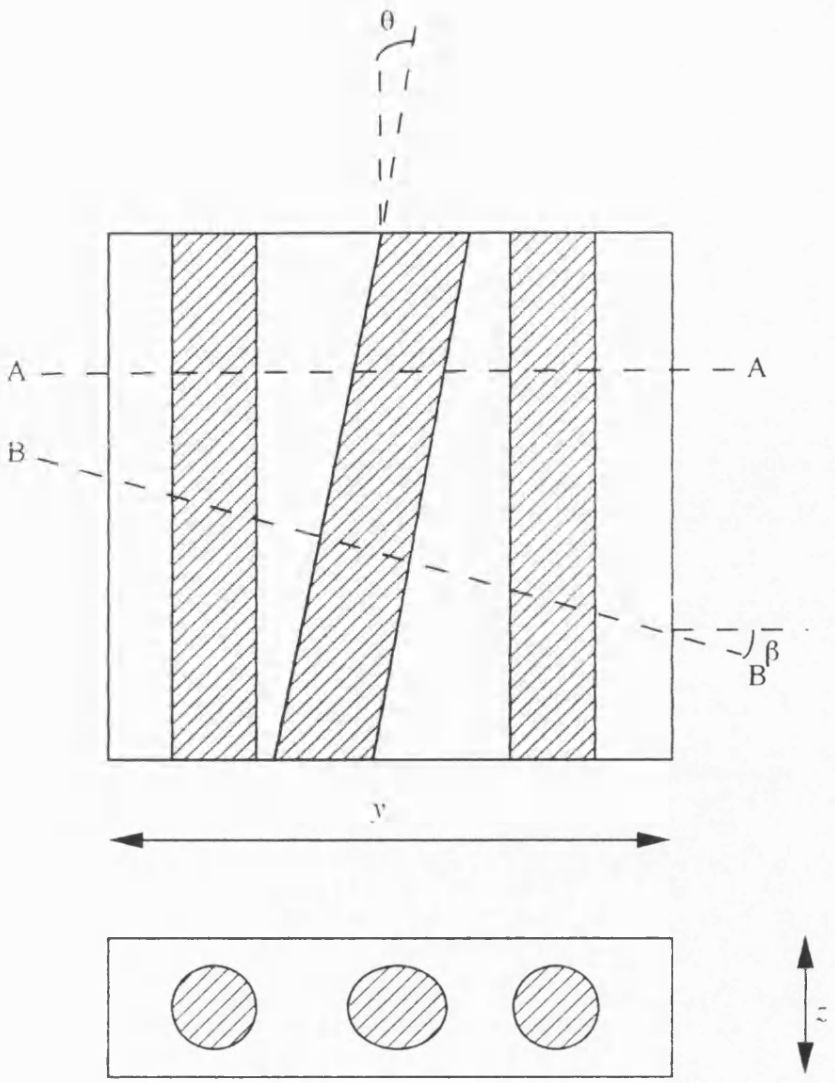

$$A_f'' = \frac{2\pi r^2 + \frac{\pi r^2}{\cos\theta}}{y \times z} \qquad A_f'' \neq A_f \neq V_f$$

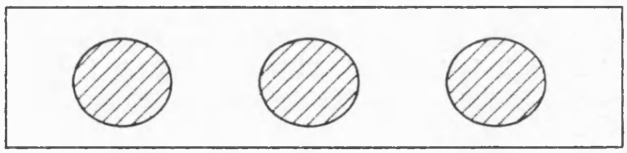

Section BB

$$A_f''' = \frac{\frac{2\pi r^2}{\cos\beta} + \frac{\pi r^2}{\cos(\theta+\beta)}}{\frac{y}{\cos\beta} \times z} \qquad A_f''' = A_f = V_f \quad \text{for} \quad \frac{\cos\beta}{\cos(\theta+\beta)} = 1$$

Figure 4.7: Diagram showing the effect of section angle on the measured fibre volume fraction of angle-ply composite laminates

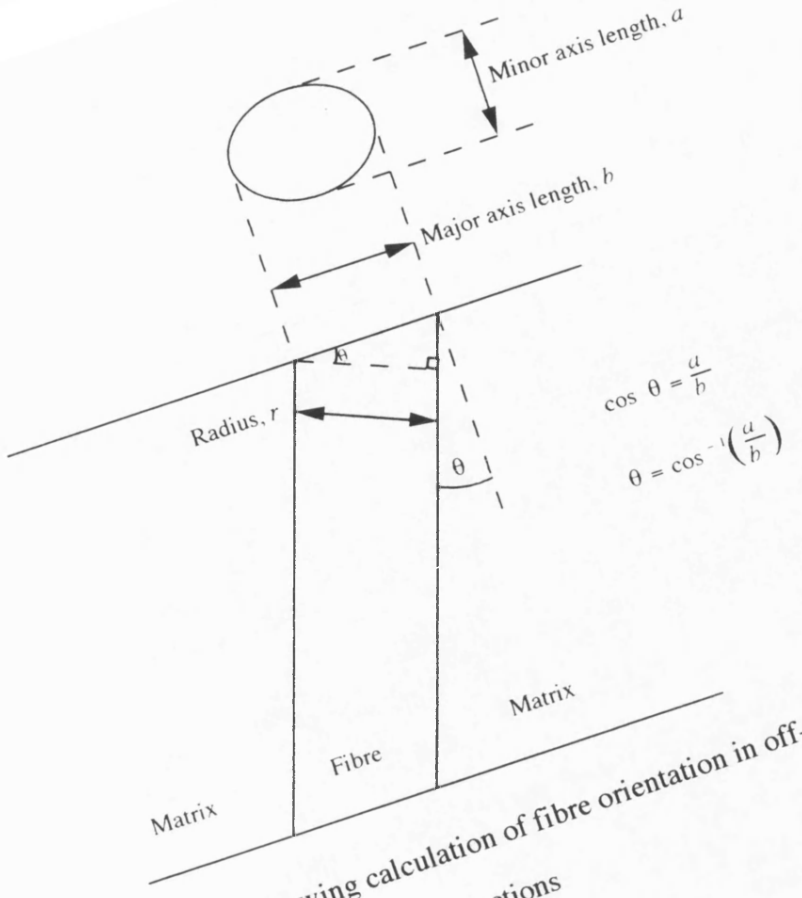

Figure 4.8: Diagram showing calculation of fibre orientation in off-axis composite sections

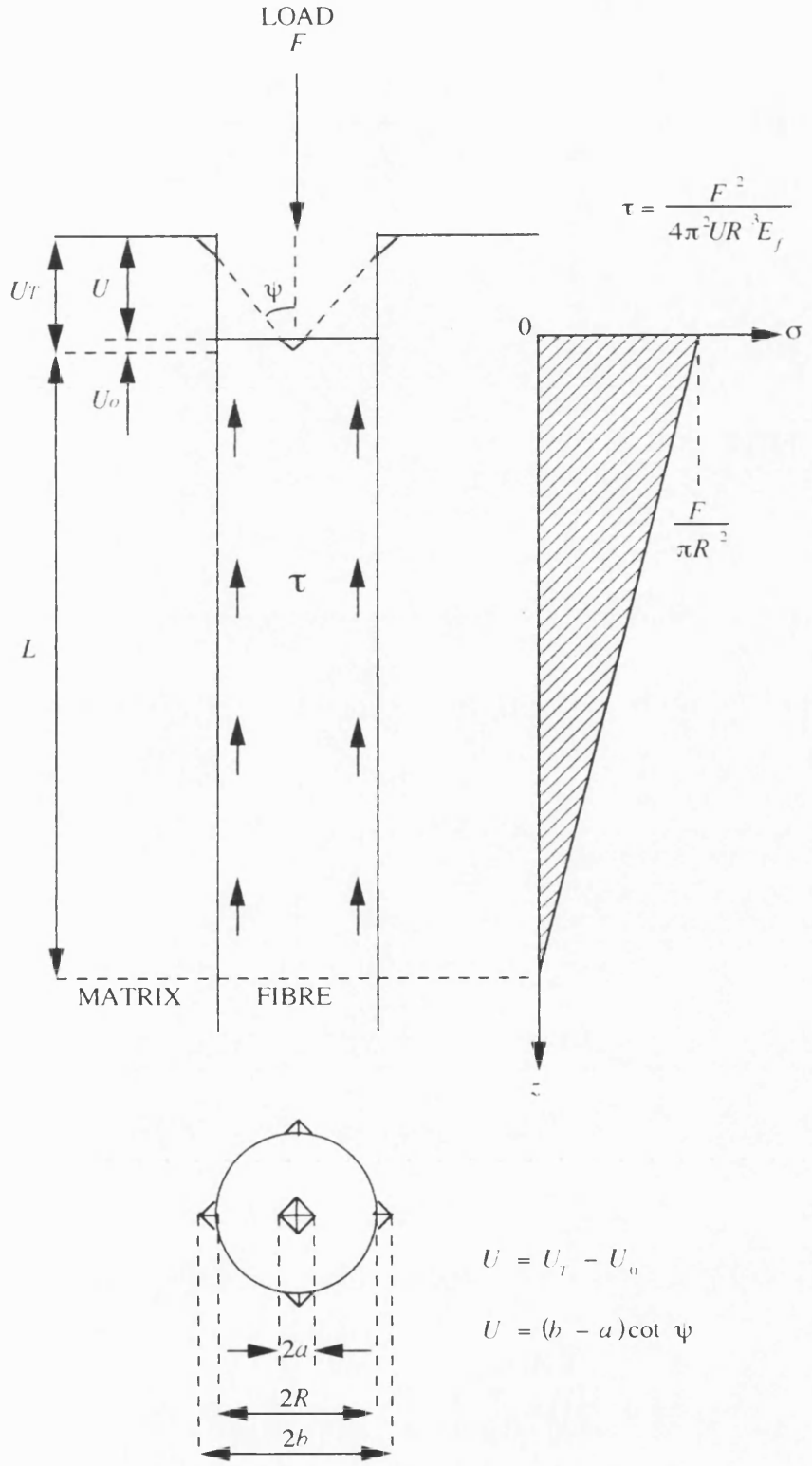

Figure 4.9: Schematic representation of the microindentation test as a method of measuring fibre-matrix interfacial friction stress

CHAPTER 5 : MONOLITHIC CAS

5.1 Introduction

A number of models are available in the literature which consider the matrix cracking behaviour of unidirectional brittle-matrix composites loaded parallel to the fibre direction, and these have been discussed in Chapter 2.

Attempts have been made by many workers to describe the stress-strain behaviour of Nicalon fibre-reinforced CAS composite by use of these models and these have been outlined in Chapter 3. However, it became apparent that the accuracy of predictions based on these models was highly sensitive to the chosen values of matrix properties, in particular the matrix fracture surface energy (γ_m), and that those values had generally been assumed. Little experimental data exists on the properties of monolithic CAS and an attempt to address this is made in the present chapter.

Initially it is necessary to establish whether the monolithic CAS made available is of the same structure and composition as that reported for the Nicalon/CAS composite matrix. The results of these findings are presented and discussed, together with the experimentally determined physical, elastic and mechanical properties of the monolithic CAS.

5.2 Results

5.2.1 Microstructural Analysis

X-ray diffraction analysis of the bulk CAS revealed that the material was highly crystalline and that the major constituent was anorthite ($CaAl_2Si_2O_8$), together with much smaller amounts of Al_2O_3 and possibly Zr_3Si_2. SEM examination of a polished sample (Figure 5.1 a)) showed that the material was quite porous (although it was thought that many of the surface features were due to polishing damage). Back-scattered electron imaging of the sample in the SEM (Figure 5.1 b)) revealed a microstructure of evenly-distributed white particles on a grey background, with

darker areas corresponding to the porosity. Quantitative analysis by EDS and WDS in the electron-probe microanalyser showed that the sample contained 45 wt.% oxygen, 20 wt.% aluminium, 20 wt.% silicon, 13 wt% calcium and 2 wt.% zirconium. The light phase was found to be rich in zirconium and the grey background corresponded to anorthite. The zirconium-containing compound was thought to have been added to the glass-ceramic as a nucleating agent. Further examination of the specimen revealed the presence of a few isolated features, as shown in Figure 5.2, which were thought to be unfused zirconium-rich particles. Analysis of a x 800 optical image of a specimen that had been polished in accordance with the routine for composite material outlined in Appendix 3 gave a porosity level of the order of 1 % with the largest pores being approximately 18 - 25 μm in diameter.

5.2.2 Physical and Elastic Properties

The values of Young's modulus (E), shear modulus (G) and Poisson ratio (ν) for the monolithic CAS determined by resonant frequency are given in Table 5.1, together with measured values of density (ρ) and thermal expansion coefficient (α). The thermal expansion coefficient was found to be constant up to 900°C.

5.2.3 Flexural Strength Properties

Specimens failed in a flexural manner from the tensile face with a 'mirror, mist and hackle' fracture typical of monolithic ceramics - as shown in Figure 5.3. The average bend strength and standard deviation of the 93 samples are given in Table 5.1 and a Weibull treatment of the data is shown in Figure 5.4. A Weibull modulus of 5.4 was obtained from the gradient of the graph, indicative of a large degree of scatter in the results. Fractography of selected samples suggests fracture initiation to have been caused by features or flaws in the microstructure of the order of 20 μm in diameter (as shown in Figure 5.5), although this was by no means definitive.

5.2.4 Single Edge-Notched Bend Test Results

The stress-strain curve obtained from the un-notched specimen, with the strain reading being obtained directly by strain-gauge measurement, is given in Figure 5.6. The stress-strain curve is linear to failure with an ultimate strength of 230 MPa, a modulus of 111 GPa and a strain to failure of 0.21 %. The deflection calculated from either the strain gauge or load readings, using simple beam-theory equations, was found to be of the order of 1/10th that of the corresponding cross-head movement and it was therefore not possible to perform a compliance analysis on data obtained from tests on notched specimens. Figures 5.7 shows representative force-deflection curves from specimens with notch-to-depth ratios of ≤ 0.4. All specimens failed catastrophically into two pieces at the maximum load. A small number of specimens with notch-to-depth ratios of 0.5 and 0.6 exhibited some degree of stable crack growth and continued to deflect after the maximum load. Representatve force-deflection curves of specimens exhibiting this type of failure are shown in Figure 5.8. The peak load in these cases was less than that observed for catastrophic failures of the same crack length - as depicted in Figure 5.9. The gradient of the force-defelection curve for each specimen was measured and the variation of this parameter with notch-to-depth ratio is given in Figure 5.10. It should be noted that although this quantity is referred to as 'stiffness' it includes an element corresponding to the stiffness of the test apparatus and as such can only be discussed relatively. However, a generally decreasing trend with increasing a/W is observed. Figure 5.11 shows the variation of fracture energy (obtained by calculating the stress intensity factor from the maximum load by using equation 4.3).

5.3 Discussion

Microstructural analysis of the monolithic CAS has shown that the material consists almost entirely of the crystalline phase anorthite with small amounts of alumina and a

zirconium-containing compound. These results are in excellent agreement with the findings of Bleay and Scott[116] (as discussed in section 3.4) on the structure and composition of the Nicalon/CAS composite matrix. It is thought that the zirconium-containing compound resulted from the addition of ZrO_2 as a nucleating agent.

The Young's modulus of the monolithic CAS measured by both resonant frequency and mechanical methods (106 GPa and 111 GPa respectively) was found to be around the upper limit of the range quoted by the manufacturer (Table 3.3). It is expected that dynamic methods would generate higher modulus values than mechanical methods in view of the low strains involved in the former and the unlikelihood of any damage being sustained. However, the mechanical value is based on the results of only one test.

When considering the measured density of the monolithic CAS, at 2.86 gcm^{-3}, it becomes apparent that this is greater than the theoretical density of anorthite (2.76 gcm^{-3}) and also greater than that quoted by the manufacturer (2.45 gcm^{-3}). However, whilst the presence of a zirconium-containing compound together with Al_2O_3 (having densities of about 6.6 gcm^{-3} and 3.9 gcm^{-3} respectively[146]) would increase the value relative to the theoretical density, the presence of porosity would cause a decrease in the value.

For a homogeneous brittle solid it is possible to relate the three-point bend and tensile strengths of a constant volume of material with a given probability of survival by the expression:

$$\frac{\sigma_{3b}}{\sigma_t} = \left[2(m+1)^2\right]^{1/m} \qquad (5.1)$$

Taking the mean bend strength (σ_{3b}) of 290 MPa and a Weibull modulus, m, of 5.4, this gives a predicted tensile strength (σ_t) for the same volume of material as 128

MPa which is in the middle of the range quoted by the manufacturer for monolithic CAS.

By fractographic examination of monolithic bend-test specimens, the critical initial flaw size, $2C$, was determined to be of the order of 20 μm. From this, a crude estimate of the matrix fracture surface energy, γ_0, can be derived from consideration of the Griffith criterion in its simplest form:

$$\sigma_f = \left(\frac{2E\ \gamma_0}{\pi C}\right)^{1/2} \qquad (5.2)$$

where σ_f is the fracture stress (291 MPa) and E the modulus (106 GPa). This gives an estimated value for the fracture surface energy of 12.5 Jm^{-2} which is in excellent agreement with that measured from chevron-notched specimens by Beyerle et al[107] and which is given in Table 3.2.

In the case of single edge-notched bend test results, only a very small number of specimens exhibited what might be considered stable crack growth. In the majority of cases specimens failed catastrophically, as the stored elastic energy of the test apparatus at the point of fracture initiation was far in excess of that required to cause complete failure. Elastic deformation of the test jig resulted in the cross-head displacement being far greater than the displacement of the specimen and rendering measurements of stiffness meaningless. From these tests, only the fracture initiation energy could be calculated (γ_i) from the peak load and stress intensity factor. Figure 5.12 shows a fairly random variation in this parameter with increasing notch-to-depth ratio. The average of all values is 52 Jm^{-2}, whereas the average of the three samples exhibiting stable crack growth is 18 Jm^{-2}.

For the specimens exhibiting controlled or semi-controlled failure it may also be possible to obtain a value for the energy to propagate a crack (i.e. γ_f) by assuming that, once the crack is initiated, all the stored energy in the jig is dissipated and that

any further energy supplied to the system (i.e. due to movement of the cross-head) is available for stable crack propagation. Thus, in the 'tail' region of the force-deflection curve, the cross-head deflection equals the specimen deflection. If one estimates that the crack has propagated half way through the specimen from the original crack tip before the onset of stability, then the work of fracture can be calculated by measuring the area of the 'tail' and dividing by twice the area ahead of the crack. For the three specimens exhibiting some stable crack growth, this gives values of γ_f as 12, 11 and 9 Jm^{-2} which are close to the value calculated from an estimate of the critical initial flaw size and again close to the value obtained by Beyerle et al[107].

5.3 Conclusions

The measured physical, elastic and mechanical properties of the monolithic CAS were found to be in good agreement with those quoted by the manufacturer, and its microstucture was found to be in accord with that reported for the Nicalon/CAS composite matrix.

Determination of the fracture mechanics parameters of the monolithic material by a single-edge notched bend test technique was largely unsuccessful as few of the test pieces exhibited stable crack growth. However, estimates of the matrix fracture surface energy were obtained by a number of techniques and were found to be in good agreement with that measured by other workers. This gives greater confidence in quantifying the matrix fracture surface energy and the published value for γ_m of 12.5 Jm^{-2} (obtained by Beyerle et al[107] from chevron-notched bend specimens) is to be used in any subsequent calculations of composite matrix cracking stress.

Dynamic Properties:	
Young's Modulus, E (Flexural)	105.6 ± 1.5 GPa
Young's Modulus, E (Longitudinal)	106.7 ± 0.3 GPa
Shear Modulus, G	41.9 ± 0.5 GPa
Poisson Ratio, ν (Calculated)	0.26
Physical Properties:	
Thermal Expansion Coefficient, α	5.3 x 10^{-6} /°C
Density, ρ	2.86 gcm^{-3}
Mechanical Properties:	
Bend Strength, σ_b	290 ± 150 MPa
Strain to Failure, ε_f	0.21 %
Young's Modulus, E	111 GPa

Table 5.1: Measured Properties of Monolithic CAS

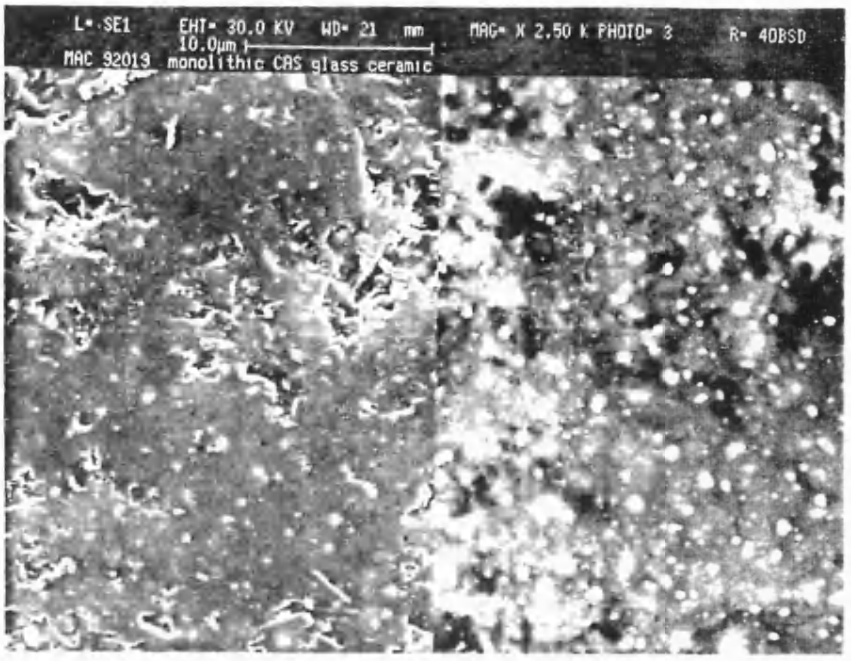

Figure 5.1: SEM micrograph of the as-received monolithic CAS in (a) secondary electron imaging mode and (b) back-scattered electron imaging mode

Figure 5.2: SEM micrograph showing region of unconsolidated zirconia-rich particles within monolithic CAS

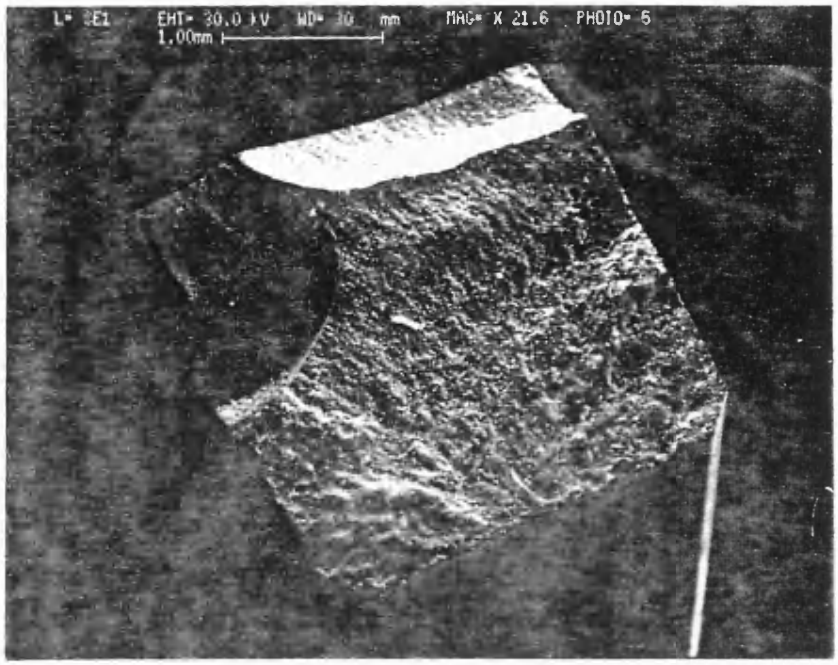

Figure 5.3: SEM micrograph of a typical monolithic CAS fracture face

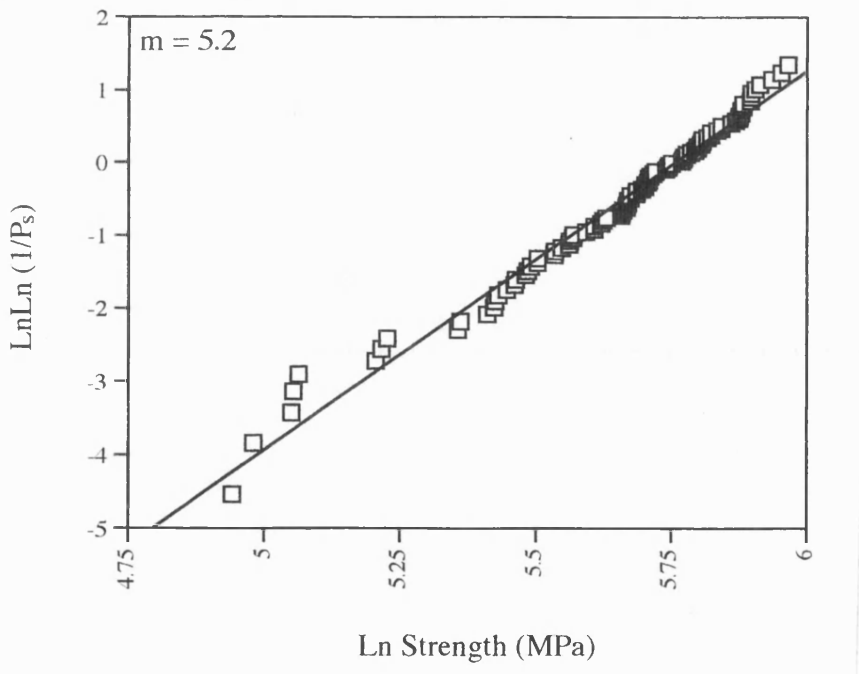

Figure 5.4: Weibull analysis of monolithic CAS bend strength data

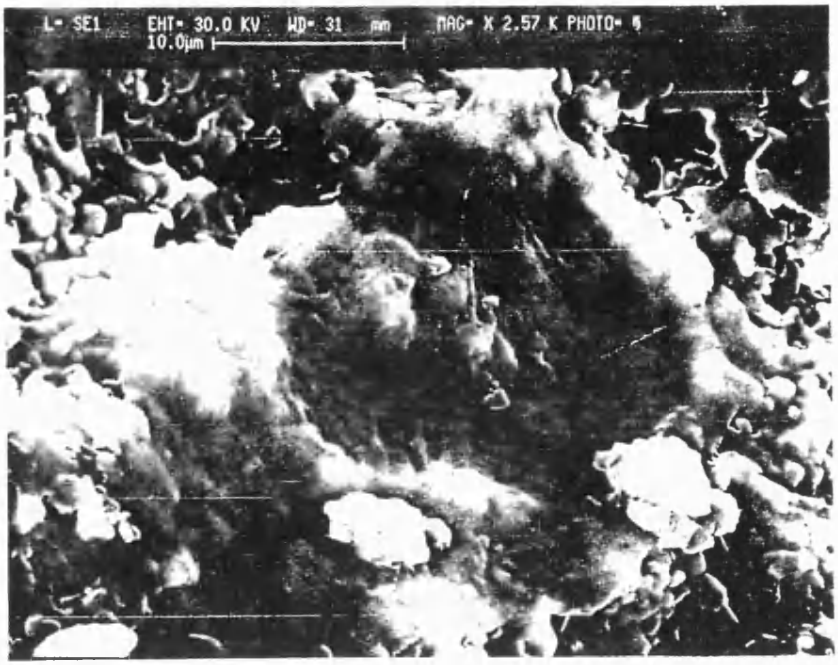

Figure 5.5: SEM micrograph showing a potentially critical flaw within monolithic CAS

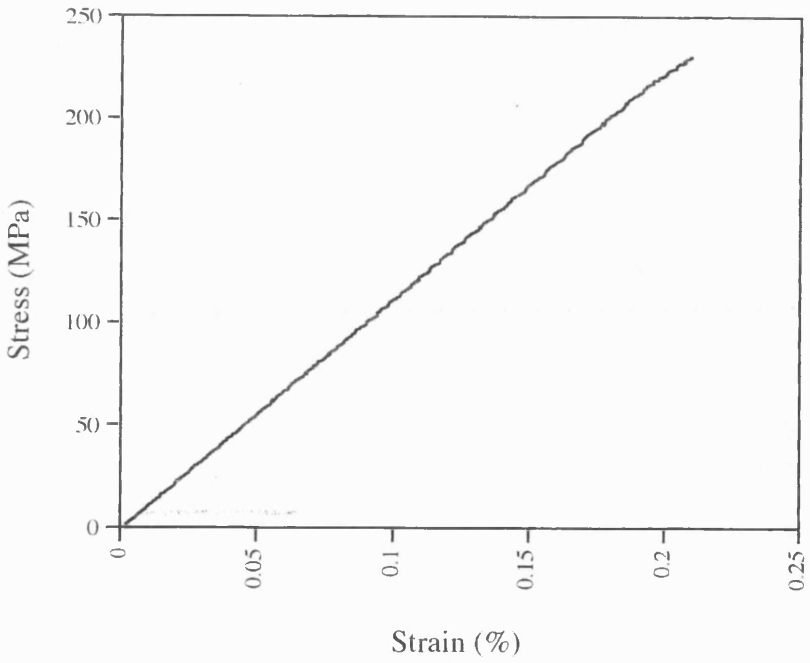

Figure 5.6: Monolithic CAS stress-strain curve obtained from un-notched SENB test

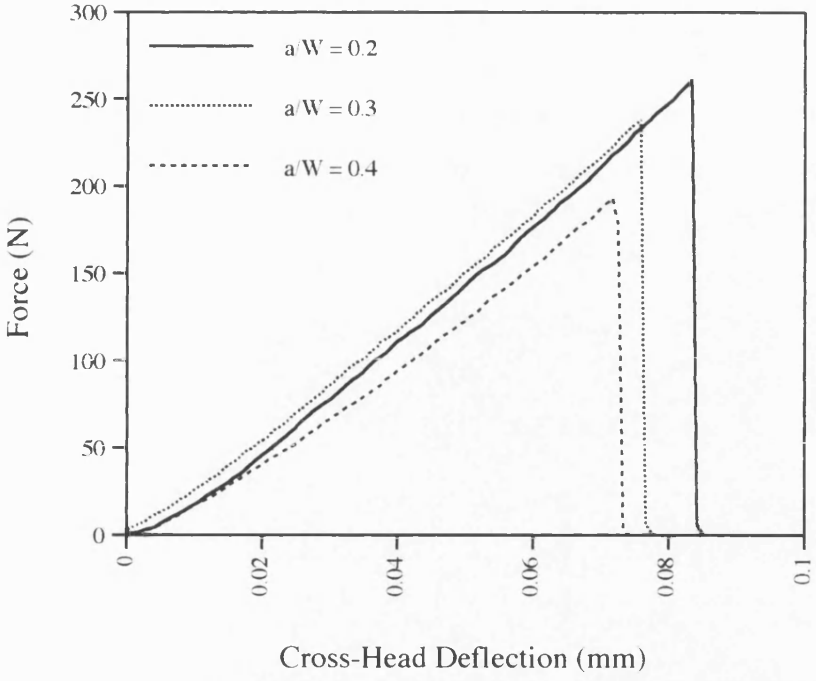

Figure 5.7: Force-deflection curves of monolithic CAS SENB specimens exhibiting unstable crack growth

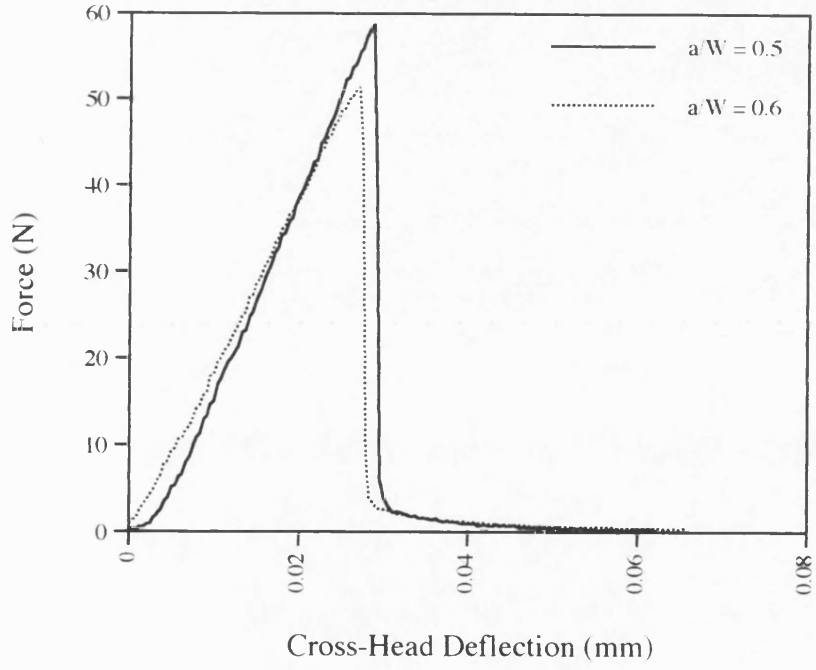

Figure 5.8: Force-deflection curves of monolithic CAS SENB specimens exhibiting some crack growth stability

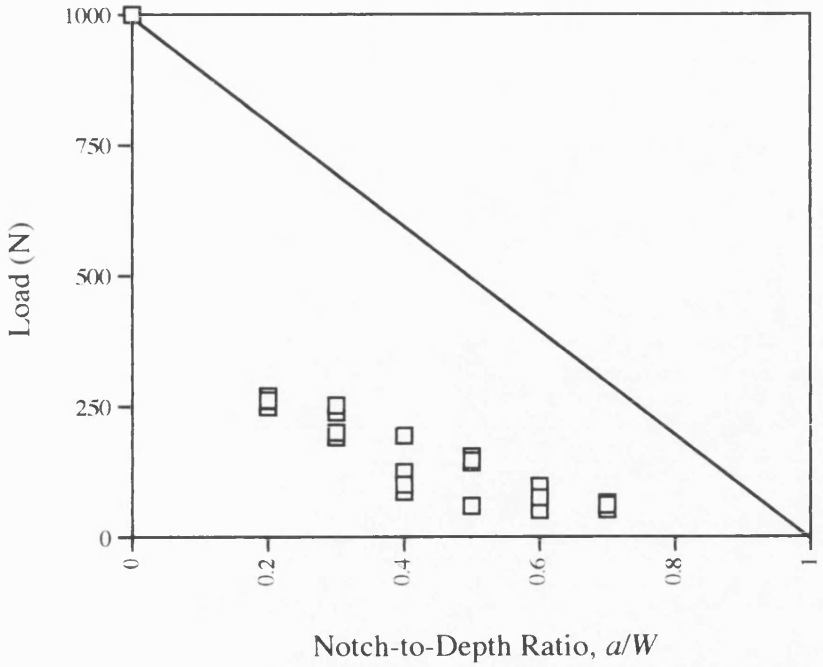

Figure 5.9: Peak load versus notch-to-depth ratio for monolithic CAS SENB tests

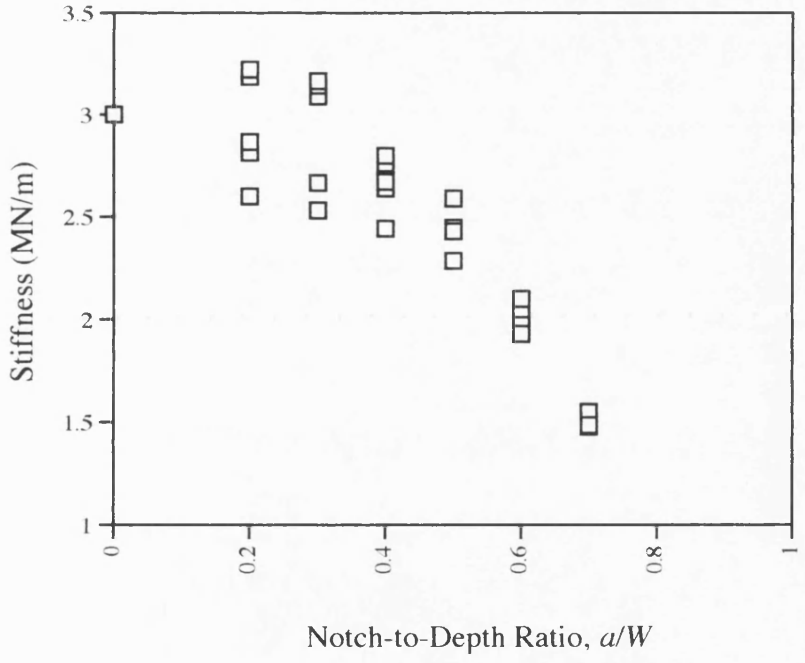

Figure 5.10: Gradient of force-deflection curves as a function of notch-to-depth ratio

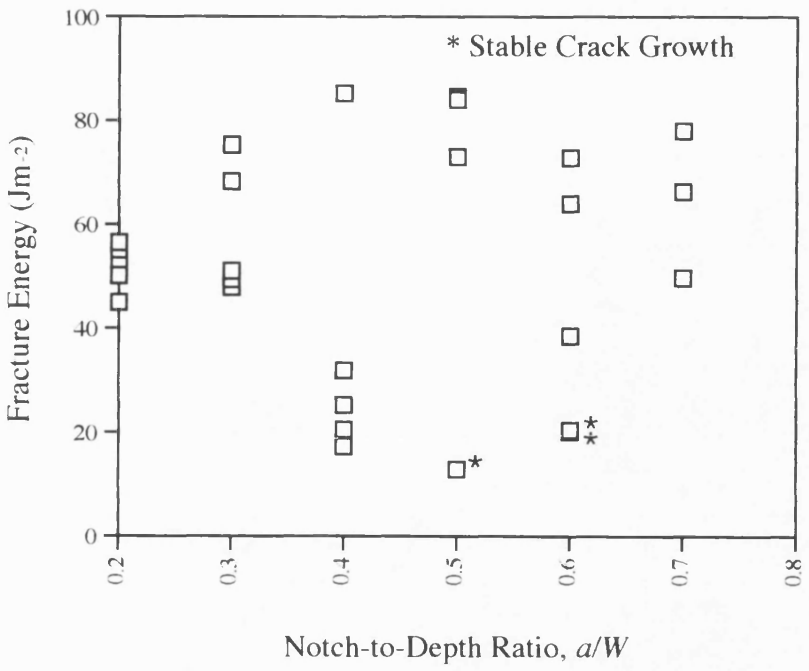

Figure 5.11: Variation of fracture energy (calculated from stress intensity factor) as a function of notch-to-depth ratio

CHAPTER 6 : UNIDIRECTIONAL NICALON/CAS COMPOSITE

6.1 Introduction

In order for ceramic-matrix composites to be used in engineering applications it is necessary to know and understand their mechanical behaviour under a range of loading conditions. In the present chapter, the room-temperature properties of unidirectionally reinforced Nicalon/CAS composite under uniaxial loading conditions are discussed. The stress-strain and acoustic emission responses of the composite during continuous and discontinuous tensile tests are presented, together with observations of damage development.

As outlined in Chapter 2, there are a number of models in existence which consider the properties and matrix cracking behaviour of unidirectional fibre-reinforced brittle-matrix composites when loaded parallel to the fibre direction. The results of the present chapter are discussed in terms of the available models.

6.2 Results

6.2.1 Microstructural Characterisation

The microstructure of the as-received unidirectional Nicalon/CAS composite is shown in Figure 6.1. All material tested was of 12-ply construction having an overall thickness of ~ 2.3 mm. Image analysis of representative sections by the method outlined in Chapter 4 gave an average fibre volume fraction of 0.34. Voids were present in the matrix in the form of closed pores of the order of 1 μm in diameter and were likely to have been due to air and volatiles being trapped during laminate processing. Matrix-rich regions separating the plies were generally evident which were likely to be due to the nature of the pre-preg manufacture, the low pressures involved during composite manufacture and the viscosity of the melt.

6.2.2 Stress-Strain Behaviour

a) Continuous Loading

A typical stress-strain curve of Nicalon/CAS unidirectional composite tested in tension is shown in Figure 6.2. It can be seen from the stress-strain curve that an initial linear region is followed by a region in which the strain increases with little increase in load, followed by a second linear region which tails off at stresses approaching the ultimate strength.

The general shape of the stress-strain curve is in agreement with that observed by other workers, as discussed in section 3.4, and in accord with that first predicted by Aveston, Cooper and Kelly (section 2.4) for a material in which the strain to failure of the matrix is less than that of the fibres. In such a material the matrix fails first and, where there are sufficient fibres to sustain the extra load thrown upon them after formation of the first matrix crack, cracking of the matrix continues with little increase in load until a saturation crack spacing is reached. The second linear region of the curve is then assumed to correspond to elastic deformation of the fibres alone followed by ultimate failure of the composite as a result of fibre fracture.

From these tests values of longitudinal elastic modulus, stress and strain at first discontinuity, ultimate strength, strain to failure and Poisson ratio were determined. Data from all unidirectional tensile tests are given in Table 6.1 and are within the range of published values given in Table 3.2, giving a degree of confidence in the techniques used to generate the results. Also included in the table are values for the shear modulus and shear strength obtained by Rolls-Royce from tensile tests on $\pm 45^{\circ}$ specimens and the transverse modulus obtained by Harris et al[111] from ultrasonic measurements.

Not included, are values for the gradient of the second linear region of the stress-strain curve (generally found to be between 35 - 45 GPa) and the strain at which this commences (~ 0.4 % in the example shown), as these parameters were difficult to determine with reproducible accuracy.

The transverse strain response of the unidirectional composite is shown in Figure 6.3. It can be seen that the strain becomes increasingly more negative with inceasing stress and reaches a minimum at a stress roughly coincident with the limit of proportionality on the longitudinal strain-stress curve. The transverse strain then becomes less negative with increasing stress and, in the case shown, actually becomes positive thus yielding a negative value of Poisson ratio. This transverse strain reversal is also in accord with the findings of other workers for both glass and glass-ceramic matrix composites (e.g. Kim & Katz[78], Habib et al[79], Nardone & Prewo[85], Kim & Pagano[106], Harris et al[111]). Nardone & Prewo attribute the transverse strain reversal to the brooming out of fibres during matrix cracking, whereas Harris et al suggest that it is due to the relaxation of normal elastic constraints during cracking and renders the determination of Poisson ratio invalid in this region. Values of Poisson ratio were calculated from strain measurements made within the initial linear region of the stress-strain curve.

In the particular case shown, the transverse strain achieves a maximum value at a stress roughly coincident with the onset of the second linear region of the longitudinal strain-stress curve and remains constant at this level until ultimate failure of the composite. It appears therefore that the failure mechanism operating in this region has no effect on the transverse strain. Assuming that little further matrix damage takes place and that the failure mechanism is one of fibre-matrix sliding and fibre fracture, then the fibres are able to slide within their matrix sockets and, since the strain gauge is placed on the matrix-rich surface, any effect on the lateral strain may thus be imperceptible.

A Weibull analysis was performed on the ultimate tensile strength data from tests on unidirectional composite (including data provided by Roll-Royce, giving a total of 26 results) and a Weibull modulus, m, of 13 was obtained.

b) Discontinuous Loading

Figure 6.4 shows the loading stress-strain curves of a specimen loaded in increments of 0.1 % strain from zero strain to ultimate failure of the composite. The overall outline of the curves is similar to the stress-strain response obtained from continuous tests as described above.

It can be seen from Figure 6.4 that at low strains (< 0.5 %) the stress-strain curves appear to be linear up to the point of previous loading, after which they bend over. However, at higher strains, stress-strain curves are non-linear from zero load. It can also be seen that after each successive unloading an increasingly large residual strain accumulates in the material. The largest increase in residual strain occurs when unloading from 0.3 % strain. The cumulative residual strain is shown in Figure 6.5 as a function of applied stress. It can be seen that the cumulative residual strain continues to increase, although to a lesser extent, at high loads.

A selection of loading/unloading curves are depicted in Figure 6.6 and show the increasing non-linearity of the stress-strain curves and the gradual closure of the hysteresis loops. It should be noted that the loops are separated along the horizontal axis for clarity only. Stiffness values from loading and unloading curves, normalised with respect to the initial Youngs modulus, are given in Figure 6.7 as a function of strain. The composite stiffness decreases with each successive loading giving an overall reduction to about 60 % of its original value. Ultimate failure of the composite occurred at a stress and strain within the range of values obtained from continuous tests (see Table 6.1).

6.2.3 Damage Observations

a) Continuous Loading

Samples failed in a fibrous manner with typical fibre pull-out lengths in the range 0.5 - 2.5 mm. Optical examination of the polished edges of failed tensile specimens showed that a periodic array of microcracks had formed in the matrix, as shown in Figure 6.8, with an average crack spacing of the order of 200 μm.

In the case of the continuously loaded specimen shown, the average crack spacing was 185 ± 66 μm. Figure 6.9 shows the crack space distribution measured from the specimen edge in an unloaded state. Weibull analysis of the distribution of crack spacings, S, gives a Weibull modulus, m, of the order of 3 with the best fit to the data obtained for a location parameter, S_u (lowest possible crack spacing), of 40 μm. This was less than the minimum measured value of 75 μm. The scale parameter, S_0, was calculated from the intercept of the $\mathrm{LnLn}[1/(P_S)]$ versus $\mathrm{Ln}(S - S_u)$, shown in Figure 6.10, which is equal to $m\,\mathrm{Ln}S_0$. The Weibull analysis was performed on the data in the assumption that the distribution corresponded to the different levels of stress required to propagate matrix cracks.

b) Discontinuous Loading

During discontinuous loading, tests were stopped at the maximum load and acetate replicas made of the polished specimen edge under load, by the method outlined in section 4.3.3, so that the evolution of cracks within the matrix could be monitored. Crack spacings were measured along an arbitrary line over the whole length of the replica. Figure 6.11 shows the increasing crack density (1/crack spacing) as a function of applied stress. It can be seen that the shape of this curve is very similar to that of the cumulative residual strain as a function of stress. Initial examination of this particular specimen prior to loading had not revealed the presence of any cracks and it

may therefore be deduced that the onset of cracking occurred at a strain of less than 0.1 %, even though the stress-strain curve was linear up to this point. The majority of matrix cracking had occurred during the region of almost constant stress and was accompanied by a large increase in cumulative residual strain together with a reduction in overall composite stiffness. Little further matrix cracking took place during this second linear region although a number of factors indicate that significant damage continued to occur during this region, namely the continuing increase in cumulative residual strain and a further reduction in composite stiffness. However, although fibre slippage and/or fibre fracture are thought to be failure mechanisms occuring in this region of the stress-strain curve these features are not readily identified from replicas. It should also be noted that although the final crack density appears to be less than that of the previous loading, this measurement was made from the actual specimen edge in an unloaded state and it is therefore evident that a number of cracks have closed and become invisible on unloading. Figure 6.12 is a micrograph of one replica showing clearly visible cracks.

In the particular case shown, the specimen did not fail into two pieces and separation of the two main crack faces was by a distance of about 700 μm.

6.2.4 Acoustic Emission Response

a) Continuous Loading

The acoustic emission response shown in Figure 6.13 a) is typical of that obtained in the current study from tensile tests carried out on unidirectionally reinforced Nicalon/CAS composite. The onset of acoustic emission occurs at a strain significantly below the limit of proportionality on the stress-strain curve, as observed by Kim & Pagano[106] and Harris et al[111], commencing in this case at a stress of 85 MPa and a strain of 0.08 % (cf proportional limit of 150 MPa and 0.14%) and is marked, as in many cases, by a small peak in the AE rate. Clearly, the onset of

damage events, indicated by acoustic emission activity, occurs at very low strains yet its effect is generally imperceptible on the stress-strain curve.

The acoustic emission rate then increases sharply as the stress increases, reaching a maximum as the stress begins to level off. The AE rate then decreases and reaches a minimum at a strain roughly coincident with the onset of the second linear region of the stress-strain curve, suggesting that the matrix saturation crack spacing had been reached. This is then followed by a steady increase in the level of acoustic emission activity with increasing stress until ultimate failure of the composite.

A plot of log N(x) versus amplitude channel, x, (Pollock method of amplitude distribution analysis, as defined in Appendix 2) is shown in Figure 6.14. The overall slope of the curve is - 0.208 (= - 0.12 b) which gives a value for b of 1.73. However, the curve appears to have two gradients, with the change in slope occurring at about x = 15. Further examination of the amplitude distribution of events by the above method, within the strain ranges 0 - 0.1 %, 0.1 - 0.2 % etc. up to failure of the composite, revealed that values of b fell into two distinct bands as shown in Figure 6.13 b) - indicative of failure by two separate mechanisms. Only the 0.3 - 0.4 % b-plot showed a bimodal distribution. All other b-plots were linear, suggesting failure by a single mechanism, with low values of b at low strain (mean ~ 1.5) and high values of b above 0.4 % strain (mean ~ 2.5). A graph showing the accumulation of events within different amplitude channel ranges is given in Figure 6.15. This demonstrates that the majority of acoustic emission events are of low amplitude and that the highest amplitude events only occur over a similar strain range to that of matrix crack formation.

The total number of acoustic emission events detected up to the failure load is of the order of 150,000 (with ~ 15,000 detected up to the point of minimum AE rate). All acoustic emission data after the peak load have been ignored.

An estimate of the total number of fibres within the tensile specimen may be calculated from the fibre volume fraction, average fibre diameter and overall cross-section of the composite and it is found to be of the order of 60,000. The number of acoustic emissions detected over the second linear region of the continuous stress-strain curve is over twice that value which may indicate that fibre sliding is a significant source of low amplitude AE activity and/or that multiple fracture of individual fibres occurs.

b) Discontinuous Loading

Acoustic emission activity was monitored during each loading and unloading, although the AE transducer had to be removed whilst replicas were taken at the maximum load. Figure 6.16 shows the variation of acoustic emission rate as a function of strain for each loading. In all cases, no acoustic emissions were detected on unloading until zero load was reached. Again, the overall outline of the curves is similar to the AE response obtained from continuous tests on the same material. However in this particular discontinuous test, the total number of acoustic emissions recorded was significantly less than that from continuous tests (~ 1/10 th). This may be as a result of failure continuing to occur under constant load whilst replicas were being taken and whilst the AE transducer was detached and also because a proportion of fibres did not fracture since the specimen remained intact on failure.

Values of b were calculated for each loading by using Pollock's method of amplitude distribution analysis (outlined in Appendix 2) and those are shown in Figure 6.17 as a function of strain. Again the value of b appears to fall into two distinct regions, taking a low value (~ 1.5) at low strains and a high value (~ 2.5) at high strains. This suggests that a change in failure mechanism takes place as the stress-strain curve becomes linear again, with subsequent failure occurring by a single mechanism emitting a large number of low amplitude events (high value of b).

It is clear that the Kaiser effect is only obeyed on certain loadings but is not obeyed on loading to 0.3 %, 0.6 %, 0.7 % strains or to failure. These results appear to correspond to loadings exhibiting the greatest degree of curvature on the stress-strain curves and implies that certain stages of damage are able to continue with only small additional applied load.

6.2.5 Interfacial Friction Stress Measurements

Measurement of the fibre-matrix interfacial friction stress by the Marshall method described in section 4.3.5, with a Vickers microhardness indentor, was performed on a polished section taken from a region within the end tabs of tensile test specimens. For the cases shown, values for τ of 9 ± 4 MPa and 11 ± 3 MPa were obtained for the continuously and discontinuously loaded specimens respectively. These results are in accord with the value quoted by Evans et al[96] for a Nicalon/CAS composite and with those found most appropriate by Beyerle et al[107] and Pryce & Smith[112] in their attempts to model the behaviour of Nicalon/CAS. However, a number of problems associated with the technique were found in the present study. In order to calculate the displacement of the fibre by the indentor, it is necessary to ensure that the indentation extends into the surrounding matrix. Inevitably this requires that the chosen fibre be sufficiently isolated from its neighbours to avoid interaction of the indentor with other fibres and so that the extent of the indentation into the matrix may be clearly measured. Obviously, the interfacial friction stress of isolated fibres may not be representative of the composite as a whole and the distribution is therefore biased. Powell et al[113] suggest that the compressive radial stress on fibres in regions of low fibre volume fraction is higher than in areas of high fibre volume fraction and that the interfacial friction stress of isolated fibres is therefore likely to be relatively large. They suggest that a large number of readings should be taken at random across a specimen in order to obatin a meaningful average of the interfacial friction stress. This does not appear to be possible by this method.

Other factors influencing the calculated value of τ are due to the limitations of the equipment used in terms of loads and optical magnifications available. The load is limited to 10, 25, 50 and 100 gf with the maximum load being insufficient to indent large fibres. The lower loads are used to obtain fibre hardness values whereby the fibre is indented but not displaced. As these indentations are small ($\sim 6\ \mu m$) the maximum magnification of the microscope at x400 is insufficient for the size of the indentation to be measured accurately ($\pm 0.1\ \mu m$). This then leads to significant errors in the fibre hardness value obtained (a $\pm 0.1\ \mu m$ error may give a difference in H_v of over 70) and in turn to the value of interfacial friction stress calculated. Attempts to measure indentations by alternative methods proved unsuccessful. In view of the poor reflectivity of the Nicalon/CAS composite, measurement of indentations by the use of reflected light microscopy at higher magnifications was impossible. This could be overcome to a certain extent by gold coating although the layer of gold masked previously-made indentations when observed optically. However, work by Shin[147] on a Nicalon/Pyrex composite has shown that gold coating prior to indentation gives values of interfacial friction stress significantly different from that obtained from the identical un-coated material (with both sets of measurements being made within an SEM). This type of experiment was not repeated in the present study.

Thus, all indentation tests performed in the present study were conducted on un-coated material and the dimensions were measured optically in situ at a magnification of x400. Bearing in mind the limitations of the equipment highlighted above, the values of interfacial friction stress generated by this technique should be treated as comparative rather than absolute.

6.3 Discussion

6.3.1 Elastic Properties

A rule-of-mixtures (ROM) approach (described in section 2.3.2) was taken in order to obtain a prediction for the initial Young's modulus of the composite. The value of modulus calculated by this approach corresponds to elastic deformation of fibres and matrix in proportion to their respective moduli and volume fractions. By taking measured values of matrix modulus, fibre volume fraction and fibre manufacturer's data a value of 131 GPa was obtained and this compares reasonably well with the mean experimental value of 127 GPa. A degree of scatter is observed in the results and this may be due to a number of reasons e.g. variability in the properties of the constituent materials and their relative proportions, subjectivity in the measuring technique, or the presence of matrix cracks in the as-received material. This latter point will be addressed in the following chapter. Rule-of-mixtures predictions based on the observed variation in fibre volume fraction give a range in modulus values of only 129 - 133 GPa which reflects the substantial contribution of the matrix to the overall composite modulus.

Prediction of the composite transverse modulus by the Reuss approximation (equation 2.12) yields a value of 123 GPa which is outside the range of quoted values. This approach assumes that the load applied transverse to the fibres acts equally on the fibres and matrix and that the stress in the fibres is equal to that in the matrix. It is also assumed that a perfect fibre-matrix bond exists and that fibres are isotropic - all of which may be inappropriate to the present system. An alternative approach is to assume that the transverse modulus is controlled by the matrix (i.e. $E_{22} = (1 - V_f)E_m$) which gives a value of 70 GPa. Pryce & Smith[110] calculate E_{22} to be within the range 85 - 115 GPa from laminate plate theory analysis of a range of cross-ply lay-ups. Clearly the measured value of 100 GPa (Table 6.1), obtained by Harris et al[111] from

ultrasonic measurements, lies roughly midway within these two ranges and may thus represent an average. This value is to be used in subsequent analyses.

A value of 0.24 was obtained for the Principal Poisson ratio, ν_{12}, of the unidirectional Nicalon/CAS composite and this is in accord with the findings of other workers (Table 3.2). Back-calculation of the fibre Poisson ratio from measured values of ν_{12} and ν_m (0.26 ± 0.1 from Table 5.1), again using a rule-of-mixtures approach, implies a value for ν_f of ~ 0.2. In the absence of any published values for this parameter, no comparisons with predictions may be made. However, the matrix Poisson ratio was derived from values of E and G obtained via resonant frequency methods (by assuming the isotropic relationship $\nu = (E / 2G) - 1$), whilst the composite Poisson ratio was determined from biaxial strain gauge within the initial linear region of a tensile stress-strain curve. Resonant frequency methods are generally expected to give higher modulus values than mechanical methods as the former effectively represents a zero strain measurement with less likelihood of damage. Calculation of Poisson ratio from uniaxial tensile tests requires the simultaneous reading of longitudinal and transverse strains and large errors are thus introduced at low strain values. The quoted value for a given specimen is that of a region prior to the limit of proportionality over which the Poisson ratio was approximately constant.
These two techniques may not therefore be comparable nor the rule-of-mixtures approach valid.
A value of 0.19 is predicted for ν_{21} from the measured transverse and longitudinal moduli together with measured ν_{12} and may not therefore be considered equal to ν_{12} as is assumed in many cases.

6.3.2 Residual Thermal Stresses

Prior to any modelling of matrix cracking in a unidirectonal composite it is necessary to take account of the residual stresses generated in the laminate during cooling from

the processing temperature which arise as a result of a mismatch in thermal coefficients between the fibre and matrix.

Taking the approach of Phillips et al[61], the axial residual stress within the matrix, σ_{ra}, may be approximated from the following expression

$$\sigma_{ra} = \frac{(\alpha_m - \alpha_f)E_f V_f \Delta T}{1 + V_f\left(\frac{E_f}{E_m} - 1\right)} \qquad (6.1)$$

where ΔT is the difference between the processing temperature and room-temperature, assuming that the composite is stress-free at the processing temperature. The expression is only approximate as it is one-dimensional and thus ignores radial stresses. Powell et al[113] in their model of residual stresses determine radial residual stresses to be negligible in the matrix of a Nicalon/CAS composite.

By taking measured values of matrix properties and fibre volume fraction, together with fibre manufacturer's data, and assuming a ΔT of 1200 °C (as discussed in Chapter 4), equation 6.1 gives an estimate of σ_{ra} as 113 MPa (tensile).

Many estimates for the axial residual stress in the CAS matrix have been quoted in the literature, ranging from 76 MPa (Pryce & Smith[110]) to 140 MPa (Harris et al[111]), with a measured value of 89 MPa being obtained by Beyerle et al[107]. The estimate given by the above lies roughly midway between the two extremes.

Powell et al[113] concluded in their modelling of residual stresses that regions of high fibre volume fraction experience larger tensile hoop and axial residual stresses in the surrounding matrix than regions of low fibre volume fraction and also suggest that at room temperature a portion of fibres close to free surfaces may be debonded.

It is possible that the matrix could be cracked after manufacture as the tensile strength of the unreinforced CAS calculated in Chapter 5 is of a similar magnitude to that of the tensile axial residual stress in the composite matrix calculated here.

6.3.3 Onset of Matrix Cracking

As discussed in Chapters 2 & 3, a number of models have been developed in an attempt to predict the onset of matrix cracking in a unidirectional composite when tested parallel to the fibres and which have subsequently been applied to Nicalon/CAS composite. Aveston et al[4] obtained an expression for the strain in the matrix, ε_{mu}, (which is assumed to equal the composite strain) when the stress in the matrix is equal to the matrix failure stress, σ_{mu}. This expression (referred to as ACK) is derived by considering the overall energy decrease that occurs when a crack forms in the matrix, assuming that the stress in the matrix is σ_{mu}, that the composite is under fixed loading conditions and that the rule of mixtures applies (with the implicit assumption that the Poisson ratios of the fibres and matrix are equal). Later work by McCartney[22] has shown that a fracture mechanics approach for predicting the formation of steady-state cracks in the matrix of such a composite (i.e. long pre-existing cracks that propagate across the entire width and thickness of the matrix) yields an expression for the matrix cracking strain identical to that obtained from an ACK-type energy balance approach (which McCartney modified for plane strain conditions) in which a crack forms instantaneously across a previously uncracked matrix. The strain at which matrix cracking occurs in a composite (under conditions of plane strain) may thus be found by the following expression (irrespective of the approach used to derive it):

$$\varepsilon_{mu} = \left\{ \frac{12\gamma_m \tau V_f^{\,2}(1-\nu^2)^2 E_f}{r V_m E_m^{\,2} E_c} \right\}^{\frac{1}{3}} \qquad (6.2)$$

where: E_m, E_f and E_c are the moduli of the matrix, fibre and composite, respectively; Vf is the fibre volume fraction such that the volume fraction of matrix, V_m is equal to

$(1 - V_f)$; r is the fibre radius; γ_m is the fracture surface energy of the matrix and τ the fibre-matrix interfacial shear stress (assumed to be constant).

Incorporation of average measured values where possible into the above expression, together with manufacturer's data for the Nicalon fibre (Table 3.4), gives a value for the matrix cracking strain of 0.17 %. The stress in the composite at this strain (= $E_c\varepsilon_{mu}/(1-\nu^2)$) is then 229 MPa, whilst the stress in the matrix, σ_{mu} (= $E_m\varepsilon_{mu}/(1-\nu^2)$), is 191 MPa. These calculated values of the composite stress and strain at the onset of matrix cracking are generally in excess of the measured limit of proportionality on the stress-strain curve and this may be for a number of reasons. Firstly, as discussed in the previous section, a tensile state of stress exists in the matrix prior to the application of load to the composite. This means that a much smaller stress (often termed σ_0) than that predicted need be applied before the composite matrix cracking stress is reached and this can be calculated from

$$\sigma_0 = \left(\frac{\varepsilon_{mu}}{(1-\nu^2)} - \frac{\sigma_{ra}}{E_m}\right)E_c \qquad (6.3)$$

where σ_{ra} is the axial residual stress within the matrix calculated in the previous section. Thus, the applied composite stress and strain necessary for matrix cracking to commence is only 94 MPa and 0.07 % respectively with only small differences in the calculated results being obtained if $(1-\nu^2)$ terms are excluded from each equation. McCartney, in fact, compares his results with those of other workers by putting ν equal to zero.

It can be seen that the applied composite matrix cracking stress and strain calculated above are of a similar order to the stress and strain in the composite at which the first few acoustic emission events are detected during tensile tests on unidirectional Nicalon/CAS. Examination of specimens during discontinuous loading shows that a small number of matrix cracks are present in a previously uncracked specimen after detection of the first few acoustic emission events but that these cracks did not appear to span the entire specimen thickness.

Acoustic emission results show that damage continues to occur with increasing stress as opposed to the constant stress predicted by ACK, whilst crack density measurements made during discontinuous tests show that the stress has to be increased well above this initial cracking level before large numbers of cracks form at almost constant load. The observation that matrix cracking occurs over a range of applied stress has been made previously by other workers and this has generally been attributed to a distribution of flaw sizes being present within the matrix. The variation of acoustic emission rate with increasing strain takes the form of a 'bell-shaped' curve in this region, with the maximum rate occurring during the region of almost constant stress, and it is possible that the the shape of this curve may correspond to a statistical distribution of matrix failure stresses with the peak representing the average matrix strength during which most cracks are formed. (This will be discussed in section 6.6). The predicted matrix cracking stress and strain calculated above represent lower-bound steady-state values for the onset of matrix cracking, requiring the presence of 'long' pre-existing cracks. The stress has to be increased before defects smaller than a critical size (calculated by McCartney[22] to be of the order of a 20 -30 μm) are able to propagate. Since good agreement is found between the onset of acoustic emission and the calculated matrix cracking stress it is possible that defects of critical-size are initially present in the specimens tested. Defects of this size may be introduced, for example, on cooling from the processing temperature or during specimen machining. Other factors which would influence the onset of matrix cracking are local variations in fibre volume fraction which may lead to variations in matrix residual stress and interfacial shear stress. Beyerle et al[107] tried to account for the observed variation in matrix cracking stress and showed that ACK predictions were in acccord with measured results provided that τ was in the range 10 - 15 MPa and for a matrix residual stress of 80 - 100 MPa.

6.3.4 Matrix Crack Spacing

Aveston et al[4] state that matrix cracking will continue at constant stress until the matrix is broken into a set of blocks of between x' and $2x'$ in length. They consider the length x' to be controlled by the rate of stress transfer across the fibre-matrix interface and derive the following expression for x' by assuming that continued matrix cracking is limited by the maximum stress which the interface can sustain:

$$x' = \left(\frac{V_m}{V_f}\right)\frac{\sigma_{mu} r}{2\tau} \qquad (6.4)$$

Results of tensile tests made in the present study show that matrix cracking does not occur at a constant stress and that the matrix crack spacing decreases with increasing stress.

By taking σ_{mu} to be 191 MPa, together with a fibre radius of 6 μm and measured values for the remaining parameters, the transfer length x' is calculated to be 111 μm. Kimber & Keer[26] showed, by purely statistical considerations, that the average saturation crack spacing is equal to 1.337 x'. In the present case, the average crack spacing is thus about 150 μm which is approximately 3/4 of the average measured value. Zok & Spearing[28] consider the interaction of slip lengths betweeen random cracks and propose that the saturation crack spacing is of the order of 1.75 x', giving a predicted average crack spacing of almost 200 μm in this case. This value is clearly closer to the average measured value. The latter also predict that crack saturation occurs at a stress 1.3 times greater than the ACK predicted matrix cracking stress. This is difficult to verify since the point at which crack saturation occurs is difficult to determine. Crack density measurements indicate that a small number cracks form even during the second linear region of the stress-strain curve. An indication of the stress or strain after which few matrix cracks form may be given by the minimum of the acoustic emission rate bell-curve, and is estimated in the case shown to be at a

stress of about 200 MPa and a strain of 0.38 % which are much greater than 1.3 times the measured cracking onset stress and strain although is approximately 1.3 times the limit of proportionality. However Zok & Spearing, in their derivation of the above, have ignored the effect of residual stresses on the onset of matrix cracking and the statistical nature of the failure process. The significance of their approach would seem to be that, by considering the formation of a random array of interacting cracks, they predict an overall decrease in crack spacing with increasing stress and obtain a reasonable estimate of the saturation crack spacing.

6.3.5 Modulus Reduction

As mentioned previously the onset of matrix cracking, determined by both direct and indirect (AE) observation, occurs at a stress well below the knee of the stress-strain curve and thus the formation of the first few cracks has little effect on the composite stiffness. From the results of discontinuous tests it can be seen that subsequent matrix cracking causes a decrease in composite stiffness reaching a plateau level corresponding to 60 - 70 % of its initial value.

Appication of the rule-of-mixtures to predict the slope of the second linear region on the continuous stress-strain curve, assuming elastic deformation of the fibres alone i.e. $E_f V_f$, gives a value of 67 GPa. Many factors can account for discrepancies between measured and predicted stiffness values in this region of the curve. For example, crack density measurements show that a small amount of matrix cracking occurs in this region, indicating that the matrix still bears a proportion of the load. This would lead to a larger stiffness than that predicted. Any initial fibre damage introduced during composite processing would lead to a stiffness decrease, which if it were the case would also have manifested itself in a similar reduction of the initial elastic modulus. Acoustic emission activity in this region of the curve tends to indicate that further damage is taking place as does the continuing increase in cumulative residual strain. These observations may be caused, for example, by fibre failure or by fibre-

matrix sliding making a contribution to the overall deformation. Both would lead to a decrease in stiffness compared to predicted values based on $E_f V_f$.

6.3.6 Ultimate Strength

Predictions of the tensile strength of unidirectional composite, by use of the models described in section 2.6.2, requires a knowledge of the as-processed strength of individual fibres within the composite. Such information was not obtained in the present study. However, it may be possible to make predictions about composite failure by taking the in situ strength of Nicalon fibres obtained by Beyerle et al[107]. They measured an average fibre strength, σ_c, of 2.0 GPa with a Weibull modulus, m, of 3.6 from fracture mirror radii within failed Nicalon/CAS composite. It may be supposed that Nicalon fibres would have a similar strength in the current Nicalon/CAS composite. These values of σ_c and m may be incorporated in Curtin's model of composite strength (section 2.6.2), from which a number of parameters may be predicted. The ultimate strength of a composite having a fibre volume fraction of 0.34, a characteristic fibre strengh of 2.0 GPa and a Weibull modulus of 3.6 is predicted to be 446 MPa (from equation 2.25). This is less than the strength predicted by Beyerle et al[107] for a Nicalon/CAS composite having a fibre volume fraction of 0.37 (as expected) but is larger than the average composite strength of 390 MPa measured in the present study. Curtin admits that his approach is likely to give an upper-bound strength prediction as additional fibre failures may be present due to processing damage and due to failure of some fibres within the wake of matrix cracks. The predicted strength will also be sensitive to variations in fibre volume fraction. However, it is interesting to note that the composite strength is predicted to be less than a quarter of the strength of individual fibres.

Curtin predicts that the proportion of failed fibres at the ultimate tensile strength of the composite is $2/(m+2)$ per length δ_c, where δ_c is the characteristic length of fibres having a characteristic strength of σ_c. In the present case the proportion of failed

fibres within a length δ_c would be 0.36. It is clear that in a number of cases specimens remain intact after the maximum load, implying that a proportion of the fibres have not failed.

The characteristic length can be calculated from $r\sigma_c/\tau$ where r is the fibre radius and τ the fibre-matrix interfacial friction stress. Taking a fibre radius of 6 μm and an average measured value of 10 MPa for τ, gives a characteristic length of 1.2 mm. This is clearly greater than the stress transfer length during matrix cracking, x', as Curtin suggests. For a composite with a test gauge length of 50 mm, as in the present case, the theory implies that each fibre will fail on average 15 times along its length. It is also predicted from the theory that the average pull-out length will be approximately $\delta_c/4$ and thus 300 μm in the present case. Pull-out was generally found to be greater than this value. However, the theory does not take account of local variations in fibre-matrix interfacial shear strength which are expected to affect the characteristic, and hence pull-out, lengths significantly.

In order to determine the accuracy of this approach, it is clear that future work should include measurements of as-processed and/or in situ fibre strengths, fibre pull-out lengths and ideally the average distance between fibre breaks.

6.3.7 Acoustic Emission

Optical examination of specimens during discontinuous tensile tests on unidirectional Nicalon/CAS has confirmed that the first few acoustic emission events correspond with the formation of the first few cracks in the matrix. This, together with the observation that on loading/unloading/reloading cycles the Kaiser effect is obeyed at some stress levels but not at others, would tend to indicate that the acoustic emission activity detected is mainly due to real damage events within the specimen as opposed to extraneous noise from the atmosphere and test apparatus.

Further examination of the acoustic emission data by using the Pollock method of amplitude distribution (b-plot) analysis within increments of strain gave two distinct

values of b, a low value (~1.5) at low strains and a high value (~ 2.5) at high strains, with the change in slope coinciding with a minimum in the rate of AE activity (Figure 6.13). The b-plot at this cross-over point was generally bi-modal as indeed was the b-plot of the overall AE activity. In the case of bi-modal b-plots, the two slopes bore little relation to those obtained from linear plots within individual strain increments. Other points to note about this type of analysis before drawing conclusions from it, are that large errors in b may be introduced in cases where the overall number of acoustic emission events is small. Another point to note is that in the present case, high values of b which indicate a large number of low amplitude events may be measured over a smaller amplitude range (1-15 compared with 1-26) and may also be prone to error. Notwithstanding these possible sources of inaccuracy, it would appear that the unidirectional Nicalon/CAS composite fails by two distinct mechanisms with high amplitude events caused by matrix cracking at low strains and large numbers of low amplitude events occuring after matrix crack saturation. Both fibre failure (a large number of small-area, low-energy failures) and fibre-matrix sliding (rubbing noises) would be expected to yield the latter type of events. The exact mechanism(s) are not known here, and the activity in this region is also likely to include a small number of matrix cracking events. However, for convenience it may be supposed that the AE events in this region originate from a single type of source.

It may therefore be possible to deconvolute the overall AE reponse obtained from continuous tensile tests into those of the two separate mechanisms. With reference to Figure 6.13 a), the first stage in deconvoluting the AE data is to fit a curve to the upper part of the AE response. This was found to obey a power law of the form $y = Cx^k$ (where C and k are constants). The next stage was then to subtract the fitted curve from all AE data in order to isolate the bell-shaped curve associated with the lower strain failure mechanism. The two fitted curves are shown in Figures 6.18 a) and b) with Figure 6.18 a) also showing the original AE rate data. The bell-shaped curve associated with the failure mechanism operating at low strains is that of a normal

distribution and coincides with the range of strain over which almost all matrix cracking occurs. The only data available for comparison is that of the increasing crack density with strain obtained in the present study from crack spacing measurements made during discontinuous loading. Figure 6.19 shows the crack density (normalised with respect to the maximum), together with the cumulative AE rate (again normalised with respect to the maximum), plotted as a function of strain. The acoustic emission data shown is that of the fitted normal distribution. The shape of the two curves in Figure 6.19 are similar although the measured strain-range over which matrix cracking occurs is somewhat wider than that indicated by the acoustic emission rate. It may be noted that the AE data and crack density measurements are obtained from two different specimens and may not be directly comparable. A number of factors may account for differences in the strain- or stress-range over which matrix cracking occurs - for example, the matrix flaw size distribution, the fibre-matrix interfacial friction, and the matrix residual stress. The possible effect of a variation in these parameters on the increasing crack density with applied stress is illustrated schematically in Figure 6.20 (after Beyerle et al[107]). From this diagram it can be seen that a reduction in the matrix flaw size distribution (indicated by an increase in the Weibull modulus, m) would give a narrower stress-range over which matrix cracking occurs. It is possible that the matrix flaw size distribution may be different in the continuously and discontinuously loaded specimens as both specimens were obtained from different plates. It may also be noted that the measured interfacial friction stress of the discontinuously loaded specimen was slightly higher than that of the continuously loaded specimen. Both of these factors may account for the discrepancy between the measured AE and crack density data. Clearly a method of obtaining the two results simultaneously is required to enable direct comparison.

6.4 Conclusions

The room-temperature tensile properties of unidirectional Nicalon/CAS composite have been studied by using a wide range of experimental techniques.
Data obtained from continuous tests were found to be in good agreement with those of other workers. Composite elastic properties were found to be in reasonable agreement with predictions based on available models.

The stress-strain behaviour and acoustic emission responses of the composite, during both continuous and discontinuous loading, were discussed in terms of the observed evolution of damage within the composite. The observed damage was primarily in the form of parallel matrix cracks spanning the thickness of the specimen. This was then thought to be followed by fibre slippage and/or fibre failure.

The onset of matrix cracking was found to coincide with detection of the first acoustic emission events and was in good agreement with predictions based on the Aveston, Cooper & Kelly (ACK) model once the tensile residual thermal stress in the matrix was taken into consideration.

The limit of proportionality on the stress-strain curve appeared to have little physical significance and may merely indicate the presence of sufficient cracks to noticeably reduce the composite modulus.

Continued matrix cracking occurred over a range of applied stress and this was thought to be due to the presence of a distribution of flaw sizes within the matrix and which was not taken into account by the ACK model.

A method of incremental amplitude distribution analyis of acoustic emission data appeared to be successful in discriminating between failure mechanisms.

It was thought that values of the fibre-matrix interfacial friction stress obtained by the microindentation method were comparative rather than absolute.

Fibre Volume Fraction, V_f	0.34 ± 0.03
Longitudinal Modulus, E_{11} (GPa)	127 ± 7
Transverse Modulus, E_{22} (GPa)	100 ± 4[#]
Shear Modulus (± 45°), G_{12} (GPa)	55 ± 4[$]
Poisson Ratio, ν_{12}	0.24 ± 0.02
Proportional Limit Stress (MPa)	167 ± 29
Proportional Limit Strain (%)	0.12 ± 0.02
Ultimate Tensile Strength, σ^*_{11} (MPa)	390 ± 36
Strain to Failure, ε^*_{11} (%)	0.76 ± 0.12
Shear Strength (± 45°), τ^*_{12} (MPa)	59 ± 5[$]
Average Crack Spacing, S (μm)	194 ± 68

Table 6.1: Room-temperature mechanical properties of unidirectional Nicalon/CAS composite

[#] Harris et al[111]

[$] Rolls-Royce data

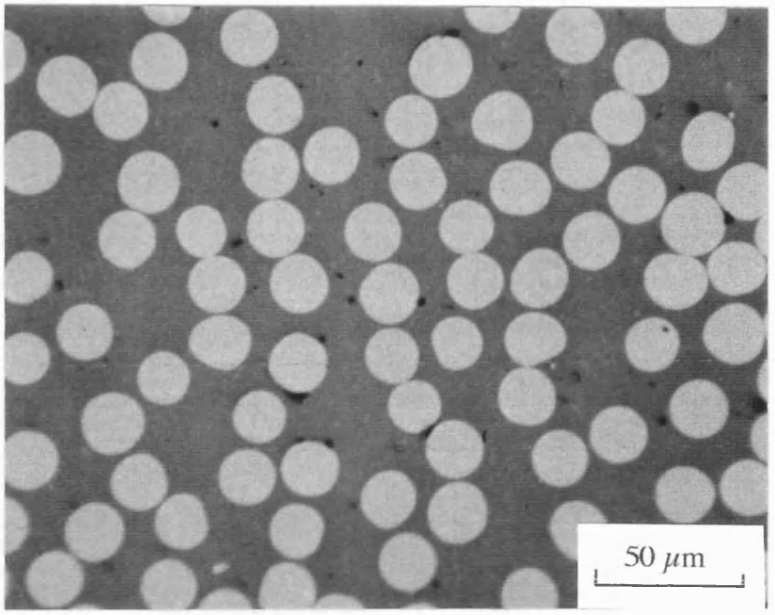

Figure 6.1: Optical micrograph showing the microstructure of as-received unidirectional Nicalon/CAS composite(x 400)

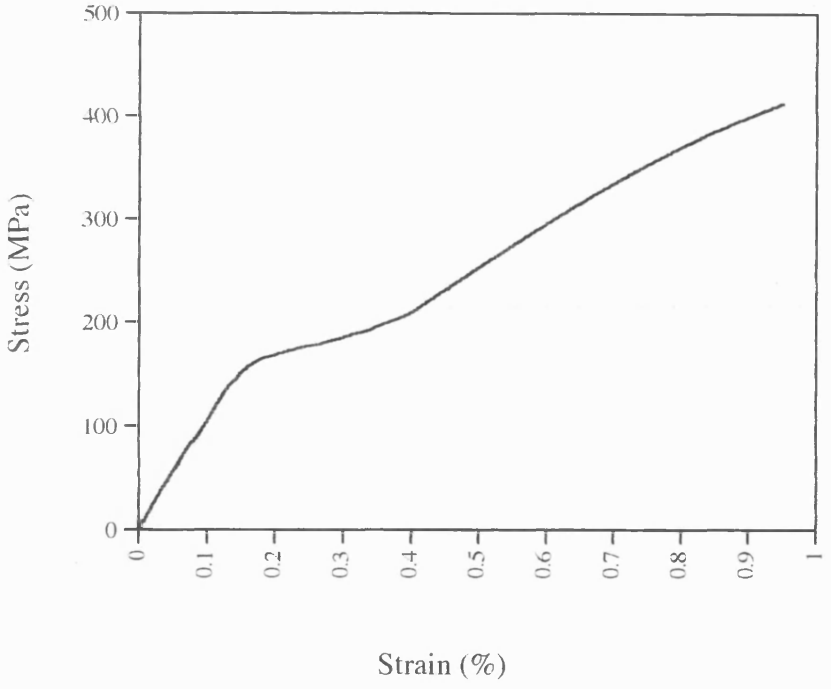

Figure 6.2: Typical room-temperature stress-strain response of unidirectional Nicalon/CAS composite

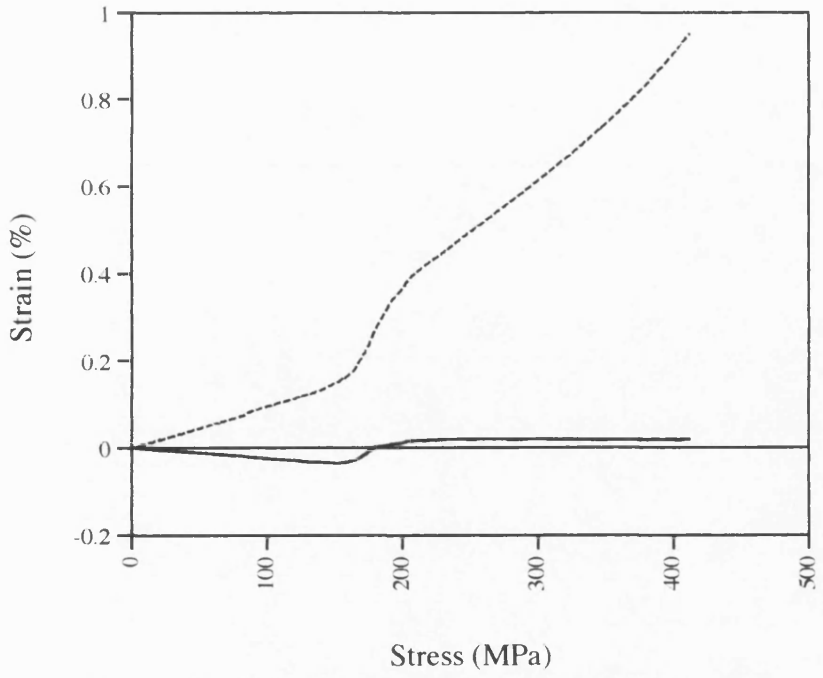

Figure 6.3: Longitudinal and transverse strain response of unidirectional Nicalon/CAS composite during continuous tensile tests

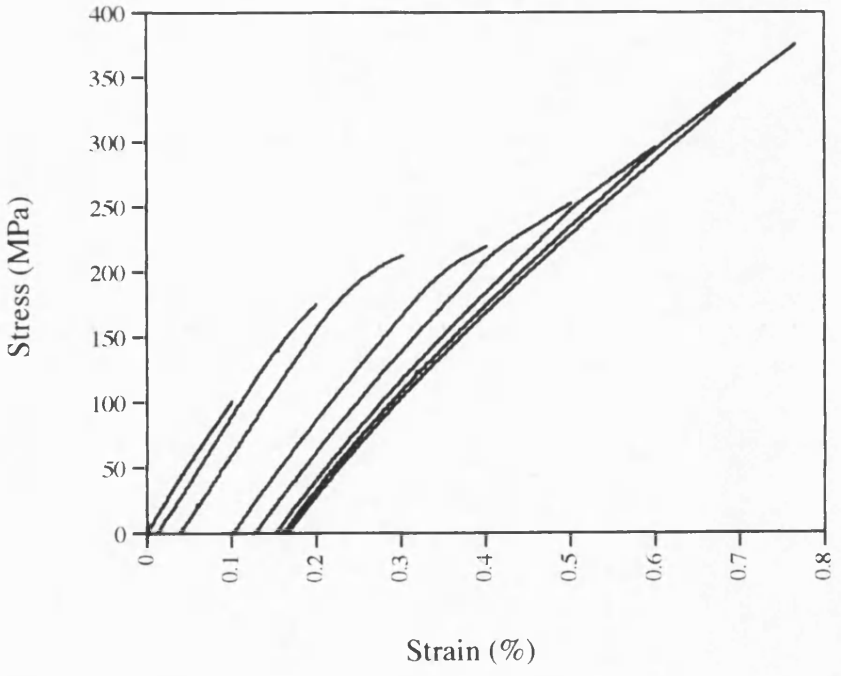

Figure 6.4: Cumulative stress-strain response of unidirectional Nicalon/CAS during discontinuous tensile loading

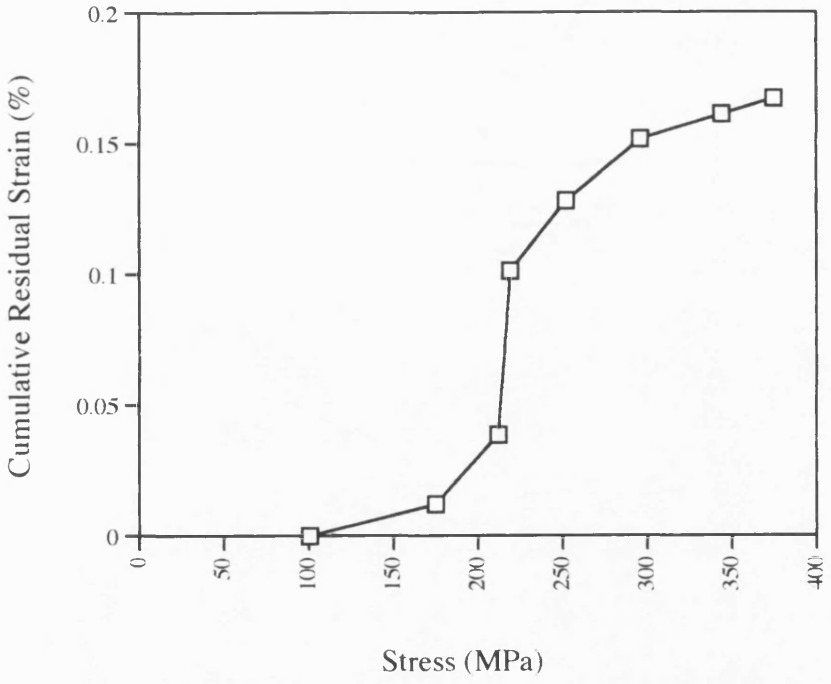

Figure 6.5: Cumulative residual strain as a function of applied stress during discontinuous tensile testing of unidirectional Nicalon/CAS

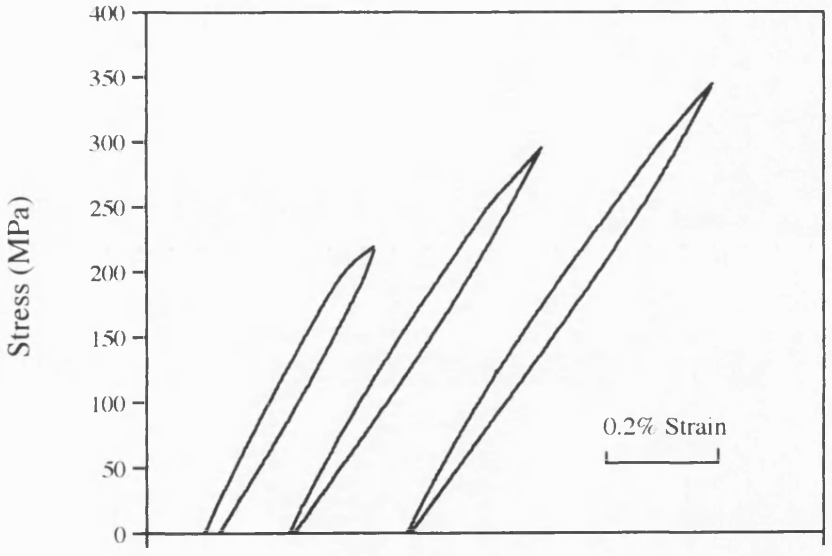

Figure 6.6: Loading/unloading curves from discontinuous tensile testing of unidirectional Nicalon/CAS

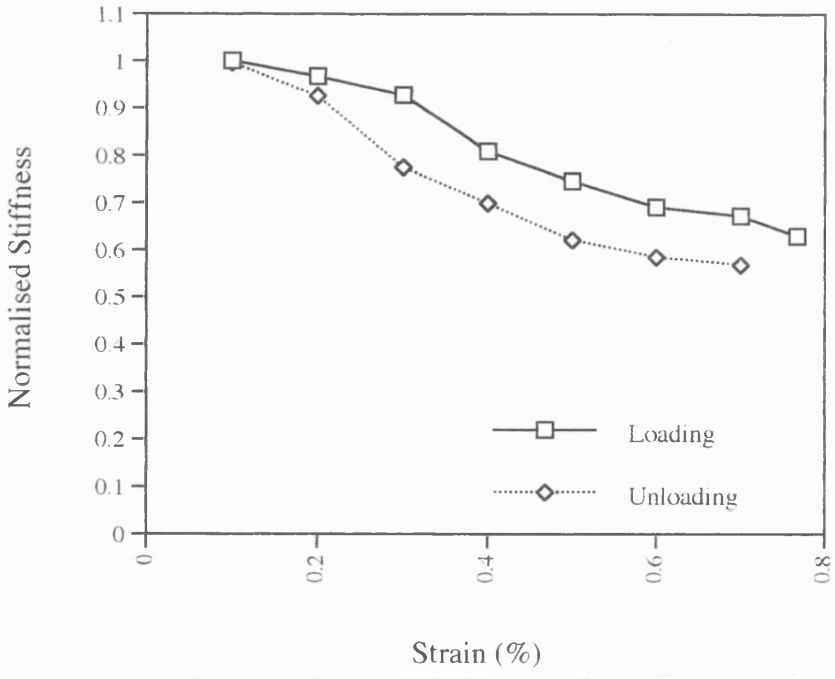

Figure 6.7: Normalised loading and unloading stiffness as a function of applied stress during discontinuous tests on unidirectional Nicalon/CAS

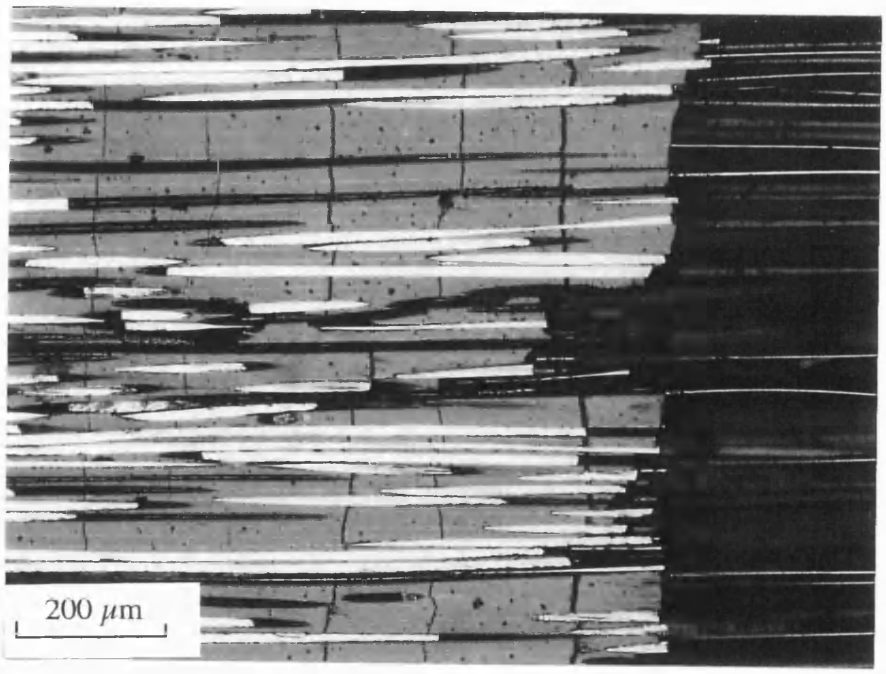

Figure 6.8: Optical micrograph showing matrix cracking and fibre pull-out in failed unidirectional Nicalon/CAS composite tensile specimen (x100)

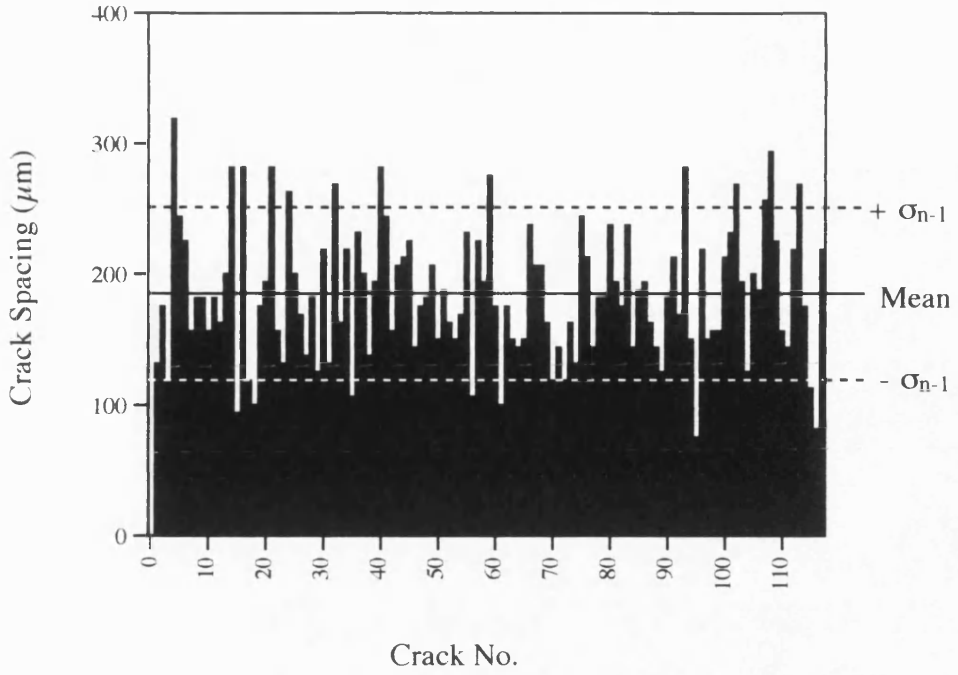

Figure 6.9: Histogram showing variation of matrix crack spacing in failed unidirectional Nicaon/CAS composite (crack number 1 being adjacent to the location of failure)

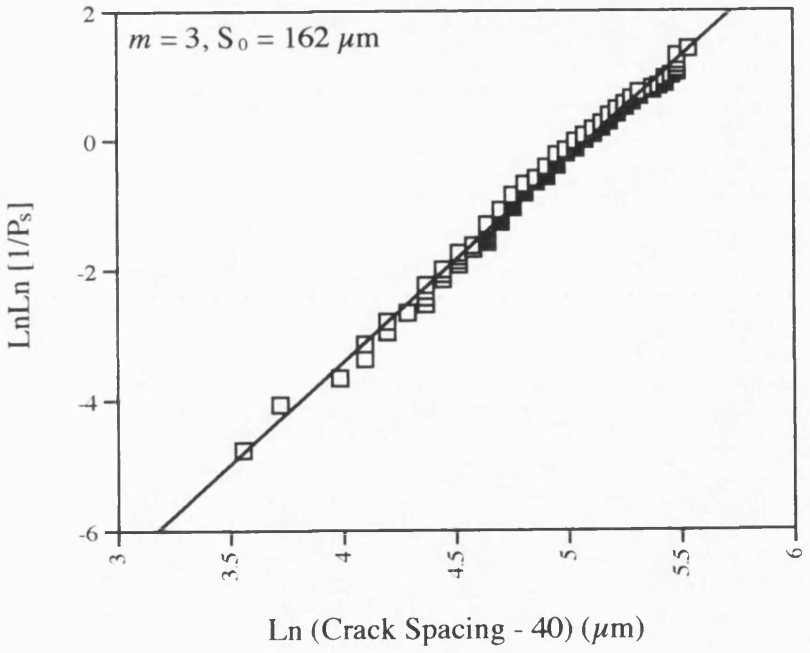

Figure 6.10: Weibull treatment of crack spacing data from failed unidirectional Nicalon/CAS composite

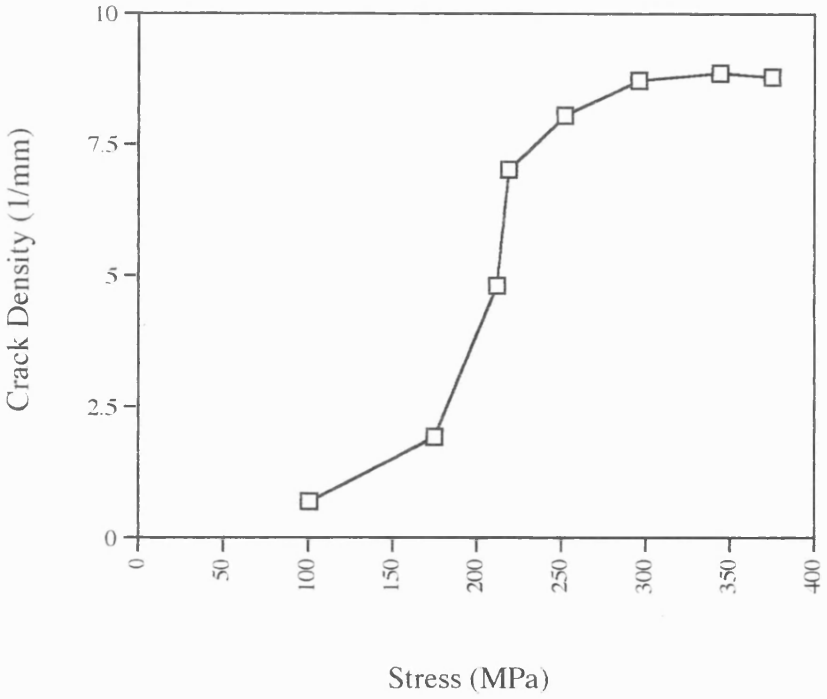

Figure 6.11: Variation of crack density as a function of applied stress during discontinuous tensile tests on unidirectional Nicalon/CAS

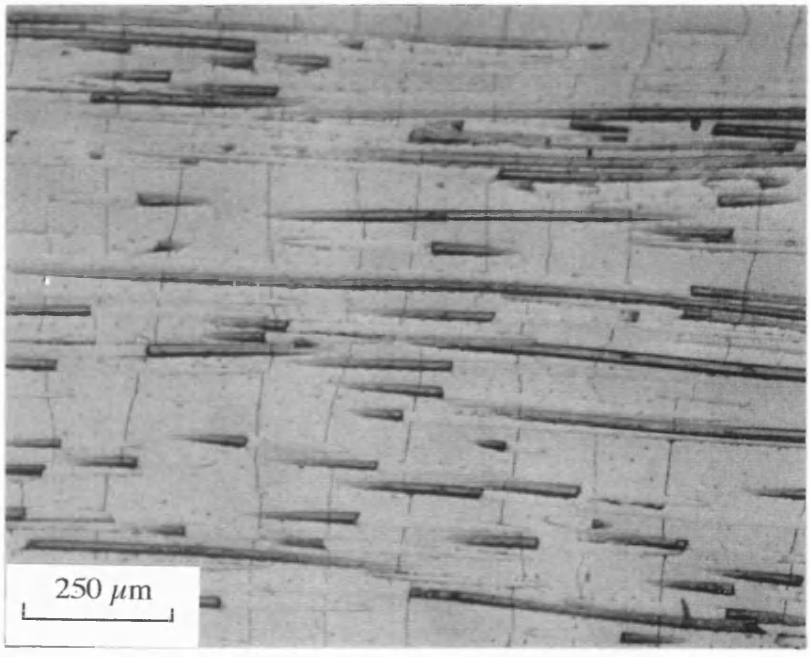

Figure 6.12: Optical micrograph of an acetate replica taken under load, showing matrix microcracking along the polished edge of a unidirectional test specimen (x 80)

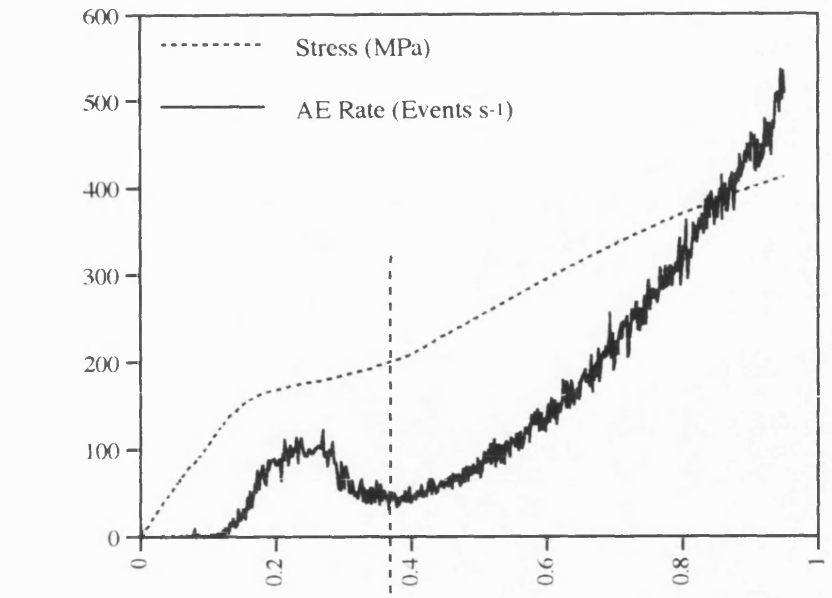

a)

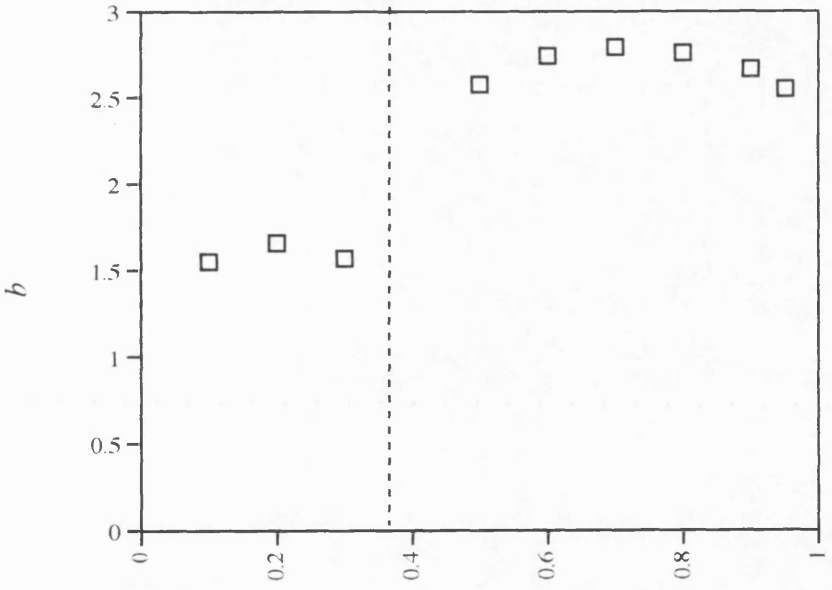

b)

Figure 6.13: Acoustic emission response of unidirectional composite shown as a) AE rate and b) *b* value as a function of applied strain

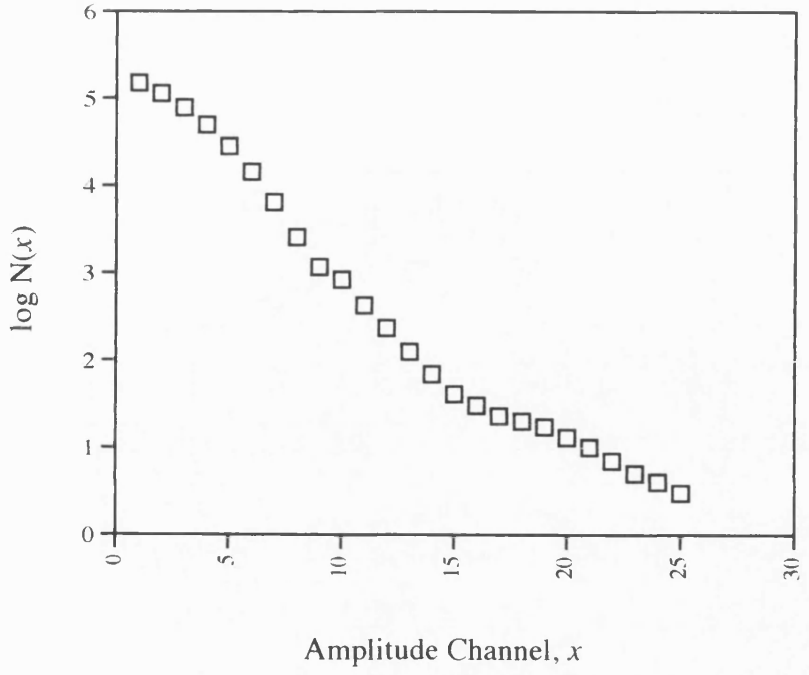

Figure 6.14: Amplitude distribution analysis of acoustic emission data from unidirectional Nicalon/CAS by the Pollock method

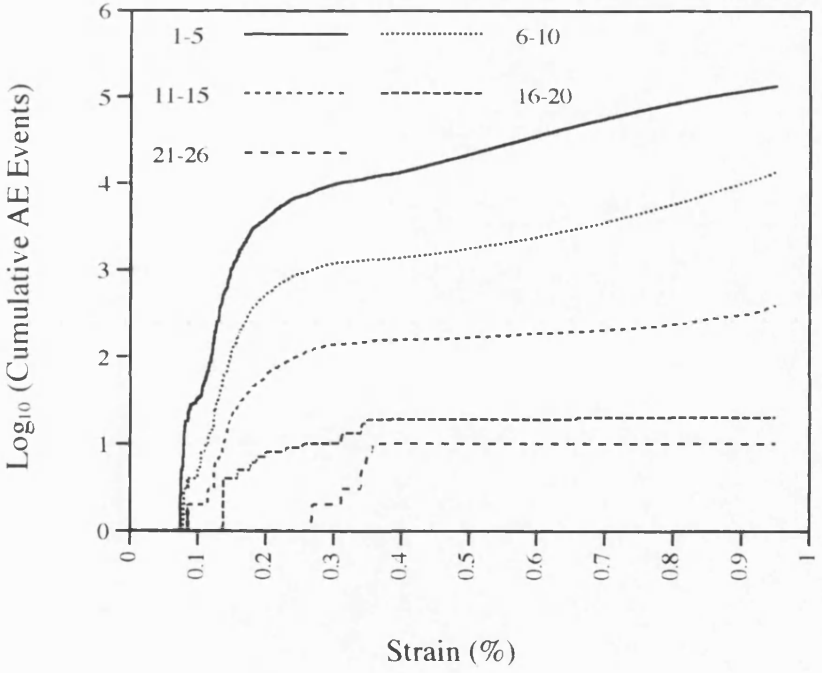

Figure 6.15: Accumulation of acoustic emission events within different amplitude ranges for unidirectional Nicalon/CAS

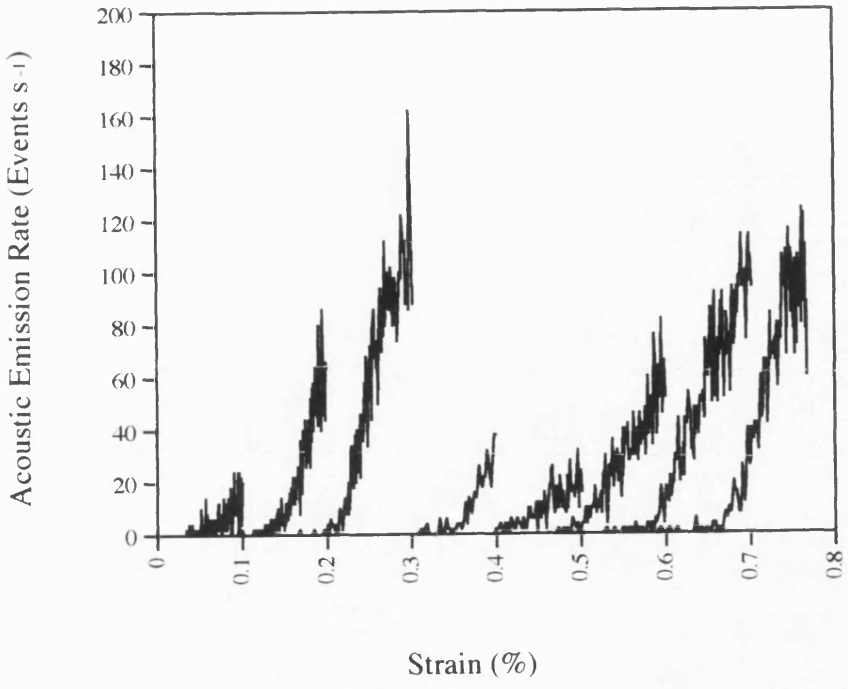

Figure 6.16: Acoustic emission rate as a function of applied strain during discontinous tensile tests on unidirectional Nicalon/CAS

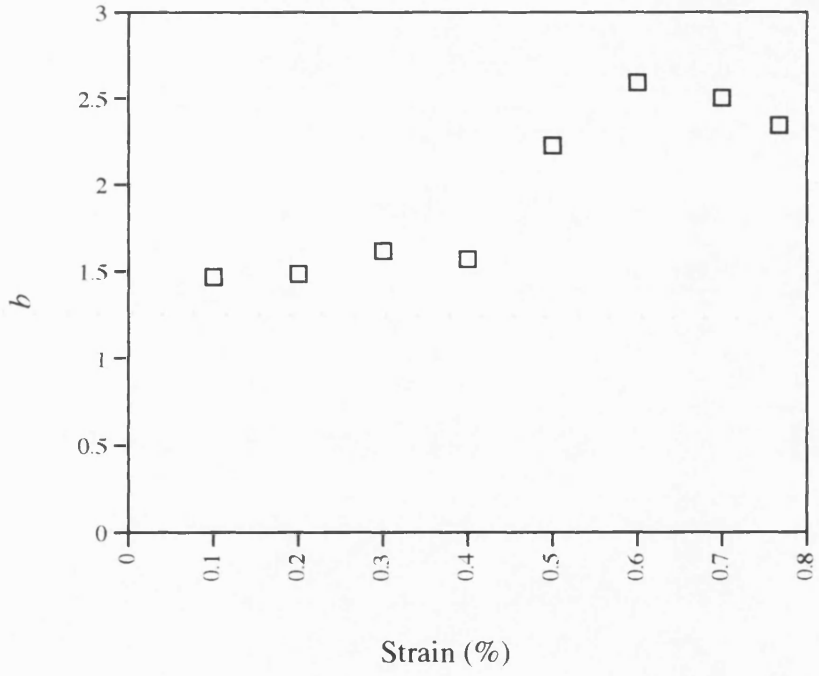

Figure 6.17: Variation in *b* value as a function of applied strain during discontinuous tensile tests on unidirectional Nicalon/CAS

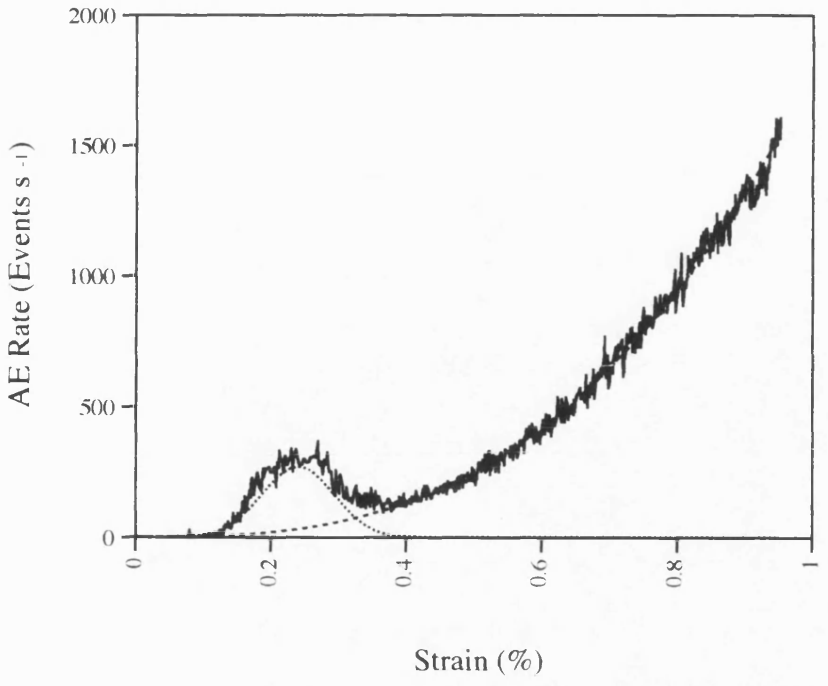

a)

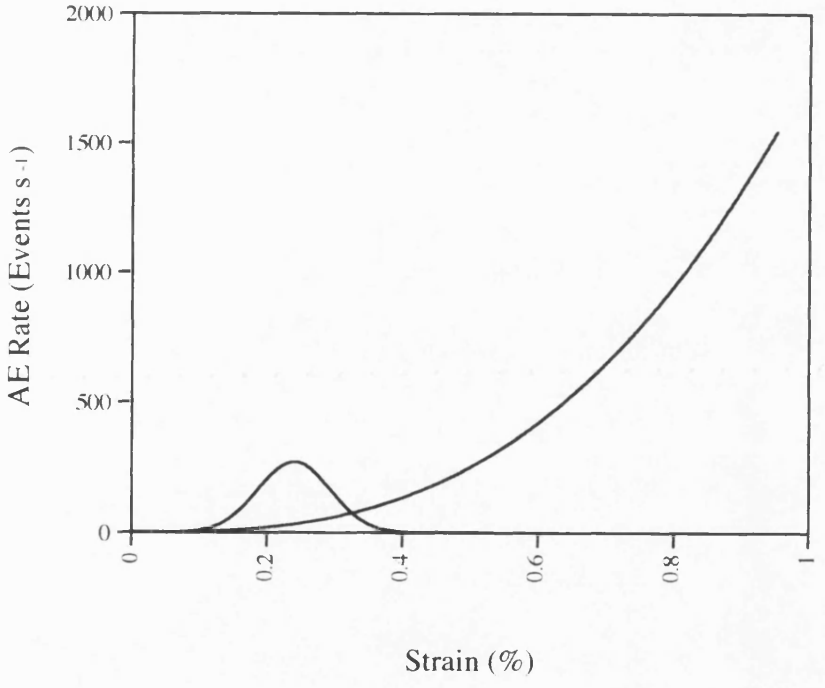

b)

Figure 6.18: Deconvoluted acoustic emission rate response of unidirectional Nicalon/CAS shown a) with original signal and b) without

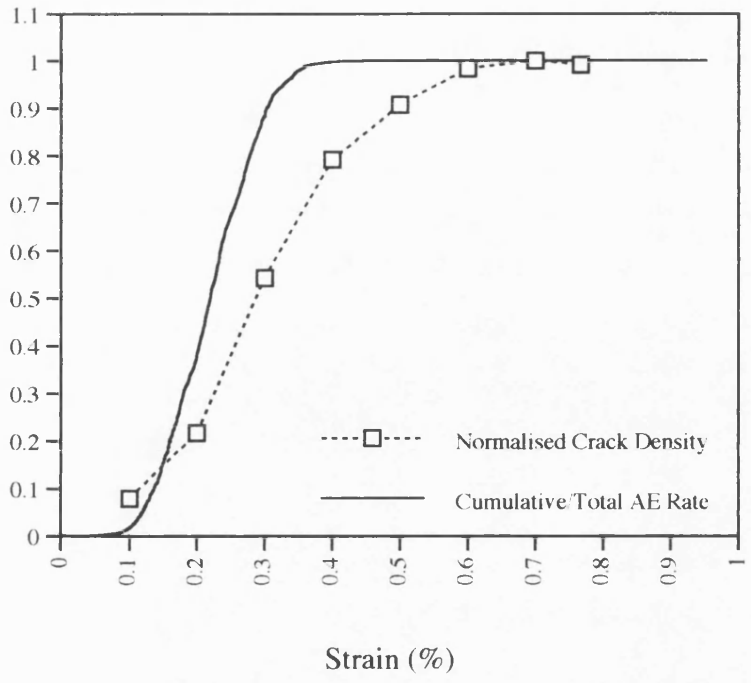

Figure 6.19: Fitted AE data, expressed as a normalised cumulative AE rate, and normalised crack density - plotted as a function of applied strain

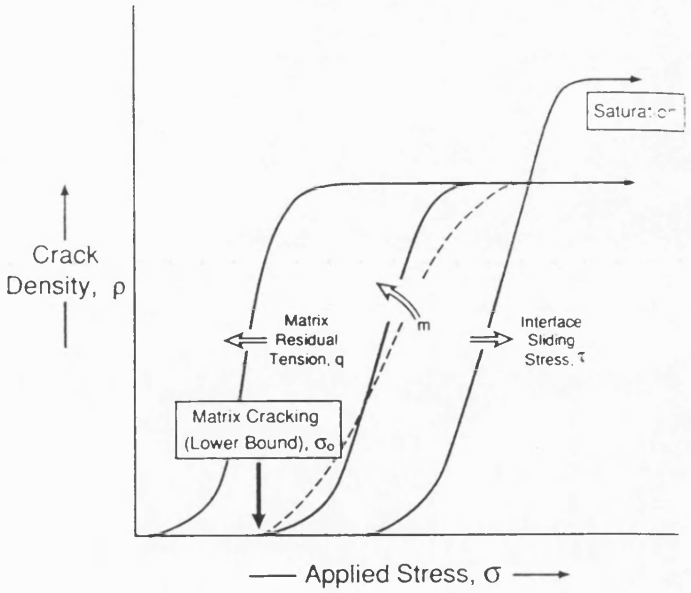

Figure 6.20: Schematic diagram showing possible variation in matrix cracking stress range with changes in interfacial friction stress, matrix residual stress and flaw size distribution (after Beyerle et al[107])

CHAPTER 7 : OFF-AXIS NICALON/CAS COMPOSITE

7.1 Introduction

In Chapter 6 experimental data were presented describing the mechanical behaviour of unidirectional Nicalon/CAS composite when tested parallel to the fibres. The stress-strain and acoustic emission responses were discussed in terms of progressive matrix cracking followed by fibre failure.
However, few structural applications exist for unidirectional composites and as a precursor to the investigation of more practical angle-ply laminates it is necessary to study the effect of fibre orientation on the mechanical behaviour of unidirectional Nicalon/CAS composite.

As discussed in Chapter 2, a number of models exist for predicting the effect of fibre orientation on the ultimate strength of polymer-matrix composites although little experimental data allowing such models to be tested on ceramic-matrix composites are available in the literature.

In the present chapter the room-temperature mechanical properties of Nicalon/CAS tested at a range of fibre orientations are discussed in terms of the available models. The stress-strain and acoustic emission responses during continuous tensile testing are presented together with damage observations.

7.2 Results

7.2.1 Microstructural Characterisation

Material available for off-axis testing was in the form of two unidirectionally-reinforced 150 mm x 150 mm plates of 12-ply construction - identified as # 9012101 L and # 9012102 L (hereafter termed plates 1 and 2 respectively). The consecutive

numbering may indicate that the plates were made from the same pre-preg batch and/or pressed in the same die-stack.

Prior to machining specimens from the two plates, both were examined by a non-destructive ultrasonic c-scan technique which gave the results shown in Figures 7.1 a) and b). The two tests were carried out consecutively under identical conditions and the results may therefore be compared directly. Dark areas show little difference between the input and detected signal whereas lighter areas are associated with greater attenuation and are thus indicative of the presence of features within the material which scatter the ultrasound waves. These features may be defects such as porosity, delamination, fibre misalignment or local variations in fibre volume fraction but, as the tests were carried out in through-transmission mode, may also be due to variations in plate thickness or surface features. For example, labels situated on the underside of each plate (bottom centre) can clearly be identified. Examination of the c-scan results obtained from each plate shows that uniform signal attenuation has occurred over the whole of plate 1 whereas a greater degree of signal attenuation has been caused in parts of plate 2. This may indicate significant differences in the quality of the two plates.

Specimens were machined from the two plates according to the cutting plans given in Figures 7.2 a) and b). In view of the large amount of material wastage in machining off-axis specimens both plates had to be used and not all orientations could be obtained from each plate. As material was limited, and in view of the extreme fragility of 90° composite noted by Harris et al[111], no attempt was made to measure the transverse properties of the composite and the only cross-check between plates was from the properties of 0° specimens.

Image analysis of representative sections by the method outlined in Chapter 4 showed little difference in the volume fraction and distribution of fibres within each plate and gave values for V_f of 0.33 ± 0.02 and 0.32 ± 0.03 from plates 1 and 2 respectively.

Optical examination of the polished edges of specimens prior to testing revealed extensive delamination within the 0°, 5°, 30° and 60° test pieces obtained from plate 2. Figure 7.3 shows a replica taken from an as-received 5° off-axis specimen. Severe delamination is clearly visible. No such flaws were identified in specimens from plate 1.

All three 60° test specimens failed during preparation, as did two of the 30° specimens.

7.2.2 Stress-Strain Behaviour

Typical stress-strain curves from each of the orientations tested are shown in Figure 7.4. From these tests values of elastic modulus, stress and strain at first discontinuity, ultimate strength, strain to failure and Poisson ratio were determined and these are given in Table 7.1. It should be noted that the 0° and 45° properties of plate 1 and 30° properties of plate 2 are the results of single tests whilst all other values are average results from 2 or 3 specimens.

Comparison of 0° data from plates 1 and 2 may indicate that the pre-existence of delamination within plate 2 has the effect of decreasing the measured properties, including composite strength. This latter point may indicate that fibre breakage (for example, due to handling or pressure during manufacture) and/or fibre property degradation (perhaps as a result of fibre compositional changes during composite manufacture) have also taken place in plate 2 prior to testing. However, it should also be noted that the strength and modulus of the 0° specimen from plate 1 are outside the range of measured values given in Table 6.1 of the previous chapter.

With reference to Figure 7.4, it can be seen that the stress-strain responses of 5° and 10° specimens exhibit some of the features of the 0° stress-strain curve (described in Chapter 6), with an initial linear region being followed by a region of almost constant stress. The limit of proportionality on the 5° stress-strain curve is less than that

observed from tests on 0° and 10° composites (by a factor of ~ 1.3) and this is thought to reflect the prior existence of cracks within the matrix of 5° specimens.
After the region of almost constant stress, the slope of the 5° stress-strain curve appears to increase (at a strain of ~ 0.4 %) prior to ultimate failure, as in the case of 0° composite, whilst the 10° specimen fails at this constant stress level at a strain of about 0.4 %.
Stress-strain curves for 20°, 30° and 45° specimens show linear elastic behaviour to failure. The extremely low strength of the 30° specimen again reflects the significant amount of cracking present in the matrix prior to testing and is therefore not thought to be representative of the behaviour of 30° material in relation to other orientations.

The transverse strain behaviour of 5° and 10° composite (Figures 7.5 and 7.6 respectively) also shows similarities to that of 0° specimens by initially decreasing, reaching a minimum at a stress roughly coincident with the limit of proportionality on the longitudinal strain-stress curve, then increasing and in both cases becoming positive. Again Poisson ratio values were determined from strain measurements made within the initial linear portion of the stress-strain curve. Figure 7.6 also shows the strain response of 10° composite at + 45° and - 45° to the loading axis (where + 45° is along the 'grain' of the reinforcement whilst - 45° is against the 'grain'). It can be seen that in both cases the strain is positive and initially linear with good agreement between the two measurements. However, at a stress roughly coincident with the limit of proportionality on the longitudinal strain-stress curve, the + and - 45° strain readings begin to deviate with the - 45° increasing sharply prior to failure and the + 45° decreasing slightly. This will be discussed in section 7.2.5 in terms of the Chamis & Sinclair method for determining composite shear properties from a 10° off-axis test (as outlined in Appendix 1).
The transverse strain response of all other off-axis specimens was negative and linear to failure.

One of the 10° off-axis specimens was loaded to failure in three increments - the first to the onset of acoustic emission activity, the second roughly to the limit of proportionality (as determined from the other 10° tests) and the third to failure. Stress-strain curves for the first two loadings were linear, whereas that of the third loading exhibited the same overall shape as the continuously loaded specimens. Replicas were taken of the untested specimen and at each load, by the method described in Chapter 4, and specimens were unloaded prior to reloading.

7.2.3 Damage Observations

Optical macrographs of representative failures at each orientation are shown in Figures 7.7 (a) to (f). Both 0° specimens failed in a fibrous manner, with overall fracture occurring in a plane perpendicular to the direction of applied load. Fibre pull-out in the plate 1 specimen was found to be much less than that in plate 2 specimens (~ 300 μm and ~ 1 mm respectively). Ultimate fracture of 5°, 10°, 20°, 30° and 45° specimens occurred at different angles to the direction of applied load and at an orientation roughly equivalent to that of the fibres. All 5° and 10° fracture faces exhibited regions of longitudinal-type failure with fibre pull-out. In the 5° composite this region extended from one edge of the specimen to approximately half the specimen width but was much less than this in 10° specimens. Some 5° and 10° specimens did not fail into two pieces but remained intact after the maximum load. Little fibre pull-out was observed in 20°, 30° or 45° specimens and the failure mechanism was predominantly, if not exclusively, shear.

Microscope examination of the polished edges of failed specimens in the region of the main failure site revealed that a regular array of microcracks had formed perpendicular to the fibre direction in all 0° specimens, with the average crack spacing in the 0° specimen from plate 1 (~ 175 μm) being less than that in plate 2 specimens (~ 200 μm). The perpendicular matrix cracks in plate 2 specimens did not appear to

have interacted with the delamination cracks already present in the composite apart from a region directly adjacent to the position of ultimate failure. In this region an interconnecting network of cracks was evident.

Regular arrays of matrix cracks had also formed in 5° and 10° specimens although these were much more widely spaced than in 0° specimens and their spacings were therefore more difficult to measure accurately by optical microscopy techniques. However, an estimate of 600 - 800 μm was made for the average crack spacing in both 5° specimens and 10° specimens by crack counting over the entire gauge length. This gives no information on the crack spacing distribution although it was observed that the maximum crack spacing was of the order of 2 - 3 mm and that the smallest crack separations were found on either side of the fracture site. Although the cracks appeared to be roughly perpendicular to the loading axis in both types of specimen, the orientation of cracks within the body of the composite was not known since only one edge was examined. However, it appeared that the propagation of cracks through the matrix of 10° specimens was by a far more tortuous path than in the 0° composite. Figure 7.8 shows the deviation of a matrix crack from a perpendicular path in the vicinity of fibre-matrix interfaces in a 10° composite. This phenomenon was observed to a lesser extent in 5° specimens.

Microscope examination of replicas from an incrementally loaded 10° specimen showed that at a stress of 140 MPa and a strain of 0.11 % only one matrix crack was visible from the specimen edge and this did not extend across the entire thickness of the specimen. Further examination of this replica revealed that the fibres were more clearly delineated than in that of the untested specimen. Comparison of the same region within these two replicas can be made from Figures 7.9 (a) and (b). A number of factors may contribute to the different appearance of the two replicas. It is important to remember that replicas are an imprint of the specimen surface onto an acetate film and require the application of pressure. The detail obtained on the replica may therefore be sensitive to the amount of pressure applied. Also, the application of

pressure and the removal of the replica from the surface may actually cause damage to the specimen (dislodging fibres or their surrounding matrix perhaps). It should also be noted that the replica of untested material was, by definition, taken when the specimen was in an unloaded state and thus any pre-existing damage may not be evident. However, it may also be possible that the increased delineation of fibres under load is a result of fibre-matrix interface failure.
Optical examination of the polished edges of failed 20°, 30° and 45° specimens did not reveal the presence of any regular cracking patterns and damage appeared to be confined to the location of failure.

7.2.4 Acoustic Emission Response

The acoustic emission response of 0° composites has been described in the previous chapter and it is not proposed to repeat the analysis here. It is sufficient to say that the overall shape of the AE rate versus strain curve and its relation to the stress-strain curve, for material from both plates, was similar to that presented earlier.

Typical acoustic emission responses of 5°, 10° and 20° specimens are shown in Figures 7.10 (a), 7.11 (a) and 7.12, respectively. Again, it can be seen that certain similarities exist between the AE responses of the 5° composite and 0° composites, with the onset of AE activity occurring at a stress well below the limit of proportionality on their respective stress-strain curves, followed by a gradual increase in AE rate until reaching a maximum during the region of almost constant stress. In both 0° and 5° cases the AE rate then decreases with increasing strain, reaching a minimum at a strain roughly coincident with the onset of the second linear region of the stress-strain curve (although it is difficult to determine whether this is in fact linear in the 5° specimen) and gradually increasing until ultimate failure of the composite. No significance should be attached to the vertical axis of the AE rate in

relation to the stress-strain response as, for clarity in presentation, the AE rate was generally scaled down in order to fit on the same axes.

In the case of 10° tensile tests, the AE rate continued to increase from AE onset, at a stress below the limit of proportionality on the stress-strain curve, to ultimate failure of the composite. The AE rate increased sharply prior to failure and this was observed in all 10° tests. In 20° specimens, acoustic emission activity commenced shortly before failure and corresponded to a slight deviation from linearity on the stress-strain curve. However, in 30° and 45° specimens, events were only detected at failure.

The total number of AE events counted for each orientation, expressed in orders of magnitude, are given in Table 7.1. As found by both Valentin et al[142] and Guild et al[143] the total number of emissions tended to decrease with increasing fibre angle, θ, although, in the present study, the total numbers from 5° and 10° specimens are of a similar magnitude.

Amplitude distribution analysis by the Pollock method used in Chapter 6 was performed on the acoustic emission data from all off-axis tests. Representative *b*-plots obtained from analysis of all AE data (up to failure) for each orientation are shown in Figure 7.13 with average values of *b* given in Table 7.1. All values of *b* are of a similar magnitude (~ 1.5 ?), apart from that of the 45° composite. In view of the small number of AE events recorded from 45° specimens and the narrow amplitude range over which *b* is measured, it is thought that the actual value of *b* is unreliable although sufficient to show that all emissions are of low amplitude.

As concluded in the previous chapter, the above type of *b*-plot analysis is unsatisfactory for distinguishing between different failure mechanisms. A more rigorous analysis may be achieved by calculating values of *b* within increments of strain from zero to failure. This has been carried out on 5° and 10° AE data for strain intervals of 0.05% and is shown in Figures 7.10 (b) and 7.11 (b) respectively. These graphs show some surprising similarities with those obtained from the 0° composite, with the average value of *b* over the region of almost constant stress being ~ 1.5. In

Figure 7.10 the vertical dashed line corresponds to the AE rate minimum. The value of b lying on this line was the overall gradient of the bi-modal b-plot obtained within the 0.4 - 0.45 % strain increment. The value of b at strains beyond this line was ~ 2.5. This result is in excellent agreement with those for 0° composites and tends to indicate that a change in failure mechanism takes place within the 0.4 - 0.45 % strain increment, with failure beyond this strain range occurring by a large number of low energy damage events. The increased scatter in b values for 5° and 10° specimens may be attributable to the smaller strain increments over which b is calulated (cf 0.1 % for 0° AE data) and the correspondingly fewer events within each, but it may also be due to the operation of a different type of failure mechanism at low strains. This latter point is most noticeable in the results of 10° composite (Figure 7.11 (b)), where values of b are 0.6 and 0.7 prior to the limit of proportionality.

If one examines the accumulation of events within different amplitude ranges for both 5° and 10° specimens (Figures 7.14 and 7.15 respectively), it can be seen that in 10° composites high amplitude events occur prior to the limit of proportionality on the stress-strain curve, whilst in 5° composite high amplitude events occur only after this point. No high amplitude events (> channel 15) occurred at other orientations.

7.2.5 The 10° Off-Axis Test

The intralaminar shear stress and shear strain were calculated from the measured stress and strain results of 10° off axis material according to the method outlined in Appendix 1. A value of 34 MPa was obtained for the intralaminar shear strength by direct transformation of the measured tensile strength. This is less than both the Iosipescu shear strength and interlaminar shear strength of Nicalon/CAS measured by Harris et al[111] (88 MPa and 41 MPa respectively) and less than the value of ± 45° shear strength quoted by Rolls-Royce as 59 MPa (see Table 6.1). However the result

is at the lower end of the range of ± 45° shear strengths (35 - 42 MPa) quoted by Corning[122].

Calculations based on readings from 0°, 45° and 90° strain gauges yielded negative values of intralaminar shear strain which is in direct opposition to the findings of Chamis & Sinclair[56] for their carbon/epoxy composite 10° off-axis test. This result is thought to reflect the much smaller shear and transverse strains relative to the longitudinal strain in ceramic-matrix composites and may indicate that the technique is inappropriate for a composite in which a substantial contribution to the overall elastic properties is made by the matrix. However, although the slope of a graph of intralaminar shear strength versus intralaminar shear strain was negative, the gradient of the initial linear region of this curve had a magnitude of 46 GPa. This again is less than values for the ± 45° shear modulus of Nicalon/CAS composite quoted by both Harris et al[111] and Rolls-Royce, at 53 GPa and 55 GPa respectively (the former of the two measurements being made by ultrasonic techniques), but nearer to the 49 GPa quoted by Corning[122].

7.2.6 Determination of Fibre Orientation

An attempt to determine the accuracy of fibre orientation in off-axis specimens was made by using the image analysis technique described in section 4.3.4. The technique was initially applied to a 45° composite as the fibres clearly presented elliptical cross-sections to the polished surface and the greatest major axis to minor axis ratio. Measurements of the major axis length, minor axis length and area were made for each selected ellipse and two values of orientation calculated for each. Figure 7.16 shows the distribution of fibre orientation obtained by each method. Calculation of fibre orientation from the area and major axis length of ellipses, as opposed to major and minor axes lengths, gives a narrower distribution which is in accord with the findings of Toll & Anderson[145]. This may reflect the greater accuracy of area

measurement compared to length measurement by having eliminated the smaller and therefore more error-prone minor axis length.

Application of this technique to a 20° off-axis composite gave a much wider range of fibre orientation with values ranging from 0° to 25° and this was not thought to reflect the true fibre orientation distribution. Figure 7.17, which shows the variation of $\cos^{-1}$ (a/b) with a/b (such that when a/b is equal to 1, the fibre is circular and its orientation is thus 0°), illustrates clearly that at high values of a/b (i.e. as b approaches a) small variations in a/b lead to large variations in the calculated fibre orientation. From Figure 7.17 it is evident that the mesurement of fibre ellipse dimensions is an unsuitable technique for fibre orientation determination where the orientation is expected to be less than ~ 40°.

7.2.7 Interfacial Friction Stress Measurements

Measurements of the fibre-matrix interfacial friction stress, τ, were made by the Marshall micro-indentation method described in section 4.3.5. Values of 11 ± 3 MPa and 9 ± 5 MPa were obtained from polished 0° sections of composite from plates 1 and 2 respectively. Again, a number of problems with the technique were highlighted i.e. that satisfactory indentation of fibres in plate 2 (without causing shattering of the surrounding matrix or interaction with adjacent fibres) required only half the applied load necessary for fibres in plate 1. This is not accounted for in the overall results from the two plates as the force applied to the fibre end is calculated from the measured indentation in the fibre (prone to error) and the (assumed constant) fibre hardness. This calculation is necessary because some of the total applied load is borne by the matrix. No variation in matrix properties is considered and the extent of the indentation in the matrix is assumed to be a direct result of fibre depression. Clearly the conclusion drawn in the previous chapter, that the technique is suitable as a

comparator, is not necessarily the case and the validity of this approach must be questioned.

7.3 Discussion

7.3.1 Elastic Properties

The variation of elastic modulus, E_x, with changes in fibre orientation, θ, can be predicted from the following equation

$$\frac{1}{E_x} = \frac{1}{E_{11}}\cos^4\theta + \left(\frac{1}{G_{12}} - \frac{2\nu_{12}}{E_{11}}\right)\sin^2\theta\cos^2\theta + \frac{1}{E_{22}}\sin^4\theta \qquad (7.1)$$

This requires knowledge of the longitudinal, transverse and in-plane shear moduli (E_{11}, E_{22} and G_{12} respectively) and the major Poisson ratio, ν_{12}. The average longitudinal modulus of unidirectional Nicalon/CAS composite given in Table 6.1 of the previous chapter was 127 GPa, whereas the average measured value for the three 0° specimens from plates 1 and 2 is only 118 GPa. The latter value reflects the reduced elastic moduli of plate 2 specimens due to the pre-existence of cracks within the matrix and will be used in the present calculations.

The magnitude of the shear modulus (46 GPa) obtained from 10° off-axis tests has been put into the context of published data for Nicalon/CAS in section 7.2.5 and will be used in the present calculations. The applicability of the test for obtaining such data from ceramic matric composites will be further discussed at the end of this chapter.

The major Poisson ratio of the 0° unidirectional composite was found to be 0.24 (Tables 6.1 and 7.1) and this is in accord with the findings of other workers.

Figure 7.18 gives a comparison of the measured and predicted variation of elastic modulus with fibre orientation. The variation of measured values reflects the

difference in quality between plates 1 and 2, with lower values generally being attributable to the pre-existence of matrix cracks in plate 2. However, it can be seen that the predicted trend is generally followed with the line representing the average behaviour.

The variation of the Poisson ratio, ν_{xy}, with fibre orientation can be predicted in a similar manner from the following equation

$$\nu_{xy} = E_x\left[\frac{\nu_{12}}{E_{11}}(\sin^4\theta\cos^4\theta) - \left(\frac{1}{E_{11}} + \frac{1}{E_{22}} - \frac{1}{G_{12}}\right)\sin^2\theta\cos^2\theta\right] \qquad (7.2)$$

where E_X is the value of elastic modulus calculated above for each value of θ. Figure 7.19 compares the variation in measured and predicted values of Poisson ratio with fibre orientation. It can be seen that measured values are generally higher than predicted and may be considered roughly constant between 0° and 20°.

7.3.2 Matrix Cracking

Previous work on unidirectional Nicalon/CAS composites tested parallel to the fibres (Chapter 6) has shown that matrix crack formation and propagation perpendicular to the fibres occurs over a longitudinal strain range of ~ 0.1 % to 0.4 % during which the composite stress is approximately constant. Associated with this damage is also a reversal of transverse strain from negative to positive and an increase in acoustic emission activity (with amplitude distribution analysis giving a *b* value of ~ 1.5 throughout this region).

Similarities between the stress-strain and acoustic emission responses of 0°, 5° and 10° off-axis composites have been identified in the present chapter. The stress-strain curves of all samples at these orientations exhibit a region of constant stress over a strain range of ~ 0.1 % to 0.4 %, during which a transverse strain reversal occurs and a rapid rise in acoustic emission activity is detected. Again, amplitude distribution

analysis gave a b value of ~ 1.5 over this range. Since a regular array of matrix cracks is present in failed specimens of both 5° and 10° off-axis composites, it may be supposed that these cracks form and grow in a manner similar to those in 0° composites.

In 0° composites, formation of the first few microcracks was found to have occurred at stresses well below the limit of proportionality on the stress-strain curve and was coincident with detection of the first few acoustic emission events. The onset of acoustic emission activity occurred in 5° and 10° off-axis composites at a stress and strain similar to those in 0° material, this stress level again being well below the limit of proportionality, although it was not confirmed whether this coincided with the onset of matrix cracking at these fibre orientations.

It should be noted that amplitude distribution analysis of 5° and 10° AE data gave much lower values of b at low strains (~ 1 and ~ 0.6 respectively compared to the 1.5 thought to be associated with matrix cracking). A discontinuous tensile test on a 10° off-axis composite showed that within a strain range of 0.06 % to 0.11 %, during which several (~ 40) acoustic emissions were detected, only one crack had become visible on the specimen edge whilst the only other noticeable difference in appearance was an increased delineation of fibres, possibly owing to interface failure. It is possible therefore that initial damage in 10° specimens is by interface failure and that the onset of matrix cracking does not occur until stresses approaching the limit of proportionality. Interface failure has previously been suggested as a source of acoustic emissions at low strains in unidirectional Nicalon/Pyrex composite (Ford et al[77]) although evidence of this is by no means conclusive in the present study, nor in fact in any other studies.

Little comment can be made regarding the onset of cracking in the 5° composite in view of the presence of cracks in as-received specimens, although it may be noted that acoustic emissions were not detected from zero strain nor did the perpendicular

cracks appear to interact with delamination cracks apart from at the location of ultimate failure.

In the 0° composite, the onset of matrix cracking was found to be in good agreement with that predicted by ACK theory when modified for the residual thermal stress in the matrix and this was found to coincide with the onset of acoustic emission activity. Expressions derived by Aveston et al[4] and McCartney[22] indicate that the composite matrix cracking strain is mostly dependent on the intrinsic properties of the constituent materials. It is therefore possible that small changes in fibre orientation would have little effect on the onset of matrix cracking.
However, since radial residual thermal stresses are negligible in the CAS matrix[113] it is possible that the effective residual matrix stress may decrease with increasing θ which may in turn lead to an apparent increase in the stress required to cause matrix cracking (although this is likely to be a small effect at angles of 20° and less).
Evidence of the effect of residual thermal stresses on the propagation of cracks through the matrix of 10° composite has been shown in Figure 7.8.

Continued matrix cracking in 0° composites is made possible by load transfer between fibres and matrix across the fibre-matrix interface and can only occur if the fibres are able to withstand the additional load thrown upon them. Since multiple matrix cracking occurs in both 5° and 10° composites it may be assumed that load transfer between fibres and matrix remains possible and that fibres at these orientations still have sufficient load-carrying capability.
According to Aveston, Cooper & Kelly[4], continued matrix cracking is limited by the stress that short lengths (x') of interface can withstand and the saturation crack spacing will thus be between x' and $2x'$. In the previous chapter, the average crack spacing in the 0° composite at failure was shown to be in the region of 200 μm. The average crack spacings in 5° and 10° composites at failure were found to be of the order of 600 - 800 μm. This increase in crack spacing may be due to an effectively

reduced interfacial shear strength in the direction of applied load, thus giving a greater stress transfer length and it may be possible to modify the ACK expression for x' to accommodate changes with orientation.

Microscope examination of failed 20° off-axis specimens indicated that little or no cracking had occurred in the matrix beyond the main failure site. A slight deviation from linearity occurred on the stress-strain curve of 20° composite at stresses approaching the ultimate strength (i.e. at a much lower stress than in 0° and 5°) and coincided with the onset of acoustic emission activity. However, since the onset of AE activity occurs at a similar stress and strain for $0° \leq \theta \leq 20°$ it is possible that interface failure and/or matrix cracking also occurs at this stress level in the 20° composite. The lack of any periodic microcracking may indicate that formation of the first few cracks in the matrix of a 20° off-axis composite is far more critical than at lower angles as fibres at this orientation are not able to withstand the additional load and ultimate fracture of the composite occurs.

7.3.3 Ultimate Strength

Predictive models for the variation in composite ultimate strength with fibre orientation have been described in section 2.6. In order to compare predictions based on these models with measured off-axis composite strengths, values for the longitudinal, shear and transverse strengths of the unidirectional lamina are required (σ^*_{11}, τ^*_{12} and σ^*_{22} respectively). Taking measured values of σ^*_{11} and τ^*_{12} as 430 MPa (mean tensile strength) and 34 MPa (from 10° off-axis tests), respectively, together with a transverse strength of 28 MPa quoted by Corning[122], we obtain the predicted variation in composite strength as a function of fibre orientation shown in Figures 7.20, 7.21 and 7.22 (based on the maximum stress theory, maximum strain theory and Tsai-Hill failure criterion, respectively). Good agreement is found between the measured and predicted strengths of all samples from plate 1. It is inevitable that the strength of 10° composite agrees with predictions based on the maximum stress

theory, as the value of shear strength incorporated in this failure criteria was calculated from the 10° off-axis strength by using the same transformation equations. However, the large discrepancy between the measured and predicted strengths of 5° and 30° off-axis composite is thought to reflect the poor quality of plate 2, thus hindering a full discussion and interpretation of the data. The strength of the 5° composite is predicted to be ~ 290 MPa by the Tsai-Hill model and ~ 390 MPa by the maximum stress and strain theories, compared to an average measured value of 170 MPa. It may be noted that errors in fibre orientation are most critical at small angles. Maximum strain theory predicts a variation in strength of the order of ±50 MPa for a ±1° error in fibre orientation at 5°. Errors of this type may be expected to contribute to the overall discrepancy between measured and predicted strengths.

Maximum stress and strain theories predict a transition from longitudinal tensile to shear failure at 5° although fractographic examination of failed tensile test specimens tends to indicate that both 5° and 10° specimens failed by combined tension and shear as fracture faces exhibit features of both types of mechanism. This is in agreement with the findings of Dawson et al[86] who observed a transition from longitudinal tensile to shear failure between 5° and 10° for their Nicalon/Pyrex composite.

The variation of resolved stresses (longitudinal, transverse and shear) with fibre orientation was calculated for the Nicalon/CAS composite from failure stresses predicted by the Tsai-Hill failure criterion with the standard transformation equations. It was predicted from this that the actual maximum shear stress occurred at an orientation of 14° with little change over the range 10° - 18°. It was also predicted that for a measured shear stress of 34 MPa at 10°, the actual shear strength would have to be 40 MPa. It may be concluded that the 10° off-axis test is an unsuitable method of determining the shear strength of this composite.

Since all three failure criteria investigated assume linear elastic behaviour with fracture dominated by fibre failure, only the occurence of ultimate failure is predicted and no information on the matrix cracking behaviour may be gained. However, it is interesting to note that the predicted strength of 20° composite is in good agreement with measured values and that this is only marginally greater than the stress at the onset of acoustic emission activity and tends to confirm the lack of matrix cracking prior to failure at this orientation. On the basis of this reasoning it may be supposed that specimens tested at fibre orientations between 10° and 20° would exhibit lessening degrees of matrix cracking.

7.4 Conclusions

The effect of fibre orientation on the room temperature tensile properties of unidirectional Nicalon/CAS composite has been investigated. Discussion and interpretation of the data was hindered by differences in quality between the two plates tested.
A difference in material quality was successfully highlighted by a non-destructive ultrasonic c-scan technique and was identified by microstructural examination as being due to delamination in one of the plates.

Results of microindentation tests were not thought to reflect differences in the properties of the two plates.

Measurement of the dimensions of fibre ellipses was found to be an unsuitable method of fibre orientation determination.

The 10° off-axis test was thought to be inappropriate for a composite in which the matrix makes a significant contribution to the overall elastic properties.

The tensile stress-strain and acoustic emission responses of 0°, 5° 10° and 20° off-axis composite were discussed in terms of interface failure and matrix cracking.

Incremental amplitude distribution analysis of AE data was again successful in discriminating between failure mechanisms.

The properties of the non-delaminated plate were found to be in good agreement with predictions of available failure criteria.

Orientation, θ	0°	0°	5°	10°	20°	30°	45°
Specimen Origin*	1	2	2	1	1	2	1
Elastic Modulus (GPa)	135	109	104	119	119	77	104
Poisson Ratio	0.24	0.24	0.22	0.25	0.25	-	0.21
Proportional Limit (MPa)	-	150	115	159	87	N/A	N/A
Proportional Limit (%)	-	0.14	0.11	0.15	0.07	N/A	N/A
AE Onset (MPa)	92	85	60	66	85	27	50
AE Onset (%)	0.07	0.08	0.06	0.06	0.07	0.04	0.05
Strength (MPa)	473	408	170	203	115	28	50
Strain to Failure (%)	0.95	0.87	0.46	0.38	0.1	0.04	0.05
Total AE Events	100,000	100,000	10,000	10,000	1000	100	10
***b* value**	1.7	1.7	1.5	1.2	1.4	1.3	3.5

Table 7.1: Room-temperature tensile properties of unidirectional off-axis Nicalon/CAS composite

(* Plate 1 = # 9012101 L, Plate 2 = # 9012102 L)

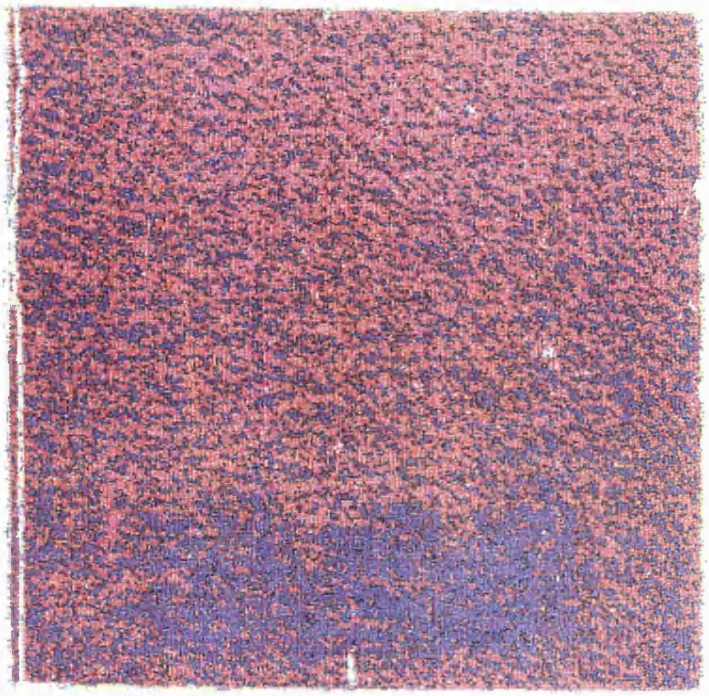

Figure 7.1 (a): Ultasonic c-scan of plate 1

Figure 7.1 (b): Ultrasonic c-scan of plate 2

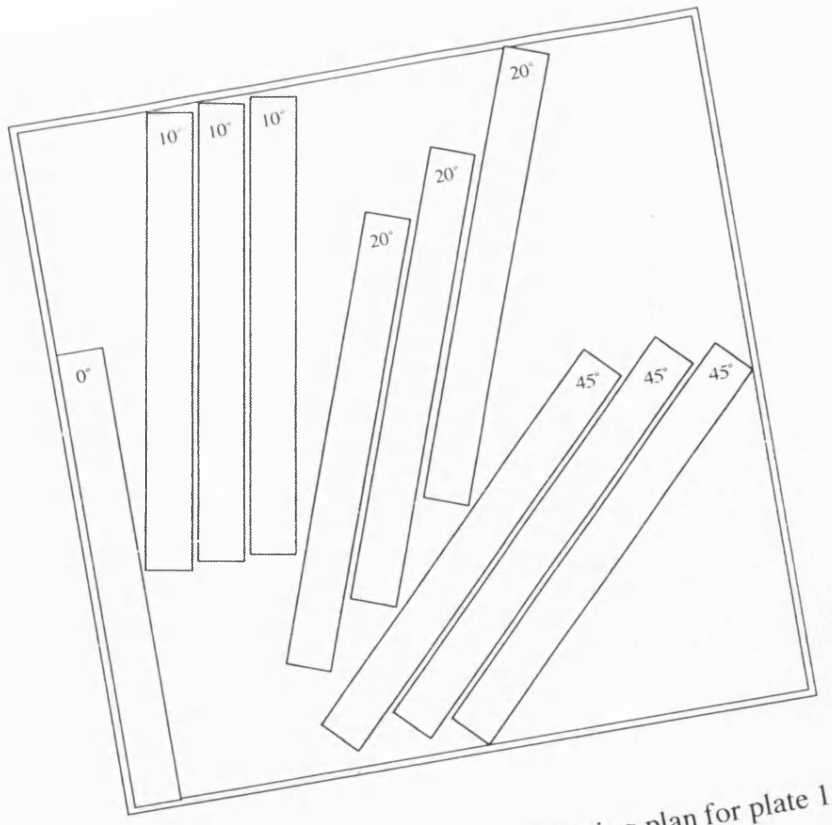

Figure 7.2 (a): Specimen machining plan for plate 1

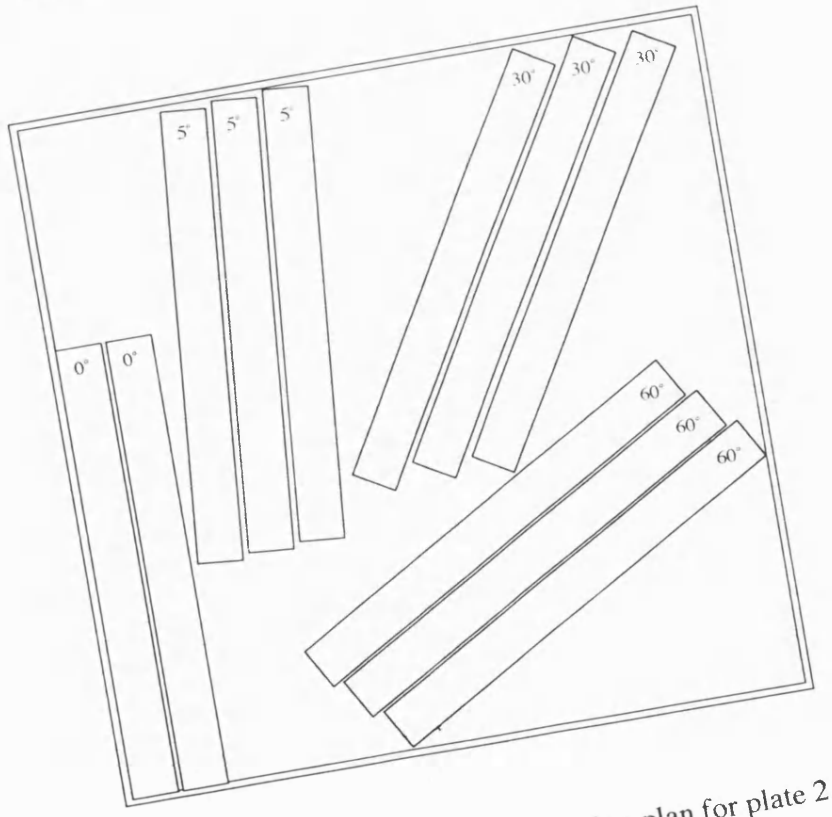

Figure 7.2 (b): Specimen machining plan for plate 2

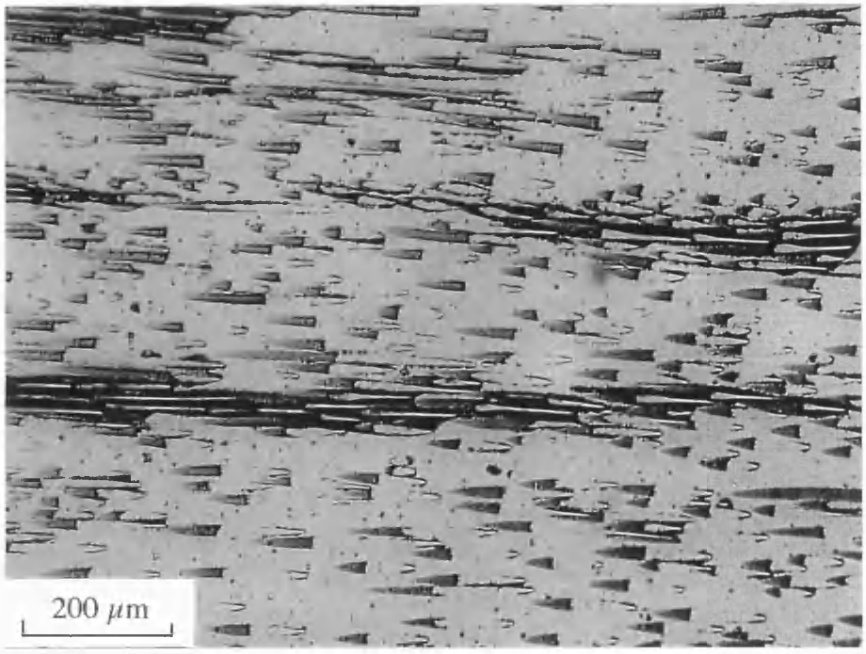

Figure 7.3: Optical micrograph of replica taken from as-received 5° off-axis composite showing delamination (x100)

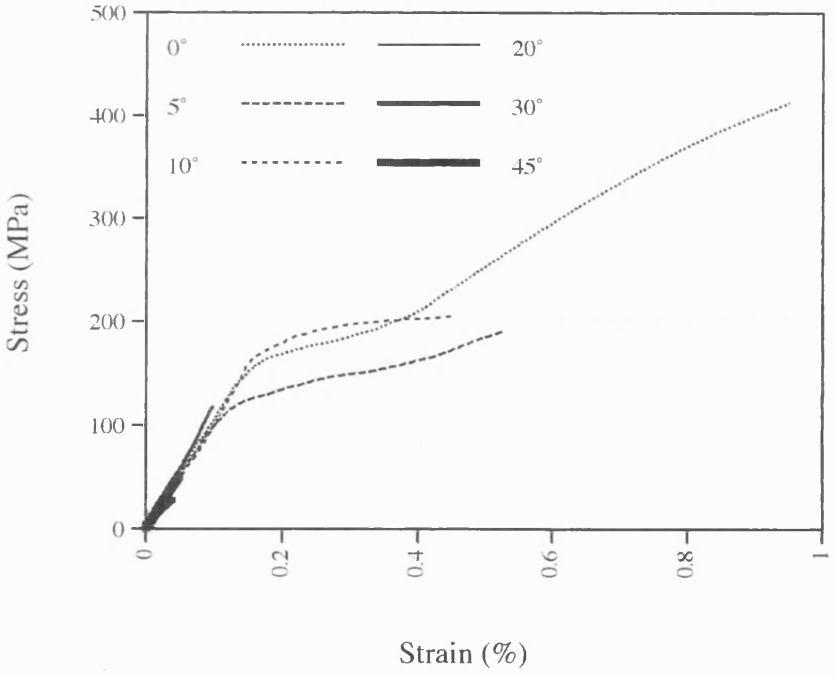

Figure 7.4: Typical room-temperature tensile stress-strain behaviour of unidirectional off-axis Nicalon/CAS composites

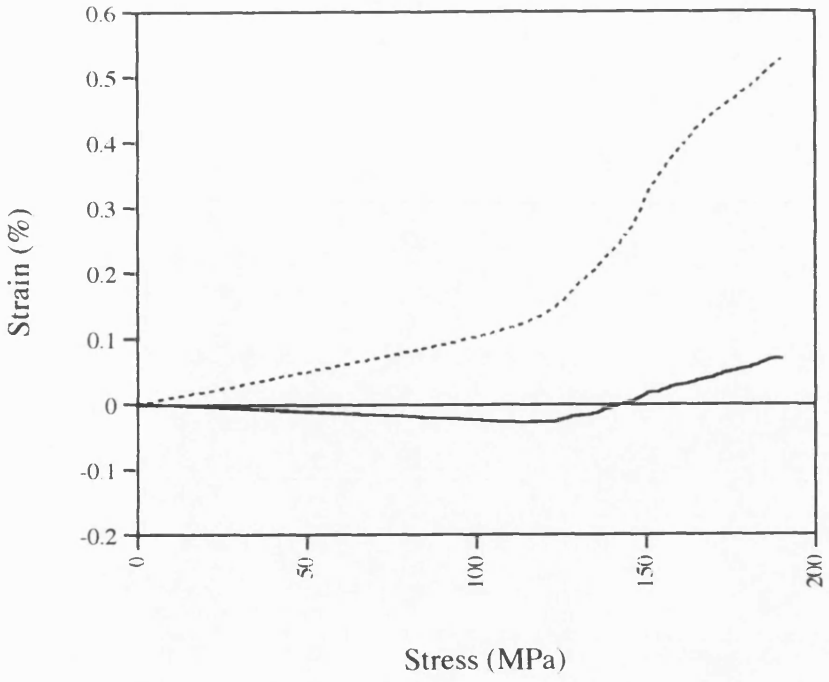

Figure 7.5: Transverse strain behaviour of 5° off-axis Nicalon/CAS composite

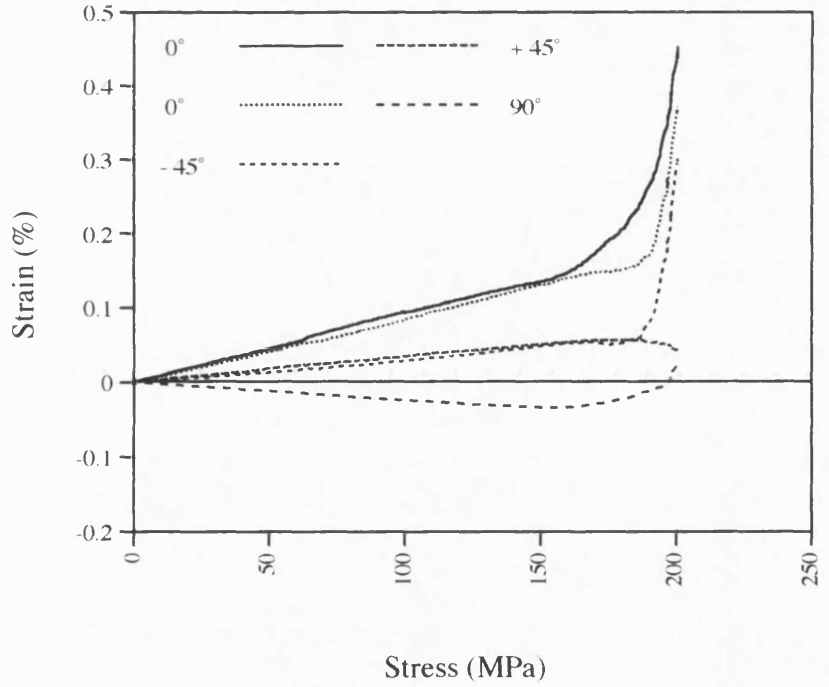

Figure 7.6: Transverse strain behaviour of 10° off-axis Nicalon/CAS composite

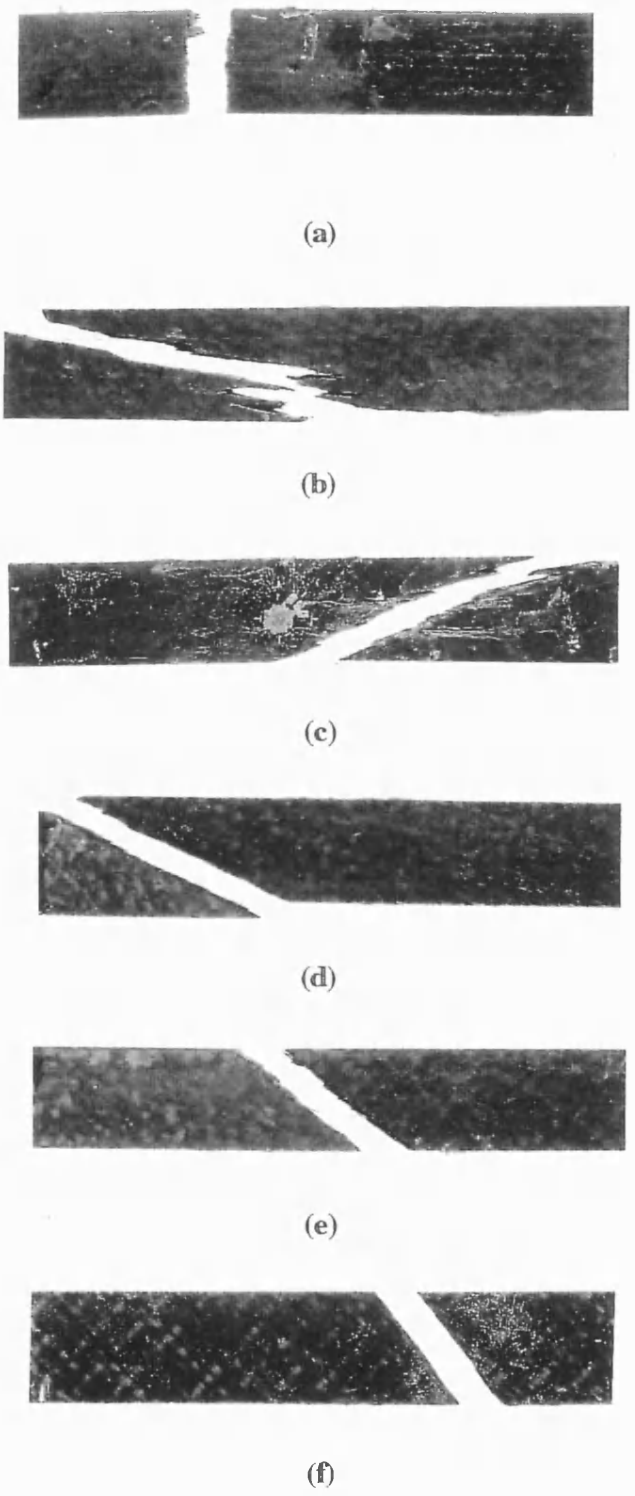

Figure 7.7 : Optical macroscopic photographs showing typical fracture profiles of (a) 0°, (b) 5°, (c) 10°, (d) 20°, (e) 30° and (f) 45° off-axis composite (x 1.5)

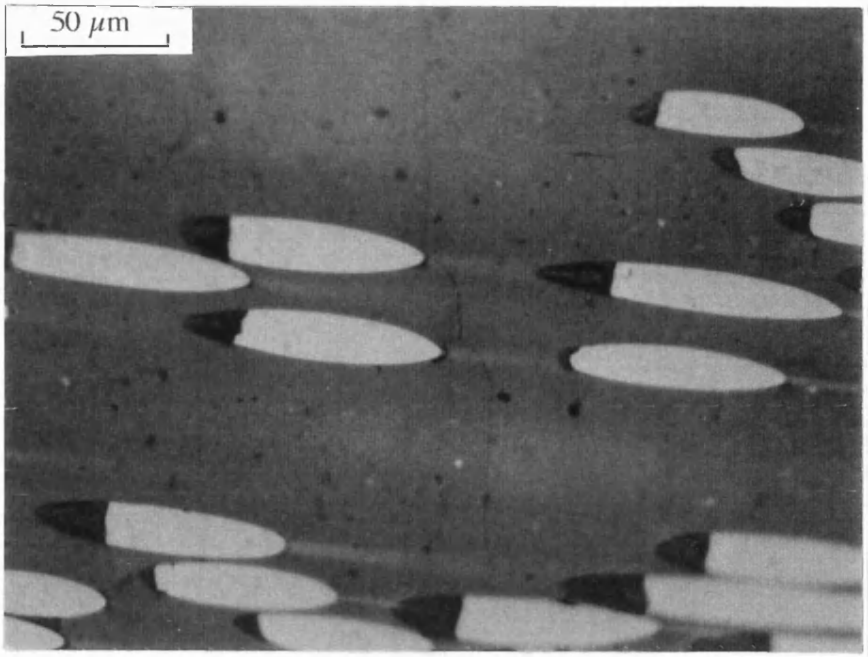

Figure 7.8: Optical micrograph showing deviation of matrix cracking towards fibre-matrix interfaces in 10° off-axis Nicalon/CAS composite (x 400)

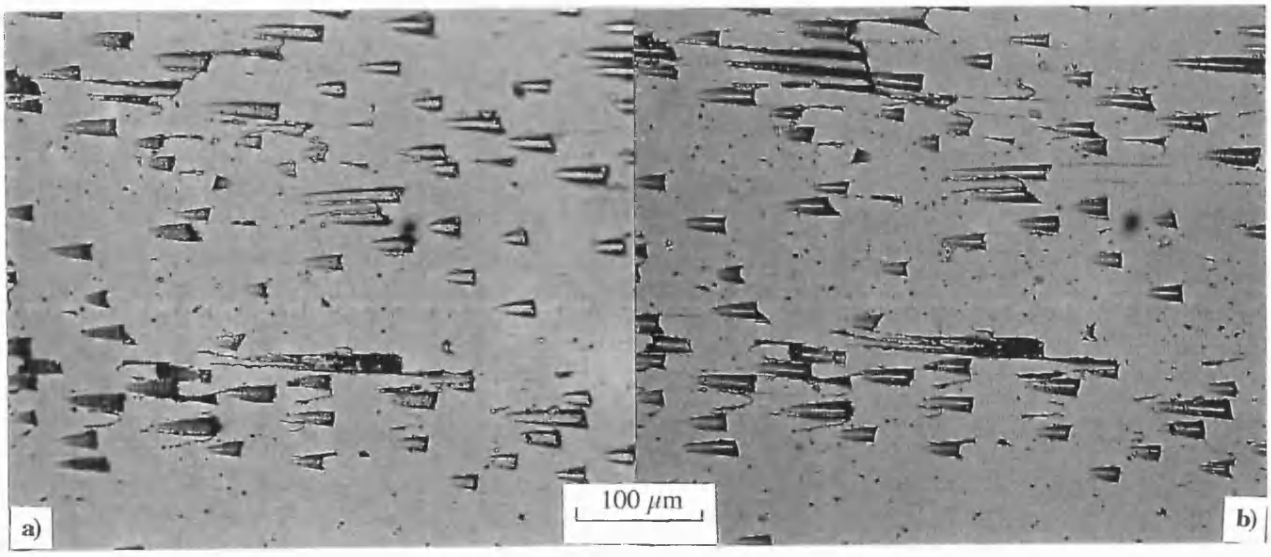

Figure 7.9: Comparison of optical micrographs from identical areas on replicas taken from (a) as received 10° off-axis composite and (b) at 140 MPa (x 200)

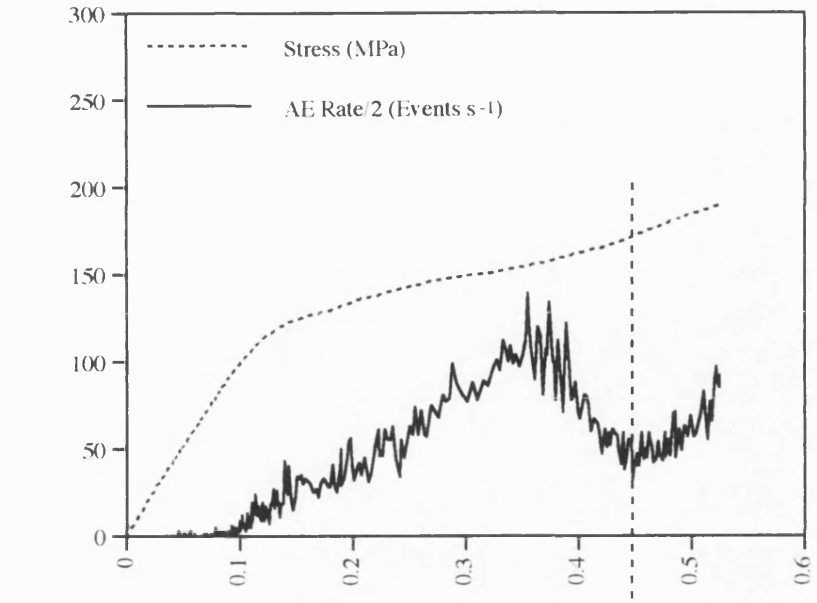

a)

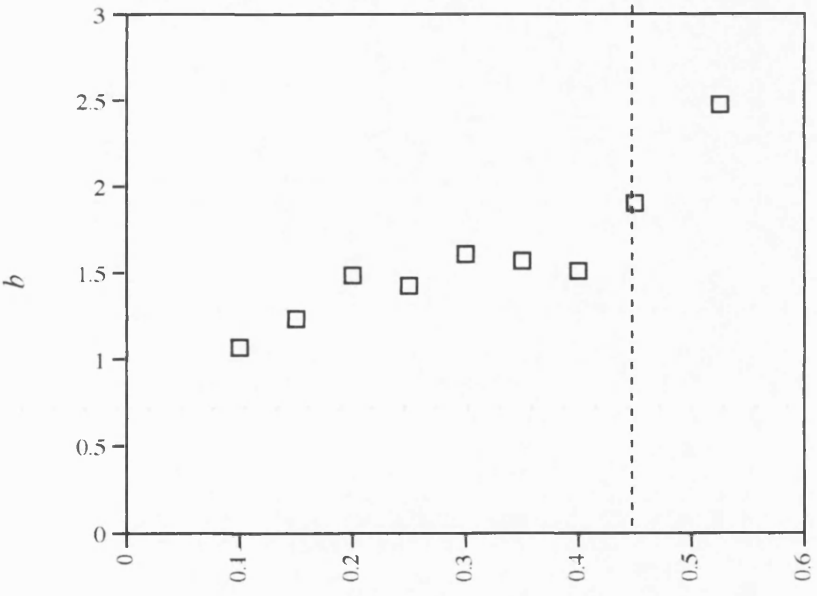

b)

Figure 7.10: Acoustic emission response of Nicalon/CAS 5° off-axis composite shown as a) AE rate and b) *b* value as a function of applied strain

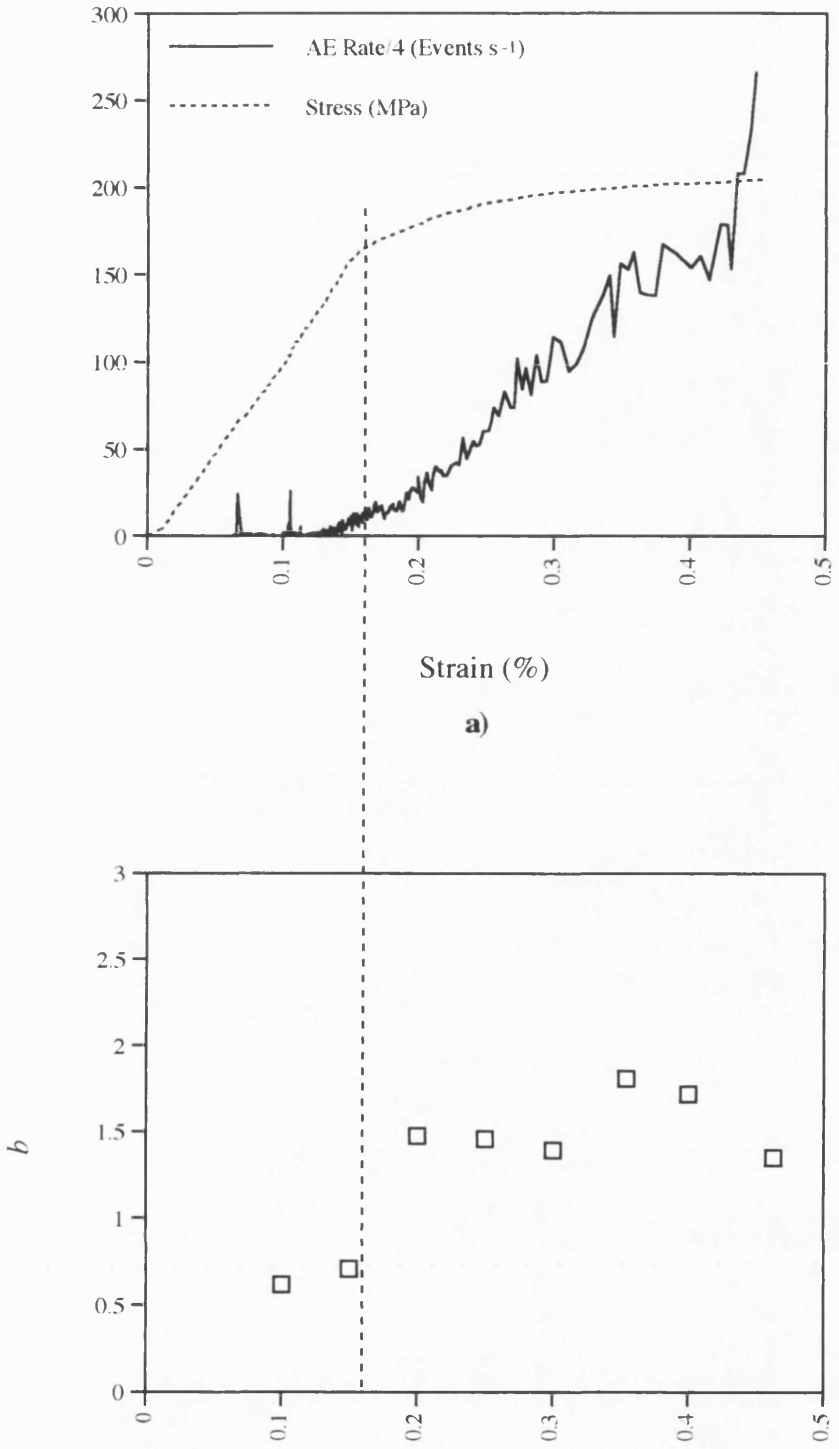

Figure 7.11: Acoustic emission response of Nicalon/CAS 10° off-axis composite shown as a) AE rate and b) *b* value as a function of applied strain

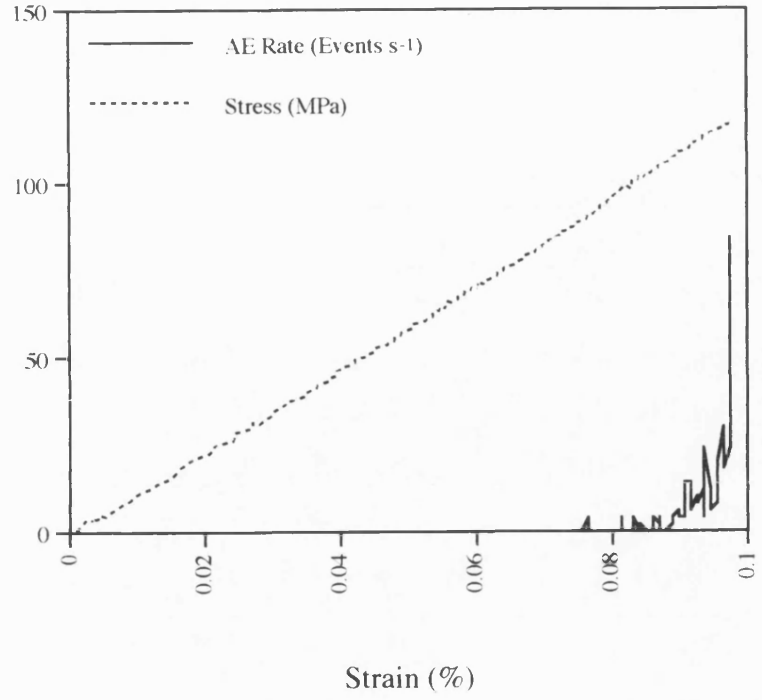

Figure 7.12: Acoustic emission response of 20° off-axis Nicalon/CAS composite as a function of applied strain

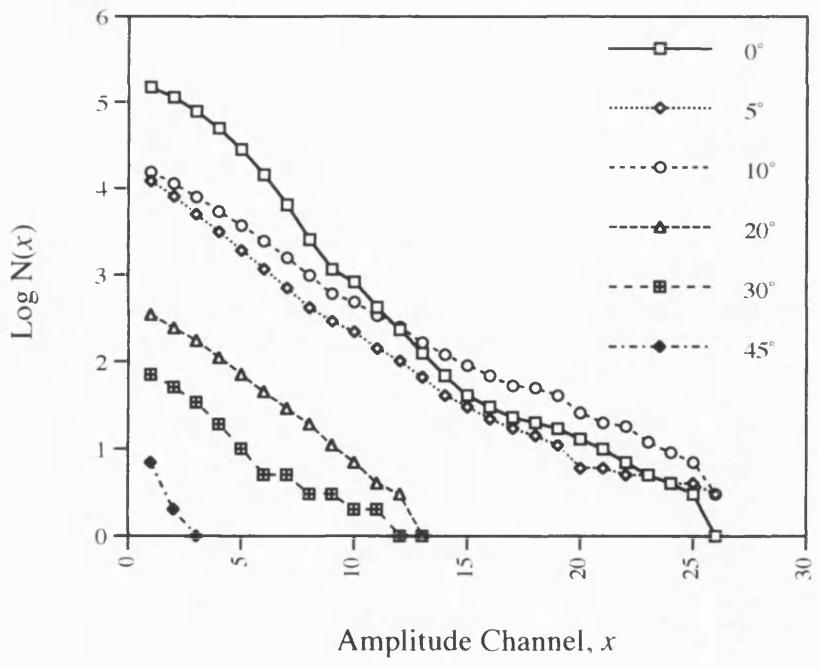

Figure 7.13: Representative *b*-plots of all Nicalon/CAS off-axis composites

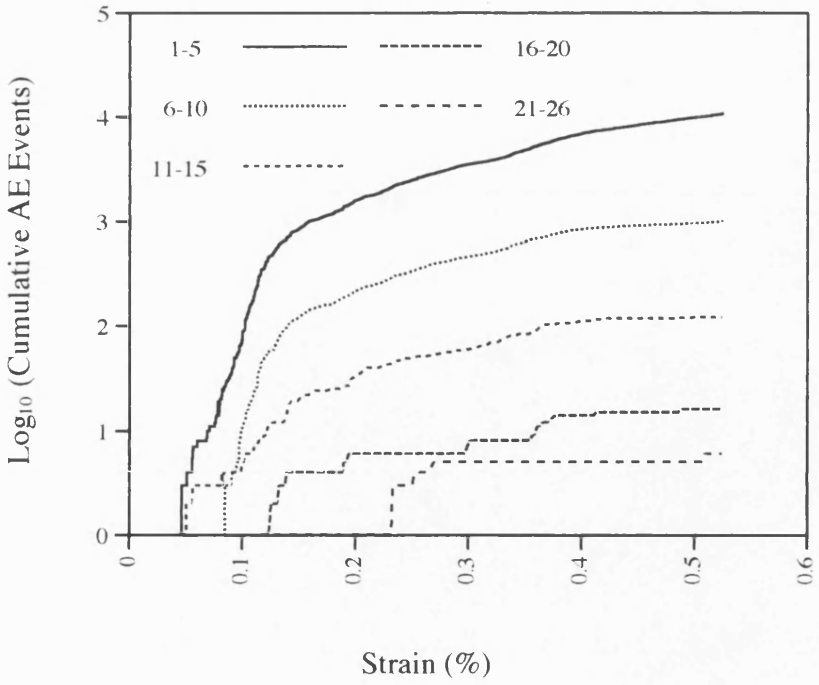

Figure 7.14: Accumulation of acoustic emission events within different amplitude channels for 5° off-axis composite

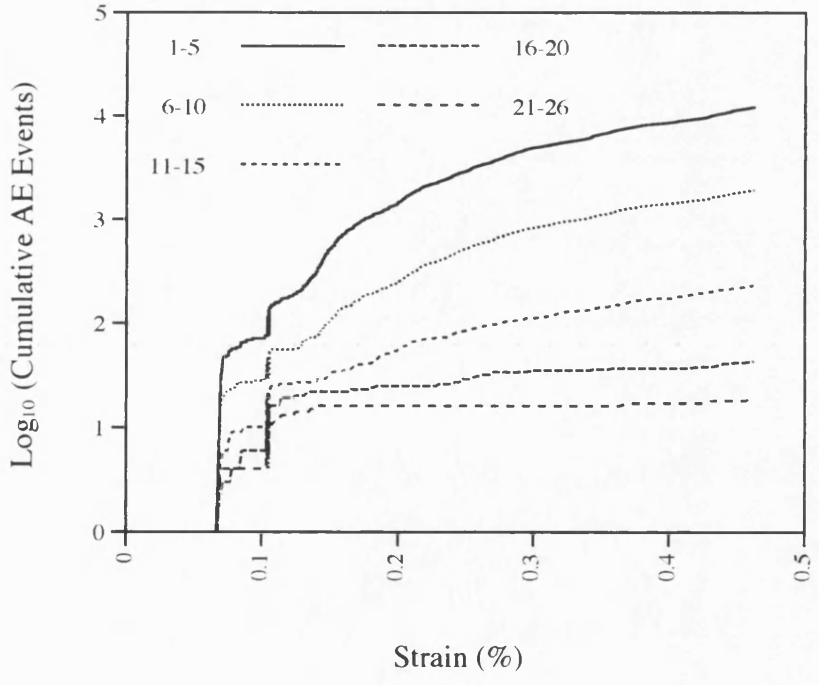

Figure 7.15: Accumulation of acoustic emission events within different amplitude channels for 10° off-axis composite

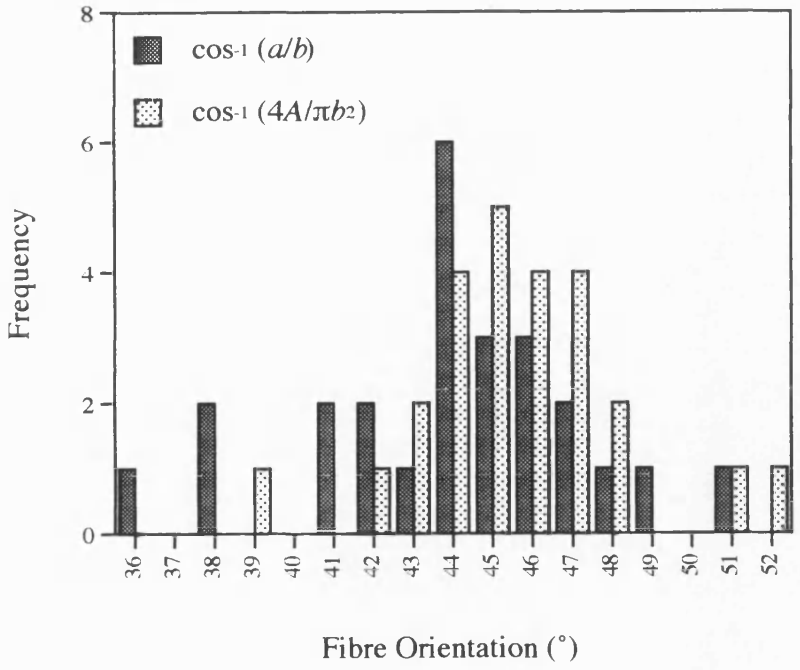

Figure 7.16: Histograms showing fibre orientation distribution within 45° off-axis composite measured from (a) major and minor axis lengths and (b) major axis length and area

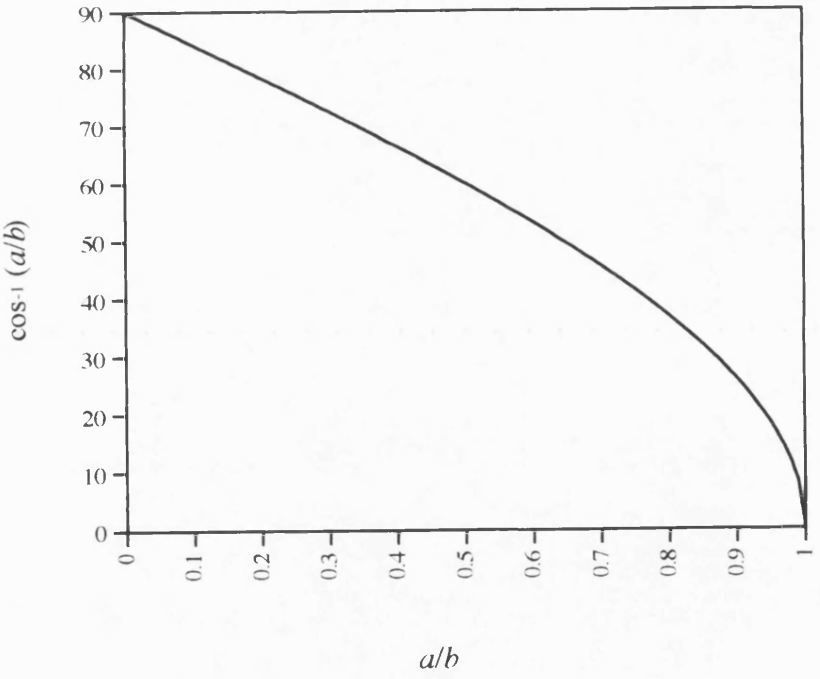

Figure 7.17: Variation of $\cos^{-1}(a/b)$ as a function of a/b

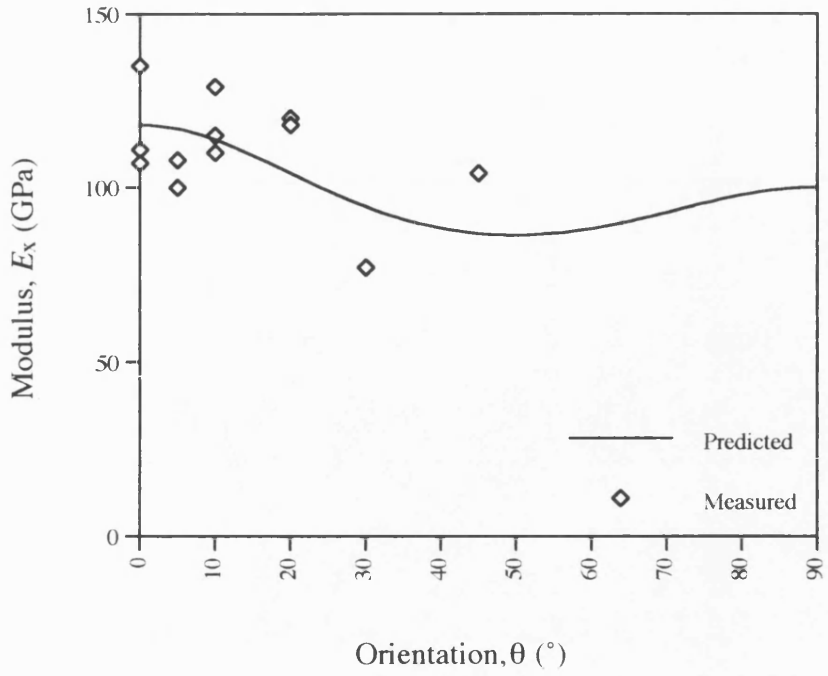

Figure 7.18: Comparison of measured and predicted elastic moduli as a function of fibre orientation

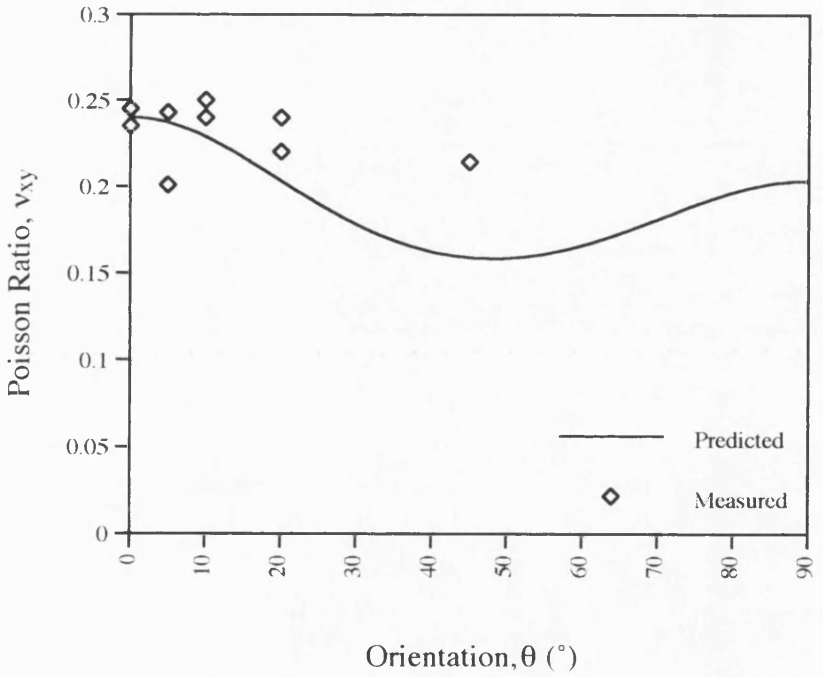

Figure 7.19: Comparison of measured and predicted Poisson ratio as a function of fibre orientation

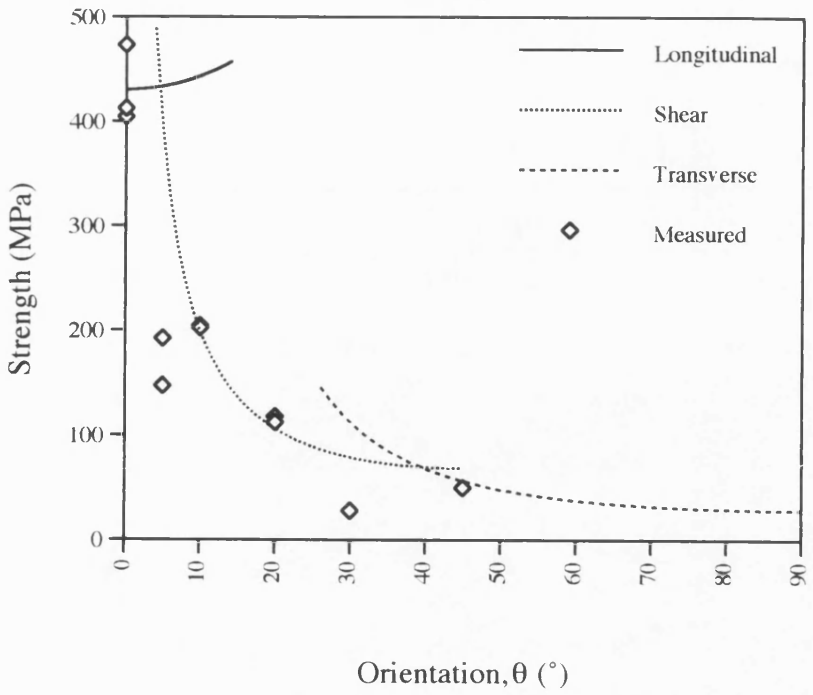

Figure 7.20: Comparison of measured and predicted fracture strength as a function of fibre orientation based on the maximum stress theory

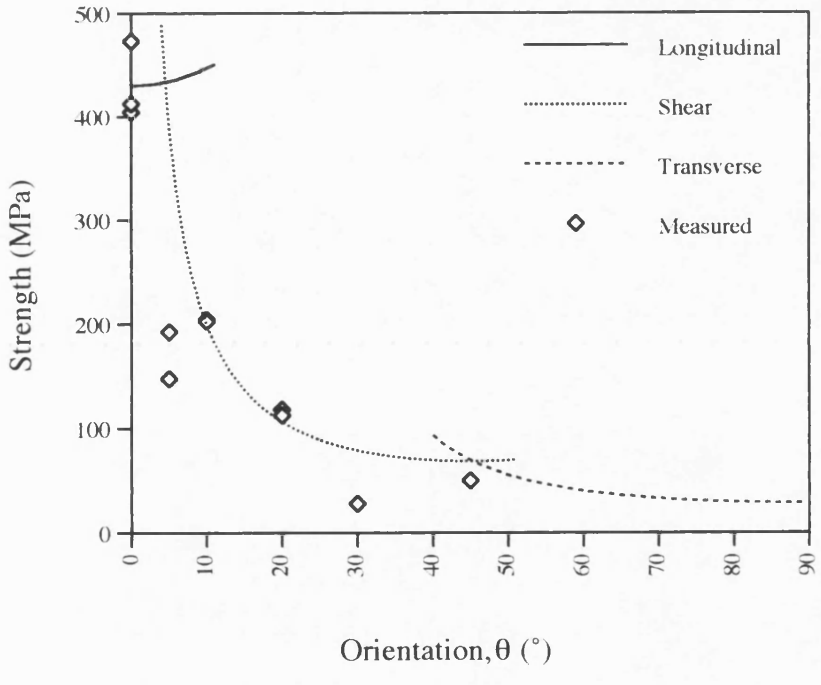

Figure 7.21: Comparison of measured and predicted fracture strength as a function of fibre orientation based on the maximum strain theory

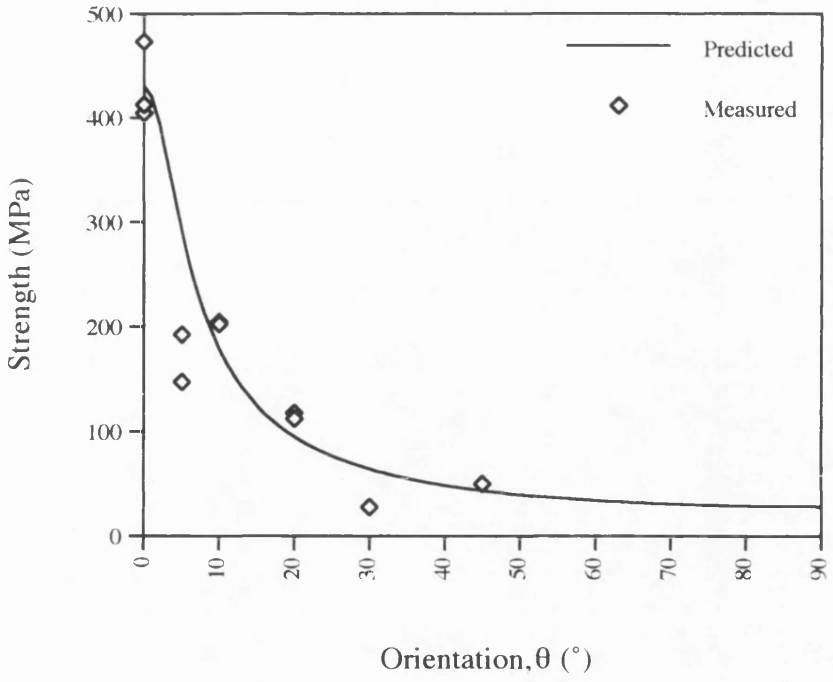

Figure 7.22: Comparison of measured and predicted fracture strength as a function of fibre orientation based on the Tsai-Hill failure criterion

CHAPTER 8 : ANGLE-PLY NICALON/CAS COMPOSITE

8.1 Introduction

In Chapter 7 experimental data were presented describing the mechanical behaviour of unidirectional Nicalon/CAS composite as a function of fibre orientation. The stress-strain and acoustic emission responses were discussed in terms of matrix cracking and measured strengths were compared to predictions based on available failure criteria.

In the present chapter the room-temperature mechanical properties of a range of model Nicalon/CAS angle-ply laminates are discussed in the light of results from unidirectional and off-axis composite. The stress-strain and acoustic emission responses during continuous tensile tests are presented together with damage observations.

8.2 Results

8.2.1 Microstructural Characterisation

Material was made available in the form of six Nicalon/CAS plates having a (0/θ/0) laminate construction, where θ was equal to 0°, 5°, 10°, 20, 45° and 90° (as detailed in Table 4.1). Again, consecutive identification numbers may indicate that some of the plates were pressed together in the same die-stack and/or made from the same pre-preg batch. Twelve to fourteen specimens were cut from each plate in a direction parallel to the fibres in the outer plies. Microstructural characterisation was carried out on samples taken from within the end tabs of failed test specimens. Delamination was generally present along the centre of θ plies in all material examined and large matrix-rich regions were evident between plies and along the specimen edges. A typical microstructure of as-received (0/θ/0) composite is shown in Figure 8.1. Microscopic examination of $(0)_3$ composite revealed the presence of micropores

situated around the edges of fibres (as shown in Figure 8.2) and to a greater extent than seen in any other composite. Measurement of the interfacial friction stress within this sample, by the Marshall microindentation method used previously, gave a value of 23 ± 5 MPa. This is far in excess of values obtained from other unidirectional composites. However, bearing in mind comments made about this technique in Chapters 6 and 7, this result is by no means absolute. Interfacial friction stress measurements of this type were not performed on other (0/θ/0) laminates.

As discussed in section 4.3.4, the measured fibre volume fraction of angle-ply laminates is only equal to the true fibre volume fraction when determined from sections taken at -(θ/2) to the 0° fibres. In view of the difficulty of cutting such sections accurately, fibre volume fractions were measured only from $(0)_3$ composites cut at 90° and from (0/90/0) composites cut at 45°. Image analysis of these sections gave values of V_f as 0.29 ± 0.03 and 0.29 ± 0.02 respectively. On the basis of these results, it was assumed that all other laminates would have similar fibre volume fractions. This is clearly less than the value obtained from thicker unidirectional material and reflects the presence of a large matrix-rich interply region seen in the (0/θ/0) composites.

8.2.2 Stress-Strain Behaviour

Room temperature tensile tests were carried out on specimens of each lay-up. Six to eight specimens from each plate were loaded continuously to failure whilst the remainder were loaded to different levels of strain (chosen in relation to features of the continuous stress-strain curve) in order to assess the extent of damage at each stage.

Representative stress-strain curves from continuous tensile tests for each of the angle-ply laminates (excluding a unidirectional composite) are shown in Figure 8.3. From

these tests values of elastic modulus, stress and strain at the first discontinuity, ultimate strength, strain to failure and Poisson ratio were determined. Average values of these data for each plate are given in Table 8.1, each value being based on a minimum of six results and up to a maximum of fourteen (e.g. elastic modulus, which could be obtained from all tests).

Comparison of the unidirectional data given in Table 8.1 with those obtained previously (Tables 6.1 and 7.1) shows that the stress and strain to failure of the $(0)_3$ composite is much lower than expected although the elastic moduli are in excellent agreement.

The elastic moduli of $(0/\theta/0)$ composites change little for $\theta \leq 20^\circ$ but decrease at higher θ ply orientations to a value at (0/90/0) approaching that of the un-reinforced matrix.

Again, Poisson ratio values were determined from an almost constant region within the linear part of the stress-strain curve and show little difference from the unidirectional value of 0.24 for $\theta < 90^\circ$. The value of Poisson ratio obtained from (0/90/0) tests is similar to the ν_{21} value predicted in Chapter 6.

The $(0)_3$ limit of proportionality is within the range of measured values obtained previously from unidirectional composites although less than that of the (0/5/0), (0/10/0) and (0/20/0) composites, which are all of the same order at ~ 180 MPa and 0.15 % strain. The proportional limits of (0/45/0) and (0/90/0) composites are much lower than this value.

The ultimate strengths of the composites show a generally decreasing trend with increasing θ ply angle, although all are greater than their corresponding unidirectional off-axis strengths.

The strains to failure of laminates again show a decreasing trend with increasing θ ply angle, reaching a minimum at 20° and then increasing again. A large degree of scatter was observed in measured values of failure strain with coefficients of variation being of the order of 30 - 40 % of the average value.

With reference to Figure 8.3, it can be seen that a typical stress-strain curve from (0/5/0) specimens is similar in shape to that of the unidirectional composite with an initial linear region followed by a region of decreasing slope and then a second linear region up to ultimate failure. The strain at which this second linear region commences (~ 0.4 %) and its slope (~ 40 GPa) are again similar to those observed in the unidirectional composite.

Stress-strain curves of the (0/10/0) and (0/20/0) laminates appear to follow that of the (0/5/0) composite, with an initial linear region followed by a region of gradually decreasing slope. (Some of the curves superimposed exactly although these were not shown for purposes of clarity). However, the extent of this region of decreasing slope in these cases was limited by failure of the composite and, although the strains to failure of (0/10/0) composites are generally greater than those of (0/20/0) materials, the average failure stresses are similar. This illustrates that the failure of these two laminates occurs during a region where a large increase in strain gives little increase in stress - the converse of which may also be the reason for the large degree of scatter in the measured failure strains.

The stress-strain curve of the (0/45/0) composite appears to be similar shape to those of (0/10/0) and (0/20/0) lay-ups, although the first deviation of linearity occurs at a much lower stress and strain. The (0/90/0) stress-strain curve, however, appears far more complex with an initial knee at an even lower level.

Figure 8.4 shows the longitudinal and transverse strain behaviour with stress for all (0/θ/0) laminates. The transverse strain response for all lay-ups is initially negative and linear with a minimum roughly corresponding to the limit of proportionality on the longitudinal strain-stress curve. The transverse strains of all the examples shown then increase whilst remaining negative. However, it was observed that the transverse strain of some (0/5/0) became positive prior to ultimate failure (as also observed in previous unidirectional tests). This may merely be a consequence of the position of

the strain gauge relative to the position of ultimate failure. The transverse strain in both (0/5/0) and (0/90/0) laminates reached a plateau level prior to failure.

8.2.3 Damage Observations

Optical macrographs of representative failures from each laminate are shown in Figures 8.5 (a) to (f). The $(0)_3$ composite failed in a longitudinal tensile manner with overall fracture occurring in a plane perpendicular to both the fibres and direction of applied load. Fracture profiles of all angle-ply laminates are similar to those of their unidirectional off-axis counterparts with fracture in (0/5/0) and (0/10/0) composites appearing to be by a combination of longitudinal tensile and shear failure, in (0/45/0) by shear and in (0/90/0) material by transverse tensile failure. Very little fibre pull-out was observed in any of those specimens. A number of (0/5/0), (0/10/0) and (0/20/0) specimens remained intact after the maximum load.

Failed tensile specimens of each lay-up were edge polished (with the end tabs removed) and examined with the aid of an optical microscope. It was seen that damage in the majority of $(0)_3$ specimens was generally confined to the location of failure and although some matrix cracks were present perpendicular to the fibres, these tended to be isolated and few specimens exhibited the regular cracking pattern of the type observed in other unidirectional composite. One specimen that did show a periodic cracking pattern had an average crack spacing of $\sim 270\ \mu$m.
Observations of damage in other laminates are summarised below. It should be noted that delamination was present within the θ ply of the majority of specimens and failure of the composite appeared to have occurred in a region where several types of failure were present - i.e. matrix cracking, delamination and fibre failure.

a) (0/5/0) Composite

Separate (0/5/0) specimens were loaded to the onset of acoustic emission activity, to strains of 0.2 %, 0.25 %, 0.3 %, 0.4 % and to failure. Subsequent microscopic examination of polished edges revealed that initial damage (first evident at 0.2 % strain) was in the form of isolated matrix microcracks within the 0° plies (with an average spacing of ~ 2.5 mm) which appeared to have propagated from the specimen edges, together with a number of cracks within the 5° ply which appeared to have been arrested by 0° fibres. At both 0.25 % and 0.3 % strain, a regular array of matrix microcracks had developed within the 0° plies (with average spacing ~ 400 μm). Some of these cracks appeared to have been arrested by the first 5° fibres whilst others propagated through the 5° ply to the opposite 0° ply. By 0.4 % strain the matrix crack spacing had reached ~ 230 μm, with many cracks traversing the entire specimen thickness, and fibre failures were first observed in both 0° and 5° plies.
Examination of a failed (0/5/0) composite again revealed a regular array of matrix cracks within the 0° plies having an average crack spacing of the order of 230 ± 130 μm and with the narrowest crack separation being at either side of the main failure site. Figure 8.6 shows the distribution of crack spacings within the 0° plies of (0/5/0) composite. All of the cracks within about ± 5 mm of the main failure site had propagated through the entire thickness of the specimen (i.e. through the central 5° ply) and the average crack spacing in this region of the specimen was of the order of 150 ± 50 μm. Failed fibres were seen throughout the 5° ply whereas 0° fibre failures were only seen adjacent to the main failure site. Figure 8.7 shows the main failure site typical of (0/5/0) composite.

b) (0/10/0) Composite

Separate (0/10/0) specimens were loaded to the onset of acoustic emission activity, to strains of 0.2 %, 0.25 %, 0.3 % and to failure. The first evidence of damage was in the

form of edge-initiated matrix microcracks within the 0° plies at 0.2 %, as in the (0/5/0) composite, with very few 10° ply initiated cracks. The crack spacing at this strain level was in excess of 6 mm. Similar damage was observed at 0.25 % strain (allbeit in a different sample) with a crack spacing now of the order of 1 mm. By 0.3 % strain, many 0° ply cracks traversed the entire thickness of the specimen (i.e. through the central 10° ply). Deviation of cracks adjacent to 10° fibres, of the form observed in 10° off-axis composite, was also seen in the (0/10/0) composite. The crack spacing within the 0° plies was now ~ 600 μm. Examination of failed (0/10/0) specimens revealed that a regular array of matrix microcracks had formed within the 0° plies but very little damage was evident within the 10° ply apart from a region directly adjacent to the main failure site where cracks traversed the entire thickness of the specimen. Cracks within the 0° plies away from this region appeared not to have propagated into the 10° ply. The average matrix crack spacing within the 0° plies at failure was of the order of 400 μm although cracks were much closer together at and around the main failure site.

c) (0/20/0) Composite

Separate specimens of the (0/20/0) composite were tested to the onset of acoustic emission activity, to strains of 0.2 %, 0.23 %, 0.25 % and to failure. Initial damage (again only evident at 0.2 % strain) appeared to be a combination of 0° ply edge-cracks and 'interface failures' (these will be discussed more fully in the sections d) and e) in which this type of failure was more easily discerned). Matrix crack spacing within the 0° ply was of the order of 3 - 4 mm. Damage observed in the sample tested to 0.23 % strain was very similar to this with a crack spacing of a similar order although possibly more interface failures. By 0.25 % strain, the average crack spacing of 0° ply matrix cracks was ~ 600 μm with some traversing the entire specimen thickness. However, examination of a failed specimen revealed that damage was confined to the region of the main failure site. This indicates that there may be a large

variation in the extent of matrix cracking within (0/20/0) composite as was observed in a 20° off-axis composite.

d) (0/45/0) Composite

Separate specimens of the (0/45/0) composite were tested to the onset of acoustic emission activity, to strains of 0.2 %, 0.25 %, 0.3 %, 0.35 % and to failure. Initial damage (evident at 0.2 % strain) was mostly in the form of 'interface failures' within the 45° ply (as depicted in Figure 8.8) and a very small number of edge-initiated 0° ply matrix cracks. The 'interface failures' in Figure 8.8 do not appear to be linked by matrix cracks although at lower magnification they give the impression of resembling a transverse ply crack of the type seen in cross-ply composite (discussed in section 2.5). There were several clusters of these type of failures observed in the sample tested to 0.2 % strain.

At 0.25 % strain many more interface failures were present in the 45° ply and these had propagated as matrix cracks out towards the 0° plies. Similarly, many more edge-initiated matrix cracks were present in the 0° plies and had propagated inwards towards the 45° ply, giving an average spacing of cracks in the 0° plies of ~ 600 μm. Some cracks traversed the entire thickness of the 45° ply and it is possible that these formed when the above two mechanisms occurred at the same location. Damage in 0.3 %, 0.35 % and failed test specimens was in the form of a regular array of parallel matrix cracks in the 0° plies, some of which traversed the entire thickness of the specimen, with an average spacing of 450 - 550 μm. Fibre failures could be seen within the 0° ply adjacent to the fracture faces in the failed test specimen. Again, cracks traversed the entire specimen thickness in this region and were generally closer together than elsewhere.

d) (0/90/0) Composite

Separate specimens of the (0/90/0) composite were tested to the onset of acoustic emission activity, to strains of 0.2 %, 0.3 %, 0.4 % and to failure. Once again, initial damage was in the form of interface failures first evident at 0.2 % strain, although no 0° ply cracks were seen in this specimen. By 0.3 % strain, matrix cracks had appeared in the 0° plies and many more interface failures were present. Figure 8.9 shows interface failures within the 90° ply of a (0/90/0) composite tested to 0.3 % strain, some of which are seen to be joined by matrix cracks. At 0.4 % strain some of the interface failures had become full transverse ply cracks which appear to have been arrested by fibres in the 0° plies, as shown in Figure 8.10, and a regular array of parallel cracks was present in the 0° plies. The average spacing of matrix cracks in the 0° plies of a failed (0/90/0) composite was of the order of 250 μm ± 100 μm. Figure 8.11 shows the damage in a (0/90/0) composite at the location of failure. Cracks in this region traverse the entire specimen thickness and a number of fibre failures can also be seen within the 0° ply. It is interesting to note that one fibre failure (top right of the picture) has occurred away from the path of an adjacent matrix crack which is in agreement with the Curtin model[49] of fibre fragmentation in unidirectional composites.

8.2.4 Acoustic Emission Response

Table 8.1 gives the stress and strain at the onset of acoustic emission activity, together with the total number of AE events recorded during continuous tensile tests on (0/θ/0) composites. It can be seen that for composites in which $\theta \leq 45°$, the AE onset occurs at a similar stress and strain in each and which is of the same order as that previously reported for unidirectional composites (Chapters 6 and 7). In (0/θ/0) laminates where $\theta \leq 20°$, the onset of acoustic emissions occurs at a stress and strain much less than (~1/2) the limit of porportionality on the stress-strain curve (which is also roughly

constant over this range) and is again in agreement with the results from unidirectional material. However, in (0/45/0) and (0/90/0) composites the AE onset occurs at a lower stress and strain which is roughly the same as the corresponding limit of proportionality.

It can also be seen from Table 8.1 that the total number of acoustic emissions (and scatter) decreases with increasing θ, to a minimum at (0/20/0), and then increases again. This trend is similar to that observed by Valentin et al[142] for their carbon/epoxy cross-ply composites tested at different orientations and, in the present case, is also similar in trend to the variation of measured strain to failure with θ ply orientation.

Amplitude distribution analysis (by the Pollock method used previously and described in Appendix 2) was carried out on the overall acoustic emission data from all (0/θ/0) laminates. Representative *b*-plots from each lay-up are shown in Figure 8.12. There appears to be little difference in the gradient, *b*, of each plot (all of which lie within the range 1.2 - 1.4). The relative positioning of each line on the vertical scale is merely dictated by the overall number of emissions from each laminate and follows the trend described above. As discussed in earlier chapters, this type of continuous *b*-plot is generally unsatisfactory in discriminating between failure mechanisms as it averages the amplitude distribution over the whole failure process.

Amplitude distribution analysis within predetermined strain increments was performed on the acoustic emission data from (0/θ/0) composites with the results given in Figures 8.13 (b) to 8.17 (b). These are shown below and to the same scale as the corresponding stress and AE rate versus strain curves (Figures 8.13 (a) to 8.17 (a)) to enable direct comparison. Strain increments of 0.05 % were generally chosen.

It can be seen in many cases, that at low strains (up to ~ 0.2 %) *b* takes a value of ≤ 1. Exceptions to this are (0/20/0) and (0/45/0) composites where the values of *b* at low strains are generally higher at ~ 1.2. In all cases *b* then appears to increase with

increasing strain and in many cases (apart from (0/20/0)) reaches the value of ~ 1.5 thought to be due to matrix cracking (Chapter 6). This is followed in some cases (not (0/10/0) and (0/20/0)) by a decrease in b prior to failure. Values of b of the order of 2.5, thought to be attributable to fibre sliding and/or fibre failure, were not obtained by analysis of the AE data from any (0/θ/0) composite.

Figures 8.13 (a) to 8.17 (a) show the stress-strain response of each laminate together with the variation of acoustic emission rate with strain. Certain similarities exist between the AE rate response of (0/θ/0) composites and that of unidirectional material. In the all cases the acoustic emission rate increases rapidly with increasing strain, reaching a maximum within the region of decreasing slope on the stress-strain curve. The AE rate maximum coincides with failure of the (0/20/0) composite, however in all other cases it is followed by a rate decrease prior to ultimate failure. In the case of the (0/90/0) composite a small additional peak in the AE rate is observed at low strains, its maximum being coincident with the first discontinuity on the stress-strain curve.

8.3 Discussion

8.3.1 Elastic Properties

Predictions of composite elastic modulus were made by using the laminated plate theory computer program, Lamanal[16], described in section 2.3.3. This required input of the longitudinal modulus (E_{11}), transverse modulus (E_{22}), shear modulus (G_{12}) and Poisson ratio (ν_{12}) of unidirectional laminae. Measured values of 127 GPa, 100 GPa, 55 GPa and 0.24 were taken from Table 6.1 for E_{11}, E_{22}, G_{12} and ν_{12} respectively. Figure 8.18 shows the variation of measured and predicted elastic moduli with θ for all (0/θ/0) laminates. It can be seen that elastic moduli are predicted to be approximately constant for $\theta \leq 20^\circ$ and this is in agreement with measured values.

However, modulus predictions for θ of 45° and 90° are an overestimate compared with measured values and this may be attributable to the presence of delamination within the θ ply which may reduce the contribution of that ply to the overall modulus. The degree of delamination in each plate was not quantified although it is clear that, with a composite transverse strength of as little as 28 MPa (Corning data[122]) and a residual tensile stress in the matrix possibly in excess of 100 MPa (section 6.3.2), there is every chance that 45° and 90° plies would be cracked prior to testing and to a greater degree than other laminates tested.

8.3.2 Matrix Cracking

Examination of the failed (0/θ/0) composites by optical microscope revealed that in the majority of cases a regular array of matrix cracks, of the type seen in unidirectional composite, had formed within the 0° plies during tensile testing. By taking the ACK approach used in section 6.3.3, it is possible to obtain a prediction for the onset of matrix cracking in the 0° plies of (0/θ/0) composites. Incorporating previously determined values for the matrix fracture surface energy (12.5 Jm^{-2}), matrix modulus (106 GPa), composite modulus (127 GPa), Poisson ratio (0.24) and taking manufacturer's data for the fibre radius (6 μm) and modulus (180 GPa) together with a measured fibre volume fraction of 0.29, gives a predicted matrix cracking strain (ε_{mu}) of 0.15 % and a composite matrix cracking stress of 200 MPa. This is clearly of the same order as the limit of proportionality on the stress-strain curve for (0/θ/0) composite when $\theta \leq 20°$. The stress in the matrix (σ_{mu}) at the predicted composite matrix cracking stress is calculated to be 169 MPa.

Previous work (Chapter 6) has shown that matrix cracking in a unidirectional composite commences at a stress and strain much lower than those predicted. However, it was shown that the onset of acoustic emissions coincided with formation of the first few microcracks and that this was in agreement with the predicted matrix

cracking stress once the residual thermal stresses had been taken into account. In the case of (0/θ/0) composites, the onset of acoustic emission activity occurs at a similar stress and strain as in unidirectional composites for $\theta \leq 20°$. The difference between the predicted matrix cracking stress and the onset of acoustic emission activity suggests that for $\theta \leq 20°$ the thermal residual stress in the matrix is similar to that in unidirectional composites.

Microscope examination of failed test specimens showed that there was a large variation in the extent of damage in (0/θ/0) composites and even in those of the same lay-up. However very little, and in some cases no, periodic matrix cracking had taken place in $(0)_3$ and (0/20/0) composite prior to ultimate failure. In the case of $(0)_3$ composites, this is thought to be a result of a high fibre-matrix interfacial shear strength (23 MPa) - shown by the lack of interface debonding and fibre pull-out compared with other unidirectional composite. In the case of the (0/20/0) composite, the lack of matrix cracking may be attributable to the type of failure predicted in the previous chapter, where the stress range over which matrix cracking occurs is of the same order as that of fibre failure. This would limit the degree of continued matrix cracking in this type of composite as, in the vicinity of matrix cracks, the fibres may not be able to withstand the extra load thrown upon them. It may be noted that the total number of emissions from the (0/20/0) composite is of the same order as the total number of fibres within that laminate (calculated from the fibre volume fraction, area etc.).

Again taking the ACK approach used in Chapter 6, a prediction for the stress transfer or slip length, x', may be calculated and from this the saturation crack spacing determined. Incorporating previous values for the fibre-matrix interfacial shear strength and fibre radius, together with the measured fibre volume fraction of 0.29 and the predicted matrix cracking stress, σ_{mu}, of 169 MPa, a value of 124 μm is calculated for x'. The results of Chapter 6 showed that the measured saturation crack

spacing was closer to the 1.75 x' predicted by Zok & Spearing[28], which in this case gives a value of ~ 220 μm. Pryce & Smith[110], in their paper on the behaviour of both unidirectional and cross-ply Nicalon/CAS laminates, note that matrix cracking in the 0° plies of all laminates tested tended towards the same saturation spacing, irrespective of lay-up and ply thickness.

The predicted saturation crack spacing in the present study is similar to the crack spacings in 0° plies measured from the edges of failed (0/5/0) and (0/90/0) composites and may indicate that matrix crack saturation has been achieved in these laminates. This is in agreement with the observed stress-strain behaviour of these laminates which shows a second linear region of the type seen in unidirectional composites which is thought to result from the load being carried almost totally by the fibres and during which little further cracking of the matrix occurs. However, the observed phenomena in (0/5/0) and (0/90/0) laminates may occur by two completely different mechanisms. For example, in the previous chapter the results tended to show that a 5° off-axis composite behaves in a very similar manner to that of a unidirectional composite tested parallel to the fibres, with the 5° fibres apparently having little effect on the cracking behaviour of the matrix. If this were the case, then the (0/5/0) composite may also behave very much like a 0° composite with continued matrix cracking occurring throughout, followed by fibre deformation and fibre failure. In the case of the (0/90/0) composite, the 90° ply is expected (in view of the low transverse strength of a unidirectional composite) to fail first, as is observed, and may thus become ineffective at low strains. The 0° plies alone may then continue to deform as in a unidirectional composite, with matrix cracking continuing until crack saturation followed by ultimate fracture as a result of fibre failure. In both laminates, it is observed that the composite transverse strain becomes constant prior to failure which may indicate that the matrix has ceased to deform. As stated previously (Chapter 6), it is possible that the transverse strain behaviour is most closely associated with matrix cracking and that any changes in lateral strain due to fibre deformation are imperceptible from a strain gauge bonded to the matrix-rich surface.

The final crack spacing in all other laminates ((0/10/0), (0/20/0) and (0/45/0)) is much greater than the predicted saturation crack spacing (400 - 600 μm cf 220 μm respectively) and may indicate that matrix crack saturation has not been achieved in these cases. Again, this is supported by the stress-strain behaviour of these composites as failure has occurred during a region of decreasing slope. The results of Chapter 6 have shown that the majority of matrix cracking occurs during a region of decreasing slope on the stress-strain curve. It is thought that failure of a composite within the matrix cracking regime leads to highly unpredictable behaviour and that this is likely to be undesirable in terms of composite design. A more successful composite would be one in which crack saturation is achieved such that the ultimate strength is determined by fibres in the longitudinal plies.

Although not confirmed, it appears that in (0/5/0) and (0/10/0) laminates the stress range over which the slope of the stress-strain curve decreases is much wider than in unidirectional 0° composite. Previous work (Chapter 6) has shown that the second linear region of the stress-strain curve commences at a stress of approximately 1.3 times the stress at the limit of proportionality in a 0° composite. In (0/5/0) composites this ratio is of the order of 1.6 which may indicate that continued matrix cracking in this and (0/10/0) laminates requires a greater increase in stress than in a 0° composite. This is not thought to be the case. A number of other possible explanations exist - for example, it is possible (as suggested in Chapter 7) that the stress-transfer length between fibres and matrix in the 5° and 10° ply is greater than that in a 0° composite. This would mean that θ fibres would carry load over a greater length and thus the probability of finding a critically sized flaw within that region is greater. Expressed in another way, the orientation of the fibres causes a reduction in their failure strength. In both cases this may lead to progressive θ fibre failure in the matrix-cracking regime. This may render the θ ply locally ineffective so that progressively more load is carried by the 0° plies which may lead to a gradually increasing slope on the stress-strain curve. Alternatively, load transfer back into the matrix may not be possible in

some case, possibly as a result of interface failure, so that θ fibres carry progressively more load (without failure) leading to a gradually increasing slope of the stress-strain curve with fibre failure at higher stresses.

It is also interesting to note that measured crack densities in the 0° plies of failed (0/θ/0) composites, 1/(average crack spacing in 0° plies at failure), follow the same trend as that of the strain to failure and total number of acoustic emissions with θ ply orientation. Figure 8.19 shows the variation of strain to failure, total AE count and crack density with θ ply orientation with the values for each parameter normalised with respect to the corresponding maximum value (which in all three cases was that of the (0/5/0) composite). The crack density, strain to failure and total AE count of the (0/5/0) composites thus become unity.

Another point worthy of mention is the observation that for all (0/θ/0) composites the spacing of cracks adjacent to the position of ultimate fracture is smaller than the average value. There may be a number of reasons for this. Firstly, it may be supposed that in a densely cracked region of composite, a higher proportion of the load would be carried by the fibres. The likelihood of fibre failure in this region would therefore be higher and a progressively weakening plane of the composite may develop leading to ultimate failure at that position. Alternatively, rapid dissipation of energy on composite failure may have the residual effect of causing additional damage in the form of cracks and failed fibres adjacent to the main failure site. The exact mechanism may only be determined by careful observation of the accumulation of damage during loading.

Discussion of matrix cracking in (0/θ/0) composites has so far concentrated on cracking in the longitudinal plies. Microstuctural observation of damage in (0/θ/0) composites loaded to different levels of strain has shown that, at low fibre angles, matrix cracks had formed at low strains in both the 0° and θ plies. The results in

Chapter 7 implied that, for $\theta \leq 20^{\circ}$, matrix cracks formed and grew in a similar manner to those in unidirectional composites and that continued cracking may have been limited by the ability of the fibres to carry extra load. It is possible that, for $\theta \leq 20^{\circ}$, the θ ply in (0/θ/0) composites would also behave in a similar manner to unidirectional composites. This is borne out by the onset of acoustic emission activity and the limit of proportionality on the stress-strain curve, which occur at similar stresses and strains to unidirectional composites.

However, microstructural observation of (0/90/0) composites tested to different levels of strain indicated that initial damage was in the form of debonded fibre-matrix interfaces in the 90° ply and that these debonds developed to form full transverse ply cracks. This type of behaviour is in agreement with the constrained cracking first observed by Garrett and Bailey[29] in cross-ply polymeric composites having thin transverse plies. Pryce and Smith[110] estimated that the critical flaw size to cause cracking in the transverse ply of a range of cross-ply Nicalon/CAS laminates was less than the ply thickness and they thus concluded that cracking was 'unconstrained' - i.e. that fully transverse cracks formed instantaneously.

8.3.3 Ultimate Strength

The first-ply-failure strengths of (0/θ/0) laminates may be predicted by using the laminated plate theory computer program, Lamanal[16], and by the application of composite failure criteria. This requires values of longitudinal, shear and transverse strengths of the unidirectional laminae (σ^{*}_{11}, τ^{*}_{12} and σ^{*}_{22} respectively), in addition to the previously input elastic properties.

Comparison of strength data from Tables 6.1, 7.1 and 8.1 shows that the ultimate strength of the $(0)_3$ composite is less than that obtained from other, thicker composites and is also less than that of the (0/5/0) composite. It has also been shown that the fibre-matrix interfacial friction stress in the $(0)_3$ composite is greater than that obtained from other unidirectional composites. Although the maximum stress and

strain theories discussed in Chapters 2 and 7 predict an increase in strength for small deviations in fibre angle from 0°, it is thought that the properties of the $(0)_3$ laminate are not representative of unidirectional composites and are not directly comparable with the strength of other (0/θ/0) laminates. It is possible that the propagation of matrix cracks through a composite with a high interfacial shear strength may be detrimental to the ultimate strength as little debonding and crack deflection can occur and cracks are able to propagate rapidly through the sample.

Measured values for the longitudinal and ±45° shear strengths of unidirectional laminae were taken from Table 6.1 as 390 MPa and 59 MPa respectively. The work of Harris et al[111] has shown that the first-ply-failure stress of cross-ply composites was in good agreement with predictions based on laminate plate theory for a tranverse strength 50 MPa (cf 28 MPa from Corning data[122]). As first-ply failure stresses of (0/90/0) composites are similar to those reported by Harris et al, it may be supposed that the transverse strength of 50 MPa may be taken in the present study. The lay-up and ply thickness for each laminate to be analysed were also entered and a nominal load applied to the system. The Tsai-Hill failure criterion was then applied to the stresses in each ply and a verdict (i.e. reserve factor) given as to the likelihood of failure having occurred in any ply. From the reserve factor and applied load, the first-ply-failure stress could be calculated for each lay-up analysed.

Figure 8.20 shows values of ultimate tensile strength and stress at the limit of proportionality on the stress-strain curve, together with the stress at the onset of acoustic emission activity and the predicted first-ply-failure stresses based on the Tsai-Hill failure criterion, for all (0/θ/0) composites. It can be seen that for θ values of 5° and 10°, the predicted failure stress of the θ ply lies within the strength range of the laminate. If one takes the ineffectiveness of the failed θ ply into consideration by taking the modulus of that ply as zero and re-analysing the laminate under the same applied load, it is predicted that for a (0/5/0) composite the load redistribution due to

failure of the θ ply is sufficient to cause failure of the 0° plies and hence ultimate failure of the composite. This is borne out by the experimental results. In the case of the (0/10/0) composite, failure of the 0° plies on failure of the 10° ply (by the above method) is marginal and this too is in agreement with the experimental data as clearly the predicted first-ply-failure stress lies towards the bottom of the range of strengths of that laminate indicating that some specimens had load carrying capability after 10° ply failure.

For θ of 20°, 45° and 90° the Tsai-Hill predictions of first-ply-failure stress are in good agreement with the limits of proportionality on the stress-strain curve of each laminate, which for θ of 45° and 90° are also the same as the AE onset stresses. At these high angles, the ultimate strength of the composite tends towards an almost constant value which is approximately two-thirds of the unidirectional strength. This implies that for θ of 45° and 90°, once failure of the θ ply has occurred the stress is transferred to the longitudinal plies and the ultimate strength is solely determined by the fibres in the 0° plies. Since one divides the failure load by the original cross-sectional area, this reduces the strength by one third.

A number of points are worthy of note at this juncture. Firstly, that the Tsai-Hill and other failure criteria (as discussed in section 2.6) assume linear-elastic behaviour to the point of failure and predict that this occurs when the stress exceeds a level determined by considering the interaction or transformation of longitudinal shear and transverse failure strengths with increasing θ. As such, any damage prior to failure is ignored and in all cases failure is assumed to be fibre-dominated. Furthermore, it has previously been shown (Chapter 6, Kim & Pagano[106], Harris et al[111]) that little physical significance can be attributed to the limit of proportionality. It is thought to be merely indicative of the presence of sufficient matrix cracks noticeably to reduce the composite modulus.

If one considers the failure of the (0/20/0) composite, it can be seen from Figure 8.21 that the limit of proportionality on the stress-strain curve is of the same order as the Tsai-Hill prediction for first-ply-failure stress and that the ulimate strength lies someway between that of unidirectional composite and the plateau strength of (0/45/0) and (0/90/0) composites. This tells us nothing of the failure processes within this laminate. One might easily assume from these results that the limit of proportionality merely represented failure of the 20° fibres, which made the 20° ply completely ineffective and that this was followed by 0° fibre failure at a higher stress. However, it has previously been shown that for a 20° off-axis unidirectional composite damage in the form of matrix cracking occurs prior to the limit of proportionality. Results of 20° off-axis tests (Chapter 7) suggest that the extent of cracking is limited by the ability of the fibres to carry extra load in the vicinity of cracks, which in turn limits the load-carrying capability of the composite as a whole. These failure processes occur with little increase in applied load and are statistical in nature. Thus, although the limit of proportionality and strength are almost coincident, neither is a true reflection of the extent of damage within the composite. Similarly, microstructural examination of (0/20/0) composites at different levels of strain has shown that several different failure mechanisms may be in operation at any given strain, with matrix cracking and fibre failure occurring in both 20° and 0° plies.

This leads one to propose the type of approach recommended by Hart-Smith[54,55], whereby individual failure envelopes are superimposed rather than interacted. He suggests that the superimposed failure envelopes would truncate each other locally and that the intersection of failure envelopes would predict failure to occur simultaneously by a number of mechanisms. This type of approach may be appropriate to angle-ply laminates for predicting the evolution of damage with stress. An attempt to illustrate this behaviour schematically is shown in Figure 8.21. For simplicity in presentation, the smooth curve of the Tsai-Hill failure criterion has been shown and is merely taken to indicate the fibre-dominated failure within the θ plies .

Hart-Smith derides the Tsai-Hill failure criterion and recommends use of the maximum strain theory. The results of the present study have shown the maximum strain theory to predict failure strengths of unidirectional off-axis composite (Chapter 7) with reasonable accuracy. In this case, the theory predicts that a transition from longitudinal tensile failure to shear failure should occur at 5° and that the transition from shear failure to transverse tensile failure should occur at a fibre orientation of about 45°. Hart-Smith also suggests that residual thermal stresses may be incorporated easily in this approach by off-setting the failure envelopes by the requisite amount. This has effectively been done in the case of matrix cracking stress predictions and indicated in Figure 8.21 by the AE onset stress at low orientations.

However, for the proposed approach to be useful, a number of factors need to be addressed. Firstly, the orientation dependences of the apparent and predicted matrix cracking stress are not known (the apparent matrix cracking stress being the ACK prediction off-set by the matrix residual stress). It has previously been noted (Chapter 7) that both the residual thermal stresses and the resolved interfacial shear strength are likely to be orientation dependent. The horizontal lines in Figure 8.21, representing the ACK matrix cracking stress and AE onset, are therefore for illustrative purposes only and are not intended to imply that fibre angle has no effect but merely that it is expected to be less than that of Tsai-Hill predictions. Secondly, the statistical nature of the failure processes needs to be taken into account as this will clearly give a greater likelihood of overlapping failure envelopes and thus failure by a number of mechanisms simultaneously. Once these factors have been addressed it may be possible to predict the extent of damage within the composite at any given stress.
In its current state, the approach predicts that at low fibre angles the initial damage will be in the form of matrix cracking perpendicular to the fibres (of the type seen in unidirectional composites), followed by θ fibre failure and then 0° fibre failure. If the statistical nature of the failure processes is taken into account, it is possible that the range of stresses over which fibres in the θ ply fail and stress-range over which matrix

cracking occurs may overlap and the extent of matrix cracking will then be truncated. Similarly, the ultimate strength of the composite may be limited by the degree of overlap between the stresses for failure of the 0° and θ fibres.

At high fibre orientations, it is predicted that transverse tensile failure of the θ ply will occur initially, followed by matrix cracking and then 0° fibre failure. Again, the extent of each damage mechanism may depend on the degree of overlap between the stress-range of each type of failure with the higher stress mechanisms truncating the lower stress mechanism in each case.

In all cases the predicted behaviour is in accord with experimental observations of damage.

8.3.4 Acoustic Emission

It appears that the Pollock method of AE amplitude distribution analysis (both methods employed) is not able to differentiate between the failure mechanisms in (0/θ/0) composites as clearly as for unidirectional composites. This may be due to a number of factors - for example: i) the number of failure mechanisms may have increased, with the possibility that several are in operation simultaneously at any given strain (e.g. interface failure, matrix cracking, θ fibre failure, 0° fibre failure), in which case all b values would be averages; ii) the acoustic emissions from one failure mechanism may dominate and may mask acoustic emissions from other sources, giving an approximately constant value of b for all strains; iii) attenuation of some acoustic emissions at internal surfaces (e.g. delamination) would lead to a decrease in their amplitude and may give rise to a higher value of b which may not be representative of the actual population of source emissions. As regards point iii), Pollock suggests that if all amplitudes were attenuated by the same factor, the value of b would be unaffected. Delamination within the θ ply may mean that emissions as a result of damage within that ply are attenuated more than those from damage within the 0° ply adjacent to the transducer. Thus the value of b associated with the former

mechanism may be distorted and perhaps obscured. All of these examples are possible explanations of the lack of discrimination between failure mechanisms by this analysis method.

Valentin et al[142] obtained bi-modal *b*-plots for all of their cross-ply composite tested at different orientations. They attributed high *b*-values (1.2 to 1.7) to fibre failures and interlaminar effects and low *b*-values (0.2 to 0.7) to rapid failure associated with the fibre-matrix interface. They also concluded that cracking normal to fibres was an insignificant source of AE activity. However, their interpretation was not based on definitive experimental observations of damage but on supposed failure mechanisms. To reiterate, high values of *b* are associated with a large number of low-energy failure events whilst low *b* values correspond to failure by a small number of higher-energy damage events.

It has been shown in the present study that progressive matrix cracking perpendicular to 0° fibres in a unidirectional composite occurs over a region of decreasing slope on the stress-strain curve and is a significant source of AE activity, having a *b* value of the order of 1.5, and that a peak in the AE rate is detected during this region. There is also evidence to suggest that initial damage in a 10° off-axis composite is by interface failure with an initial *b* value of ~ 0.7. This result is in agreement with that of Valentin et al[142].

Incremental analysis of the AE data from (0/10/0) composite showed that initial *b* values were again of the order of 0.7, although there was no evidence to suggest that initial damage was in the form of interface failure. It is possible that interface failures cannot be seen by direct observation in composites with low-angle fibres.

There is, however, microstructural evidence of initial damage in the form of interface failures within the θ ply at orientations of 20°, 45° and 90°. In the majority of these cases, damage only became evident at strains of 0.2 % at which point transverse matrix cracks were also present. This is not to suggest that there was no damage present in composites tested to the onset of acoustic emission activity but that it may

have been undetectable by the observation technique employed. It is possible that interface failures and matrix cracking occur simultaneously in these composites which, based on b values of 0.7 and 1.5 respectively, would give an average b value of ~ 1 initially. This was found to be the case.

It is possible, therefore, that different failure events occur simultaneously and that their acoustic emissions superimpose to give an average b value. This is in acoord with the model proposed in the previous section whereby failure mechanisms are superimposed. Figure 8.22 shows schematically how the acoustic emission rate may vary for the separate failure mechanisms and includes the variation of AE rate with strain determined in Chapter 6 to be associated with the evolution of matrix cracks. Superposition of the AE rate curves for matrix cracking, θ fibre failure and 0° fibre failure for each laminate would then generate the type of overall curves witnessed during tensile tests on (0/θ/0) composites.

Again, this type of approach requires knowledge of the statistical distibution of fibre strengths within the composite and an understanding of how the distribution varies with θ. Beyerle et al[107] measured a fibre strength distribution with a mean of 2 GPa and a Weibull modulus, m, of 3.6 from fibre fracture mirror radii in unidirectional Nicalon/CAS composite. From this, and by using the Curtin[49] model, the strength of unidirectional composite having a fibre volume fraction of 0.29 is predicted to be 380 MPa. It may be possible to adapt this type of model in order to predict the orientation dependence of fibre strength, its distribution and the position on the distribution which constitutes failure. The latter point arises from the observation that a number of (0/θ/0) specimens remained intact after the ultimate stress, indicating that not all fibres had failed. An estimate of the proportion of fibre failures necessary for the remainder to be unable to withstand the applied load is therefore also required. Curtin suggests that the proportion of failed fibres at the ultimate strength of a unidirectional composite will be approximately $2/(m+2)$ per length δ_c (where δ_c is a characteristic

sliding length). It is possible that the length δ_c and the total number of fibres within that distance will change with orientation and it is anticipated that this is calculable.

With reference to Figure 8.22, the approach also assumes that matrix cracking occurs over the same strain range in both θ and 0° plies and that this is the same as in the unidirectional 0° composite. Microstructural examination of separate specimens loaded to different strain levels has shown that the majority of matrix cracking occurs between 0.2 and 0.4 % strain. This is in accord with observations of unidirectional 0° composites and it is possible that the assumption is valid.

8.4 Conclusions

The tensile stress-strain and acoustic emission responses of a range of Nicalon/CAS (0/θ/0) laminates have been investigated. The results have been discussed in terms of microstructural observations of damage accumulation and in the light of results from unidirectional and off-axis composites.

Similarities between the results for (0/θ/0) laminates and those for unidirectional and off-axis composites were identified and existing models were found accurately to predict a number of stages of damage development.

A tentative behaviour model has been proposed in which the failure envelopes of individual damage mechanisms are superimposed and which can be used to predict the stress-strain behaviour, acoustic emission response and damage evolution in these types of composite.

Laminate	0/0/0	0/5/0	0/10/0	0/20/0	0/45/0	0/90/0
Elastic Modulus (GPa)	127 ±4	122 ± 9	125 ± 15	123 ± 11	114 ± 10	108 ± 8
Poisson Ratio	-	0.25 ± 0.01	0.22 ± 0.04	0.25 ± 0.03	0.24 ± 0.02	0.17 ± 0.03
Proportional Limit (MPa)	150 ± 50	183 ± 49	182 ± 40	172 ± 35	94 ± 17	66 ± 13
Proportional Limit (%)	0.12 ± 0.04	0.16 ± 0.03	0.15 ± 0.04	0.15 ± 0.02	0.09 ± 0.02	0.06 ± 0.02
AE Onset (MPa)	-	91 ± 16	89 ± 13	94 ± 22	94 ± 17	60 ± 9
AE Onset (%)	-	0.07 ± 0.01	0.08 ± 0.02	0.08 ± 0.02	0.08 ± 0.02	0.06 ± 0.01
Strength (MPa)	311 ± 23	342 ± 65	284 ± 61	272 ± 42	212 ± 29	221 ± 44
Strain to Failure (%)	0.44 ± 0.09	0.58 ± 0.18	0.43 ± 0.14	0.29 ± 0.14	0.41 ± 0.11	0.50 ± 0.2
Total AE Events	-	80,000 ± 10,000	30,000 ± 5,000	15,000 ± 500	50,000 ± 10,000	60,000 ± 20,000

Table 8.1: Room-temperature tensile properties of Nicalon/CAS pomposite angle-ply laminates

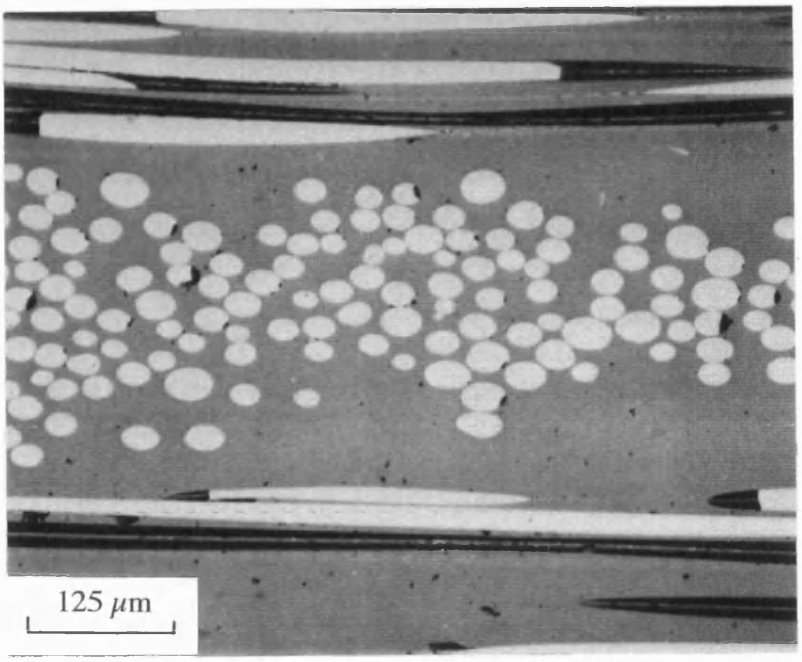

Figure 8.1: Optical micrograph showing typical marix-rich regions (x 160)

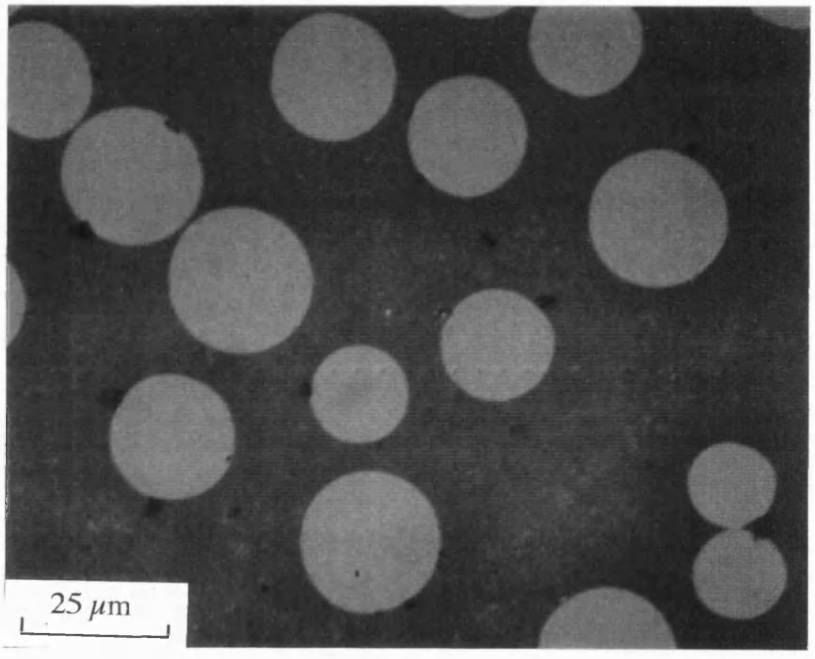

Figure 8.2: Micrograph showing pores around fibre edges in $(0)_3$ Nicalon/CAS composite (x 800)

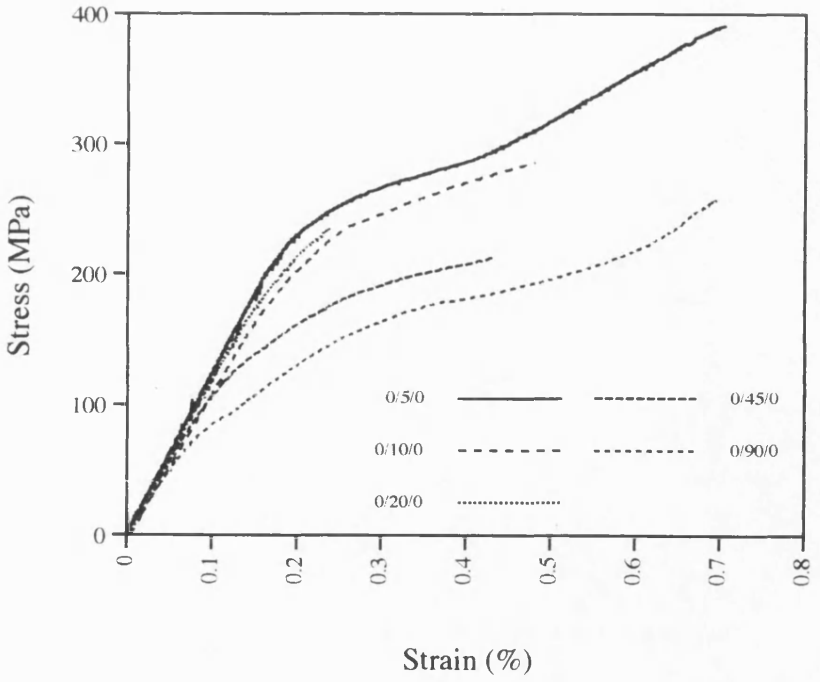

Figure 8.3: Typical room-temperature tensile stress-strain curves of Nicalon/CAS (0/θ/0) laminates

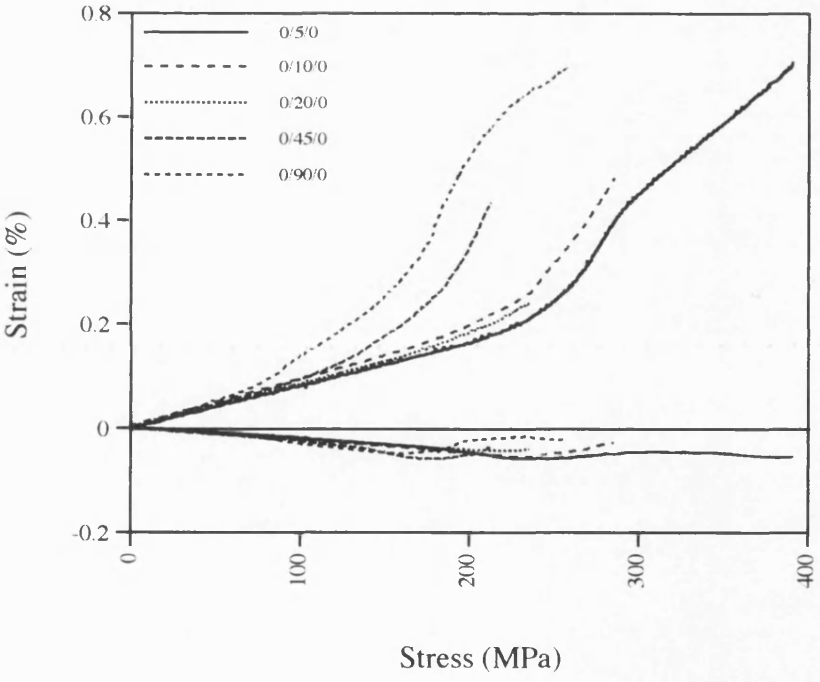

Figure 8.4: Longitudinal and transverse strain behaviour of Nicalon/CAS (0/θ/0) laminates

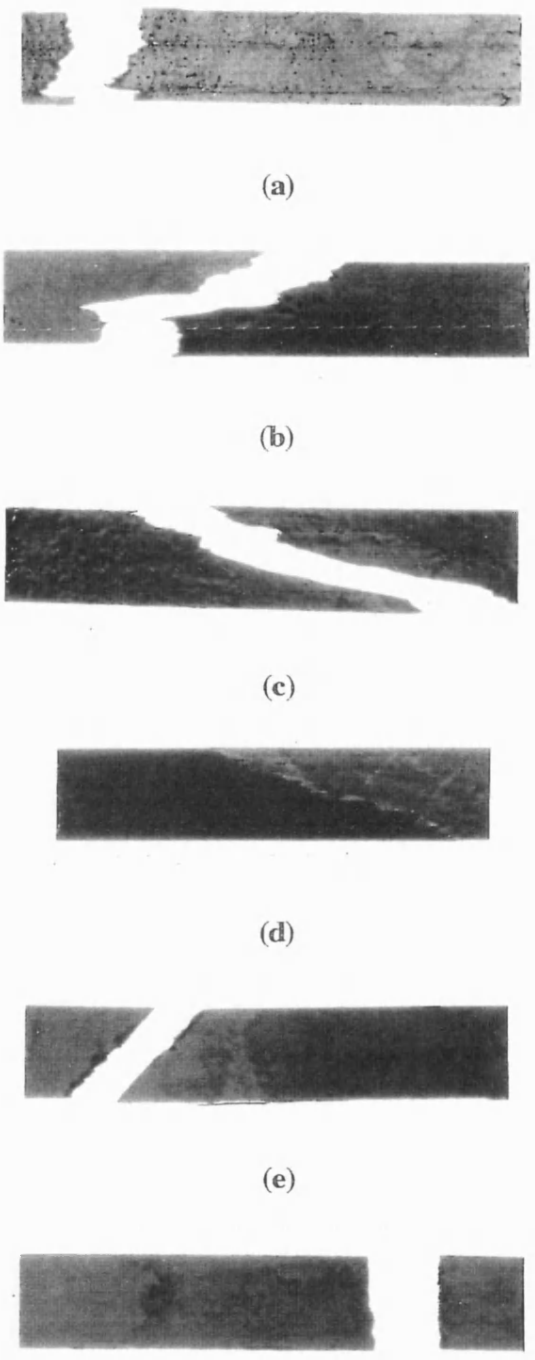

Figure 8.5 : Optical macroscopic photographs showing typical fracture profiles of failed (0/0/0) tensile test specimens - (a) (0/0/0), (b) (0/5/0), (c) (0/10/0), (d) (0/20/0), (e) (0/45/0), (f) (0/90/0) (x 1.5)

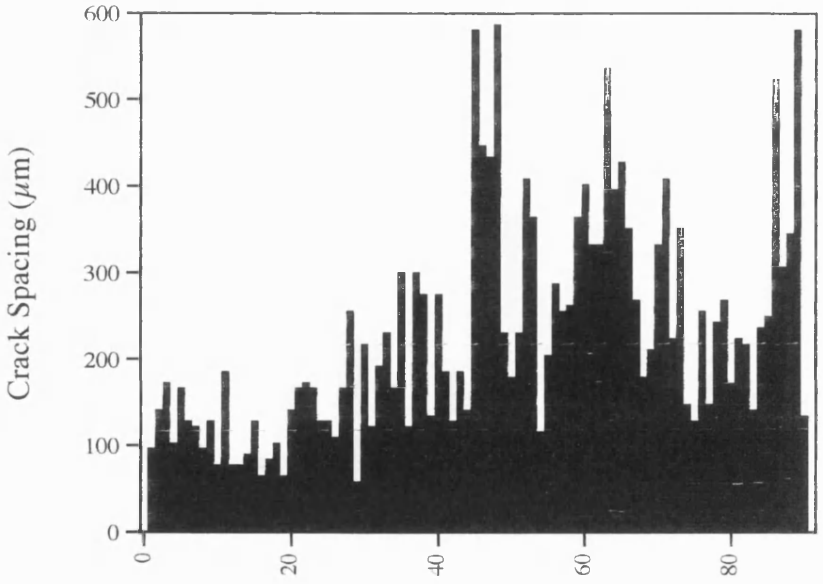

Figure 8.6: Distribution of crack spacing in a failed (0/5/0) test piece (numbered from failure site)

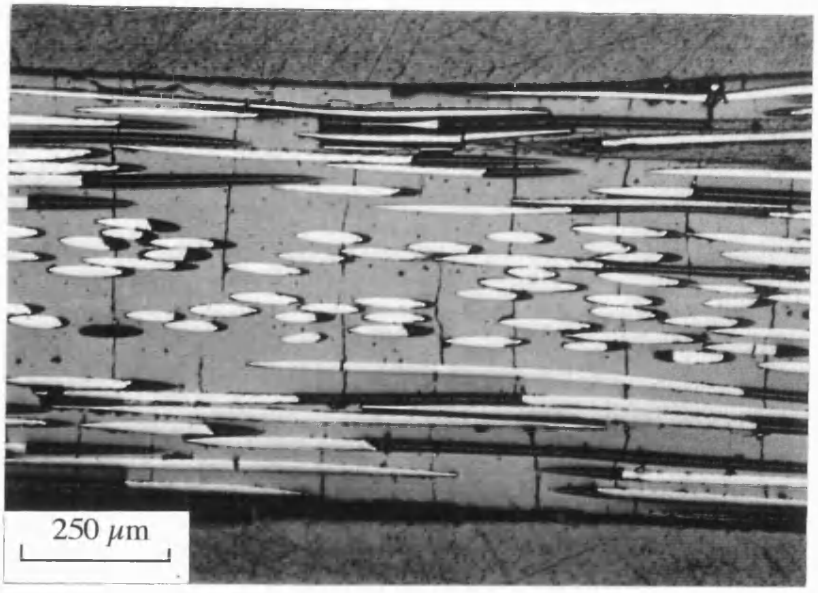

Figure 8.7: Optical micrograph showing edge of a failed (0/5/0) test specimen (x 80)

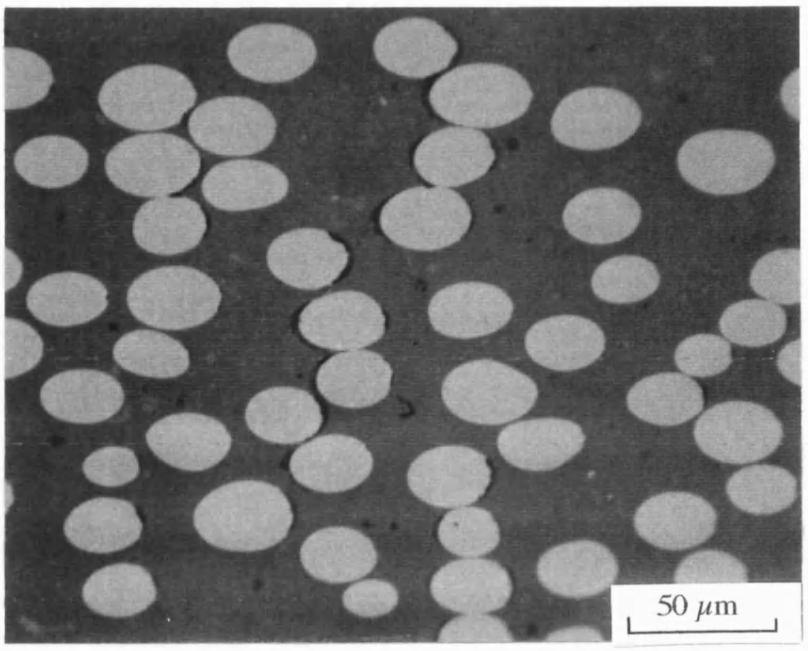

Figure 8.8: Optical micrograph showing interface failures in (0/45/0) composite tested to 0.2 % strain (x 400)

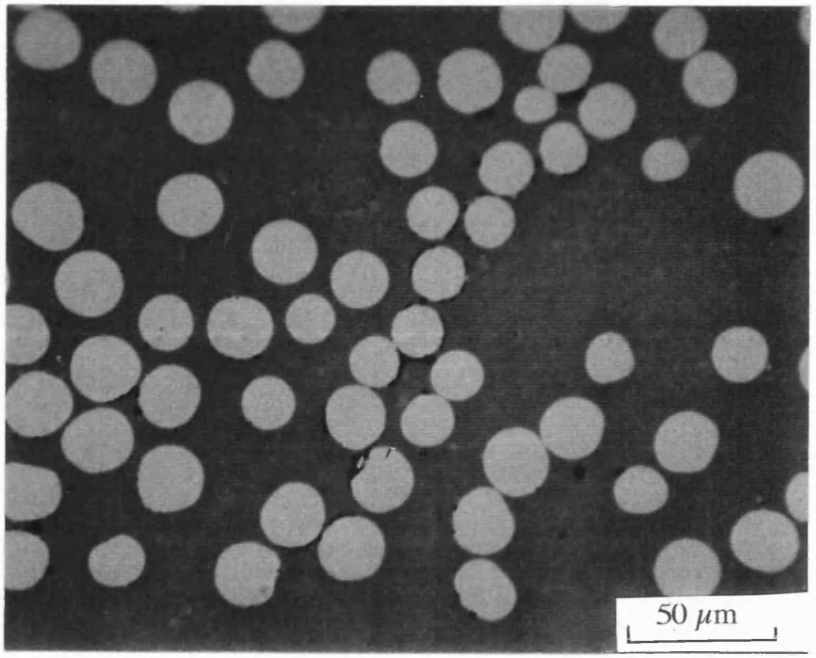

Figure 8.9: Optical micrograph of showing interface failures within the 90° ply of (0/90/0) composite tested to 0.3 % strain (x 400)

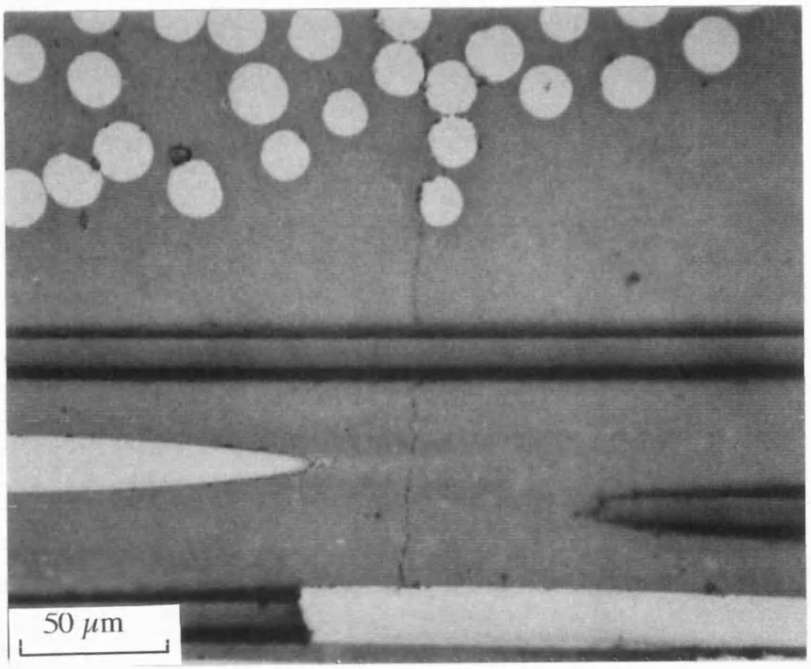

Figure 8.10: Optical micrograph of (0/90/0) composite tested to 0.4 % strain showing the propagation of a transverse ply crack being arrested by fibres within the 0° ply (x 400)

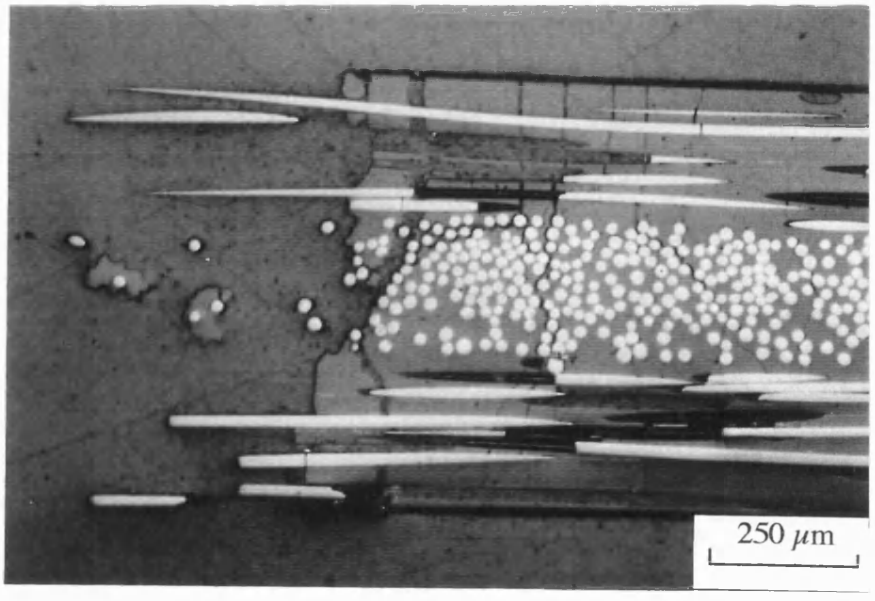

Figure 8.11: Optical micrograph showing the edge of a failed (0/90/0) test specimen (x 80)

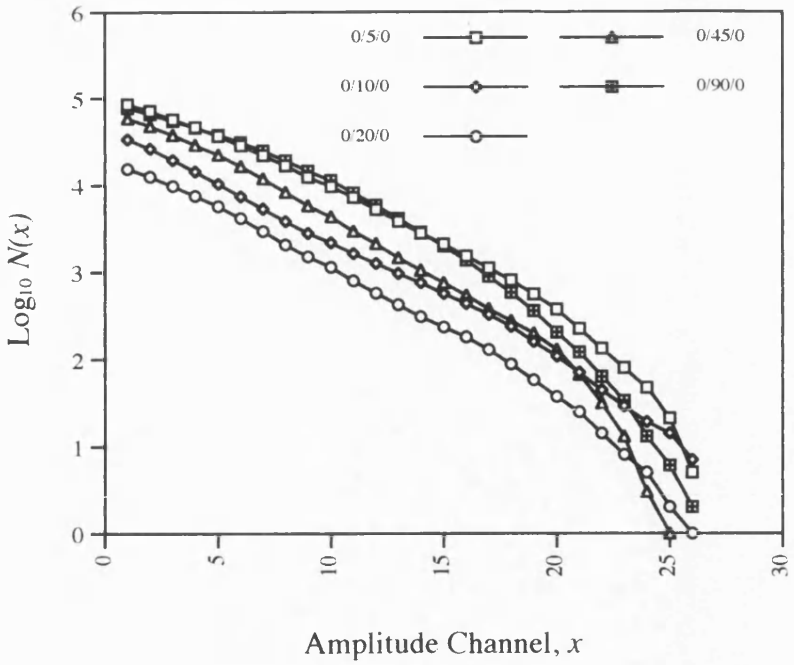

Figure 8.12: Amplitude distribution analysis of all (0/θ/0) composite

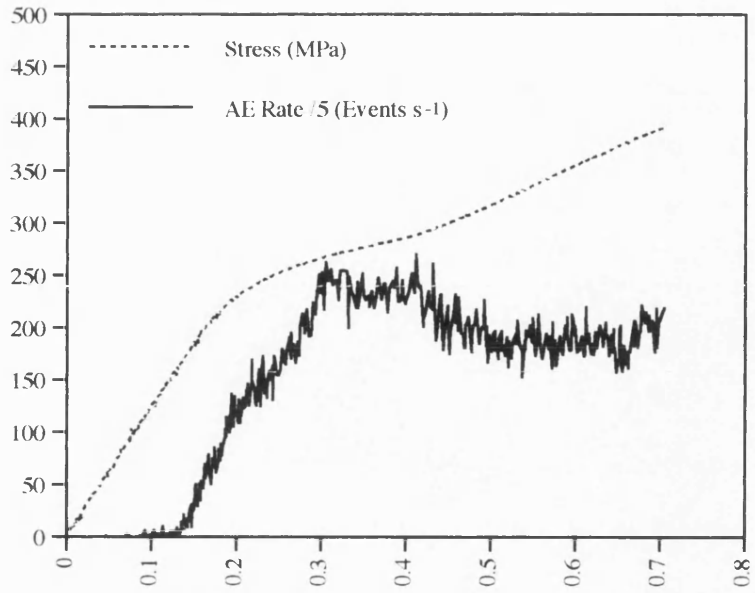

Strain (%)

a)

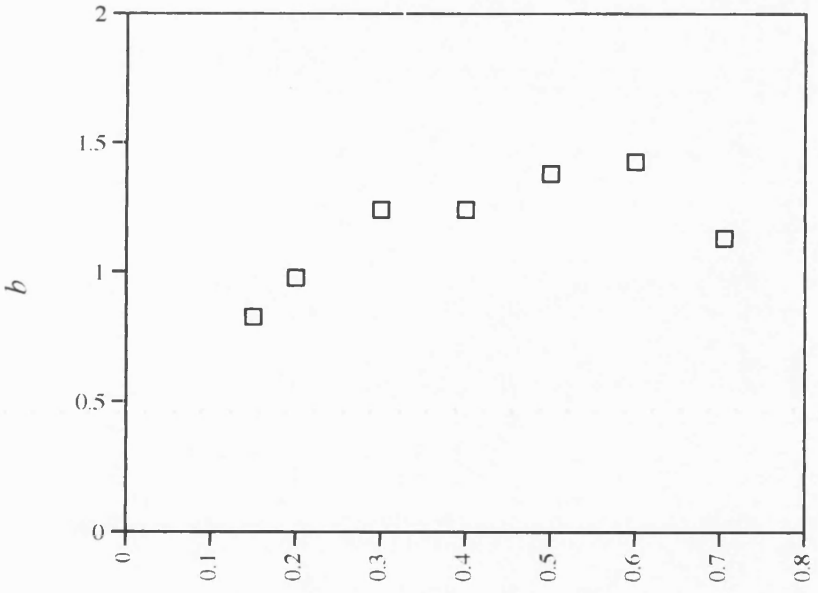

Strain (%)

b)

Figure 8.13: Acoustic emission response of Nicalon/CAS (0/5/0) composite shown as a) AE rate and b) *b* value as a function of applied strain

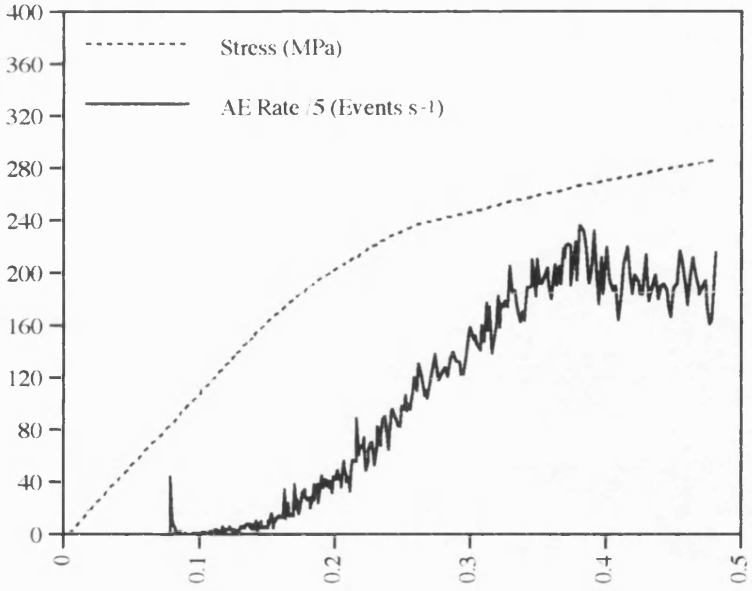

a)

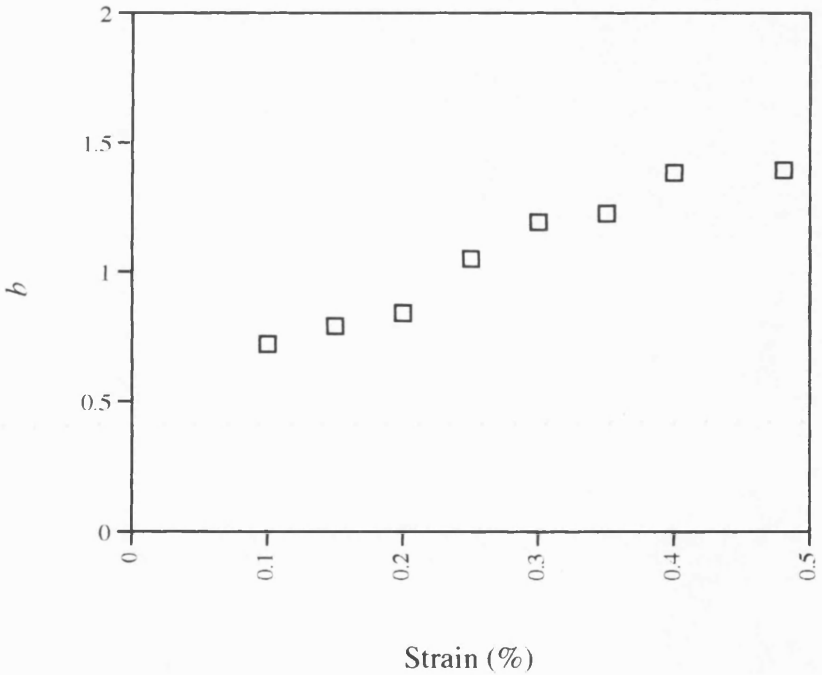

b)

Figure 8.14: Acoustic emission response of Nicalon/CAS (0/10/0) composite shown as a) AE rate and b) *b* value as a function of applied strain

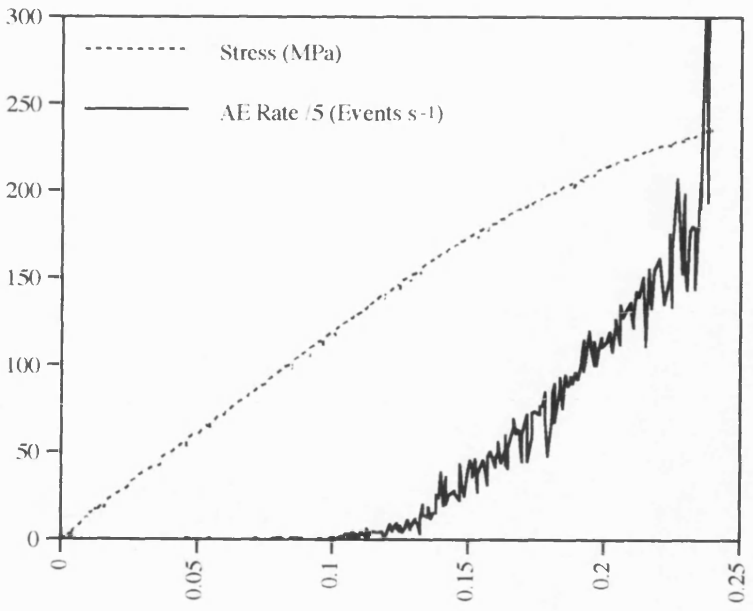

a)

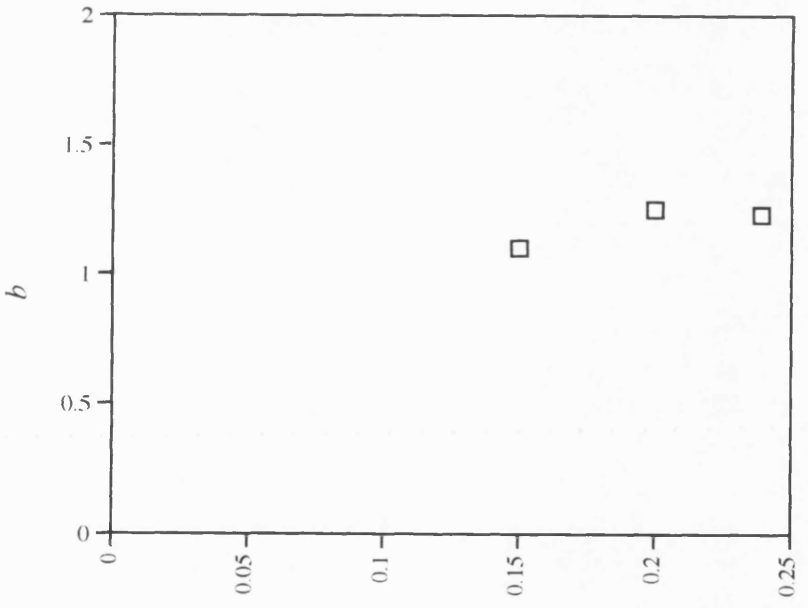

b)

Figure 8.15: Acoustic emission response of Nicalon/CAS (0/20/0) composite shown as a) AE rate and b) *b* value as a function of applied strain

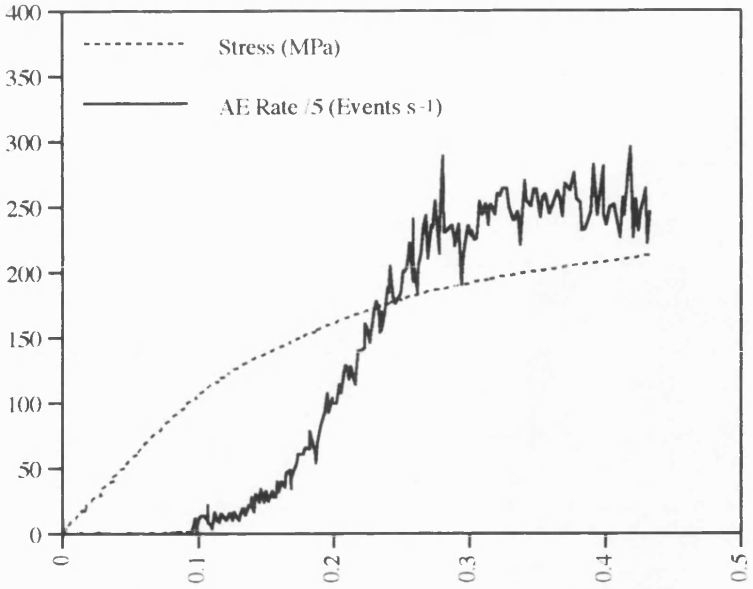

a)

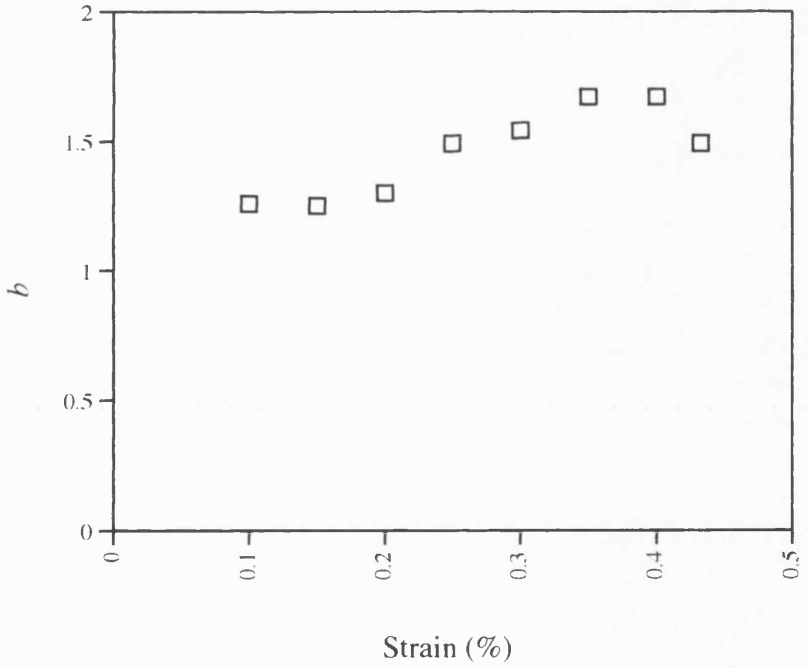

b)

Figure 8.16: Acoustic emission response of Nicalon/CAS (0/45/0) composite shown as a) AE rate and b) *b* value as a function of applied strain

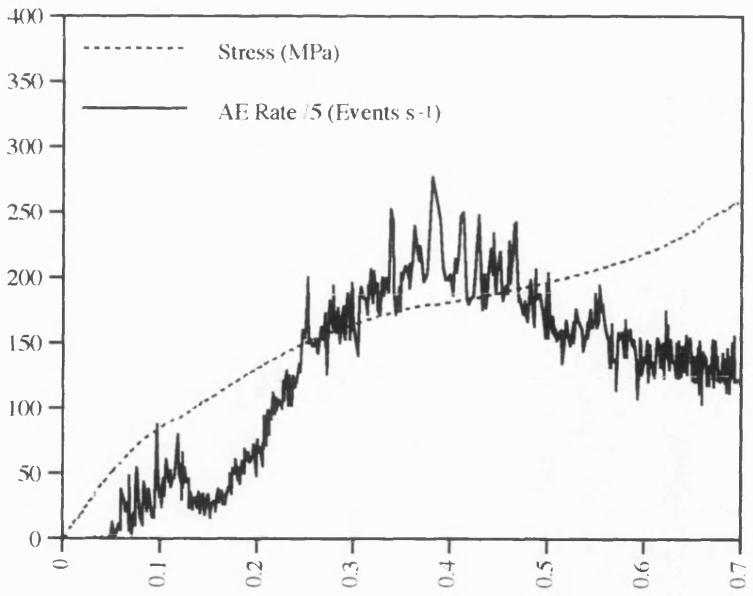

a)

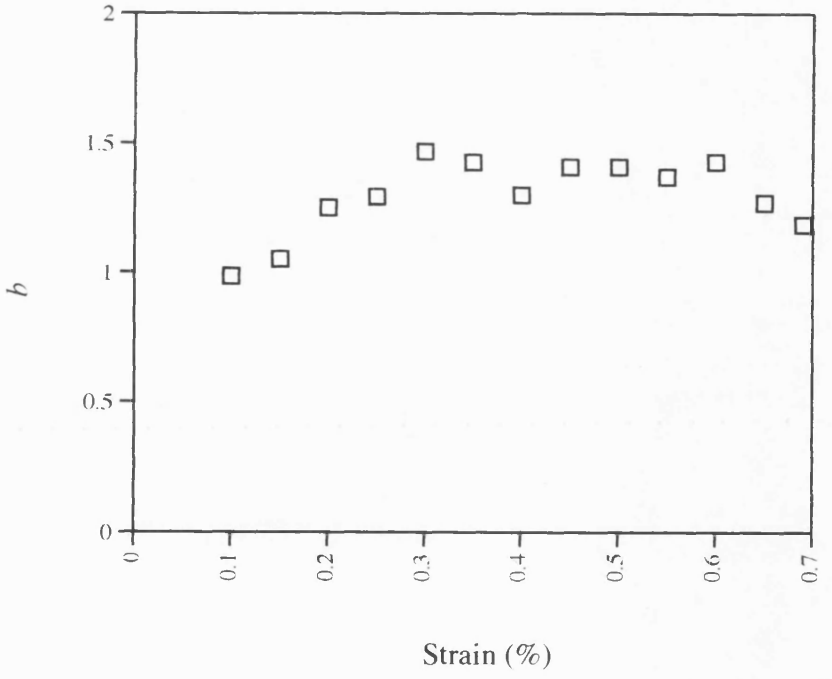

b)

Figure 8.17: Acoustic emission response of Nicalon/CAS (0/90/0) composite shown as a) AE rate and b) *b* value as a function of applied strain

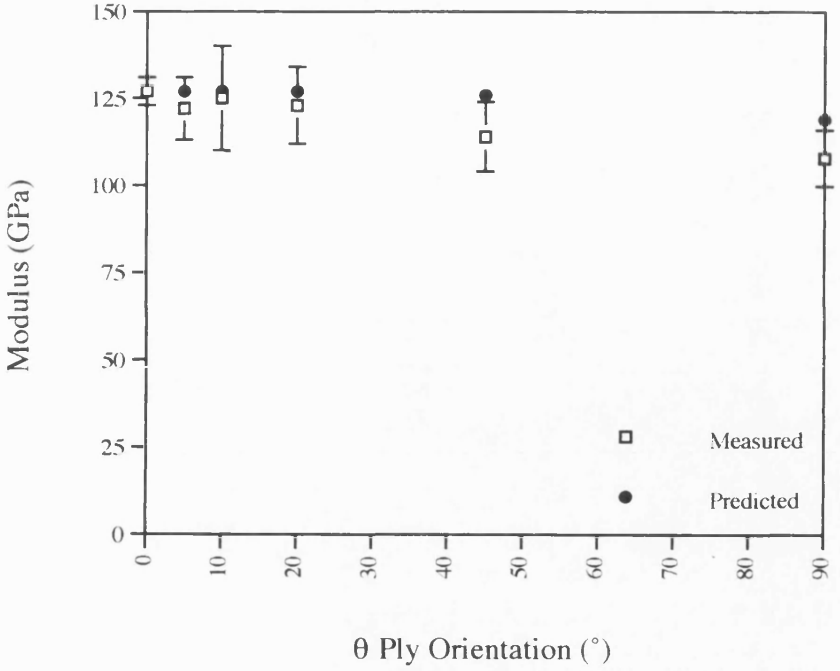

Figure 8.18: Comparison of measured and predicted composite modulus as a function of θ ply orientation

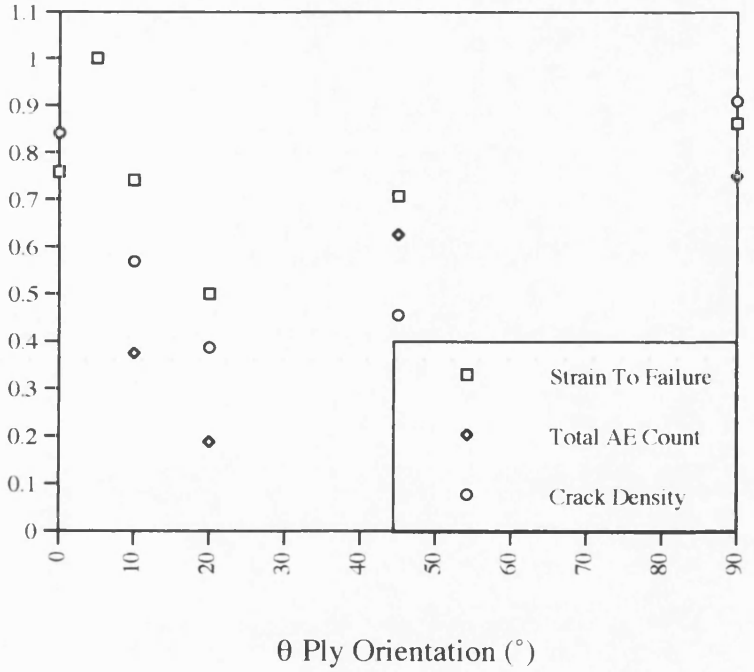

Figure 8.19: Strain to failure, total AE count and final crack density of (0/θ/0) composites (normalised wrt maximum) as a function of θ ply orientation

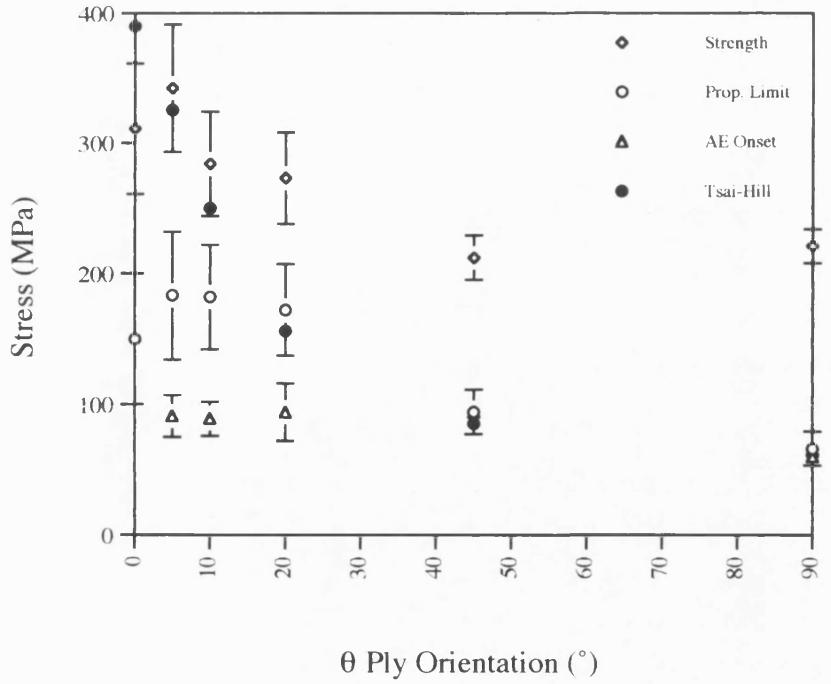

Figure 8.20: Ultimate strength, limit of proportionality and acoustic emission onset stress of (0/θ/0) composite plotted as a function of θ ply orientation, together with first-ply failure stress based om predictions of Tsai-Hill failure criterion

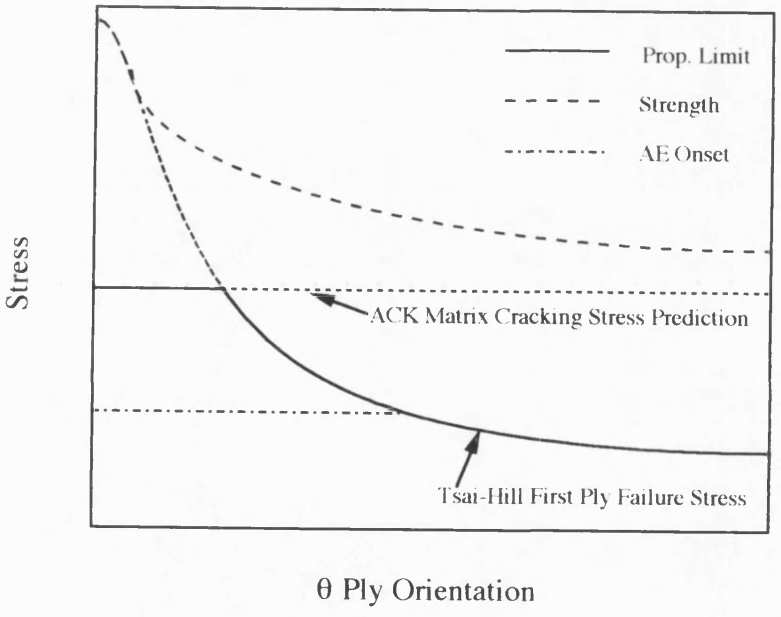

Figure 8.21: Schematic representation of mechanical behaviour of Nicalon/CAS (0/θ/0) laminates

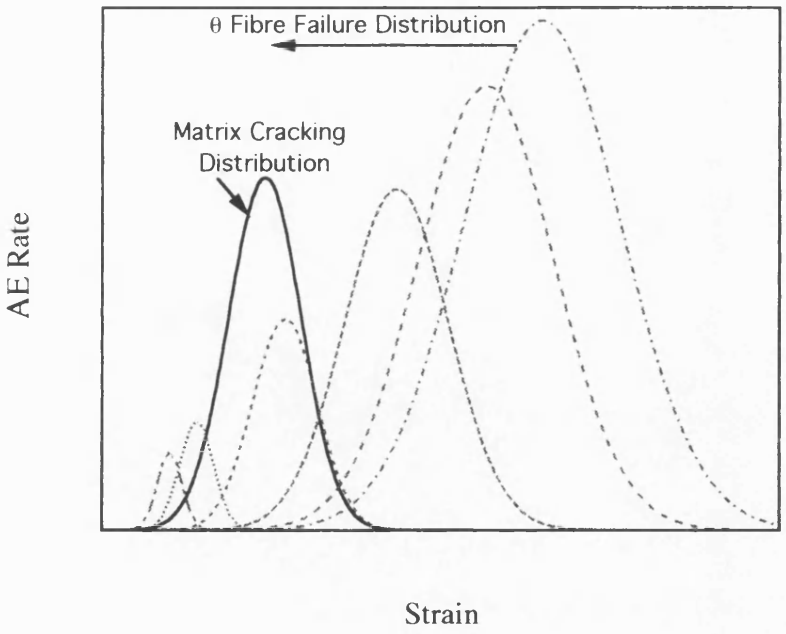

Figure 8.22: Schematic representation of acoustic emission response of Nicalon/CAS (0/θ/0) laminates

CHAPTER 9 : CONCLUSIONS AND FUTURE WORK

9.1 Conclusions

In order for the potential of ceramic-matrix composites to be fully exploited, a detailed understanding of the micro-mechanics of failure under a wide range of loading conditions is required. The aim of the present study was therefore to investigate the damage processes which occur in unidirectional, off-axis and simple angle-ply laminates of a Nicalon/CAS glass-ceramic matrix composite in an attempt to understand the material's stress-strain behaviour.

Examination of published literature revealed that several workers had attempted to describe the stress-strain behaviour of unidirectional glass-ceramic matrix composites in terms of the onset and development of cracks within the matrix. It also became apparent that the accuracy of their predictions, based on available models of matrix cracking in brittle-matrix composites, was highly sensitive to the chosen values of matrix properties and that little experimental data on the properties of monolithic CAS existed.

An attempt to address this shortfall in data was made in Chapter 5. The microstructural, physical, elastic, and mechanical properties of monolithic CAS were studied in detail by using a wide range of experimental techniques. The microstructure of the monolith was found to be in excellent agreement with published results on the structure and composition of the Nicalon/CAS matrix. The physical, elastic and mechanical properties were also found to be in accord with those quoted by the manufacturer. Fracture mechanics parameters of the monolithic CAS were measured and estimated by a number of methods. The single-edge notched bend test was a largely unsuccessful method, as few specimens exhibited any form of crack growth stability. Estimates of the matrix fracture surface energy (γ_m) were obtained from specimens that did fracture in a stable manner and also from estimates of the

critical flaw size. This gave greater confidence in selecting a value of γ_m to be used in any subsequent modelling exercises.

The stress-strain behaviour and acoustic emission response of unidirectional Nicalon/CAS composite during continuous and discontinuous tensile tests were examined in Chapter 6. The overall shape of the stress-strain curve was in reasonable accord with that predicted by the Aveston, Cooper and Kelly[4] (ACK) model. The slope of an initial linear region was in good agreement with rule-of-mixtures predictions of composite modulus. The limit of proportionality on the stress-strain curve was followed by a region of decreasing slope and it was confirmed, by optical examination of replicas made during discontinous tests, that the majority of observable damage occurred during this region and was in the form of a parallel array of matrix cracks, situated perpendicular to the fibres and spanning the entire specimen thickness. It was observed that the formation of the first few matrix cracks coincided with the onset of acoustic emission activity and that this occurred at a stress well below the limit of proportionality. The onset of matrix cracking was found to be in good agreement with the predictive models of Aveston, Cooper and Kelly[4] and McCartney[22] once the tensile residual thermal stress in the matrix was taken into consideration. The physical significance of the limit of proportionality was not understood and its suitability as a design stress should thus be questioned.
Continued cracking of the matrix, up until crack saturation, was found to occur over a range of stress and not the constant stress predicted by ACK and this was thought to be due to the presence of a distribution of flaw sizes in the matrix. This was reflected in the changing rate of acoustic emission activity during matrix cracking. The saturation crack spacing was found to be in reasonable agreement with the combined models of ACK and Zok & Spearing[28].
Amplitude distribution analysis of acoustic emission data, by novel application of the Pollock method[144], gave a constant value for the parameter b during the matrix cracking regime. This is thought to indicate that failure occurs by a single mechanism,

whilst the value of b in this region implied that matrix cracking damage events gives rise to high amplitude emissions and are thus of high energy.

The region of decreasing slope on the stress-strain curve was followed by a second linear region during which little futher matrix cracking occurred. Amplitude distribution analysis of acoustic emissions throughout this region, by the above method, indicated that failure of the composite occurred by a different mechanism comprising a large number of low energy events. This was thought to be progressive fibre fragmentation of the type predicted by Curtin[49], and/or fibre-matrix sliding due to elastic deformation of the fibres within their matrix sockets (of the type proposed by ACK). It was found that the failure mechanism operating in this region of the stress-strain curve had no perceivable effect on the composite transverse strain. However, the exact mechanism remained unconfirmed.

The effect of fibre orientation on the room-temperature tensile properties of Nicalon/CAS was studied in Chapter 7. However, discussion and interpretation of the data was hindered by differences in quality between the two plates tested. A difference in material quality was highlighted successfully by a non-destructive ultrasonic c-scan technique and was subsequently identified by microstructural examination as being due to delamination in one of the plates.

Similarities were found between the behaviour of 5° and 10° off-axis composites and that of a unidirectional composite tested parallel to the fibres. Observable damage was again in the form of a parallel array of matrix cracks. However, some evidence of interface failure prior to matrix cracking was gained by examination of replicas made during discontinous tests on 10° off-axis composite. The average crack spacing in failed 5° and 10° composites was found to be larger than in 0° specimens. This may be due to a number of factors, for example: (i) the stress transfer length, x' (predicted from the ACK model), may be greater in composites with orientated fibres due to a lower effective interfacial friction stress in the direction of applied stress, and (ii) that continued matrix cracking is limited by the ability of fibres to carry the additional

load and this ability may decrease with increasing fibre angle, thus limiting the extent of cracking.

The variation of composite strength with fibre orientation was found, for the non-delaminated plate, to be in good agreement with predictions based on available failure criteria. However, these failure criteria assume linear elastic behaviour and fibre-dominated failure which ignore the significant contribution of matrix cracking to the overall damage in the composite.

Another conclusion drawn from Chapter 7 is that the 10° off-axis test, originally proposed by Chamis and Sinclair[56], appears to be an unsuitable method for obtaining the shear properties of a composite in which the matrix makes a substantial contribution to the overall elastic deformation.

It was also found that measurement of the dimensions of fibre ellipses is an unsuitable method for determining the fibre orientation and that this is mostly due to the shape of the trigonometric function $\cos^{-1}$ in addition to experimental error.

The stress-strain behaviour and acoustic emission responses of simple Nicalon/CAS angle-ply laminates (Chapter 8) were then interpreted in the light of results from Chapters 6 and 7. A series of model (0/θ/0) laminates were tested continuously in tension to failure and to different levels of strain. Damage accumulation in the laminates was studied in detail. Similarities between the results for (0/θ/0) laminates and those for unidirectional and off-axis composites were identified and existing models were found accurately to predict a number of stages of damage development. The observable damage was predominantly that of matrix cracking in both the 0° and θ plies. However, crack saturation was not achieved in the 0° plies of all (0/θ/0) materials tested. The transverse strain behaviour, again, appeared to be most closely associated with matrix cracking, reaching a plateau level only in those specimens achieving crack saturation in the 0° plies. It was thought that continued matrix cracking was limited in many cases by the ability of fibres to withstand additional load.

A tentative behaviour model was proposed in which the failure envelopes of individual damage mechanisms are superimposed and which can be used to predict the stress-strain behaviour, acoustic emission response and damage evolution in these types of composites. It was thought that the extent of each damage mechanism depended on the degree of overlap between the strength distributions of the matrix, θ and 0° fibres, with the higher stress mechanism truncating the lower stress mechanism in each case.

9.2 Conclusions in Context

Glass-ceramic matrix composites are currently being considered by aero-engine manufacturers for use in high-temperature structural applications. It is believed that incorporating strong ceramic fibres into a glass-ceramic matrix can prevent the catastrophic brittle fracture, traditionally associated with monolithic ceramics, by providing various energy dissipation processes during failure. In unidirectionally reinforced glass-ceramic composites tested at room-temperature in a direction parallel to their fibres, this type of property enhancement is achieved to an extent - with a high fracture energy resulting from crack deflection, crack bridging and fibre pull-out, all of which require a weak fibre-matrix interfacial bonding.

The mechanical behaviour of unidirectional glass-ceramic matrix composites has been reported elsewhere[106-112] and the results of the present study are in agreement with those workers. The behaviour is generally found to be in accord with that predicted by the Aveston, Cooper and Kelly model[4] (ACK) and initial damage is found to be in the form of matrix cracking perpendicular to the fibres. The formation of matrix cracks leads to a reduction in composite stiffness and a loss of protection for the fibre-matrix interface against oxidation and composite embrittlement. Matrix microcracking is therefore deemed to be a fundamental life-limiting issue for ceramic-matrix composites and as such is likely to be the design limit for this class of material.

The ACK theory predicts that the stress at which matrix cracking initiates is enhanced, above that of the monolithic matrix, and that it corresponds to the limit of proportionality on the stress-strain curve. However, this was not found to be the case for a Nicalon/CAS composite. It was found that the onset of matrix cracking occurred at stresses well below the limit of proportionality on the stress-strain curve. It appeared that any enhancement of the matrix crack initiation stress was, to some extent, negated by the thermal stresses induced in the material due to the different thermal expansion coefficients of the fibres and matrix. Kim and Pagano[106] infer from their results that no enhancement occurs and that the matrix crack initiation stress is similar to that of the unreinforced matrix. However, in both the present work and that of Kim and Pagano, it is concluded that the limit of proportionality on the stress-strain curve has little physical significance and its use a design stress should be questioned. A number of factors may increase the matrix cracking initiation stress - e.g. elimination of larger flaws in the matrix, a higher fibre volume fraction, a reduction in fibre radius, a slight increase in fibre-matrix interfacial friction stress (this point will be discussed further), or ideally a matrix with a thermal expansion coefficient closer to that of the fibres. Clearly, some of these so-called solutions may introduce problems of their own. It is also possible that a zero damage design criterion is impractical for this type of composite. It may be possible that a degree of matrix cracking may be tolerated by means of fibre coating and or component coating.

Continued matrix cracking occurs with increasing applied stress as a result of stress transfer between the fibres and matrix via the fibre-matrix interface. Again this requires a weak fibre-matrix interface. The present study has shown (if the results of microindentation tests are to be believed) that there is a thin dividing line between continued matrix cracking and brittle fracture of the composite. This is shown by the difference in the behaviour of $(0)_3$ composites having an interfacial friction stress of 23 MPa, which were of low strength and exhibited little matrix cracking or fibre pull-out, and the more conventional composite behaviour of unidirectional composites

having a fibre-matrix interfacial friction stress of about 9 - 11 MPa. It was also shown that continued matrix carcking occurs over a range of stress, rather than the constant stress assumed in the ACK theory. The range of stress over which matrix cracking occurs may be reduced by decreasing the mean and distribution of flaw sizes in the matrix.

Discussion of possible improvements in unidirectional properties is of academic interest in terms of design, as few engineering applications exist for this type of laminate. It should also be noted that the property which gives unidirectionally reinforced composite desirable behaviour is the very property that leads to the low transverse and shear strength of that laminate - i.e. a weak fibre-matrix bond. Most aero-engine components will be subjected to multiaxial loads and will require the use of composites containing fibres orientated in directions of applied load.
In the present study, the behaviour of a (0/θ/0) laminates have been investigated. Although this not a conventional lay-up it is conceviable that the design of certain components may require sections of ≤ 0.5 mm thickness. In the case of (0/90/0) composites, a first-ply failure stress of 50 - 60 MPa was measured which corresponded to cracking in the transverse ply. Clearly, a material with a design stress as low as this is of little practical use in an aero-engine. However, it is interesting to note that the tranverse cracking appeared to be constrained - i.e. that progressive crack progagation across the 90° ply occurred as opposed to the instaneous formation of a full transverse ply crack. The threshold for this type of cracking is dependent on the ply thickness and thus it may be possible to further constrain the cracking by decreasing the ply thickness. It is not known by the author whether this is a practical proposition. The production of very thin pre-preg may lead to handling problems and the application of greater pressure during manufacture may lead to excessive fibre damage. These are just two of the many considerations.
The results from tests on (0/θ/0) laminates indicate that a (0/20/0) composite is the worst scenario in terms of desirable behaviour, as few of the energy absorbing

processes are operative. It is concluded that the behaviour of composites which fail in the matrix cracking regime is unpredicable and and should be avoided. The most successful composites appear to be those in which crack saturation is achieved and where ultimate fracture is controlled by fibres in the 0° plies.

9.3 Future Work

In the present study, observation of damage development have been restricted to that of matrix cracking. In order to interpret the behaviour of unidirectional composites more fully it is necessary to determine the damage mechanism operating in the second linear region of the stress-strain curve. It is thought that this may only be achieved by direct observation of fibre deformation and fracture, and a suitable method for obtaining this type of information is required.

Further work on the effect of fibre orientation on the matrix cracking behaviour of a more consistent quality ceramic-matrix composite should be carried out at 5°, 10°, 15° and 20° (smaller intervals might not be possible as machining errors may become more significant) as it is thought that this would yield vital information on the changing rôle of the fibre-matrix interface and residual thermal stresses in the matrix, and would enable further development of models for predicting matrix cracking stress, stress transfer across the interface, and saturation crack spacing in unidirectional material.

In order to develop the behaviour model proposed in the present study, it is necessary to quantify the strength distribution of fibres at different orientations. This may be achieved by a combination of the above, i.e. direct observation of fibre fracture in off-axis composites.

It is suggested that a study of more conventional angle-ply and cross-ply laminates be carried out and that the effect of ply thickness on the cracking behaviour be investigated, in particular the effect of decreasing the ply thickness.

REFERENCES

1. E.G.Butler, M.H.Lewis - 'Prospects for Ceramics in Airborne Gas Turbine Engines', 4th Int.Symp. on Ceramic Materials and Components for Engines Ed. R.Carlsson, Elsevier, 32-49 (1992)

2. R.W.Davidge - 'Perspectives for Engineering Ceramics in Heat Engines', High Temperature Technology, **5** (1), 13-21 (1987)

3. D.B.Marshall, J.E.Ritter - 'Reliability of Advanced Structural Ceramics and Ceramic Matrix Composites - A Review', Ceram.Bull., **66** (2), 309-317 (1987)

4. J.Aveston, G.A.Cooper, A.Kelly - 'Paper 2 - Single and Multiple Fracture', Conference Proceedings of the National Physical Laboratory, IPC Science and Technology Press Ltd., Guidford, Surrey, 15-26 (1971)

5. O.H.Wyatt & D.Dew-Hughes - 'Metals, Ceramics and Polymers', Cambridge University Press (1974)

6. J.F.Knott - 'Fundamentals Of Fracture Mechanics', Butterworths (1973)

7. A.A.Griffith - 'The Phenomena of Rupture and Flow in Solids', Trans.Royal.Soc.London, **A221**, 163-198 (1920)

8. C.E.Inglis -' Stresses in a Plate due to the Presence of Cracks and Sharp Corners', Trans.Instn.Nav.Archit., **55**, 1, 219- (1913)

9. G.R.Irwin - 'Fracture', in Handbuch der Physik, Volume 6, Springer-Verlag, Berlin (1958)

10. W.Weibull - 'A Statistical Distribution Function of Wide Applicability', J.Appl.Mech., **18**, 293-297 (1951)

11. R.W.Davidge - 'Mechanical Behaviour of Ceramics', Cambridge Solid State Science Series, Cambridge University Press, London (1979)

12. D.Hull - 'An Introduction to Composite Materials', Cambridge Solid State Science Series, Cambridge University Press (1981)

13. R.M.Jones - 'Mechanics of Composite Materials', Scripta Book Company, Washington D.C. (1975)

14. S.W.Tsai - 'Composites Design - 3rd Edition', Think Composites, Dayton, Ohio (1987)

15. A.Kelly, N.H.Macmillan - 'Strong Solids', Third Edition, Clarendon Press, Oxford (1986)

16. R.J.Butler, A.L.Butler - 'LAMANAL - A Program for the Design and Analysis of a Laminated Plate', Cranfield Press (1986)

17. G.A.Cooper, J.M.Sillwood - 'Multiple fracture in a Steel Reinforced Epoxy Resin Composite', J.Mat.Sci., **7**, 333-352 (1972)

18. J.Aveston, A.Kelly - 'Theory of Multiple Fracture of Fibrous Composites', J.Comp.Mat., **8**, 325-362 (1973)

19. B.Budiansky, J.W.Hutchinson, A.G.Evans - 'Matrix Fracture in Fibre-Reinforced Ceramics', J.Mech.Phys.Solids, **37** (1), 167-189 (1986)

20. D.B.Marshall, A.G.Evans - 'Failure Mechanisms in Ceramic-Fibre/Ceramic-Matrix Composites', J.Am.Ceram.Soc., **68** (5), 225-231 (1985)

21. D.B.Marshall, B.N.Cox, A.G.Evans - 'The Mechanics of Matrix Cracking in Brittle Matrix Fibre Composites', Acta.Metall., **33** (11), 2013-2021 (1985)

22. L.N.McCartney - 'Mechanics of Matrix Cracking in Brittle Matrix Fibre Reinforced Composites', Proc.Roy.Soc.London, **A 409**, 329-350 (1987)

23. L.N.McCartney - 'New Theoretical Model of Stress Transfer Between Fibre and Matrix in a Uniaxially Fibre-Reinforced Composite', **A425**, 215-244 (1989)

24. A.S.D.Wang, M.W.Barsoum, X.G.Huang - 'Matrix Crack Initiation in Ceramic Matrix Composites Part II : Models and Simulation Results', Comp.Sci.&Tech., **44**, 271-282 (1992)

25. J.Aveston, R.A.Mercer, J.M.Sillwood - Proc. NPL conference on Composites - Standards, Testing and Design, IPC Science and Technology Press, 93-102 (1974)

26. A.C.Kimber, J.G.Keer - 'On the Theoretical Average Crack Spacing n Brittle Matrix Composites Containing Continuous Aligned Fibres', J.Mat.Sci.Lett., **1**, 353-354 (1982)

27. X.F.Yang, K.M.Knowles - 'The One-Dimensional Car Parking Problem and Its Application to the Distribution of Spacings Between Matrix Cracks in Unidirectional Fibre-reinforced Brittle Materials', J.Am.Ceram.Soc., **75** (1), 141-147 (1992)

28. F.W.Zok, S.M.Spearing - 'Matrix Crack Spacing in Brittle Matrix Composites', Acta Metall.Mater., **40** (8), 2033-2043 (1992)

29. K.W.Garrett, J.E.Bailey - 'Multiple Transverse Fracture in 90° Crossply Laminates of Glass-Fibre reinforced Polyester', J.Mat.Sci., **12**, 157-168 (1977)

30. A.Parvizi, K.W.Garrett, J.E.Bailey - 'On Multiple Transverse Cracking in Glass Fibre Epoxy Crossply Laminates', J.Mat.Sci., **13**, 2131-2136 (1978)

31. J.E.Bailey, A.Parvizi - 'On Fibre Debonding Effects and the Mechanism of Transverse-Ply Failure in Cross-Ply Laminates of Glass Fibre/Thermoset Composites', J.Mat.Sci., **16**, 649 - 659 (1981)

32. A.S.D.Wang, P.C.Chou, S.C.Lei - ' A Stochastic Model for the Growth of Matrix Cracks in Composite Laminates', J.Comp.Mat., **18**, 239 - 254 (1984)

33. S.L.Ogin, P.A.Smith - 'A Model for Matrix Cracking in Cross-Ply Laminates', Scripta Met., **19**, 779 - 784 (1987)

34. N.Laws, G.J.Dvorak - 'Progressive Transverse Ply Cracking in Composite Laminates', J.Comp.Mat., **22**, 900 - 916 (1988)

35. H.Fukanaga, T.W.Chou, P.W.M.Peters, K.Schulte - 'Probabilistic Failure Strength Analyses of Graphite/Epoxy Cross-ply Laminates', J.Comp.Mat., **18**, 339 - 356 (1984)

36. A.L.Highsmith, K.L.Reifsnider - 'Stiffness-Reduction mechanisms in Composite Laminates', in 'Damage in Composite Materials', ASTM STP 775, 103 -117 (1982)

37. R.E.Rowlands - 'Strength (Failure) Theories and Their Experimental Correlation', in Handbook of Composites (Volume 3 - Failure Mechanics of Composites), Eds. G.C.Sih & A.M.Skudra, Elsevier, Amsterdam, 71-125 (1985)

38. D.E.Tripp, J.H.Hemann, J.P.Gyekenyesi - 'A Review of Failure Models for Ceramic Matrix Composite Laminates Under Monotonic Loads', Transactions of the ASME, 112, 492-501 (1990)

39. A.Kelly - 'Materials Science and Technology - Chapter 1: Fibrous Composite Materials', Ed. T.-W.Chou, VCH Publishers Inc., New York, Vol. **13**, 1-24 (1993)

40. R.Y.Kim - 'Materials Science and Technology - Chapter 11: Strength of Fibre Composites', Ed. T.-W.Chou, VCH Publishers Inc., New York, Vol. **13**, 495-532 (1993)

41. H.E.Daniels - 'The Statistical Theory of the Strength of Bundles of Threads', Proc.Roy.Soc.Lond., **A183**, 405-435 (1945)

42. B.D.Coleman - 'On the Strength of Classical Fibres and Fibre Bundles', J.Mech.Phys.Solids, **7**, 60-70 (1958)

43. B.W.Rosen - 'Tensile Failure of Fibrous Composites', AIAA Journal, **2** (11), 1985-1991 (1964)

44. C.Zweben - 'Tensile Failure of Fibre Composites', AIAA Journal, **6** (12), 2325-2331 (1968)

45. C.Zweben, B.W.Rosen - 'A Statistical Theory of Material Strength with Application to Composite Materials', J.Mech.Phys.Solids, **18**, 189-206 (1970)

46. M.D.Thouless, A.G.Evans - 'Effects of Pull-Out on the Mechanical Properties of Ceramic-Matrix Composites', Acta.Metall., **36** (3), 519-522 (1988)

47. H.Cao, M.D.Thouless - 'Tensile Tests of Ceramic-Matrix Composites: Theory and Experiment', J.Am.Ceram.Soc., **73** (7), 2091-2094 (1990)

48. W.A.Curtin - 'Exact Theory of Fibre Fragmentation in a Single-Filament Composite', J.Mat.Sci., **26**, 5239-5253 (1991)

49. W.A.Curtin - 'Theory of Mechanical Properties of Ceramic-Matrix Composites', J.Am.Ceram.Soc., **74** (11), 2837-2845 (1991)

50. W.A.Curtin - 'Ultimate Strengths of Fibre-Reinforced Ceramics and Metals', Composites, **24** (2), 98-102 (1993)

51. S.W.Tsai - 'Strength Theories of Filamentary Structures', in Fundamental Aspects of Fibre-Reinforced Plastic Composites, Eds. R.T.Schwarz and H.S.Schwartz, Wiley, New York, 3-11 (1968)

52. S.W.Tsai, E.M.Wu - 'A General Theory of Strength for Anisotropic Materials', J.Comp.Mat., **5** (1), 58-80 (1971)

53. E.M.Wu - 'Phenomenological Anisotropic Failure Criterion', Mechanics of Composite Materials, Ed. G.P.Sendeckyj (Composite Materials vol. 2 Ed. L.J.Broutman), Academic Press, New York, 353-431 (1974)

54. L.J.Hart-Smith - ' A New Approach to Fibrous Composite Laminate Strength Prediction', Proc. 8th DOD/NASA/TAA Conference on Fibrous Composites in Structural Design, NASA-3087, 663-693 (1989)

55. L.J.Hart-Smith - 'The Role of Biaxial Stresses in Discriminating Between Meaningful and Illusory Composite Failure Theories', Composite Structures, **25**, 3-20 (1993)

56. C.C.Chamis, J.H.Sinclair - 'Ten-Deg Off-Axis Test for Shear Properties in Fibre Composites', Experimental Mechanics, **17** (9), 339-346 (1977)

57. A.Puck, W.Schneider - 'On Failure Mechanisms and Failure Criteria of Filament-Wound Glass-Fibre/Resin Composites', Plastics & Polymers, 33-42, (February 1969)

58. R.Hill - 'The Mathematical Theory of Plasticity', Oxford University Press, London, 318-320 (1950)

59. R.A.J.Sambell, D.H.Bowen, D.C.Phillips - 'Carbon Fibre Composites with Ceramic and Glass Matrices - Part 1 Discontinuous Fibres', J.Mat.Sci., **7**, 663-675 (1972)

60. R.A.G.Sambell, A.Briggs, D.C.Phillips, D.H.Bowen - 'Carbon Fibre with Ceramic and Glass Matrices - Part 2 Continuous Fibres', J.Mat.Sci., **7**, 676-681 (1972)

61. D.C.Phillips, R.A.J.Sambell, D.H.Bowen - 'The Mechanical Properties of Carbon Fibre Reinforced Pyrex Glass', J.Mat.Sci., **7**, 1454-1464 (1972)

62. D.C.Phillips - 'The Fracture Energy of Carbon-Fibre Reinforced Glass', J.Mat.Sci., **7**, 1175-1191 (1972)

63. D.C.Phillips - 'Interfacial Bonding and the Toughness of Carbon Fibre Reinforced Glass and Glass-Ceramics', J.Mat.Sci., **9**, 1847-1854 (1974)

64. S.Yajima, K.Okamura, J.Hayashi, M.Omori - 'Synthesis of Continuous SiC Fibres with High Tensile Strength', J.Am.Ceram.Soc., **59**, 324-327 (1976)

65. K.Okamura - 'Ceramic Fibres from Polymer Precursors', Composites, **18** (2), 107-120 (1987)

66. K.M.Prewo, J.J.Brennan -'High Strength Silicon Carbide Fibre-Reinforced Glass-Matrix Composites', J.Mat.Sci., **15**, 463-468 (1980)

67. K.M.Prewo, J.J.Brennan - 'Silicon carbide Yarn Reinforced Glass Matrix Composites', J.Mat.Sci., **17**, 1201-1206 (1982)

68. J.J.Brennan, K.M.Prewo - 'Silicon Carbide Fibre Reinforced Glass-Ceramic Matrix Composites Exhibiting High Strength and Toughness', J.Mat.Sci., **17**, 2371-2383 (1982)

69. K.M.Prewo - 'Tension and Flexural Strength of Silicon Carbide Fibre Reinforced Glass-Ceramics', J.Mat.Sci., **21**, 3590-3600 (1986)

70. K.M.Prewo - 'Fatigue and Stress Rupture of Silicon Carbide Fibre-Reinforced Glass-Ceramics', J.Mat.Sci., **22**, 2695-2701 (1987)

71. D.B.Marshall - 'An Indentation Method for Measuring Matrix-Fibre Frictional Stresses in Ceramic Composites', J.Am.Ceram.Soc., **67** (12), C259-C260 (1984)

72. T.Mah, M.G.Mendiratta, A.P.Katz, R.Ruh, K.S.Mazdiyasni - 'Room-Temperature Mechanical Behaviour of Fibre-Reinforced Ceramic-Matrix Composites', J.Am.Ceram.Soc., **68** (1), C27-C30 (1985)

73. T.Mah, M.G.Mendiratta, A.P.Katz, R.Ruh, K.S.Mazdiyasni - 'High-Temperature Machanical Behaviour of Fibre-Reinforced Glass-Ceramic-Matrix Composites', J.Am.Ceram.Soc., **68** (9), C248-C251 (1985)

74. J.F.Mandell, D.H.Grande, J.Jacobs - 'Tensile Behaviour of Glass/Ceramic Composite Materials at Elevated Temperatures', Journal of Engineering for Gas and Turbine Power, **109**, 267-273 (1987)

75. E.Y.Luh, A.G.Evans - 'High Temperature Mechanical Properties of a Ceramic Matrix Composite', J.Am.Ceram.Soc., **70** (7), 466-469 (1987)

76. D.M.Dawson, R.F.Preston, A.Purser - 'Fabrication and Materials Evaluation of High Performance Aligned Ceramic Fibre-Reinforced Glass Matrix Composite', Ceram.Eng.Proc., **8**, 815-821 (1987)

77. B.A.Ford, R.G.Cooke, S.Newsam - 'Failure Mechanisms in Silicon Carbide Fibre Reinforced Borosilicate Glass', Proc.Brit.Ceram., **39**, 229-234 (1987)

78. R.Y.Kim, A.P.Katz - 'Mechanical Behaviour of Unidirectional SiC/BMAS Ceramic Composites', Ceram.Eng.Sci.Proc., **9** (7-8), 853-860 (1988)

79. F.A.Habib, R.G.Cooke, B.Harris - 'Cracking in Brittle Matrix Composites', Brit.Ceram.Trans.J., **89**, 115-124 (1990)

80. R.W.Davidge, A.Briggs - 'The Tensile Failure of Brittle Matrix Composites Reinforced with Unidirectional Continuous Fibres', J.Mat.Sci., **24**, 2815-2819 (1989)

81. O.Sbaizero, A.G.Evans - 'Tensile and Shear Properties of Laminated Ceramic Matrix Composites', J.Am.Ceram.Soc., **69** (6), 481-486 (1986)

82. A.Seerat Un Nabi, B.Derby - 'Mechanical Properties of Laminated Pyrex Matrix Composites', Proc.9th Risø Int.Symp. on Metallurgy and Materials Science, 463-468 (1988)

83. K.M.Prewo - 'Carbon Fibre Reinforced Pyrex Glass Matrix Composite Tension and Flexure Properties', J.Mat.Sci., **23**, 2745-2752 (1988)

84. K.M.Prewo, B.Johnson, S.Starret - 'Silicon Carbide Fibre-Reinforced Glass-Ceramic Composite Tensile Behaviour at Elevated Temperature', J.Mat.Sci., **24**, 1373-1379 (1989)

85. V.C.Nardone, K.M.Prewo - 'Tensile Performance of Carbon-Fibre-Reinforced Glass', J.Mat.Sci., **23**, 168-180 (1988)

86. D.M.Dawson, A.Binstead, F.K.Ko - 'The Mechanical Properties of Crossply and 3-D Braided Nicalon SiC Fibre Reinforced Pyrex Composites', Brit.Ceram.Trans.J., **88**, 226-228 (1989)

87. V.S.R.Murthy, M.H.Lewis - 'Interface Structure and Matrix Crystallisation in SiC(Nicalon)-Pyrex Composites', J.Mat.Sci.Lett., **8**, 571-572 (1989)

88. S.M.Bleay, V.D.Scott - 'Microstructure Property Relationship in Pyrex Glass Composites Reinforced with Nicalon Fibres', J.Mat.Sci., **26**, 2229-2239 (1991)

89. S.M.Cox, P.L.Kirby - 'Rate of Crystal Growth in Glass', Nature, **159**, 162-163 (1947)

90. S.G.Clarke, S.M.Bleay, V.D.Scott - 'An Investigation into the Formation of Second-Phase Crystals in Amorphous Pyrex Glass', J.Mat.Sci.Lett., **10**, 149-153 (1991)

91. A.W.Pryce, M.C.Hill, P.A.Smith - 'Damage Development in Glass Matrix Composite Laminates', Proc. 4th IMechE Int. Conf. (FRC'90 Fibre Reinforced Composites), Liverpool, UK, 263-271 (1990)

92. D.W.Shin, K.M.Knowles - 'Microstructure-Property Relationships in SiC Fibre-Reinforced Borosilicate Glass Composites', Ibid., 163-168

93. R.J.Kerans, R.S.Hay, N.J.Pagano, T.A.Parthasarathy - 'The Role of the Fibre-Matrix Interface in Ceramic Composites', Ceram.Bull., **68** (2), 429-442 (1989)

94. M.D.Thouless, O.Sbaizero, L.S.Sigl, A.G.Evans - 'Effect of Interface Mechanical Properties on Pull-Out in a SiC-Fibre-Reinforced Lithium Aluminium Silicate Glass-Ceramic', J.Am.Ceram.Soc., **72** (4), 525-532 (1989)

95. H.C.Cao, E.Bischoff, O.Sbaizero, M.Ruhle, A.G.Evans - ' The Effect of Interfaces on the Mechanical Performance of Fibre Reinforced Brittle Materials', J.Am.Ceram.Soc., **73** (6), 1691-1699 (1990)

96. A.G.Evans, F.W.Zok, J.Davis - 'The Role of Interfaces in Fibre-Reinforced Brittle Matrix Composites', Comp.Sci. & Tech., 42, 3-25 (1991)

97. R.Chaim, A.H.Heuer - ' The Interface Between (Nicalon) SiC Fibres and a Glass-Ceramic Matrix', Advanced Ceramic Materials, **2** (2), 154-158 (1987)

98. R.F.Cooper, K.Chyung - 'Structure and Chemistry of Fibre-Matrix Interfaces in Silicon Carbide Fibre-Reinforced Glass-Ceramic Composites: an Electron Microscopy Study', J.Mat.Sci., **22**, 3148-3160 (1987)

99. E.Bischoff, M.Ruhle, O.Sbaizero, A.G.Evans - ' Microstructural Studies on the Interfacial Zone of a SiC-Fibre-Reinforced Lithium Aluminium Silicate Glass-Ceramic', J.Am.Ceram.Soc., **72** (5), 741-745 (1989)

100. M.Y.Chen, J.M.Battison, T.Mah - Interface Analysis of Si-C-O Fibre/Magnesium Aluminosilicate Matrix Composites', J.Mat.Sci., **24**, 3213-3220 (1989)

101. L.A.Bonney, R.F.Cooper - Reaction-Layer Interfaces in SiC-Fibre_reinforced Glass-Ceramics: A High Resolution Scanning Transmission Electron Microscopy Analysis', J.Am.Ceram.Soc., **73** (10), 2916-2921 (1990)

102. D.B.Marshall, W.C.Oliver - 'Measurement of Interfacial Mechanical Properties in Fibre-Reinforced Ceramic Composites', J.Am.Ceram.Soc., **70** (8), 542-548 (1987)

103. J.F.Mandell, K.C.C.Hong, D.H.Grande - 'Interfacial Shear Strength and Sliding Resistance in Metal and Glass-Deramic Matrix Composites', Ceram.Eng.Sci.Proc., **7** (7-8), 937-940 (1986)

104. M.H.Lewis, A.M.Daniel, A.Chamberlain, M.W.Pharaoh, M.G.Cain - Microstructure-Property Relationships in Silicate-Matrix Composites', Journal of Microscopy, **169** (2), 109-118 (1993)

105. K.Chyung - U.S.Patent No. 4615987, October 7th (1986)

106. R.Y.Kim, N.J.Pagano - 'Crack Initiation in Unidirectional Brittle-Matrix Composites', J.Am.Ceram.Soc., **74** (5), 1082-1090 (1991)

107. D.S.Beyerle, S.M.Spearing, F.W.Zok, A.G.Evans - 'Damage and Failure in Unidirectional Ceramic-Matrix Composites', J.Am.Ceram.Soc., **75** (10), 2719-2725 (1992)

108. I.M.Daniel, G.Anastassopoulos, J.-W.Lee - 'The behaviour of Ceramic Matrix Fibre Composites Under Longitudinal Loading', Comp.Sci.&Tech., **46**, 105-103 (1993)

109. P.Karandikar, T.-W.Chou - 'Characterisation and Modelling of Microcracking and Elastic Moduli Changes in Nicalon/CAS Composite', Ibid.

110. A.W.Pryce, P.A.Smith - 'Behaviour of Unidirectional and Cross-Ply Ceramic Matrix Composites Under Quasi-Static Tensile Loading', J.Mat.Sci., **27**, 2695-2704 (1992)

111. B.Harris, F.A.Habib, R.G.Cooke - 'Matrix Cracking and the Mechanical Behaviour of SiC-CAS Composite', Proc.Roy.Soc.Lond., **A437**, 109-131 (1992)

112. A.W.Pryce, P.A.Smith - Modelling the Stress-Strain Behaviour of Unidirectional Ceramic Matrix Composite Laminates', Br.Ceram.Trans., **92** (2), 49-54 (1993)

113. K.L.Powell, P.A.Smith, J.A.Yeomans - 'Aspects of Residual Thermal Stress in Continuous-Fibre-Reinforced Ceramic matrix Composites', Comp.Sci.&Tech., **47**, 359-367 (1993)

114. R.F.Allen, C.J.Beevers, P.Bowen - 'Fracture and Fatigue of a Nicalon/CAS Continuous Fibre-Reinforced Glass-Ceramic Matrix Composite', Composites, **24** (2), 150-??? (1993)

115. D.A.W.Kaute, H.R.Shercliff, M.F.Ashby - 'Delamination, Fibre Bridging and Toughness of Ceramic Matrix Composites', Acta.Metall.Mater., **41** (7), 1059-1970 (1993)

116. S.M.Bleay, V.D.Scott, B.Harris, R.G.Cooke, F.A.Habib - 'Interface Characterisation and Fracture of Calcium Aluminosilicate Glass-Ceramic reinforced with Nicalon Fibres', J.Mat.Sci., **27**, 2811-2822 (1992)

117. M.W.Pharaoh, A.M.Daniel, M.H.Lewis - 'Stability of Interfaces in Calcium Aluminosilicate Matrix/Nicalon SiC Fibre Composites', J.Mat.Sci.Lett., **12**, 998-1001 (1993)

118. P.W.McMillan - 'Glass-Ceramics - Second Edition', Academic Press, London (1979)

119. V.S.R.Murthy, M.W.Pharaoh, M.H.Lewis - 'Interface, Matrix and Fibre Microstructure in SiC-Reinforced Glass-Ceramic Composites', Inst.Phys.Conf.Ser. No.111, Paper presented at Int.Conf. on New Materials and their Applications, Univ. of Warwick (1990)

120. K.M.Prewo, J.J.Brennan, G.K.Layden - 'Fibre Reinforced Glass and Glass-Ceramics for High Performance Applications', J.Am.Ceram.Bull., **65** (2), 305-322 (1986)

121. R.Chaim, D.G.Brandon, L.Baum - 'Mechanical Properties and Microstructural Characterisation of SiC-Fibre-Reinforced Cordieritic Glass-Ceramics', Ceram.Eng.Sci.proc., **9** (7-8), 695-704 (1988)

122. Corning Glass - Private Communication

123. G.Simon, A.R.Bunsell - 'Mechanical and Structural Characterisation of the Nicalon Silicon Carbide Fibre', J.Mat.Sci., **19**, 3649-3657 (1984)

124. L.C.Sawyer, R.Arons, F.Haimbach, M.Jaffe, K.D.Rappaport - 'Characterisation of Nicalon: Strength, Structure and Fractography', Ceram.Eng.Sci.Proc., **6** (7-8), 567-575 (1985)

125. T.Mah, N.L.Hecht, D.E.McCullum, R.Hoenigan, H.M.Kim, A.P.Katz, A.Lipsitt - 'Thermal Stability of SiC fibres (Nicalon)', J.Mat.Sci., **19**, 1191-1202 (1984)

126. A.S.Fareed, P.Fang, M.J.Koczak, F.M.Ko - 'Thermomechanical Properties of SiC Yarn', Am.Ceram.Soc.Bull., **66** (2), 353-358 (1987)

127. G.Simon, A.R.Bunsell - 'The Creep of Silicon Carbide Fibres', J.Mat.Sci., **2**, 80-82 (1983)

128. S.M.Bleay, A.R.Chapman, G.Love, V.D.Scott - 'Electron Probe Microanalysis of Nicalon Fibre', J.Mat.Sci., **27**, 5389-5396 (1992)

129. C.H.Andersson, R.Warren - 'Silicon Carbide Fibres and Their Potential for Use in Composite Materials. Part 1', Composites, **15** (1), 16-24 (1984)

130. T.Yamamura, T.Hurushima, M.Kimoto, T.Ishikawa, M.Shibuya, T.Iwai - ' Development of New Continuous Si-Ti-C-O Fibre with High Mechanical Strength and Heat Resistance', Proc. World Congress on High Tech Ceramics, 6th CIMTEC, Milan, Italy, 24-28th June (1986)

131. T.Yamamura, Y.Waku, T.Ishikawa, T.Yamamoto, M.Shibuya, M.Suzuki, T.Nishi, T.Nagasawa - 'Compatibility of New Continuous Si-Ti-C-O Fibre for Composites', Looking Ahead for Materials and Processes, Ed., J.de Bossu, G.Briens, P.Lissac, Elsevier Science, Amsterdam (1987)

132. A.Briggs, R.W.Davidge - 'Borosilicate Glass Reinforced with Continuous Silicon Carbide Fibres: A New Engineering Ceramic', Mat.Sci.&Eng., **A109**, 363-372 (1989)

133. ASTM C 848 - 78 - ' Standard Test Method for Young's Modulus, Shear Modulus and Poisson's Ratio for Ceramic Whitewares by Resonance'

134. W.R.Davis - 'Measurement of the Elastic Constants of Ceramics by Resonant Frequency Methods', Trans.Brit.Ceram.Soc., **67** (11), 515-541 (1968)

135. prEN 843-1:1992 - Draft European Standard 'Advanced Technical Ceramics - Mechanical Properties of Monolithic Ceramics at Room Temperature - Part 1: Determination of Flexural Strength'

136. ASTM E 399-90 - 'Standard Test Method for Plane-Strain Fracture Toughness of Metallic Materials'

137. H.G.Tattersall, G.Tappin - 'The Work of Fracture and its Measurement in Metals, Ceramics and Other Materials', J.Mat.Sci., **1**, 296-301 (1966)

138. R.Morrell, L.N.McCartney - 'Measurement of Properties of Brittle Matrix Composites', Br.Ceram.Trans., **92** (1), 1-7 (1993)

139. Micro-Measurements -'Catalog 500. Part A - Strain Gauge Listings', page 6

140. R.V.Williams - 'Acoustic Emission', Adam Hilger Ltd., Bristol (1980)

141. A.Rotem - 'The Discrimination of Micro-Fracture Mode of Fibrous Composite Material by Acoustic Emission Technique', Fibre Science & Technology, **10**, 101-121 (1977)

142. D.Valentin, Ph.Bonniau, A.R.Bunsell - 'Failure Mechanism Discrimination in Carbon Fibre-Reinforced Epoxy Composites', Composites, **14** (4), 345-351 (1983)

143. F.J.Guild, B.Harris, A.J.Wills - 'Acoustic Emission from Glass/Polyester Composites: Effect of Fibre Orientation', J. Acoustic Emission, **1** (4), 244-250 (1982)

144. A.A.Pollock - 'Acoustic Emission 2 - Acoustic Emission Amplitudes', Non-Destructive Testing, **6** (5), 264-269 (1973)

145. S.Toll, P.-O.Andersson - 'Microstructural Characterisation of Injection Moulded Composites Using Image Analysis', Composites, **22** (4), 298-306 (1991)

146. M.F.Ashby, D.R.H.Jones - 'Engineering Materials - An Introduction to Their Properties and Applications', Pergamon Press, Oxford (1980)

147. D-W.Shin - 'Microstructure-Property Relationships of SiC Fibre-Reinforced Borosilicate Glass', PhD Thesis, Cambridge University (1993)

APPENDICES

Appendix 1 : The 10-degree Off-Axis Test for the Measurement of Shear Properties In Fibre Composites

Chamis and Sinclair[56] investigated the use of a 10° off-axis tensile test for the measurement of intralaminar shear characteristics of a unidirectional composite. This was first thought to be a suitable test for a unidirectional carbon fibre-reinforced epoxy composite since the intralaminar shear strain (ε_{12}) of this material, when normalised with respect to the failure strain (ε_{xx}) and plotted as a function of fibre orientation (θ), reached a critical value (as defined by the maximum strain theory) at roughly 10°. The material and structural axis co-ordinate systems are defined in Figure 2.4 and the variation of material axis stresses and strains with orientation are depicted in Figures 2.12 and 2.15, respectively.

Chamis and Sinclair used the following transformation equations which relate the ply intralaminar strain to structural axes strains for any orientation:

$$\varepsilon_{12} = (\varepsilon_{yy} - \varepsilon_{xx})\sin 2\theta + \varepsilon_{xy} \cos 2\theta \qquad \text{(A1.1)}$$

For a rectangular strain gauge rosette consisting of three gauges orientated at 0° (g1), 45° (g2) and 90° (g3) to the composite structural axes, the structural axis strains are given by:

$$\begin{aligned} \varepsilon_{xx} &= \varepsilon_{(g1)} \\ \varepsilon_{yy} &= \varepsilon_{(g3)} \\ \varepsilon_{xy} &= -\varepsilon_{(g1)} + 2\varepsilon_{(g2)} - \varepsilon_{(g3)} \end{aligned} \qquad \text{(A1.2)}$$

Thus by calculating the structural axis strains from the strain gauge readings by using equations A1.2 and substituting into equation A1.1 with θ set equal to 10°, then the intralaminar shear strain along the 10° plane can be expressed by

$$\varepsilon_{12} = -1.282\ \varepsilon_{(g1)} + 1.879\ \varepsilon_{(g2)} - 0.598\ \varepsilon_{(g3)} \qquad \text{(A1.3)}$$

Therefore, once the gauge strains are known, the intralaminar shear strain can be calculated from equation A1.3. Similarly the ply intralaminar shear stress can be calculated from the following transformation equation

$$\sigma_{12} = \sigma_{xx} \sin \theta \cos \theta \qquad \text{(A1.4)}$$

which for θ of 10° becomes

$$\sigma_{12} = 0.171\ \sigma_{xx} \qquad \text{(A1.5)}$$

The ply intralaminar shear stress can then be plotted against the ply intralaminar shear strain and a value for the initial ply shear modulus can be determined from the slope of the initial tangent to this stress-strain curve. The ply intralaminar shear strength equals the shear stress calculated at the composite fracture load and similarly for the fracture shear strain.

Chamis and Sinclair highlight a number of advantages of this technique over the commonly used ±45° tensile test or thin-tube torsion tests as a method of measuring shear properties. They suggest that the technique allows the use of long, thin specimens which may be cut from the same plate as those for longitudinal and transverse characterisation and that this is not only more economical on material but enables direct comparison of results. The test also yields values of modulus, Poisson ratio, coupling between extensional and shear deformation, and fracture stress. The specimens are free of lamination residual stresses in contrast to ±45° specimens.

However, there are also a number of disadvantages. Chamis and Sinclair found that the ply intralaminar shear strain was a maximum for carbon/epoxy composite at an orientation of 10° and appeared to be insensitive to small errors in orientation about this value, whereas the ply intralaminar shear stress was found to vary rapidly in the

region of 10°. They therefore recommended that the errors in fibre orientation, strain gauge positioning and load alignment be kept to within ±1°. The method also requires the simultaneouse measurement of strain from three gauges and that the true gauge strains (i.e. with the transverse sensitivity of the gauges accounted for) has to be calculated for each. It is also necessary to transform both stresses and strains with the possibility of further introduction of errors. Chamis and Sinclair also suggest that specimens with a relatively long gauge length to gauge width ratio (≥ 14:1) are required to minimise the restraining effect of the grips ('end-constraint effect').

Appendix 2 : A Method of Amplitude Distribution Analysis - After Pollock[144]

During a typical test, a wide range of peak amplitudes from individual emissions may be obtained. Pollock[144] suggests that it is possible to describe the distribution of peak amplitudes in terms of a function $n(a)$, where $n(a)$ is defined as the fraction of the emission population whose peak amplitude is greater than a. It is found that the experimental data often approximate to a power-law distribution of the form

$$n(a) = \left(\frac{a}{a_0}\right)^{-b} \qquad \text{(A2.1)}$$

where a_0 is the lowest detectable amplitude. The exponent b characterises the amplitude distribution and can be obtained from the gradient of a log-log plot. In the case of the Marandy MR1004 AE analyser, the minimum detectable threshold is 10 mV and each amplitude channel is 2.4 dB wide. The maximum amplitude within each channel is $2.4x$ dB, where x is the amplitude channel number. Thus the relationship between the amplitude a of an AE event, where a is in mV, and the amplitude channel is

$$2.4x = 20 \log\left(\frac{a}{a_0}\right) \qquad \text{(A2.2)}$$

Equating A2.1 and A2.2 gives the expression

$$\log n(x) = \log n(a) = -0.12bx \qquad \text{(A2.3)}$$

where $n(x)$ is the fraction of the emission population whose peak amplitude level is greater than that in channel x. The fraction, $n(x)$, of all AE events with amplitudes exceeding the minimum amplitude level, x_0, is

$$n(x) = \frac{N(x)}{N(x_0)} \qquad \text{(A2.4)}$$

where $N(x)$ is the number of events exceeding amplitude level x, and $N(x_0)$ is the total number of AE events above the minimum detectable threshold, a_0. Taking logarithms of both sides of equation A2.4 gives

$$\log n(x) = \log N(x) - \log N(x_0) \qquad \text{(A2.5)}$$

By substituting equation A2.3 into A2.5 and rearranging, an expression for the known quantity $N(x)$ may be derived

$$\log N(x) = \log N(x_0) - 0.12bx \qquad \text{(A2.6)}$$

Thus to obtain a Pollock distribution from the AE amplitude levels obtained from the Marandy system, the logarithm of the total number of AE events with amplitudes greater than level x (which includes those within level x), i.e. $\log N(x)$, versus the amplitude level x. The gradient of the line will equal $-0.12b$ and the intercept on the $\log N(x)$ axis will be equal to $\log N(x_0)$. The value of b can then be compared to that obtained form other AE detection systems.

When a deformation process occurs in a small number of large steps, each step releases a large amount of energy and, since the energy of an acoustic emission event is proportional to the square of the amplitude, there is a large proportion of high amplitude events and the value of b is therefore small. However, when deformation proceeds by a large number of small steps, low amplitude emissions tend to dominate and b is large. Pollock observed that values of b commonly lie within the range 0.4 and 2 and that if the amplitudes of all events were attenuated by the same factor, the value of b would remain unaffected.

Valentin et al[142], who investigated the effect of fibre orientation on the properties of carbon/epoxy composites, performed *b*-plot anayses on their acoustic emission data. They determined that the value of *b* decreased with increasing fibre angle in the case of unidirectional composite, whereas in cross-ply composites the value of *b* first decreased and then increased reaching a maximum at ±45°. They concluded from these results that, in unidirectional material, large amplitude events which were due to shear failure and cracking parallel to the fibres became relatively more important as the fibre angle increased and that fibre-dominated failure at low angles yielded a large amount of low-energy events. Matrix cracking perpendicular to the fibre direction was thought to be an insignificant source of AE activity.

Appendix 3 : Technique for the Preparation of Nicalon/CAS Polished Sections

The procedure detailed below was originally developed, after the Buehler Dialog method, for a Nicalon/Pyrex composite containing cristobalite and was later adapted at Bath University to the less demanding task of Nicalon/CAS preparation.

Specimens fell generally into three catagories: entire test specimens to be edge-polished prior to testing; entire specimens cast in 75mm x 25 mm blocks of epoxy resin and edge-polished after testing; or small representative sections set in 30 mm epoxy resin mounts and polished for quantitative microstructural analysis.

Specimens were mounted in Struers Epofix cold-setting resin following the manufacturer's recommended procedure. Where necessary, for example in the polishing of (0/θ/0) sections, either metal or polymer sample clips could be used to secure specimens within the resin. Care also had to be taken to ensure that the Epofix resin had fully hardened prior to specimen polishing and this was generally achieved by placing the samples in an oven at 50°C for 2 hrs once the resin was solid.

Specimens were secured in the requisite polishing holder and, whether specimens were free-mounted or set in Epofix resin, thin pieces of aluminium were placed between the sample and the grub screws of the holder to prevent gripping damage. A Buehler Motopol 12 universal grinder/polisher was used in all cases. The polishing pressure was set to 5lb per square inch of specimen (total loaded area, including resin) and was maintained at this level throughout.

The first stage of the procedure was to grind specimens flat. This could be achieved in two ways - by using a Buehler P320 grit resin-bonded diamond wheel rotating contrary to the specimen head at a speed of 120 rpm and washed with a steady flow of

water, or by using 8" 180 grit silicon carbide paper rotating at 250 rpm in the same direction as that of the specimen head and again washed with water. The second method was found to give better results in terms of less damage, and specimens were generally found to be flat within about 2 minutes. It was, however, necessary to use small diameter paper and to ensure that the specimens overlapped the edge of the paper during rotation in order to prevent uneven wearing and hence uneven grinding of the sample.

The second stage required the use of a an 8" METLAP 4 wheel rotating at a speed of 25 rpm in a contrary direction to that of the specimen head and sprayed with a thin layer of 9μm oil-based diamond spray. This was continued for 7 minutes. Again, it was necessary to ensure that the specimens overlapped the edge of the platten for the reasons given above.

The third stage was performed by using a Perforated TEXMET cloth rotating at a speed of 240 rpm in the same direction as the specimen head and sprayed with 6 μm diamond spray. This stage took a further 7 minutes. It was found that the slightly harsher, water-based diamond spray gave a better result then oil-based slurries at this stage.

Finally, samples were polished on a TEXMET cloth rotating complimentary at a speed of 240 rpm in the same direction as the specimen head and sprayed with 1 μm oil-based diamond spray. This stage was initially set for 10 minutes duration to remove completely any damage from the previous stage. However, it should be noted that this time may be altered to suit the specimen requirements. It was observed that, although a long final polish was required for aesthetic observation of the microstructure (e.g. to eliminate any chip-out of fibre ends and for image analysis), this was too long for the observation of matrix microcracks. It was found that a number of cracks visible at stage three had disappeared after only two minutes of final

polishing as the edges of the cracks were refined. Subsequent re-polishing of these specimens on stage three re-revealed the cracks.

Appendix 4 : Publications

C.M.A.Davies, B.Harris, R.G.Cooke - 'Characterisation of Damage Onset in Glass-Ceramic Matrix Composite Angle-Ply Laminates', Composites, **24** (2), 141 - 149 (1993) and was presented at 'Fatigue and Fracture of Composite Materials', Cambridge University, April 1992

INDEX OF TABLES AND FIGURES

Chapter 2: Behavioural Models

Chapter 3: Glass and Glass-Ceramic Composites

Chapter 4: Materials and Experimental Details

Chapter 5: Monolithic CAS

Chapter 6: Unidirectional Nicalon/CAS Composite

Chapter 7: Off-Axis Nicalon/CAS Composite

Chapter 8: Angle-Ply Nicalon/CAS Composite